Development of an MSC-Based Immune Checkpoint Inhibiting Cell Therapy

Serap GOKCEN

A thesis submitted for the degree of Doctor of Philosophy

in Molecular Medicine

School of Life Science

University of Essex

Date of submission for examination (October 2025)

Statement of Originality

Unless indicated otherwise, I confirm that the content of this thesis is my original work and has not been submitted for the award of any degree elsewhere. All previously published data and sources are appropriately cited and acknowledged within this thesis.

Acknowledgements

I would like to thank and express my sincere gratitude to my PhD supervisor, Dr Andrea Mohr, for her continuous support, encouragement, and patience. Despite all the challenges I have been through, her guidance throughout my PhD research lit the way from the beginning and taught me invaluable lessons in becoming a researcher. I would also like to thank Dr Ralf Zwacka for his encouragement and guiding kind presence in every step, whose wisdom was always the source of innovative ideas.

I want to thank my fellow lab members of the Molecular Medicine Lab whom I have worked, Aleyna Guney, Phoebe Blair, Tianyuan Chu, and Louis Clay, for their friendship and support. I am glad to have the opportunity to collaborate with them at the University of Essex. Special thanks to Dr Greg Brook and Aygun Azadova for their help and support.

Lastly, I would like to thank my family for their continuous love and support in every step of my life. Without you, I could not have made it this far.

Authorship and Contributions

Unless indicated otherwise here, all experiments in this thesis were conducted by the candidate. In section 4.11, establishment of the B16.F10 metastasis model, dosing, and tissue collection were performed by Dr Andrea Mohr, and Dr Tianyuan Chu conducted quantification of metastatic nodules and histological assessment. In section 4.5 cytokine array of MSC.LUC and MSC.HAC samples were carried out by Phoebe Blair.

Abstract

Cancer research has focused on targeted therapy, particularly immune checkpoint therapies, since programmed cell death protein 1 (PD1) monoclonal therapies demonstrated notable efficacy with reduced toxicity. Despite its progress to date, several challenges persist, including a non-inflammatory tumour microenvironment (TME), constraints on drug delivery, and suboptimal binding of recombinant antibodies. To overcome these challenges, we propose a pragmatic cell therapy approach in which mesenchymal stem cells (MSCs) are utilised as carriers of a soluble, high-affinity PD1 variant ($sPD1^{HAC}$). This approach aims to harness the tumour tropism and plasticity of MSCs while providing a sustained source of a highly competitive PD1 in the TME.

Our study demonstrates successful insertion of $sPD1^{HAC}$ into MSCs, leading to sufficient secretion without compromising cell viability and maintaining unperturbed cytokine profile, as shown by ELISA, apoptosis, and cytokine array assays. Across solid-phase and cell-based binding assays, including cross-species competitions, $sPD1^{HAC}$ outcompeted recombinant PD1 and anti-PDL1 monoclonal antibodies. It reduced PD1-PDL1 binding by 82-94 per cent at one-fifth the comparator concentration. Furthermore, a single intravenous dose of $MSC.sPD1^{HAC}$ significantly reduced pulmonary metastatic burden in C57BL/6 mice with B16.F10 melanoma. Additionally, at the cohort scale, TCGA PanCancer Atlas mRNA Z-scores were analysed for T-cell abundance, activation, progenitor-exhausted, and exhausted states to stratify samples as hot or cold. Melanoma showed the highest T-cell-defined inflammatory state within the dataset. We also examined a predefined set of 323 immune-related genes and their correlations with PDL1 to identify a general signature for high-PDL1 tumours. Although no universal signature emerged, PDL1 aligned with IFNγ-linked activation, as confirmed by flow cytometry in IFNγ-stimulated cancer cell lines. This reinforces the idea that delivery and continuous ligand competition may be decisive, especially in colder settings.

Together, these findings highlight an approach that is both principled and practical. Cohort data clarify where inflammation is limited and why a universal biomarker may be elusive. The MSC platform then addresses that challenge by providing tumour-tropic, continuous delivery of a high-affinity PD1 variant, achieving

robust competition in vitro and efficacy in vivo. In doing so, it augments the antibody therapy and offers a credible route to strengthen responses in cancers that are currently difficult to inflame.

List of Abbreviations

Abbreviation	Full Term
4-1BB	Tumour necrosis factor receptor superfamily member 9
5FU	5-fluorouracil
Ab	Antibody
ACT	Adoptive cell therapy
ADCC	Antibody-dependent cellular cytotoxicity
Akt	Protein kinase B
ANOVA	Analysis of variance
AP-1	Activator protein-1
APC	Antigen-presenting cells
AT-MSC	Adipose tissue-derived mesenchymal stem cell
ATCC	American Type Culture Collection
ATP	Adenosine triphosphate
BiTE	Bispecific T-cell engagers
BM-MSC	Bone marrow-derived mesenchymal stem cell
BSA	Bovine serum albumin
BTLA	B and T lymphocyte attenuator
CAF	Cancer-associated fibroblast
CAR	Chimeric antigen receptor
CD2	Cluster of differentiation 2
CD20	Cluster of differentiation 20
CD27	Cluster of differentiation 27
CD274	Programmed cell death protein 1-ligand 1 gene
CD28	Cluster of differentiation 28

CD3-BsAbs	CD3 targeted bispecific antibodies
CD4+	Helper T-cell
CD8+	Cytotoxic T-cell
CD80	Cluster of differentiation 80
CD86	Cluster of differentiation 86
cDC	Conventional dendritic cell
cGAS	Cyclic GMP-AMP synthase
CHO	Chinese hamster ovary
CK2	Casein kinase 2
CRI	Cancer Research Institute
CRS	Cytokine release syndrome
CTL	Cytotoxic T lymphocyte
CTLA-4	Cytotoxic T-lymphocyte-associated antigen 4
DAB	3,3′-Diaminobenzidine
DAG	Diacylglycerol
DAMP	Damage-associated molecular pattern
DC	Dendritic cell
DMEM	Dulbecco's modified Eagle medium
dMMR	Deficient mismatch repair
DUR	Durvalumab
ECM	Extracellular matrix
EGFR	Epidermal growth factor receptor
ELISA	Enzyme-linked immunosorbent assay
EMT	Epithelial-mesenchymal transition
Erk	Extracellular signal-regulated kinase
EV	Extracellular vesicle
FACS	Fluorescence-activated cell sorting
FBS	Fetal bovine serum
FcRn	Neonatal Fc receptor
FDA	The US Food and Drug Administration
GITR	Glucocorticoid-induced TNF receptor-related protein
GM-CSF	Granulocyte-macrophage colony-stimulating factor

H&E	Haematoxylin and eosin
HAC	High-affinity consensus
HAC-V	High-affinity consensus variant
HEK293T	Human embryonic kidney 293T
HER2	Human epidermal growth factor receptor 2
HVEM	Herpes virus entry mediator
HI	Hot intensity
hIgG1	Human immunoglobulin G1
HLA	Human leukocyte antigen
HLA-I	Human leukocyte antigen class I
hPDL1	Human PDL1
HSS	Hot summary score
HSV-1	Herpes simplex virus 1
ICANS	Immune effector cell-associated neurotoxicity syndrome
ICB	Immune checkpoint blockade
ICI	Immune checkpoint inhibitor
ICOS	Inducible T-cell costimulator
IDO1	Indoleamine 2,3-dioxygenase 1
IFNγ	Interferon gamma
Ig SF	Immunoglobulin superfamily
IgG	Immunoglobulin G
IgG1-Fc	Immunoglobulin G1 Fc fusion/domain
IL10	Interleukin 10
IL12	Interleukin 12
IL13	Interleukin 13
IL15	Interleukin 15
IL18	Interleukin 18
IL1β	Interleukin 1 beta
IL2	Interleukin 2
IL23	Interleukin 23
IL6	Interleukin 6
iNOS	Inducible nitric oxide synthase

irAEs	Immune-related adverse effects
IP3	Inositol 1,4,5-trisphosphate
ITSM	Immunoreceptor tyrosine-based switch motif
JAK-STAT	Janus kinase/signal transducer and activator of transcription
LAG3	Lymphocyte activation gene 3
mAb	Monoclonal antibody
MAD	Median absolute deviation
MAPK	Mitogen-activated protein kinase
MCP-1	Monocyte chemoattractant protein-1
MDSC	Myeloid-derived suppressor cell
MEK	Mitogen-activated protein kinase
MFI	Mean fluorescence intensity
MHC	Major histocompatibility complex
MOI	Multiplicity of Infection
mPDL1	Murine PDL1
MSC	Mesenchymal stem cell
MSI-H	Microsatellite instability-high
mTOR	Mechanistic target of rapamycin
NF-κB	Nuclear Factor kappa-light-chain-enhancer of activated B cells
NFAT	Nuclear factor of activated T-cells
NK	Natural killer cells
NKT	Natural killer T-cells
NSCLC	Non-small cell lung cancer
OD	Optical density
OV	Oncolytic virus
OX40	Tumour necrosis factor receptor superfamily member 4
p53	Tumour suppressor protein 53
PAMP	Pathogen-associated molecular pattern
PBS	Phosphate-buffered saline
PD1	Programmed cell death protein 1
pDC	Plasmacytoid dendritic cell
PDCD1	Programmed cell death protein 1 gene

PDL1	Programmed cell death protein 1-ligand 1
PDL2	Programmed cell death protein 1-ligand 2
PE	Phycoerythrin, a fluorescent tag protein
PEX	Progenitor-exhausted T-cell state
PFA	Paraformaldehyde
pFUSE	pFUSE expression vector backbone
pFUSE.sPD1^{HAC}	Plasmid construct for expressing soluble PD1^{HAC} variant
pFUSE.sPD1^{WT}	Plasmid construct for expressing soluble PD1^{WT} variant
PI3K	Phosphatidylinositol 3-kinase
PIP3	Phosphatidylinositol-3,4,5-trisphosphate
PKCθ	Protein kinase c theta
PLC-γ1	Phospholipase C-gamma 1
PROTAC	Proteolysis-targeting chimera
PTEN	Phosphatase and tensin homolog
PVR	Poliovirus receptor
Ras	Ras GTPase
RasGRP1	Ras guanine nucleotide-releasing protein 1
RCC	Renal cell carcinoma
rhPD1	Recombinant human PD1
rhPDL1	Recombinant human PDL1
rmPD1	Recombinant mouse PD1
rPD1	Biotinylated labelled programmed cell death protein 1
ROS	Reactive oxygen species
SHP2	Src homology 2 domain phosphatase 2
SLAM	Signalling lymphocytic activation molecule
SLAM6	Signalling lymphocytic activation molecule family member 6
SLP-76	Signalling lymphocyte-activated protein of 76 kDa
sPD1	Soluble PD1
sPD1^{HAC}	Soluble programmed cell death protein 1 high affinity consensus variant

sPD1^{WT}	Soluble programmed cell death protein 1 wild type
SPR	Surface plasmon resonance
STING	Stimulator of interferon genes
Strep-HRP	Streptavidin conjugated with horseradish peroxidase
Strep-PE	Streptavidin conjugated with phycoerythrin
TAA	Tumour-associated antigen
TAM	Tumour-associated macrophage
TAN	Tumour-associated neutrophil
TCF1	T-cell factor 1
TCGA	The Cancer Genome Atlas Program
TCM	Central memory T-cell
TCR	T-cell receptor
TEM	Effector memory T-cell
TEX	Terminally exhausted T-cell state
Tfh	T follicular helper cell
TGFβ	Transforming growth factor beta
TIGIT	T-cell immunoreceptor with Ig and ITIM Domains
TIL	Tumour-infiltrating lymphocyte
TIM	T-cell Immunoglobulin and Mucin
TIM3	T-cell immunoglobulin and mucin domain protein 3
TLR	Toll-like receptor
TMB	3,3′,5,5′-Tetramethylbenzidine
TME	Tumour microenvironment
TNF-R1	Tumour necrosis factor receptor superfamily member 1a
TNF-R2	Tumour necrosis factor receptor superfamily member 1b
TNFSF	Tumour necrosis factor superfamily
TNFSF10	Tumour necrosis factor-related apoptosis-inducing ligand gene
TP53	Tumour protein p53 gene
TRAIL	Tumour necrosis factor-related apoptosis-inducing ligand
Treg	Regulatory T-cells
TRM	Tissue-resident memory T-cell
UC-MSC	Umbilical cord-derived mesenchymal stem cell

VAF	Variant allele frequency
VEGF	Vascular endothelial growth factor
VISTA	V-domain immunoglobulin suppressor of T-cell activation
WHC	Width of hot coverage
XCR1	X-C motif chemokine receptor 1
ZAP70	Zeta-chain-associated protein kinase 70

List of Figures and Tables

Table of Contents

Chapter 1: Literature Review

1.1 Introduction

Immune checkpoint blockade (ICB) therapies, also termed as immune checkpoint inhibitors (ICI), have gained substantial recognition in the recent decade due to their remarkable success in treating diverse cancer types, minimal side effects, and high overall survival rates. ICB therapy is based on reactivation of the patient's immune system against cancer by targeting immune inhibitors. In this context, a range of ICB therapies have been developed. Although some of these approaches may not have been successful in either research or clinical studies, therapies targeting the immune checkpoint programmed cell death protein (PD1) and several others continue to show promising results. For instance, Cercek and her colleagues demonstrated the effectiveness of anti-PD1 monoclonal therapy in a cohort of 12 patients with locally advanced rectal cancer (Cercek *et al.*, 2022). Remarkably, complete tumour removal was achieved in all 12 patients, and no significant adverse events were reported.

Despite such success stories, significant challenges persist in the field of ICB therapies. For instance, the delivery of therapeutics into the desmoplastic stroma of tumours remains an issue that needs to be solved. Various approaches have been developed to overcome drug delivery issues, such as combination therapies and immune vaccines; however, none of them has yet achieved a robust solution for breaking the barrier of this evolving microenvironment. Here, we propose mesenchymal stem cells (MSCs) as a delivery vector that is capable of releasing mediators and migrating to the tumour site. In principle, MSCs can break the fibroblastic stroma barrier, harbour, and carry more than one therapeutic agent due to their ability to undergo genetic modifications and transport these drugs or factors to the specific location of the tumour. Therefore, they have great potential to enhance the effectiveness of treatment and shift the inflammation balance to the benefit of immunity (Hmadcha *et al.*, 2020; Seyed-Khorrami *et al.*, 2021). Furthermore, they can also be directed into the tumour tissue electromagnetically with the addition of biohybrid microrobot modification without losing their biological activities or the functionality of the therapeutic payload, as our group has shown in a previous study (Gundersen *et al.*, 2023).

While global agencies have approved many drugs for ICB therapy, key challenges remain. In addition to the stroma barrier of tumours, the immunosuppressive tumour

microenvironment (TME) and cytokine-associated cytotoxicity are the other issues that are still unsolved. Progress in decoding the intricate structure of TME, which includes the immune toxicity, therapeutic resistance, and biomarker identification, has been slower than anticipated, highlighting the need for intensified research efforts. Although tumours with microsatellite instability are known to respond well to the treatment, they represent only a small fraction of patients. On the other hand, the concept of 'hot tumours' is gaining increasing attention for its potential to benefit a broader range of patients, provide valuable insights into cancer immune evasion mechanisms, and deepen our understanding of tumour immunity. Building on this perspective, identifying a common expression profile of cytokines and immune cells that is applicable across all cancer types could expand the patient population's eligibility for treatment while guiding the selection and development of optimal immunotherapeutic agents.

Still another, and arguably the most formidable challenge that ICB therapies face, is the insufficient proliferation of tumour-infiltrating lymphocytes (TILs), primarily driven by low-affinity and short-duration binding of ICB antibodies. To address the challenge of binding affinity, Maute and colleagues engineered two libraries of PD1 variants employing the yeast surface display method (Maute *et al.*, 2015). They aimed to identify a competitive, high-affinity PD1 variant capable of binding effectively to its ligands, programmed cell death ligand 1 and 2 (PDL1 and PDL2, respectively). This approach led to the discovery of a high-affinity consensus (HAC) PD1, termed as HAC-V, which featured ten amino acid substitutions and exhibited approximately a 35,000-fold increased affinity on surface plasmon resonance (SPR) compared to the wild-type PD1. Moreover, HAC-V exhibited improved tumour penetration properties, highlighting its potential as a therapeutic candidate.

1.2 Dysregulation of immune checkpoints in cancer

The genesis and progression of cancer hinge upon complex cascades of genetic and epigenetic alterations, cumulatively resulting in an aberrant transcriptional landscape that favours tumour survival and immune evasion. These alterations occur in distinct genomic structures known as insulated neighbourhoods, where pivotal genes, ranging from tumour suppressors (TP53) and oncogenes (EGFR) to immune regulators (PDCD1), are located. Disruption of these regions contributes directly to cancer

pathogenesis by dysregulating oncogenic signalling pathways and modulating immune checkpoint gene expression (Hnisz *et al.*, 2018). Thus, dysregulation of immune checkpoints starts with tumorigenesis. On the other hand, mutations that cause genomic dysregulations in cancer have two faces for tumours; they give rise to neoantigens that render the tumour susceptible to immune surveillance, and they also give rise to expression of immune checkpoints that support them evading from immune system.

Immune checkpoints, such as PD1, PDL1, cytotoxic T-lymphocyte associated protein 4 (CTLA-4), lymphocyte-activation gene 3 (LAG-3), T-cell immunoglobulin and mucin-domain containing-3 (TIM-3), and T-cell immunoreceptor with Ig and ITIM domains (TIGIT), typically serve as key regulators of immune homeostasis, preventing excessive immune responses and autoimmune pathology. However, in the context of cancer, dysregulation and overexpression of their genes significantly contribute to tumour-mediated immunosuppression. This dysregulation stems from tumour-intrinsic genetic and epigenetic alterations, extrinsic inflammatory pressures, and metabolic cues (Kalbasi and Ribas, 2020; Vishnoi *et al.*, 2022).

At the genomic level, gene amplifications, structural variations, and oncogenic mutations directly influence transcription levels of immune checkpoints in cancer. For example, copy number gains and rearrangements at chromosome 9p24.1, where the CD274 gene (PDL1) resides, have been consistently correlated with high PDL1 expression in cancers like Hodgkin lymphoma, NSCLC, and triple-negative breast cancer (Ansell *et al.*, 2015; Guo *et al.*, 2016; Lin *et al.*, 2024b) Also, loss-of-function mutations in tumour suppressors such as TP53, and oncogenic transcription factors such as MYC and signalling cascades including PI3K/AKT/mTOR and RAS/RAF further augment PDL1 expression, making these genetic alterations foundational drivers in many tumour types. (Hargadon, 2023; Kalbasi and Ribas, 2020).

In contrast, epigenetic mechanisms, including DNA methylation, histone modifications, and noncoding RNA regulation, provide a dynamic layer of control that modulates the expression of immune checkpoints as well as PDL1 in response to environmental cues. Studies have shown that changes in promoter methylation and histone acetylation can fine-tune PDL1 levels, especially in response to inflammatory cytokines such as IFNγ (Cha *et al.*, 2019; Dai *et al.*, 2022). In terms of the regulation

of PD1 expression on T-cells, epigenetic modifications appear to be even more critical. Chronic T-cell receptor stimulation leads to durable epigenetic changes, such as irreversible demethylation of enhancer regions and histone modification patterns that drive sustained PD1 overexpression and promote T-cell exhaustion in the tumour microenvironment (Mishra and Verma, 2018; Saleh *et al.*, 2020).

Despite these distinctions, there is a significant interplay between genetic and epigenetic mechanisms. In the case of PDL1, while genetic alterations such as gene amplification set the baseline for constitutive expression, epigenetic modifications can adjust expression levels dynamically in response to external stimuli.

The idea of evolving cancer cells in response to a dynamic immune system and TME changes constitutes the immunoediting concept (Swann and Smyth, 2007). According to this hypothesis, cancer cells accomplish evading the immune system in three phases: designated elimination, equilibrium, and escape. The elimination phase of immunoediting is also called immunosurveillance, in which cancer cells are recognised and eliminated by immune cells. Although the elimination phase can be passed with complete tumour clearance, it can also be incomplete with partial tumour clearance. Incomplete elimination brings the equilibrium phase, in which cancer cells can stay dormant or evolve, acquiring further mutations and expressions. In the equilibration phase, immune pressure is still on the susceptible cancer cells to a possible extent. If this process continues and elimination cannot be done thoroughly, ultimately, this mechanism leads to the selection and escape of successful cancer cell clones. Thus, these clones become able to resist the immune system by avoiding or suppressing it, so there is an escape phase (Mittal *et al.*, 2014; Swann and Smyth, 2007).

Beyond classical immunoediting, a recent theoretical model that interprets the functional and non-functional intra-tumour heterogeneity has been elucidated, distinguishing neutral evolution of cancer cells from Darwinian evolution (Williams *et al.*, 2016). Building on this foundation, Efremova et al. initially suggested that the neutral accumulation of mutations exerts a greater influence on cancer cells than immunoediting. They investigated hypermutated and microsatellite-instable colorectal cancer cell lines to elucidate tumour dynamics in the context of immunoediting and immune checkpoint therapies. To ascertain the driving forces behind cancer evolution, they characterised neoantigens, assessed their binding affinity, and evaluated the

retention of neoantigen-generating mutations in both wild-type and immunodeficient tumour-bearing mice using whole-exome sequencing to identify somatic mutations, Affymetrix Mouse Diversity SNP array profiling for genome-wide copy number analysis, variant allele frequency (VAF)-based cancer cell fraction estimation to assess clonal architecture, RNA sequencing for expression profiling, and peptide-Major histocompatibility complex (MHC) binding prediction algorithms to characterise neoantigen landscapes. Their findings revealed that the impact of T-cell-dependent immunoediting was relatively minor compared to neutral evolution. Notably, the study showed that anti-PDL1 therapy markedly altered this equilibrium, shifting the dynamics from neutral to non-neutral evolution among the cancer clones, enforcing intense immuno-selective pressure (Efremova *et al.*, 2018). This transition was accompanied by increased tumour homogeneity, suggesting that checkpoint blockade can intensify immunoediting to the extent that resistant clones may eventually dominate, potentially explaining the development of resistance to ICB therapy. It is important to note that this study was conducted on hypermutated and microsatellite-unstable colorectal cancer cell lines, which are among the most responsive cancer types to ICB therapy.

Collectively, these multilayered and context-dependent mechanisms of checkpoint dysregulation highlight the complexity of tumour-immune interactions and the inherent limitations in current ICB therapies. Tumour cell-intrinsic genetic and epigenetic alterations, evolutionary dynamics, and extrinsic inflammatory signals collectively contribute to therapeutic resistance and incomplete clinical responses observed in cancer immunotherapy.

1.3 Tumour microenvironment and inflammation

Closely linked to the genetic and epigenetic dysregulation of immune checkpoint molecules, the TME represents another significant and complex barrier to effective ICB therapies. When the focus shifts from molecular regulators such as RNAs to the cellular and structural constituents, the TME emerges as a heterogeneous and intricate ecosystem comprising cancer cells, diverse immune cell populations, stromal elements including MSCs and cancer-associated fibroblasts (CAFs), as well as cytokines, growth factors, extracellular vesicles (EVs), immune checkpoints, and vascular networks.

Inflammation within the TME plays a dual role, exhibiting both anti-tumour and pro-tumour effects (Lan *et al.*, 2021; Zhao *et al.*, 2021). Acute inflammation is beneficial, supporting dendritic cell maturation, antigen presentation, and activating robust immune responses against cancer cells. Conversely, chronic inflammation fosters immune evasion, promotes tumour cell proliferation and metastasis, and contributes to therapy resistance. Although TME is often characterised by chronic inflammation, cytokines and chemokines, acting as crucial mediators, reflect a delicate balance between tumour-promoting and immune-activating functions. Pro-inflammatory cytokines such as TNF-α, IL-6, IL-1β, and IL-23 can initially enhance anti-tumour immunity, yet their persistent activity often drives chronic inflammation and immunosuppression (Landskron *et al.*, 2014). Anti-inflammatory cytokines like IL-10 and TGF-β similarly have dualistic roles, promoting tumour evasion and immunological tolerance under chronic inflammatory conditions.

Interactions within the TME significantly influence tumorigenesis through multiple dynamic mechanisms. Immune cell infiltration and activity within the TME differ considerably based on tumour and stromal types, creating diverse immune landscapes that vary between patients (Wang *et al.*, 2023). This diversity is attempted to be characterised by the classification of tumours into immunologically "hot" or "cold," indicating distinct levels of immune infiltration and inflammation. Hot tumours, rich in infiltrating T-cells and inflammatory signals, often respond well to immunotherapy (Jiao *et al.*, 2019). In contrast, cold tumours, with minimal immune infiltration, generally show resistance, highlighting the need for strategies to transform these cold tumours into responsive hot ones.

EVs are another factor emerging as another key component to facilitate intricate intercellular communication within the TME. EVs mediate the transfer of proteins, nucleic acids, and metabolites, actively shaping local and distant tumour microenvironments, influencing immune responses and tumour progression.

Tumour-derived EVs are found to cause therapy resistance by carrying PDL1 in an orientation that enables it to bind PD1 on T-cells, thereby inhibiting T-cell activity (Mortezaee and Majidpoor, 2022). Clinical investigations also provide evidence for the presence of PD1 on circulating EVs derived from activated T-cells in specific cancer contexts. For instance, studies in metastatic melanoma and head and neck squamous

cell carcinoma have identified PD1 on exosomes isolated from patient plasma. In these settings, higher levels of PD1-positive EVs were observed in patients who did not respond to immune checkpoint inhibitors and were associated with poor progression-free and overall survival (Chen *et al.*, 2018b; Serratì *et al.*, 2022; Theodoraki *et al.*, 2018). These findings together indicate that the therapeutic agent used in ICB therapy must have superior binding abilities to displace wild-type PD1 and should be sustained by a continuous source in the TME.

Additionally, inflammation-related intracellular signalling pathways, often referred to as downstream molecular pathways, such as nuclear factor kappa B (NF-κB), Janus kinase/signal transducer and activator of transcription (JAK-STAT), and mitogen-activated protein kinase (MAPK), as well as toll-like receptor (TLR) pathways, are pivotal regulators within the TME. These downstream signalling cascades orchestrate cytokine production, immune cell recruitment and polarisation, and modulate the inflammatory milieu, significantly shaping tumour biology and immune dynamics (Zhao *et al.*, 2021).

In summary, the TME comprises a dynamic network of interactions and inflammatory signals that critically shape cancer progression and therapeutic outcomes. Understanding, characterising, and targeting these interactions, especially by modulating acute versus chronic inflammatory responses, may lead to improved personalised strategies in cancer immunotherapy.

1.3.1 The concept of HOT-COLD tumours

Objective response rates to anti-PD1/PDL1 therapies vary greatly by tumour type and agent, reaching approximately 33 to 40% in advanced melanoma with anti-PD1 monotherapy, about 40 to 56% in Merkel cell carcinoma, around 69 to 72% in relapsed/refractory classical Hodgkin's lymphoma, and about 34 to 48% in tumours with high microsatellite instability (MSH-I) and deficient mismatch repair (dMMR) (Chen *et al.*, 2019a; D'Angelo *et al.*, 2021; Eroglu *et al.*, 2018; Nghiem *et al.*, 2016; O'Malley *et al.*, 2022). This rate in other cancer types, such as advanced non-small-cell lung cancer, advanced or metastatic urothelial cancer, and advanced renal-cell carcinoma, is generally no more than 25% with checkpoint inhibitor monotherapy in less selected settings (Disis *et al.*, 2023; Motzer *et al.*, 2015; Rosenberg *et al.*, 2016).

The reasons for this variation among patients within the same cohort remain incompletely understood. In 2009, Camus et al. discovered that the co-expression of genes related to cytotoxicity and T helper 1 (Th1) cells in adaptive immune responses could predict patient survival, independent of metastatic status in colorectal cancer. This correlation between survival and Th1 cells led to the classification of tumours into "hot," "variable," and "cold" categories based on the 2-year recurrence risk, which was found to be 10%, 50%, and 80%, respectively. The variable group was further subdivided into immunosuppressive and immune rejection subtypes (Camus *et al.*, 2009; Marei *et al.*, 2023).

Following these findings, this categorisation of tumours has been evidenced to be decisive for therapy response by numerous studies that investigated various cancer types, not only in terms of tumour size and metastatic potential but also in relation to the TME, signalling pathways, TILs, and other immune characteristics. Even though this framework was initially developed from observations of tumour-infiltrating lymphocytes and their impact on patient outcomes, the availability of large-scale datasets such as TCGA has dramatically increased its prominence over the past decade.

Currently, the classification of tumours as hot or cold is approached with a multidisciplinary strategy. Comprehensive profiling now integrates genomic, transcriptomic, proteomic, and imaging data to yield a holistic view of the TME (Chakravarthy *et al.*, 2018). Radiomics techniques, for instance, enable non-invasive prediction of immune phenotypes from computed tomography scans by quantifying features that correlate with high or low immune cell densities (Nguyen *et al.*, 2023). These methodologies, coupled with advanced machine learning algorithms, continue to enhance the accuracy and reproducibility of immune classification, thereby aiding in the design of personalised immunotherapeutic agents (Sakai *et al.*, 2025).

Although this field is advancing rapidly, deciphering the TME demands the integration of advanced methodologies, extensive datasets, and substantial time investment. Approaching this complexity from multiple perspectives, through both targeted and integrative analyses of high-quality datasets such as those from TCGA, can streamline the path toward meaningful insights. In this study, common T-cell markers and other

immune-related genes were analysed in relation to PDL1 expression to contribute to this understanding.

1.3.2 Key immune checkpoint molecules

The TME's signalling network and the resulting hot/cold tumour phenotype arise from numerous inputs (Galon and Bruni, 2019; Wang *et al.*, 2023). Among these, immune checkpoints have gained remarkable attention, as findings on specific receptor-ligand pairs, such as PD1/PDL1, show that they can calibrate the magnitude and duration of T-cell responses to such an extent that they may alter the course of tumorigenesis. Fundamentally, the function of the immune checkpoints is to define the threshold between effective immunity and tolerance within tumours by counterbalancing co-stimulation and cytokine signalling. Thus, immune checkpoints operate as gatekeepers on the T-cell receptor and co-stimulatory signalling axis, setting the activation threshold that determines whether antigen recognition matures into effective immunity or is restrained into tolerance. This framing naturally leads to the historical development of T-cell activation biology from identifying the TCR to establishing the canonical two-signal model.

The discovery of T-cell receptor (TCR) by James P. Allison and his colleagues in the early 1980s marked a significant milestone in immunology, opening a new era in our understanding of immune cell interactions and the regulation of immune response to an antigen (Allison *et al.*, 1982) was not a coincidence that years later, in 2018, he and Tasuku Honjo were awarded the Nobel Prize for their discovery of cancer therapy by inhibition of negative immune regulation. Soon after the TCR revelation, it was established that not only TCR engagement but also a second signal is needed for a fully activated T-cell (canonical two-signal model). Also, it was discovered that TCR ligation can lead to the T-cell unresponsiveness or anergy when it is provided alone (D L Mueller *et al.*, 1989; June *et al.*, 1987). Until a while ago, this signal was mainly discussed in stimulatory roles; however, inhibitory signals (co-inhibitors) exist as a secondary signal as well as stimulatory signals (co-stimulators), and each one of them plays a crucial role in the regulation of T-cell activation, acting through co-receptors in cis or trans position. On top of that, the diverse roles of secondary signals found later on have led the canonical two-signal model of naive T-cells to evolve further.

Although these co-receptors were mainly studied in the initial activation of naive T-cells, some of them to modulate effector, regulatory, and memory T-cells, determining the fate of T-cells in the spleen and lymph nodes (Tai *et al.*, 2012). The regulation of these T lymphocytes depends on the expression of signal transduction pathways. Such expression levels fluctuate and overlap according to internal and external stimuli during the regulation of T-cells to find a fine-tune for the immune response, creating a tight control on the inflammatory response with activation of naive T-cells, deactivation of previously activated cells, or unresponsiveness. This process ensures that T-cells respond to the right level while preventing autoimmunity. Based on the changes in expression levels of regulatory signalling molecules, a tidal model was proposed by Zhu and his colleagues (Zhu *et al.*, 2011). In this model, immune response rises and falls with the interplay between co-stimulatory and co-inhibitory signals while precisely determining the magnitude and direction of the response together. Therefore, instead of the two-signal model, as often attributed to the T-cell activation in the past, this model provides an intricate representation of the second co-signals, which are highly precise to environmental cues and can gradually modulate T-cell responses (Talay *et al.*, 2009).

In terms of protein structure, co-signal molecules can be classified into two main categories, the Immunoglobulin superfamily (Ig SF) and Tumour Necrosis Factor Superfamily (TNFSF). While their extracellular domain architecture defines Ig SF co-receptors, TNF is defined by a conserved cysteine-rich signature-containing domain. Ig SF further includes CD28, PVR-like protein, CD2/Signalling Lymphocytic Activation Molecule (SLAM), and T-cell Immunoglobulin and Mucin (TIM) families (Kumar *et al.*, 2018). In the wake of the clinical success of monoclonal antibodies like anti-PD1 and anti-CTLA4, which target immune activation in cancer treatment, the identification of co-stimulatory molecules has witnessed a rapid surge. Some significant examples of TNFSF co-signals are Glucocorticoid-Induced TNF receptor-related protein (GITR), Tumour necrosis factor receptor superfamily member 4 (TNFRSF4 or OX40), member 9 (TNFRSF4 or 4-1BB), member 7 (TNFRSF7 or CD27), member 1A and 1B (TNF-R1/2), Herpes Virus Entry Mediator (HVEM), etc. Ig SF member co-signals include Cluster of Differentiation 80 (CD80 or B7.1), Cluster of Differentiation 86 (CD86 or B7.2), Cluster of Differentiation 28 (CD28), B and T lymphocyte attenuator (BTLA), Cytotoxic T-lymphocyte-associated protein 4 (CTLA-4), PD1, PDL1, PD-L2, Inducible

T-cell co-stimulator ligand (ICOSL or B7-H2), Cluster of Differentiation 276 (CD276 or B7-H3), Lymphocyte-activation gene 3 protein (LAG3), T-cell immunoreceptor with Ig and ITIM domains (TIGIT) and V-domain Ig suppressor of T-cell activation (VISTA).

Having established how checkpoints tune T-cell activation, the next question is the scope. The full complement of human immune checkpoints remains unsettled and continues to expand as new receptor-ligand pairs are described. A consolidated set of well-characterised checkpoints is summarised in Figure 1.1, grouped into co-inhibitory and co-stimulatory classes. Importantly, their expression and net effect are context-dependent: even highly functional T-cells can upregulate inhibitory checkpoints during acute infection as a homeostatic brake (Wang *et al.*, 2022c).

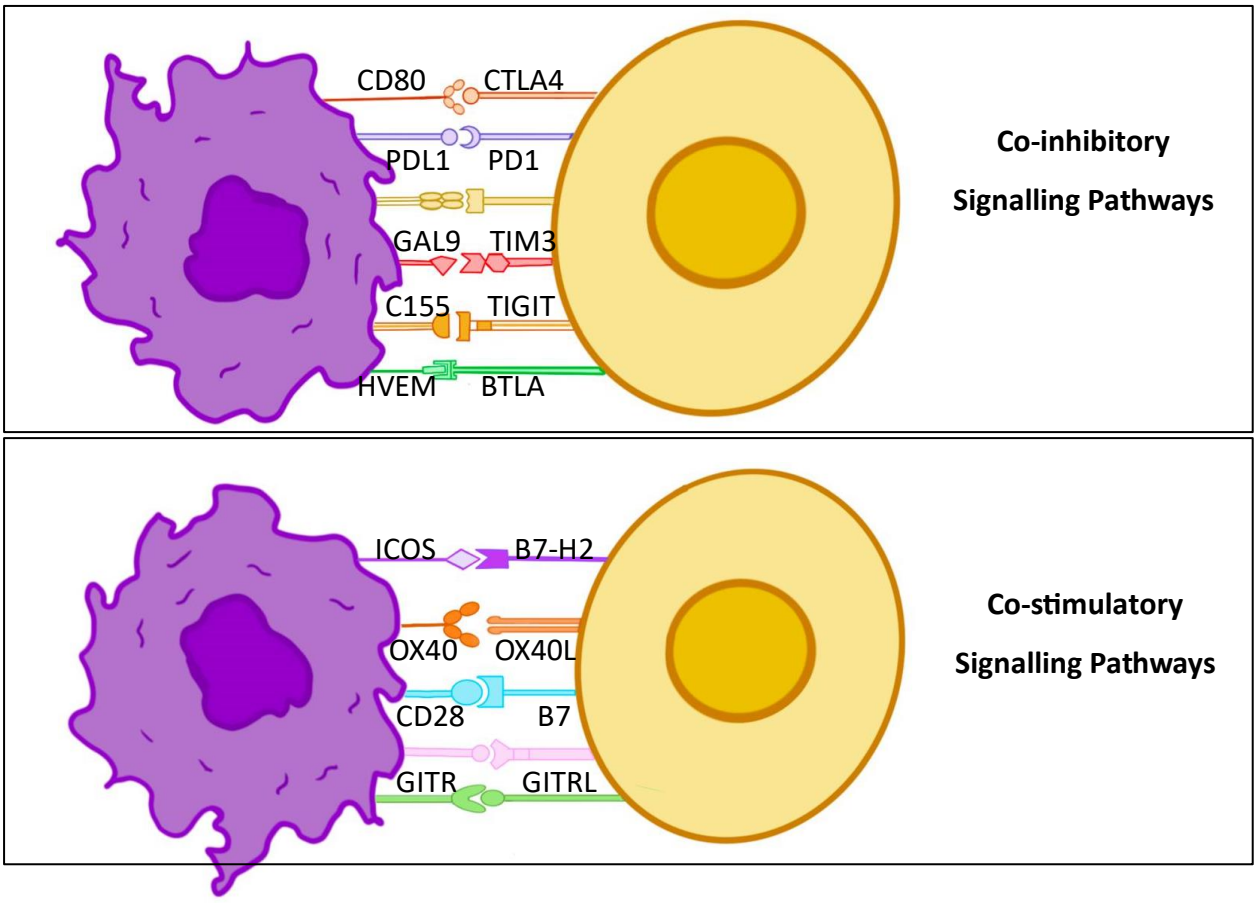

Figure 1.1 Schematic depiction of T-cell key co-inhibitory and co-stimulatory signalling pathways and molecules. T-cell (yellow; $CD8^+$ cytotoxic or $CD4^+$ helper) receptors engage ligands on antigen-presenting cells and tumour cells (purple; dendritic cells, macrophages, B cells, and cancer cells).

The influence of these checkpoints on the TME extends beyond direct inhibition of T-cell function. Their expression is often associated with an immunosuppressive milieu characterised by the accumulation of regulatory T-cells (Tregs), myeloid-derived suppressor cells (MDSCs), and M2-polarized tumour-associated macrophages, all of which further reinforce immune tolerance and impair effective anti-tumour responses (Li *et al.*, 2020). Interconnectedly, the composition, spatial organisation, and activation states of infiltrating immune cells also set the TME's tone (hot/cold), disease trajectory, and treatment responsiveness.

1.3.3 Inflammatory and anti-inflammatory cytokines

While the innate immune system spearheads the initial defence against tumours, the adaptive immune response provides the critical arsenal required for sustained tumour eradication. Cytotoxic T lymphocytes (CTLs), equipped with effector molecules such as IFNγ and granzymes, deliver precise and targeted destruction of tumour cells. However, this process is often derailed by helper T-cell subsets like Th2, Th17, and Tregs. Th2 cells, through the secretion of IL-4 and IL-13, orchestrate the polarization of tumour-associated macrophages (TAMs) into a tumour-promoting phenotype. Similarly, Th17 cells drive angiogenesis and facilitate immune evasion, while Tregs, ironically serving as mediators of immune tolerance, suppress effector T-cells, inadvertently aiding tumour progression. This intricate balance within the adaptive response underscores the profound complexity of immune dynamics in the tumour microenvironment.

Within the challenges of pro-tumour inflammation, an unexpected ally emerges: inflammation as a protector against tumour formation. While chronic inflammation often contributes to cancer development, acute immune responses can activate surveillance pathways that identify and eliminate early tumour cells. This dual role demonstrates the immune system's remarkable ability to balance destruction and protection, shaping the delicate equilibrium of tumour immunity. Understanding this balance offers significant potential for using inflammation as both a weapon and a defence in cancer therapy.

Acute inflammation is typically rapid, self-limiting, and pathogen or damage-driven, dominated by pattern-recognition signalling and bursts of IL-1β, TNFα, and IL-6 that

mobilise neutrophils, activate endothelium, and enhance antigen presentation (Chen *et al.*, 2018c; Zhao *et al.*, 2021). When efficiently resolved, acute danger signalling can promote tumour surveillance by enhancing dendritic cell activation and migration for T-cell priming, while licensed cDC1s support early CTL induction (Lei *et al.*, 2024; Moriya *et al.*, 2021). By contrast, failure of resolution sustains a chronic cytokine milieu that remodels the TME towards immune suppression, angiogenesis, and tissue repair programmes that favour tumour promotion (Fishbein *et al.*, 2021; Zhao *et al.*, 2021).

Among the immune system's massive reservoir of cytokines and chemokines, IL-6 is a key interleukin. It supports myeloid accumulation, STAT3 activation, and survival pathways in tumour and stromal cells. The cis- and trans-signalling of IL6 links chronic inflammation to tumour cell proliferation, epithelial to mesenchymal transition, and all of these events to therapy resistance (Ebbing *et al.*, 2019; Rose-John, 2021). In parallel, IL-1β propagated by inflammasome activity maintains leukocyte recruitment and endothelial activation, but in persistent settings also enhances tumour growth and accelerates a protumour chemokine network (Zhao *et al.*, 2021). On the protective side, IFNγ produced by CTLs and NK cells is a pivotal cytokine in acute anti-tumour immunity, increasing antigen processing and MHC expression, inducing CXCL9 and CXCL10 to recruit $CXCR3^{+}$ effector cells, and exerting cytostatic pressure on incipient tumours; however, prolonged or dysregulated IFNγ signalling can select for immune-edited variants and tolerance pathways, underscoring context dependence (Pattu *et al.*, 2025). Most of the chemokines themselves are bifunctional, such as CXCL9 and CXCL10. These chemokines generally correlate with T-cell inflamed phenotypes and better response to checkpoint blockade, but their gradients can also rendered ineffective therapy response due to stromal barriers and chronic exposure (Tokunaga *et al.*, 2018). On the other side, TGFβ and IL-10 consolidate the chronic state by dampening antigen presentation, promoting Treg stability, and driving TAM polarisation towards wound healing phenotypes that impede CTL access to tumour nests; TGFβ additionally reshapes metabolism and extracellular matrix to hinder T-cell infiltration. As seen in this narrow frame of cytokines, they are mostly known to have both pro- and anti-inflammatory roles (Briukhovetska *et al.*, 2021).

1.3.4 Immune cells in the TME

Immune cells secrete a range of cytokines, interleukins, growth factors, and proteolytic enzymes, including IL8, IFNγ, TNF-α, VEGF, and matrix metallopeptidases (MMP) that drive metabolic changes and thereby modulate the TME phenotype. In fact, interaction goes both ways. For example, chemotactic cues from VEGF, monocyte chemoattractant protein-1 (MCP-1/CCL2), and macrophage colony-stimulating factor-1 (M-CSF/CSF-1) also promote the accumulation of TAMs within the TME, which correlates with unfavourable prognosis across several malignancies (Elmusrati *et al.*, 2021). The TME includes cells from both adaptive and innate immunity, such as T and B lymphocytes; TAMs and tumour-associated neutrophils (TANs); myeloid-derived suppressor cells (MDSCs); mast cells; dendritic cells (DCs); and natural killer (NK) cells. In conclusion, tumour-associated immune cells within the TME comprise a heterogeneous mixture of innate and adaptive immune cells whose functions critically regulate tumour progression, metastasis, and therapeutic outcomes.

Innate immune cells have pivotal roles in tumour immunosurveillance and immunoediting processes, as well as adaptive cells. For instance, TAMs are among the most abundant immune cells within the TME and display remarkable plasticity. These cells can polarise toward an M1 phenotype, which secretes pro-inflammatory cytokines supporting tumour cell killing, or toward an M2 phenotype, which promotes tumour progression by secreting growth factors, angiogenic mediators (such as VEGF), and matrix metalloproteinases, which further facilitate tissue remodelling, invasion, and metastasis (Faget *et al.*, 2021; Peña-Romero and Orenes-Piñero, 2022). Neutrophils also exhibit a dual role, with N1 neutrophils contributing to anti-tumour immunity through production of reactive oxygen species and cytokines, whereas N2 neutrophils drive tumour progression by remodelling the extracellular matrix and enhancing angiogenesis (Faget *et al.*, 2021).

Tumour-associated macrophages (TAMs)

Tumour-associated macrophages, especially the M2-like phenotype, are significant in ICB, as key contributors to tumour-promoting inflammation. M2-TAMs foster an immunosuppressive microenvironment by suppressing cytotoxic T-cells and secreting anti-inflammatory cytokines such as IL-10, TGF-β, and VEGF. This not only

accelerates tumour growth but also supports angiogenesis and metastasis. M2-TAMs have roles in extracellular matrix (ECM) remodelling, which further promotes tumour expansion. Signals from cancer cells, T-cells, and B cells reprogramme TAMs into pro-tumour effectors that enable immune evasion and tumour progression. Beyond their direct actions, M2-TAMs orchestrate the recruitment of other immune cells, advocating their status as pivotal modulators of tumour-associated inflammation (Sun *et al.*, 2024).

Neutrophils in tumour immunity

Neutrophils, the first responders, again exhibit both anti-tumour and pro-tumour functions in cancer. While their initiation role in infection control is commendable, their chronic presence in the TME frequently influences tumour progression. Similarly to TAMs, tumour-associated neutrophils (TANs) polarise into two subsets: N1, with anti-tumour properties, and N2, which promote tumour growth. N2-TANs, through the secretion of factors like iNOS, VEGF, and Matrix metallopeptidase 9 (MMP9), enable angiogenesis, immune suppression, and metastasis. Their adaptability within the TME underscores their complexity, yet the predominance of N2-polarised TANs is associated with tumour progression (Elmusrati *et al.*, 2021).

Myeloid-derived suppressor cells (MDSCs)

MDSCs, a heterogeneous yet potent population, function as key immunosuppressive mediators in the TME. By deploying Arg-1 and iNOS and producing IL-10 and TGF-β, they suppress T-cell proliferation and effector function; additional mechanisms include cysteine depletion and NO/ROS generation that impair TCR-HLA signalling. MDSCs also promote angiogenesis, favour Treg/Th2 activation, and upregulate PDL1 to engage PD1 on T-cells, while dampening NK-cell activity. Consequently, interrupting their recruitment, survival, or suppressive pathways represents a credible therapeutic strategy (Elmusrati *et al.*, 2021).

Natural killer cells (NKs)

NKs are another important cell group which closely related to PD1 therapies. Emerging evidence indicates that NK cells, although typically exhibiting lower basal PD1 than T-cells, can upregulate PD1 after chronic tumour exposure or prolonged activation. In time-resolved in vitro systems, a terminally differentiated $CD56^{dim}$ subset of NKs acquires PD1 following sustained exposure to tumour-derived factors and cytokines, including IL-12, IL-15, and IL-18 (Bai and Cui, 2022; Buckle and Guillerey, 2021). Across studies using flow cytometry and receptor-occupancy assays, PD1 induction, while variable in magnitude, associates with reductions in degranulation (CD107a) and IFNγ secretion, with cytotoxic deficits partially restored by PD1 or PDL1 blockade by approximately 30-40% (Dong *et al.*, 2019). However, methodological differences such as stimulation duration, cytokine presets, antibody clone selection, and gating strategies contribute to variable PD1 detection.

On the other hand, MSCs exert potent, state-dependent effects on NK cells. The claim that naive MSCs may attenuate NK cell activation is supported by studies demonstrating that MSCs in an unprimed state secrete high levels of inhibitory factors such as TGFβ, PGE2, IDO, which downregulate activating receptors of NK cells (e.g., NKG2D, NKp30) and suppress IFNγ secretion in co-culture systems. In contrast, MSCs primed with IFNγ undergo a phenotypic and secretomic shift characterised by elevated production of immunostimulatory cytokines (for example, IL-15 and IL-12) that enhance NK cell cytotoxicity and may support antibody-dependent cellular cytotoxicity (ADCC) (Moloudizargari *et al.*, 2021).

The evaluation of the MSC-NK crosstalk data implies that while MSCs possess an inherent duality in modulating NK cell activity, careful optimisation of priming conditions can shift the balance in favour of an immunostimulatory profile. This is particularly significant given the potential to harness MSCs as vehicles for targeted immunomodulation in the tumour microenvironment. In other words, appropriately primed MSCs may serve not only as cell therapy agents in their own right but also as platforms for the sustained local delivery of therapeutic molecules that enhance NK cell effector function.

Dendritic cells (DCs)

Dendritic cells are functionally grouped into three subsets: conventional DCs (cDCs), plasmacytoid DCs (pDCs), and inflammatory DCs. Conventional DCs mediate anti-tumour immunity by acquiring antigens and cross-presenting them to $CD8^+$ T-cells. Within this compartment, cDC1 (including $XCR1^+$) are the principal cross-presenters and correlate with enhanced cytotoxic T-cell activity (Audsley *et al.*, 2020). However, tumour-derived IL-10, TGF-β, PGE_2, and hypoxia collectively impede DC maturation and skew differentiation towards tolerogenic states across both primary and monocyte-derived DCs. In such milieus, antigen capture may remain intact, but the expression of co-stimulatory molecules (CD80, CD86) and production of IL-12 decline, blunting T-cell priming (Mazzoccoli and Liu, 2024). These context-dependent shifts highlight the plasticity of DCs as both an opportunity and a liability in situ, and they reinforce the need for strategies that stabilise immunostimulatory programmes.

The PD1/PDL1 axis constrains DC function either by reducing T-cell priming capacity or by dampening DC co-stimulation. PDL1 expressed on DCs limits effective presentation and suppresses IL-12 secretion in vitro and in vivo, including murine melanoma models (Pittet *et al.*, 2023; Su *et al.*, 2021). Reports of PD1 expression on DCs further suggest direct inhibition of their capacity to expand cytotoxic T-cells, although epitope selection and gating differences contribute to inconsistent detection (Wang *et al.*, 2024a). Across preclinical systems, PD1/PDL1 blockade consistently augments markers of DC maturation and increases pro-inflammatory cytokines, with several studies reporting ≳2-fold gains in IL-12 versus untreated controls (Pittet *et al.*, 2023; Su *et al.*, 2021). Together, these data provide a mechanistic basis for checkpoint modulation to relieve DC-mediated suppression and to enable more durable engagement of adaptive immunity.

1.5 T-cells in cancer immunotherapy

T-cells coordinate anti-tumour immunity through direct cytotoxicity, helper cytokine production, and durable memory formation. $CD8^+$ cytotoxic T lymphocytes recognise tumour antigens on MHC class I and induce apoptosis via perforin/granzyme and Fas-FasL pathways. Lysis releases antigens that reinforce priming and amplify responses (Brunell *et al.*, 2023; Fu *et al.*, 2020). $CD4^+$ T-cells sustain these programmes by

secreting IFNγ, IL-2, and TNF-α, which support CTL differentiation and maintenance, enhance antigen-presenting cell function, and recruit additional effectors. Central, effector, and tissue-resident memory T-cell subsets provide rapid recall responses that associate with improved outcomes and sustained remission (Guo *et al.*, 2024). The clinical impact of T-cells on tumorigenesis is evident from PD1 and CTLA4 blockade, which releases inhibitory signalling and reinvigorates exhausted T-cell populations, and also from adoptive cell therapies, including CAR T-cells and TILs, that leverage and extend intrinsic cytotoxic programmes (Guo *et al.*, 2024; Moseman *et al.*, 2025; Nagasaki *et al.*, 2022; Wang *et al.*, 2024b).

T-cell development in the thymus enforces MHC restriction and self-tolerance through positive and negative selection (Lin *et al.*, 2025; Mani *et al.*, 2023). Naive T-cells, marked by CD45RA and CCR7, circulate through blood and lymphoid organs. Upon antigen encounter, naive T-cells rapidly differentiate into effector cells in response to a combination of TCR signalling, co-stimulation, and cytokine cues; a process that propels them into a robust functional state marked by increased cytotoxic molecule production and pro-inflammatory cytokine release. This effector phase is pivotal for immediate tumour clearance; however, a subset of these activated cells subsequently transitions into various memory subtypes that include central memory T-cells (T_{CM}), effector memory T-cells (T_{EM}), and tissue-resident memory T-cells (T_{RM}). Each is characterized by unique homing markers and functional profiles that support long-term immunosurveillance (Pu *et al.*, 2025). The continuum further encompasses the emergence of stem-like progenitor exhausted T-cells, which arise under conditions of chronic antigen exposure such as those present in the tumour microenvironment. These progenitor exhausted cells exhibit intermediate levels of inhibitory receptors like PD1 yet retain the transcription factor TCF1, enabling them to proliferate and differentiate upon therapeutic intervention such as PD1 blockade (Brunell *et al.*, 2023). Such cells contrast with terminally exhausted T-cells, which display high levels of PD1, loss of proliferative capacity, and irreversible epigenetic modifications that render them refractory to reactivation(Chen *et al.*, 2019b; Koh *et al.*, 2022; Wang *et al.*, 2022a; Zhang *et al.*, 2021). In parallel, $CD4^+$ T-cells diversify into Th1, Th2, Th17, and Tfh subsets that orchestrate immunity, while $FOXP3^+$ Tregs, required for peripheral tolerance, are exploited as well by tumours to suppress immune responses.

Persistent antigen, sustained inflammation, and metabolic stress drive exhaustion, with progressive loss of effector function and proliferation. Inhibitory receptors including PD1, LAG3, TIM3, and TIGIT act together to dampen TCR and co-stimulatory signalling, reduce IL-2, TNF-α, and IFN-γ production, and limit cytolytic degranulation (Brunell *et al.*, 2023; Gitto *et al.*, 2021; Pansy *et al.*, 2021).

By contrast, stem-like progenitor exhausted cells retain self-renewal and can be reprogrammed by PD1/PDL1 blockade, although efficacy depends on alleviating hypoxia, lactate accumulation, and nutrient deprivation that impair glycolysis and mitochondrial fitness. Exhaustion manifests functionally as reduced cytokine secretion, proliferation, and degranulation; in terminally exhausted populations, restoration after PD1 blockade is partial and transient due to fixed epigenetic constraints (Liu *et al.*, 2020; Reading *et al.*, 2018).

The crosstalk between MSCs and T-cells is mediated through a complex network of soluble factors and cell surface interactions. MSCs are known to secrete a range of immunosuppressive molecules, including IDO, prostaglandin E_2 (PGE_2), IL-10, and TGFβ, which modulate T-cell priming, proliferation, and trafficking (Mondino and Manzo, 2020). In addition, MSCs express HLA-I and can present antigens in a context that influences T-cell function, while the secretion of chemokines such as CXCL9, CXCL10, and CXCL11 further directs T-cell migration toward tumour sites (Nair *et al.*, 2025) (Pansy *et al.*, 2021). When MSCs are engineered to secrete sPD1, the intent is not only to neutralize PDL1 inhibitory signals but also to improve the immunological synapse between dendritic cells and T-cells, thereby preserving essential co-stimulatory interactions (Guo *et al.*, 2024; Pu *et al.*, 2025). This targeted delivery strategy aims to mitigate the off-target effects and systemic toxicities often seen with conventional immune checkpoint inhibitors, while simultaneously enhancing intratumoural T-cell activation and function (Hübbe *et al.*, 2020).

1.6 Immune therapies for cancer

Traditionally, chemotherapy and radiotherapy have been the cornerstones of cancer treatment. In recent years, targeted therapies have emerged alongside chemotherapy and radiotherapy as a third approach to cancer treatment, expanding on the progress made with immune treatments. The main characteristic separating targeted therapies

from conventional ways is that they target a gene or protein altered in cancer, thereby assuring specificity and reducing the adverse side effects significantly. Immune therapy, which is one of these targeted approaches, aims at the immune system components and fights against cancer from the inside. In this context, various strategies have been developed. Some approaches have been deprioritised due to limited efficacy, whereas others continue to mature with convincing signals in preclinical models and clinical studies (Jin *et al.*, 2019; Johnson *et al.*, 2018).

Primary research has provided distinct frameworks for classifying cancer immunotherapies by both the immune contexture of tumours and the specific therapeutic modalities employed. The classification based on tumour-immune microenvironment stratifies into three archetypes, namely, hot, variable, and cold as aforementioned. Another classification is based on the therapeutic approach underlying the mechanism of action. Immune therapies can be classified under 6 titles with this classification according to the Cancer Research Institute (CRI) Clinical Accelerator team and an analysis of the immune-oncology drug development study done by Jia Xin Yu and her colleagues in 2019. They have inspected 3,876 active immune-oncology agents and identified the 6 most developed groups. These groups are T-cell-targeted immunomodulators, other immunomodulators, cell therapy, cancer vaccines, oncolytic viruses, and CD3-targeted bispecific antibodies (Figure 1.2)(Xin Yu *et al.*, 2019b).

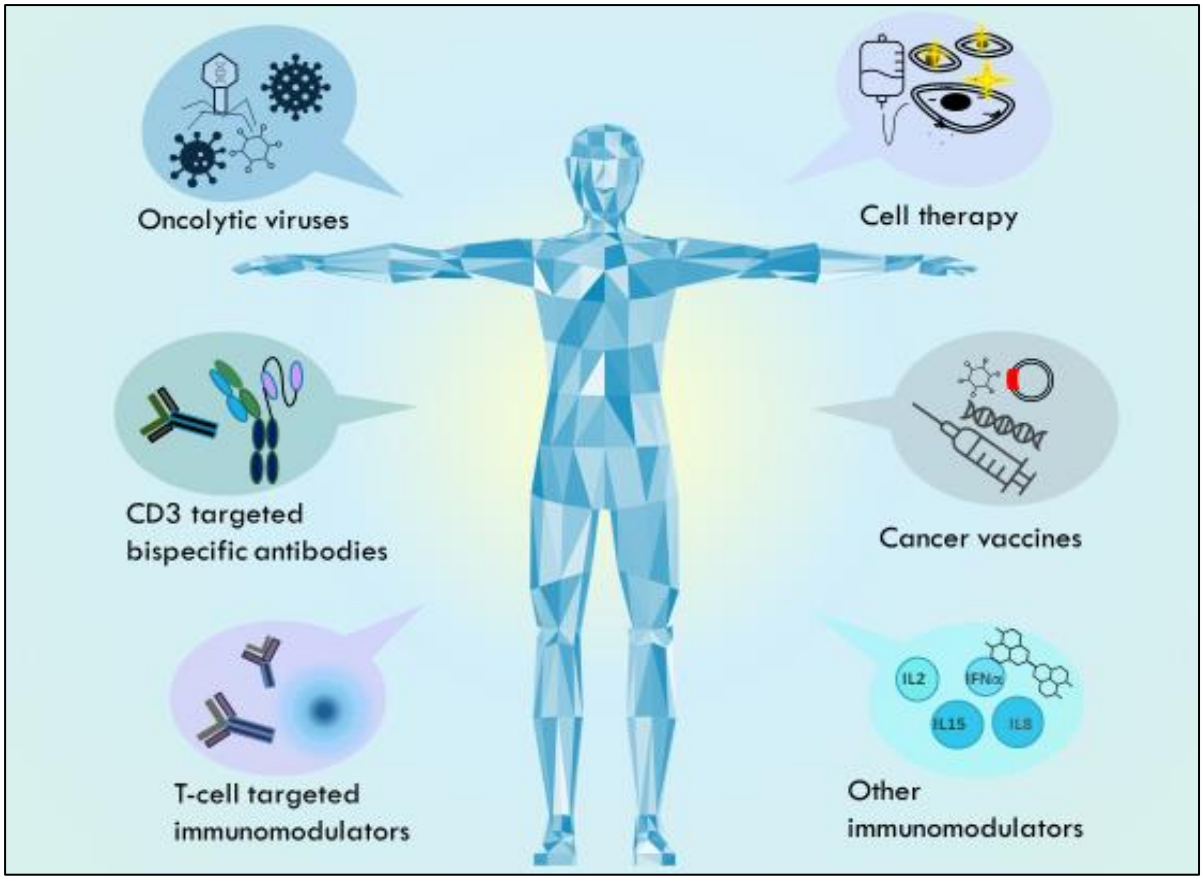

Figure 1.2. Schematic representation of immune therapy categorises. Immune therapies can be inspected under 6 main topics: oncolytic viruses (e.g. modified Adenovirus Herpes simplex virus), cell therapy (e.g. CAR-T-cells), CD3 targeted antibodies, cancer vaccines (e.g. cell-, protein-, RNA- or DNA-based), T-cell targeted immunomodulators (e.g. monoclonal antibodies), and other immunomodulators (e.g. cytokines, chemical compounds).

1.6.1 CD3 targeted bispecific antibodies

CD3 targeted bispecific antibodies (CD3-BsAbs) include cytotoxic effector cell redirectors, tumour-targeted immunomodulators, and dual immunomodulators. Different from other therapeutic antibodies that can only detect the corresponding antigen via both Fab arms, CD3-BsAbs can detect the same antigen with their antigen-binding domains. CD3-BsAbs simultaneously bind to a tumour-associated antigen (TAA) expressed on cancer cells, thereby connecting them to CD3 on T-cells. Similarly to TCR and MHC formation, this approach initiates T-cell activation and recognition of cancer cells (Dahlén *et al.*, 2018; Middelburg *et al.*, 2021).

Potent T-cell redirection by CD3-targeted bispecific antibodies depends critically on tumour antigen density, spatial geometry, and dosing parameters. Higher antigen

density on tumour cells facilitates robust immunological synapse formation and serial killing by redirection of both CD8+ and CD4+ T-cells, whereas low or heterogeneous expression can compromise efficacy and promote off-tumour toxicity (Ball *et al.*, 2023). Studies have demonstrated that epitope location and the molecular format of bispecific antibodies, such as having a small flexible structure with single-chain variable fragments (e.g., approved therapy; BiTE^{TM}) or IgG-like constructs, significantly modulate avidity, pharmacokinetics, and tissue penetration (Bergamaschi *et al.*, 2025). Evidence from quantitative pharmacokinetic/pharmacodynamic modelling indicates that step-up dosing and fractionated administration strategies effectively reduce cytokine release syndrome (CRS) and immune effector cell-associated neurotoxicity syndrome (ICANS) by moderating peak T-cell activation (Foster and Lum, 2019; Singh *et al.*, 2021). This convergence suggests that careful calibration of antigen density thresholds and geometric parameters is imperative for optimising the therapeutic window.

Adaptive resistance following CD3-bispecific treatment emerges from antigen escape mechanisms, including shedding, trogocytosis, and T-cell dysfunction marked by rapid PD1 upregulation on activated T-cells (Goebeler *et al.*, 2024). Clinical and preclinical evidence from phase 2 studies indicates that the initiation of bispecific antibody therapy frequently leads to a pronounced exhaustion phenotype, characterised by increased PD1/PDL1 expression, release of inhibitory cytokines, and an immunosuppressive tumour microenvironment (Köhnke *et al.*, 2015; Singh *et al.*, 2021). In contrast to continuous infusion paradigms, step-up dosing regimens have allowed more controlled immune activation and reduced cytokine surges in patient cohorts, thereby improving T-cell functional persistence (Ball *et al.*, 2023). Moreover, combination strategies with PD1/PDL1 blockade have demonstrated additive or synergistic effects, suggesting that checkpoint inhibition can rescue T-cell functionality and sustain cytotoxic responses over prolonged treatment courses (Ball *et al.*, 2023; Clynes and Desjarlais, 2019). It is noteworthy that direct assessments of combination therapies using CD3-bispecifics and PD1 blockade remain limited in diverse solid tumour models.

1.6.2 Oncolytic viruses (OVs)

OVs are basically native or genetically modified viruses that can selectively replicate their genetic material within cancer cells that harbour oncogenic signalling abnormalities and dysfunctional type-I interferon (IFN) responses. In contrast to some cancer vaccines that are also based on a virus, OVs directly infect and trigger the lysis process of cancer cells in situ. Their antitumour activity is based on two main mechanisms: their ability to selectively infect neoplastic cells, thereby directly killing them, and stimulation of the antitumour immunity, mostly via causing inflammatory cytokine release in TME. The foundational claim is that tumour-selective replication culminates in a robust release of intracellular components, particularly damage-associated molecular patterns (DAMPs) such as adenosine triphosphate (ATP) and high-mobility group box 1 (HMGB1), which are critical for activating local innate immune responses (Seymour and Fisher, 2016) The effectivity of these mechanisms varies depending on the properties of the virus, cancer type, and the interplay between the virus, TME and host immune system. Many double- or single-stranded DNA and RNA viruses have been proposed as vectors for research and clinical trials to date. For Instance, adenoviruses, HSV-1, poliovirus, poxviruses, measles virus, vaccinia virus, and parvovirus H1 (Kaufman *et al.*, 2013; Santos Apolonio *et al.*, 2021). Although this approach has many advantages, only a limited portion of patients can benefit from these advantages. Therefore, new developments in the genomics field are employed, and combination therapies with ICB therapies are being investigated currently (Chen *et al.*, 2018a; Mahalingam *et al.*, 2020; Ribas *et al.*, 2017). Multiple studies have demonstrated that OV platforms replicate preferentially in tumour cells, leading to selective viral propagation and a reduction in off-target toxicity. For example, HSV-1-based platforms, which include both T-VEC and less-modified strains such as HSV1716, have been shown to exploit impaired IFN pathways in cancer cells to achieve selective replication and lysis, while non-malignant tissues remain relatively protected (Ajina and Maher, 2017; DePeaux and Delgoffe, 2024).

The lytic process triggers the release of DAMPs and pathogen-associated molecular patterns (PAMPs), which then engage innate immune receptors such as Toll-like receptors (TLRs), RIG-I, and the cGAS-STING pathway (DePeaux and Delgoffe, 2024). Activation of these receptors results in type-I IFN production, which in turn

drives the activation and maturation of antigen-presenting cells (APCs), including dendritic cells (DCs). The cross-priming of tumour antigens to CD8+ T-cells is a particularly crucial step that links local oncolysis to systemic anti-tumour immunity. Data indicate that OV-mediated ICD can increase tumour-specific TCR diversity and expand cytotoxic T-cell populations, thereby converting an immunologically 'cold' tumour into an inflamed 'hot' one (Ajina and Maher, 2017; Liu and Sun, 2021). In many cases, quantitative measures have shown relative increases in activated T-cell frequencies on the order of 50% or more when comparing pre- and post-treatment samples (Jeong *et al.*, 2021).

The role of payload engineering in enhancing these immunogenic effects is central. Engineered OVs incorporating immunostimulatory transgenes, such as granulocyte-macrophage colony-stimulating factor (GM-CSF), various cytokines, such as IL-12 and IL-15, chemokines, such as CXCL9 and CXCL10, and even co-stimulatory ligands, have been shown to further amplify the recruitment and activation of APCs, thereby enhancing cross-priming and T-cell infiltration (Zamarin *et al.*, 2017). For instance, T-VEC (FDA-approved oncolytic virus, 2015), which expresses GM-CSF, not only induces local viral oncolysis but also facilitates robust DC recruitment and activation, leading to an enhanced systemic CD8+ T-cell response (Kim *et al.*, 2015; Mistarz *et al.*, 2019; Robilotti *et al.*, 2023). Comparative studies across platforms have indicated that while all OVs share the basic mechanism of inducing ICD via lysis and DAMP release, variations in cell tropism and replication kinetics lead to differences in the magnitude and duration of the immune response. Adenoviral platforms tend to generate rapid and potent oncolysis but may be more susceptible to neutralisation than HSV-1 derivatives (Ajina and Maher, 2017).

The mode of OV delivery further shapes the immunogenic outcome. Intratumoural injection is widely used to achieve high local viral concentrations, optimise direct oncolysis, and generate a local cytokine storm that triggers rapid type-I IFN responses and chemokine expression. In contrast, systemic administration is challenged by the dilution of viral particles and the presence of neutralising antibodies that can curtail viral replication before the virus reaches metastatic sites. However, innovative cell-carrier strategies, such as utilising macrophages for viral delivery, have shown promise in protecting the virus from humoral neutralisation and enabling efficient targeting of disseminated lesions (Ajina and Maher, 2017).

Despite these promising immunogenic effects, the persistence and spread of OV therapy are significantly constrained by host antiviral defences. It was claimed that pre-existing neutralising antibodies, robust interferon responses, and physical barriers within the tumour microenvironment (TME) serve as major impediments to OV efficacy (Ajina and Maher, 2017; Zheng *et al.*, 2019). Circulating neutralising antibodies, particularly in patients with prior viral exposures, have been reported to reduce effective viral titres by more than 70%, thereby impeding systemic delivery and viral bioavailability at the tumour site (Ajina and Maher, 2017). Concurrently, the innate IFN response, although pivotal for activating adaptive immunity, induces an antiviral state in adjacent normal tissues that can curtail viral replication. Data from multiple platforms indicate that overproduction of type-I IFNs is correlated with accelerated viral clearance, thus limiting both local and systemic OV effects (Ajina and Maher). This dual functionality of IFNs calls for a careful balance: while they are necessary to initiate the immune cascade, excessive IFN production may reduce viral persistence and, by extension, the magnitude of immune priming (DePeaux and Delgoffe, 2024).

Physical and pharmacokinetic limitations impose additional constraints. Tumour stroma, characterised by a dense extracellular matrix and aberrant vasculature, poses a formidable physical barrier to viral dissemination (DePeaux and Delgoffe, 2024). Viral shedding, another operational concern, has been monitored rigorously in clinical studies. The shedding is typically low and transient; however, stringent containment measures, including specialised dressings and patient education on hygiene practices, are recommended to mitigate the risks of inadvertent transmission, particularly in at-risk populations such as individuals with severe immunosuppression or active uncontrolled autoimmunity (Epstein and Rabkin, 2024). In terms of operational safety, the overall safety profile of OV therapy is acceptable, though it is platform-specific and requires careful monitoring. Common adverse events observed across OV platforms include transient pyrexia, chills, flu-like symptoms, and local injection-site reactions. (DePeaux and Delgoffe, 2024; Glorioso *et al.*, 2021).

Finally, the combination of OV therapy with immune checkpoint inhibitors, specifically PD1 and PDL1 agents, has demonstrated encouraging synergies. Preclinical data support that initial OV-induced immune priming may be amplified by subsequent checkpoint blockade, thereby reinvigorating exhausted tumour-specific T-cells. Although precise sequencing is critical to minimising immune-related adverse events

and maximising efficacy, early evidence suggests that a temporal separation wherein OV therapy precedes checkpoint inhibition yields the most robust T-cell infiltration and effector memory formation (Epstein and Rabkin, 2024).

1.6.3 Cancer vaccines

Cancer vaccines were the precursor of immunotherapy efforts. The very first cancer vaccine was invented and developed in vitro by Dr. Jian Zhou in 1991 (Zhao *et al.*, 2017). Cancer vaccination aims to induce or amplify T-cell responses against tumour-associated antigens. Approaches include peptide or protein antigens, whole cell or lysate vaccines, and antigen-loaded dendritic cells, most frequently. DCs have been favoured in cancer vaccine strategies as they have a number of desired characteristics that can be exploited by the therapy. They have the ability to absorb or present tumour-associated antigens via various mechanisms, as well as the ability to recall lymphocytes and travel between lymphoid and non-lymphoid tissues to control inflammation by modulating cytokines and chemokine gradients. Such abilities were found to be associated with systemic and long-lasting anti-tumour effects in several investigations. Although DC vaccines have demonstrated a high level of safety and immunogenicity profile, clinical responses were unfortunately insufficient (Perez and De Palma, 2019; Saxena *et al.*, 2021)

The available evidence confirms that the choice of antigen, coupled with the vaccine format, is a critical determinant of both the breadth and magnitude of antigen-specific T-cell responses. Neoantigen-personalised vaccines, which target tumour-specific mutations absent from normal tissues, consistently generate high-avidity CD8+ and CD4+ T-cell responses that overcome central tolerance, in contrast to shared tumour antigens that are liable to induce only low-affinity responses due to thymic deletion (Brentville *et al.*, 2018; Chi *et al.*, 2024). Preclinical and early clinical data further demonstrate that delivery platforms such as long peptides, mRNA or DNA formulations, dendritic cell vaccines, and viral or bacterial vectors influence antigen processing and cross-presentation by professional antigen-presenting cells. For example, long synthetic peptides require uptake and processing that facilitate presentation on both MHC class I and II molecules, leading to enhanced epitope spreading and T-cell receptor clonality compared to short peptides that may result in

an incomplete immune response (Chi *et al.*, 2024; Esprit *et al.*, 2020). Moreover, mRNA vaccines have shown rapid adaptability and potent immune activation in trials involving melanoma and gastrointestinal tumours, producing sustained IFNγ secretion and durable responses (Peng *et al.*, 2025). Similarly, dendritic cell approaches have yielded robust T-cell responses; however, the logistical challenges inherent in ex vivo manipulation often restrict their broad clinical application (Chi *et al.*, 2024). This collective evidence suggests that optimising both antigen choice and the accompanying vaccine format is instrumental in achieving high response rates and prolonged progression-free survival, thereby underpinning the rationale for personalised immunotherapy strategies that target multiple tumour neoantigens (Hu *et al.*, 2018; Li *et al.*, 2023).

Tumour evolution and the immunosuppressive TME exert a further set of constraints that shape the clinical performance and real-world utility of cancer vaccines. Evasion mechanisms, including antigen loss or HLA downregulation, can curtail the effectiveness of even the most immunogenic neoantigen vaccines, as evidenced by decreased T-cell recognition when subclonal mutations predominate (Esprit *et al.*, 2020; Fan *et al.*, 2023). The interplay between tumour heterogeneity and immune selection pressure necessitates a vaccine design that incorporates a spectrum of epitopes to induce epitope spreading and prevent immune escape (Li *et al.*, 2023). In parallel, the TME, characterised by regulatory T-cells, myeloid-derived suppressor cells, and immunosuppressive cytokines such as TGFβ, can diminish T-cell infiltration and function, further attenuating vaccine efficacy. Clinical data indicate that combining vaccines with PD1/ PDL1 inhibitors significantly enhances T-cell responses and clinical metrics such as objective response rate and progression-free survival, particularly in settings of low tumour burden (Hu *et al.*, 2018; Peng *et al.*, 2025).

Furthermore, pragmatic considerations regarding manufacturing timelines and safety profiles impact the translation of vaccine strategies into clinical practice. Neoantigen-based vaccines, while potentially more immunogenic, require extensive sequencing, computational prediction, and bespoke manufacturing that can extend production times and increase costs (Peng *et al.*, 2025). By contrast, shared antigen vaccines offer an off-the-shelf solution; however, their efficacy is often limited by central tolerance and reduced T-cell avidity (Esprit *et al.*, 2020; Fan *et al.*, 2023). Safety profiles across vaccine formats remain broadly acceptable, with local injection site

reactions and mild to moderate systemic adverse effects being the most common; nonetheless, viral vector-based vaccines may incur vector-specific adverse events, and rare cases of autoimmunity cannot be excluded (Brentville *et al.*, 2018; Peng *et al.*, 2025). Notably, combination regimens that include PD1/ PDL1 modulators have been well tolerated and have further bolstered clinical responses by countering TME-induced suppression.

1.6.4 Adoptive cell therapy

Adoptive cell therapy (ACT) aims to reinforce the immune system by ex vivo engineered human lymphocytes to the host. It includes chimeric antigen receptor (CAR) T-cells, CAR natural killer cells, TCR-engineered T-cells, and TIL-based therapy. This group of therapies has become a dominant area of clinical development globally (Upadhaya *et al.*, 2021; Xin Yu *et al.*, 2019a). While ACT can be highly effective in specific settings, particularly haematological malignancies and translation to solid tumours, it must address challenges such as antigen escape, TME heterogeneity, immunosuppression, T-cell exhaustion, and trafficking. Many of these barriers are being targeted through improved designs and through combination with immune checkpoint blockade or other modulators (Kandra *et al.*, 2022; Marofi *et al.*, 2021; Met *et al.*, 2019; Sharma and Allison, 2015)

Engineering choices and tumour context determine ACT potency and durability. ACTs are highly sensitive to design parameters and the intrinsic properties of the target tumour, which collectively dictate treatment potency and durability. In haematological malignancies, uniform and high-density antigens such as CD19 and BCMA allow CAR T-cells to elicit robust responses with reported complete response rates of 40-74% or higher, owing to efficient antigen recognition and minimal physical barriers (Azeez *et al.*, 2025; Bailey *et al.*, 2025). By contrast, solid tumours demonstrate considerable antigen heterogeneity and lower antigen density that complicate target selection and result in suboptimal infiltration due to physical stromal barriers and an immunosuppressive microenvironment (Azeez *et al.*, 2025; Gwadera *et al.*, 2025). Detailed evaluations reveal that costly trade-offs in CAR design are essential; for example, constructs incorporating CD28 co-stimulation tend to achieve rapid initial expansion and high cytokine production, yet are prone to accelerated T-cell

exhaustion, while 4-1BB domains foster prolonged persistence and memory formation, albeit with slower expansion kinetics (Crowther *et al.*, 2020). Moreover, manufacturing variables, including the fitness of the starting T-cell product, ex vivo expansion duration, dosing, and conditioning regimens, have been shown to significantly influence in vivo persistence and function (Jiang *et al.*, 2025). Complementary approaches such as TCR-engineered T-cells, which benefit from recognising intracellular neoantigens but are restricted by HLA and carry a risk of on-target/off-tumour toxicity, or tumour-infiltrating lymphocytes (TILs) that exploit a broader neoantigen repertoire in solid tumours yet require intensive preconditioning and IL2 support, further illustrate the necessity for tailored engineering decisions (Bailey *et al.*, 2025; Zhang *et al.*, 2025). Such integration of construct optimisation, target antigen profiling, and robust manufacturing practices is therefore crucial for bridging the potency gap between haematological and solid tumour settings and maximising durable clinical responses.

Toxicities and resistance mechanisms shape clinical deployment and combinations. Safety profiles and resistance mechanisms stand as critical determinants for the clinical implementation of ACT. In haematological settings, CAR T-cell therapy has consistently been associated with cytokine release syndrome (CRS) and immune effector cell-associated neurotoxicity (ICANS), which are generally managed through step-up dosing, the use of tocilizumab, and steroids, alongside predictable on-target effects such as B-cell aplasia that are acceptable given supportive care frameworks (Azeez *et al.*, 2025). Conversely, in solid tumours, on-target/off-tumour toxicity remains a significant concern due to overlap in antigen expression with normal tissues, and resistance mechanisms such as antigen loss, lineage switching, and impaired antigen presentation have been frequently documented (Azeez *et al.*, 2025). Furthermore, the tumour microenvironment exerts powerful suppressive influences via upregulated PD1 and PDL1, TGFβ and adenosine signalling, and (Oppermans *et al.*, 2020) metabolic restrictions that foster T-cell exhaustion (Zhang *et al.*, 2025). These resistance mechanisms have prompted numerous studies to explore rational combinatorial strategies, including the incorporation of PD1 and PDL1 blockade, cytokine and chemokine engineering to create 'armoured' CARs, and regional delivery to enhance tumour infiltration (Castiello *et al.*, 2022; Gwadera *et al.*, 2025). Such strategies are further supported by evidence indicating that improved T-cell manufacturing quality

and appropriate preconditioning regimens can mitigate toxicity while enhancing cellular persistence and overcoming resistance (Jiang *et al.*, 2025). Ultimately, integrated approaches that balance engineering precision with tailored management of tumour-specific toxicities and resistance factors are essential for optimising ACT deployment across diverse clinical settings, thus ensuring that the benefits of these advanced therapies are both potent and durable.

1.6.5 T-cell targeted immunomodulators and other immunomodulators

T-cell targeted immunomodulators include co-inhibitory antagonists (e.g. CTLA4, PD1, PDL1, LAG3, TIM3, VISTA) and co-stimulatory antagonists (e.g. OX40, ICOS). ICB aims to reverse tumour-induced tolerance by preventing inhibitory ligand receptor engagement, thereby restoring T-cell priming and effector function. They mainly consist of cell-surface signalling proteins responsible for negative immune regulation in self-tolerance, homeostasis, and fine-tuning of T-cell function. These regular and necessary functions are exploited by cancer cells as an immune escape mechanism. Cancer cells that survive after an immunosurveillance stay dormant or evolve, accumulating genetic changes such as mutations in DNA or changes in gene expression. Evolving cancer cells modulate tumour-specific antigens and immune checkpoint pathways that subsequently enable them to suppress the immune attack. In this mechanism, known as immunoediting, immune checkpoints are overexpressed by cancer cells. Therefore, blocking these pathways can re-establish immune control (Sharpe and Pauken, 2018; Swann and Smyth, 2007).

CTLA4 inhibitors such as ipilimumab and tremelimumab enhance T-cell priming by relieving CTLA4 competition with CD28 for their ligands CD80 and CD86 and can deplete intratumoural Tregs via Fcγ receptor engagement (Simpson *et al.*, 2013). These mechanisms yield antitumour activity in immunogenic tumours but within a narrow therapeutic window, with dose-linked immune-related adverse effects (irAEs) that require careful optimisation and monitoring. Combination regimens often use lower CTLA4 doses to retain efficacy while moderating toxicity (Augustin *et al.*, 2023; Shulgin *et al.*, 2020; Wu *et al.*, 2019).

In parallel, LAG3 inhibitors, typified by the relatlimab class, represent a novel approach to reinvigorate exhausted T-cells that frequently co-express PD1. The blockade of

LAG3 has been shown in pre-clinical models to restore proliferative capacity and cytotoxic function in subsets of T-cells that display a mixed proliferative/exhausted phenotype. Although single-agent activity is modest, clinical studies, particularly those evaluating the fixed-dose combination of relatlimab with nivolumab, have demonstrated a near doubling of progression-free survival relative to PD1 monotherapy in metastatic melanoma (Adam *et al.*, 2025; Tawbi *et al.*, 2022).

Antibodies targeting TIGIT interrupt binding to CD155/CD112, thereby mitigating the inhibitory signals that suppress T and NK cell responses. Pre-clinical evidence indicates that these agents induce partial restoration of T-cell function; however, clinical outcomes have been mixed, with response rates varying significantly across tumour types. Importantly, the efficacy of TIGIT inhibitors appears to be contingent upon concurrent PD1 inhibition; only in a background of PD1 pathway blockade do TIGIT inhibitors demonstrate enhanced antitumour activity, suggesting compensatory mechanisms that limit their benefit as monotherapies (Cui *et al.*, 2025). This dependency highlights the complex interplay between checkpoint receptors and underscores the necessity for future studies to incorporate judicious biomarker-driven patient selection to identify those most likely to benefit from monoclonal antibody inhibition.

Costimulatory receptor agonists targeting molecules such as OX40, 4-1BB (CD137), CD27, and ICOS have been developed to further enhance T-cell activation by providing a strong secondary signal that complements antigen receptor engagement. The efficacy of these agonists is highly dependent on their molecular format, with optimal activity requiring efficient cross-linking mediated by Fcγ receptor interactions, and often displays bell-shaped dose-response relationships (Crimini *et al.*, 2024; Fabian *et al.*, 2021). For 4-1BB agonists, a bell-shaped dose-response curve has been consistently observed in both pre-clinical and early clinical studies. At moderate doses, transient proliferative bursts marked by increased Ki-67 expression and clonal expansion are evident; however, supratherapeutic doses have been associated with hepatotoxicity, indicative of excessive systemic cytokine release and peripheral immune overactivation (Crimini *et al.*, 2024). This hepatotoxicity has prompted the design of lower-agonism constructs and conditional activation strategies, which are engineered to remain dormant in systemic circulation and become activated only within the tumour milieu. Such conditional formats rely on advanced Fc engineering

and precise control over antibody valency to ensure that target-specific cross-linking is achieved without triggering off-target toxicities. These findings underscore the importance of integrating pharmacodynamic readouts such as cytokine profiles and T-cell receptor clonality assessments into early phase studies to precisely titrate the dose for maximum immunostimulatory benefit with minimal toxicity.

Beyond monoclonal antibodies that directly target T-cell checkpoints or costimulatory receptors, a range of additional immunomodulatory strategies has been pursued to remodel the tumour microenvironment. Cytokine-based therapies (interleukins and interferons predominantly), exemplified by high-dose IL2, historically approved for melanoma and renal cell carcinoma, have demonstrated profound capacity to stimulate NK cells and CD8+ T-cells; however, their clinical use has been severely limited by systemic toxicities, most notably capillary leak syndrome (Butterfield and Najjar, 2024). Innate immune sensors, particularly STING and TLR agonists, are also being investigated primarily via intratumoural administration in order to bypass systemic instability and off-target effects. Pre-clinical models have consistently demonstrated that STING agonists induce robust type I interferon production, leading to enhanced dendritic cell activation and subsequent priming of CD8+ T-cells. Nevertheless, clinical trial outcomes with these agents have been mixed, with some studies reporting only modest improvements in progression-free survival. Limitations in clinical translation have been largely ascribed to suboptimal target engagement, rapid drug clearance, and the compartmentalised nature of innate immune activation that may not translate into systemic antitumour responses (Butterfield and Najjar, 2024). Progress likely depends on improved delivery and biomarker-driven selection. All these approaches have been immensely improved in recent years. While each of them has more than one FDA-approved drug for cancer treatment, combination therapies and new methods are also still being investigated widely.

Another T-cell targeted therapy includes Bacillus Calmette-Guerin, which is a live attenuated strain of Mycobacterium bovis and also causes cytokine release. While it has been promising in preclinical research like some of the other modulators, it failed to fulfil expectations in clinical trials at least as a monotherapy (Berraondo *et al.*, 2019). Still, the other two types of immunomodulators are called small-molecule-based and particle-based immunomodulators. A distinctive speciality between them is the ability

to employ each immunomodulator mentioned above in a molecular form or with the addition of a nanoparticle (Chauhan *et al.*, 2021; Grippin *et al.*, 2021).

Proteolysis targeting chimeras (PROTACs) and related targeted protein degradation technologies fit best under immune system modulators. These small molecules recruit E3 ligases to degrade selected signalling proteins in immune cells or in the TME, with the goal of enhancing antitumour immunity. Examples under exploration include degraders directed at PDL1, HPK1, and STAT3. Extracellular degradation concepts such as LYTAC extend this logic to membrane proteins. These programmes remain investigational and are typically considered as combination partners with ICB rather than as a separate established class (Cotton *et al.*, 2021; Zhou *et al.*, 2021).

Collectively, the six-category framework provides a practical structure for the field. ICIs have delivered broad survival benefits across many solid tumours. ACT has transformed outcomes in several haematological cancers and is advancing in solid tumours. Vaccines, OVs, and CD3 bispecific antibodies contribute complementary mechanisms that can possibly convert immunologically cold tumours toward inflamed states and enhance T-cell engagement. Cytokines and small molecule modulators, including targeted protein degradation, offer additional levers to reprogram the TME. Ongoing efforts increasingly focus on rational combinations, biomarker-guided selection, and delivery strategies that maximise efficacy while limiting toxicity.

1.7 PD1 and PDL1/2 signalling pathway

PD1 is a monomeric type 1 surface glycoprotein that consists of a single V-set Ig SF domain linked to a transmembrane domain and a cytoplasmic domain with tyrosine-based signalling motifs. PD1 is frequently attributed to the CTLA4/CD28 subgroup mainly because of shared functional features; however, PD1 also exhibits substantial homology with antigen receptors and CD8 subgroups. Thus, between these two subgroups, it represents an intermediate, indicating that a PD1-like protein might be the precursor of Ig SF family signalling receptors. The co-inhibitory function of PD1 on T-cells was first proved in knock-out mice in which the PDCD1 locus, which contains the murine PD1 gene, was deleted (Cheng *et al.*, 2013) (Ishida *et al.*, 1992).

The activation of CD4+ T-cells, CD8+ T-cells, natural killer T-cells (NKT), B cells, and monocytes leads to the induced expression of PD1 antigen. Besides the activated T-cells, it is also expressed in activated monocytes and dendritic cells. The inhibitory function of it, which depends on the binding to one of its ligands, PDL1 (CD274, B7-H1) or PDL2 (CD273, B7-DC), starts upon binding to dampen T-cell activation and the immune response. The expression of PDL1 was observed on T and B cells, DCs, macrophages, MSCs, bone marrow-derived mast cells, and non-homoeopathic cells, while PDL2 is only expressed on DCs, macrophages, and mast cells (Agata *et al.*, 1996; Keir *et al.*, 2008; Latchman *et al.*, 2001; Tseng *et al.*, 2001).

Although having a stronger binding affinity to PD1, PDL2 exerts a minimal impact on T-cell regulation, compared to PDL1. However, in this context, it is important to note that receptors that bind weakly can also trigger inhibitory signalling (Cheng *et al.*, 2013). Latchman and her colleagues studied PDL1 and PDL2 mRNA distribution in several healthy tissues. In accordance with their study, mRNA expression profiles were generally similar, with high expression in the placenta and low expression in the spleen, lymph nodes, and thymus. Both ligands were expressed in the heart, but PDL1 expression was slightly higher. Only PDL2-expressed tissues were the pancreas, lung, and liver, and only PDL1-expressed tissue was the foetal liver (Latchman *et al.*, 2001).

Silencing the activated effector T-cells is the fundamental function of the PD1/PDL1 signalling pathway, thereby preventing overshooting of immune attack. One other primary function of it is autoimmunity by giving rise to the development of Tregs and by inhibiting self-reactive T-cells (Francisco *et al.*, 2010). MHC presented by APCs displays a specific antigen to the reciprocal TCR on naive T-cells as the beginning of T-cell activation, but this binding is followed by a secondary signal, as mentioned. The co-stimulatory signal is imperative for a fully activated T-cell. Upon activation, induced expression of PD1 starts to hinder MHC-TCR-mediated activation if the co-inhibitory pathway is exerted via PD1/PDL1 or PD1/PDL2 binding (Sharma *et al.*, 2017).

Cytokines are critical regulators of both PD1 and PDL1 expression together with their function, establishing a bidirectional circuit that modulates immune responses in cancer, fibrosis, and transplant tolerance. On one hand, cytokines such as IL-12, IFNγ, TGFβ, and IL-18 act as upstream signals that induce PD1/PDL1 expression on tumour cells, immune cells, and stromal cells. For example, IL-12 stimulates the production of

IFNγ, which in turn upregulates PDL1 expression on tumour cells, linking innate and adaptive immune activation to subsequent checkpoint induction (Ahmadnia *et al.*, 2024; Amarnath *et al.*, 2011; Zhang *et al.*, 2023). However, IFN expression is also essential for immune-inflamed TME, so it is necessary to know its expression threshold, turning inflammation from acute to chronic. Similarly, TGFβ, well known for its role in driving epithelial-mesenchymal transition (EMT) and fibrosis, activates signalling cascades such as PI3K/AKT and MEK/ERK, resulting in PDL1 overexpression and promotion of immunosuppressive and fibrotic environments (Zhang *et al.*, 2023).

Conversely, engagement of PD1 by its ligands, predominantly PDL1, delivers inhibitory signals that suppress cytokine production. When PD1 is triggered on T-cells, phosphatases such as SHP1/2 are recruited, leading to dephosphorylation of key signalling molecules like STAT1. This dampens the transcription of critical effector cytokines, including IFNγ, IL-2, and TNF-α. This inhibitory signalling underlies the functional exhaustion observed in T-cells infiltrating tumours, contributing to a state of reduced cytokine output and impaired effector functions. Moreover, PD1-PDL1 engagement has been implicated in the phenotypic conversion of Th1 cells into Tregs, which are known to lower levels of inflammatory cytokines while upregulating FOXP3, thus further reinforcing an immunosuppressive milieu (Amarnath *et al.*, 2011; Yang *et al.*, 2011).

This bidirectional interaction is further compounded by feedback loops in the tumour context. Cytokine induction (for example, IFNγ initiated by IL-12 signalling) enhances PDL1 expression on cancer cells, which subsequently feeds back to suppress additional cytokine production by effector T-cells, thereby limiting antitumour immunity (Pasero and Olive, 2013). In fibrotic processes and during EMT, TGFβ not only acts as a primary inducer of PDL1 expression but is also upregulated as a downstream effector of PDL1 signalling; such reciprocal regulation creates a positive feedback loop that intensifies both fibrogenesis and immune suppression (Zhang *et al.*, 2023). In addition, studies in melanoma have demonstrated that the restoration of immune cell functionality via exogenous cytokine administration combined with PD1/PDL1 blockade can revitalize the dysfunctional crosstalk between plasmacytoid dendritic cells and γδ T-cells, underscoring the therapeutic relevance of modulating this interplay (Girard *et al.*, 2021).

Other cytokines, notably IL-18, further contribute to the complexity of this network by inducing PD1-dependent immunosuppressive signals (Pasero and Olive, 2013). In allogeneic transplant models, blockade of the PD1-PDL1 axis has been shown to augment cytokine production (including IFNγ, IL-4, and IL-6) and disrupt Treg maintenance, highlighting the dual regulatory role that cytokines play in both activating and responding to PD1/PDL1 signalling (Yang *et al.*, 2011).

PDL1, a key immune checkpoint protein, is expressed across a wide spectrum of human malignancies and in multiple cellular compartments, including tumour cell membranes, cytoplasm, stromal cells, and tumour-derived exosomes (Chen *et al.*, 2018b). Its expression pattern is heterogeneous both between and within cancer types, with significant implications for tumour immune evasion and responses to checkpoint blockade therapies.

In non-small cell lung cancer (NSCLC), PDL1 expression is notably high. Studies demonstrate that NSCLC tumour cells express elevated PDL1 levels when compared directly to other tumour types, and, importantly, PDL1 is also abundantly present in the tumour stroma and on tumour-derived exosomes (Kluger *et al.*, 2017). The stromal PDL1, primarily carried by exosomes, appears to contribute to resistance to immunotherapy by binding to and sequestering PDL1-targeting antibodies. Additionally, within lung cancers, NSCLC subtypes such as adenocarcinoma and squamous cell carcinoma tend to show higher PDL1 positivity compared to small cell lung cancer and pleomorphic variants, although the precise percentages vary with the assay and cutoff selected (Chen *et al.*, 2018b; Yu *et al.*, 2016a).

Renal cell carcinoma (RCC) displays an intermediate pattern of PDL1 expression. RCC tumour cells exhibit moderate levels of PDL1 that are generally lower than those observed in NSCLC but higher than in melanoma tumour cells (Kluger *et al.*, 2017). Moreover, in RCC, PDL1 can also be detected on infiltrating immune cells within the tumour microenvironment, further underscoring its role in modulating antitumour immunity (Yu *et al.*, 2016b).

Metastatic melanoma illustrates a distinctive pattern. While overall PDL1 expression on melanoma tumour cells is lower compared to NSCLC, approximately 45% of metastatic melanoma cases exhibit PDL1 positivity in at least 5% of tumour cells, with around 24% showing expression in ≥20% of tumour cells. Most notably, melanoma

frequently demonstrates higher PDL1 expression in non-tumour compartments, including stromal inflammatory cells such as macrophages and lymphocytes, which can be more predictive of treatment responses to PD1 inhibitors than PDL1 expression on tumour cells per se (Kluger *et al.*, 2017; Obeid *et al.*, 2016).

Breast cancer shows considerable variability in PDL1 expression across its subtypes. Basal and triple-negative breast cancers (TNBC) tend to express significantly higher levels of PDL1 at both the mRNA and protein levels compared to luminal subtypes (Soliman *et al.*, 2014). Basal breast cancer cell lines display not only elevated constitutive PDL1 expression but also a robust inducible response following interferon gamma exposure, suggesting an inherent aggressive phenotype coupled with immune evasion capabilities. In contrast, luminal (hormone receptor-positive) breast cancers generally exhibit lower PDL1 expression, aligning with their less aggressive behaviour and different immune microenvironment (Stovgaard (Sabatier *et al.*, 2015; Stovgaard *et al.*, 2019).

Beyond these primary cancer types, PDL1 is expressed in various other malignancies, including gastric, hepatocellular, esophageal, pancreatic, ovarian, bladder, head and neck, thyroid, and even certain hematologic cancers. In many of these cancers, high PDL1 expression is associated with adverse clinicopathological features such as increased tumour aggressiveness, invasion, and metastasis, thereby contributing to poor patient outcomes (Yu *et al.*, 2016b). However, nuances exist; for example, in Merkel cell carcinoma, PDL1 expression on tumour cells can be absent despite potential positivity in the microenvironment, and in some breast cancers, PDL1 expression correlates with better clinical outcomes (Gatalica *et al.*, 2014).

Although these studies all define and explore PD1/PDL1 expression levels in cancer types, each of them utilizes its own method (mostly immunohistochemistry and quantitative immunofluorescence techniques) and each of them inspects one or a maximum of three cancer types, leaving a gap in a comparative study on PD1/PDL1 expression in cancer types. Notwithstanding these methodological advances, the precision of PD1/PDL1 measurement remains critically undermined by several factors. A major source of imprecision is the inherent spatial heterogeneity of PDL1 expression within tumours. As expression levels can vary significantly between tumour centres, edges, or between primary and metastatic sites, small sample sizes (such as those

obtained from tissue microarrays or core needle biopsies) may not adequately capture this heterogeneity (Stovgaard *et al.*, 2019; Yu *et al.*, 2016b). This sampling bias contributes to discordance and variability in reported PDL1-positive rates. In addition, the lack of standardized scoring systems and variability in cut-off thresholds for positivity, ranging from as low as 1% to as high as 50% of cells staining positive, further compromises cross-study comparability and the reliability of PDL1 as a predictive biomarker (Kluger *et al.*, 2017).

At the molecular level, PD1 hinders TCR-mediated signalling by impairing the activity of the PI3K/Akt and the Ras/MEK/Erk pathway signalling cascades, which are both required together for the initiation of T-cell activation. One of the mechanisms of PD1 inhibition of the PI3K/Akt pathway targets PTEN phosphorylation and phosphatase activity regulated by CK2. PTEN C-terminus serine/threonine cluster S380/T382/T383 phosphorylation is operated by CK2. This cluster provides PTEN protein stability and decreases PTEN lipid phosphatase activity for the PIP3 substrate. For example, in the stimulation process led by TCR/CD3 and CD28, CK2 phosphorylates PTEN, thereby stabilizing it. Thus, its phosphatase activity is inhibited. On the contrary, PD1 recruits SHP2, a phosphatase, to the ITSM in the PD1 Tail and hampers phosphorylation of the Ser/Thr cluster in the C-terminus of PTEN, thereby inhibiting stabilization of PTEN. Therefore, PTEN phosphatase activity increases. In addition, PD1 also hampers the Ras/MEK/Erk signalling pathway. RasGRP1, one of the elements of PLC-γ1 downstream, is mediated by the Ca2+ and DAG, which together form the MEK/Erk MAP kinase pathway, the downstream of the Ras/MEK/Erk pathway. PD1 disrupts this pathway by inhibiting PLC-γ1. There are also other events that start with TCR ligation and are inhibited by PD1 ligation, such as activation of ZAP70 and PKCθ. Collectively, these event series strongly inhibit T-cell activation, proliferation, and survival by decreasing the activation of transcription factors such as activator protein 1 (AP-1), nuclear factor of activated T-cells (NFAT), and nuclear factor-κB (NF-κB) (Figure 1.3) (Bardhan *et al.*, 2016; Sharpe and Pauken, 2018).

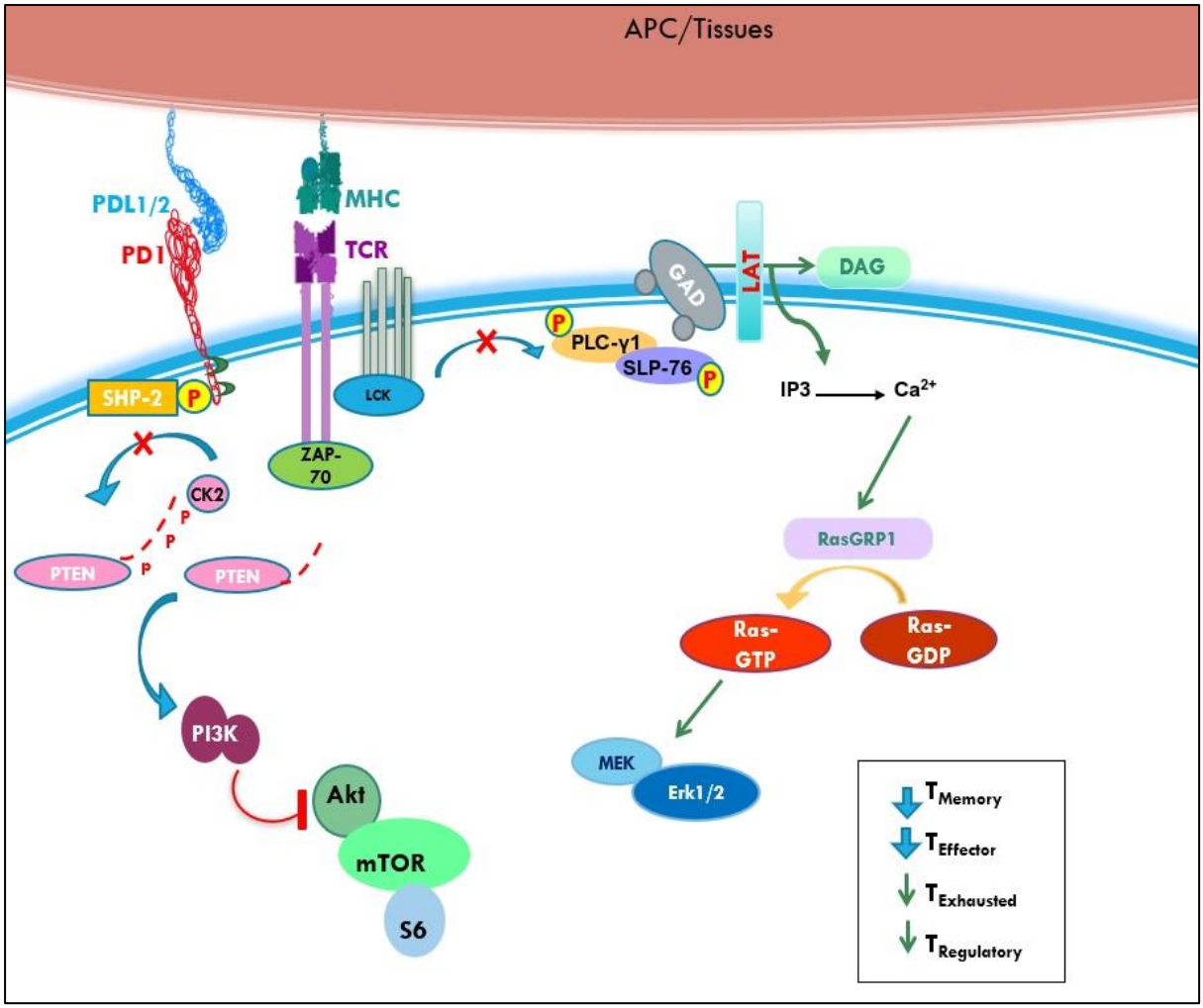

Figure 1.3 Intracellular inhibition mechanisms of PD1/PDL1 pathway in molecular level. This pathway inhibits mainly PI3K/Akt and the Ras/MEK/Erk pathway signalling cascades which are both crucial for T-cell activation and effector functions. Inhibition hinders memory and effector T-cell and causes T-cell exhaustion, increase in regulatory T-cells.

1.8 Treatments with monoclonal immune checkpoint inhibitors

In the last decade, immune checkpoint therapy came to the forefront of cancer therapies due to many plausible reasons. First of all, the success achieved with these therapies is remarkable, with prolonged overall survival, shrinkage, or even complete removal of tumours. Another reason is that ICB therapies can be applied to many diverse cancer types, regardless of the organ or tissue they stem from. Besides the positive response to the treatment and diversity of targeted tumour tissue, reduced side effects in comparison to other cancer therapies have gathered attention on this topic, and finally, it became one of the most widely prescribed cancer therapeutics. In

this context, some monoclonal antibodies target cancer cells and aim to bind tumour-associated antigens such as HER2, CD20, and VEGF, some others target directly immune checkpoint inhibitors. We can mention, for instance, the ones that target specifically T-cell immunomodulators such as PD1, PDL1, CTLA4, and IDO1. These are in respectively second, third, seventh, and twelfth places in the top 15 targets in the 2019's immune-oncology drug pipeline, showing the growth of attraction to T-cell immunomodulators (Xin Yu *et al.*, 2019a). On top of that, this growth is also expanding with active clinical trials accounting for 66% of all active immuno-oncology agents. As of 12 April 2026, a ClinicalTrials.gov search identified 3826 active interventional studies evaluating anti-PD1/PDL1 therapies in cancer, using the major approved agents as search terms.

CTLA4 blockade acts during the early priming phase by preventing CTLA4 from engaging CD80/CD86 on antigen-presenting cells. This permits the restoration of CD28-mediated co-stimulation and enhances the expansion of naive T-cells while mitigating regulatory T-cell suppression (Buchbinder and Desai, 2016; Rowshanravan *et al.*, 2018). In contrast, PD1 and PDL1 inhibitors function predominantly within peripheral tissues and the tumour microenvironment by blocking PD1 engagement, thereby reinvigorating exhausted effector T-cells and restoring essential intracellular pathways for cytokine production and cytolytic activity. The clinical efficacy of FDA-approved PD1/PDL1 monotherapies is conditioned by factors such as antigen load, T-cell abundance, and myeloid tone, which collectively determine the magnitude of T-cell receptor engagement and downstream responses (Beavis *et al.*, 2018; Dyck and Mills, 2017; Grywalska *et al.*, 2018). The monoclonal format, combined with advanced Fc engineering, contributes to improved specificity, longer half-life, and optimised tissue distribution, which are critical for achieving effective and durable immunomodulation (Grywalska *et al.*, 2018). Secondary inhibitory axes, including LAG3 and TIGIT, have been identified as additional targets that may augment the efficacy of PD1 and PDL1 blockade when applied in combination strategies. These mechanistic insights underpin current therapeutic strategies and provide the rationale for the subsequent list of approved PD1 and PDL1 antibodies, which illustrate the clinical translation of these engineering enhancements (Grywalska *et al.*, 2018).

PD1/PDL1 monoclonal antibodies are protein-based therapeutic molecules that belong to the immunoglobulin (Ig) family; in other words, they are true antibodies with

defined heavy and light chain structures arranged in a Y-shaped conformation (Bu *et al.*, 2022). Their antigen-binding fragments (Fabs) contain variable domains that provide high specificity and affinity for targeted epitopes on the PD1 receptor or its ligand PDL1, while their constant (Fc) regions can be engineered to reduce or eliminate undesired effector functions such as antibody-dependent cellular cytotoxicity (ADCC) (Li and Rudensky, 2016; Ohaegbulam *et al.*, 2015).

Physically, these antibodies are complex protein structures typically classified as IgG isotypes, for example, IgG1, IgG2a, IgG2b, or IgG4, depending on their intended application and functional engineering. They exhibit a modular architecture where the variable region is combined with an Fc domain that can be modified to optimize half-life, reduce immunogenicity, or modulate interactions with Fc receptors (Lee *et al.*, 2017; Li and Rudensky, 2016). These modifications are critical for ensuring that the antibodies act solely via checkpoint blockade rather than depleting target-expressing cells through immune effector mechanisms.

The creation of PD1/PDL1 monoclonal antibodies involves standard immunological and molecular biology methods. In preclinical settings, the process usually begins by immunizing an appropriate host animal (typically mice or rats) with the target antigen, which can be the purified PD1 or PDL1 protein, or sometimes cells expressing these proteins (Bu *et al.*, 2022; Tan *et al.*, 2016). This immunization stimulates the animal's B cells to produce a repertoire of antibodies against the antigen. Following immunization, antibody-producing B cells are isolated and fused with immortal myeloma cells using hybridoma technology, resulting in hybridoma cell lines that continuously produce a single, uniform antibody clone (Burova *et al.*, 2017; Ohaegbulam *et al.*, 2015).

For clinical applications, these initial antibody candidates are often further engineered through recombinant DNA techniques. The variable region genes encoding the antigen-specific antibodies are cloned and, if necessary, "humanized" by grafting them onto human IgG frameworks to reduce immunogenicity when administered to patients. This humanization process is critical in developing therapeutics such as nivolumab and pembrolizumab, which are designed for use in human cancer immunotherapy (Li and Rudensky, 2016; Ohaegbulam *et al.*, 2015). Furthermore, these engineered antibodies are expressed in mammalian cell systems, such as Chinese hamster ovary

(CHO) cells, to ensure proper protein folding, post-translational modifications, and consistent production quality (Wang *et al.*, 2020).

Briefly, PD1/PDL1 monoclonal antibodies are sophisticated antibodies produced via immunization, hybridoma generation, and recombinant engineering techniques. Their production involves isolating cross-species B-cell clones, fusing them with myeloma cells to create immortal hybridomas, and further engineering them as needed to optimize therapeutic efficacy and safety in clinical applications.

1.8.1 Approved antibodies and core pharmacology define class and agent differences

The first approved monoclonal ICB therapy, anti-CTLA4 (Ipilimumab), achieved substantial success in clinical trials. Therefore, Ipilimumab (Yervoy®) acquired FDA approval in 2011 for the first- and second-line treatment of malignant melanoma patients (Cameron *et al.*, 2011). Then Pembrolizumab (Keytruda®) was approved by the FDA as the first anti-PD1 monoclonal antibody for unresectable or metastatic melanoma patients in 2014 (Poole, 2014). Treatments targeting the PD1/PDL1 axis continued from 2014 to 2025 with 6 new antibodies targeting PD1 with active ingredient names: Nivolumab (2015), Cemiplimab (2018), Dostarlimab (2021), Toripalimab (2023), Retifanlimab (2023), and Tislelizumab (2024). FDA-approved agents targeting PDL1s to date are Atezolizumab (2016), Durvalumab (2017), and Avelumab (2017) for the treatment of a variety of cancer types (14 in total). This wide range of cancers includes renal cell and non-small cell lung carcinoma (NSCLC), head and neck cancer, melanoma, classical Hodgkin lymphoma, and small-cell lung carcinoma (SCLC), although most of these drugs are recommended to be prescribed to patients with any dMMR solid tumours and tumours with microsatellite instability (Table 1.1). In addition to these widely studied and FDA-approved ones , the European Union, Japan, and China have also approved 4 other anti- PD1/PDL1 monoclonal antibodies in the meantime: Toripalimab (anti-PD1), Camrelizumab (anti-PD1), Sintilimab (Tyvyt®, anti-PD1), and Tislelizumab (anti-PD1) for different cancer types (Marin-Acevedo *et al.*, 2021; Thoreau and Chudasama, 2022).

Table 1.4 FDA-Approved Anti-PD1/PDL1 Monoclonal Antibodies: Cancer Types, Approval Years, Key Reference Studies, and Ongoing Clinical Trials

	Drug Name	Active Ingredient	Cancer type	Studies	Clinical trials
anti-PD1	KEYTRUDA (2014)	PEMBROLIZUMAB	Melanoma, Merkel cell carcinoma Classical Hodgkin lymphoma Primary mediastinal large B-cell lymphoma Hepatocellular carcinoma Gastric or gastroesophageal junction AC Non-small cell lung cancer	PD-1 inhibition and treatment of advanced melanoma-role of pembrolizumab (Jazirehi *et al.*, 2016), Pembrolizumab: First Global Approval (Poole, 2014), Structural basis of checkpoint blockade by monoclonal antibodies in cancer immunotherapy (Lee *et al.*, 2016),	Total 474 active trials NCT06307093 NCT04098068 NCT03131908
	OPDIVO (2015)	NIVOLUMAB	Melanoma Metastatic squamous non-small cell lung cancer Small cell lung cancer	Nivolumab: Targeting PD-1 to Bolster Antitumor Immunity (Brahmer *et al.*, 2015), Model-Based Population Pharmacokinetic Analysis of Nivolumab in Patients With Solid Tumours (Bajaj *et al.*, 2017), Nivolumab in the treatment of malignant melanoma: review of the literature (Mashima *et al.*, 2015).	Total 412 active trials NCT03656718 NCT04704154 NCT02923934
	LIBTAYO (2018)	CEMIPLIMAB – RWLC	Cutaneous squamous cell carcinoma Basal cell carcinoma Non-small cell lung cancer	Real-world multicentre observational study of effectiveness and toxicity in patients with advanced cutaneous squamous cell carcinoma treated with cemiplimab (Faoro *et al.*, 2024), PD-1 Blockade with Cemiplimab in Advanced Cutaneous Squamous-Cell Carcinoma (Migden *et al.*, 2018)	Total 22 active trials NCT04460456 NCT04646005 NCT05064085
	JEMPERLI (2021)	DOSTARLIMAB – GXLY	Endometrial cancer Mismatch repair deficient (dMMR) solid tumours	Gynaecological Cancers Caused by Deficient Mismatch Repair and Microsatellite Instability (Deshpande *et al.*, 2020), PD-1 Blockade in Mismatch Repair-Deficient, Locally Advanced Rectal Cancer(Cercek *et al.*, 2022)	Total 14 active trials NCT03843359 NCT03981796 NCT04313504
	LOQTORZI (2023)	TORIPALIMAB – TPZI	Advanced nasopharyngeal carcinoma	Toripalimab: the First Domestic Anti-Tumor PD-1 Antibody in China (Zhang *et al.*, 2022), Toripalimab: First Global Approval(Keam, 2019).	Total 27 active trials NCT04322006 NCT04301557, NCT05830539
	ZYNYZ (2023)	RETIFANLIMAB – DLWR	Merkel cell carcinoma	Margetuximab with retifanlimab as first-line therapy in HER2+/PD-L1+ unresectable or metastatic gastroesophageal adenocarcinoma (Catenacci *et al.*, 2022).	Total 11 active trials NCT03059823 NCT03522142 NCT04989387
	TEVIMBRA (2024)	TISLELIZUMAB – JSGR	Esophageal squamous cell carcinoma	Tislelizumab Versus Chemotherapy as Second-Line Treatment for Advanced or Metastatic Esophageal Squamous Cell Carcinoma (Shen *et al.*, 2022).	Total 40 active trials NCT05036798 NCT05014828, NCT05116085
anti-PDL1	**Drug Name**	**Active Ingredient**	**Cancer type**	**Studies**	**Clinical trials**
	TECENTRIQ (2016)	ATEZOLIZUMAB	Urothelial carcinoma	Atezolizumab: First Global Approval (Markham, 2016), Clinical Pharmacokinetics and Pharmacodynamics of Atezolizumab in Metastatic Urothelial Carcinoma (Stroh *et al.*, 2017), Atezolizumab for First-Line Treatment of PD-L1–Selected Patients with NSCLC (Herbst *et al.*, 2020).	Total 50 active trials NCT02926196 NCT03617666 NCT03815643
	IMFINZI (2017)	DURVALUMAB	Non-small cell lung cancer Small cell lung cancer Biliary tract cancer Unresectable hepatocellular carcinoma	Durvalumab: First Global Approval (Syed, 2017), Three-Year Overall Survival with Durvalumab after Chem-radiotherapy in Stage III NSCLC (Gray *et al.*, 2020), Molecular mechanism of PD-1/PD-L1 blockade via anti-PD-L1 antibodies atezolizumab and durvalumab(Lee *et al.*, 2017)	Total 176 active trials NCT03737968 NCT02087423 NCT04985851
	BAVENCIO (2017)	AVELUMAB	Merkel cell carcinoma Urothelial carcinoma Renal cell carcinoma	Antibody-Dependent Cellular Cytotoxicity Activity of a Novel Anti–PD-L1 Antibody Avelumab on Human Tumor Cells (Boyerinas *et al.*, 2015), Product review: avelumab, an anti-PD-L1 antibody (Collins and Gulley, 2019), Avelumab: First Global Approval (Kim, 2017).	Total 59 active trials NCT02926196 NCT03617666 NCT03815643

PD1 antibodies are typically formulated as IgG4 isotypes that possess intrinsically low Fc receptor engagement to reduce the risk of effector cell-mediated depletion of activated T-cells (Ma *et al.*, 2016). In contrast, some PDL1 antibodies have been engineered to balance checkpoint inhibition with potential antibody-dependent cellular cytotoxicity against tumour cells (Ma *et al.*, 2016). Isotype and Fc engineering are critical given their influence on serum half-life, tissue biodistribution, and overall clinical efficacy; modifications to the Fc region, such as silencing or enhancing FcRn binding, have been implemented to optimise dosing schedules and reduce off-target effects (Gogesch *et al.*, 2021; Nguyen and Maynard, 2021). Dosing approaches vary between agents but often use fixed-dose regimens administered intravenously at intervals of two to three weeks, achieving half-lives in the order of 2-3 weeks that facilitate predictable pharmacokinetics (Goleva *et al.*, 2021).

1.8.2 Clinical benefit is tumour-type specific and shaped by immune contexture

PD1/PDL1 monotherapies have demonstrated durable responses in tumour types with a permissive immune contexture, such as melanoma, non-small cell lung cancer, and tumours characterized by high microsatellite instability or dMMR. These cancers typically exhibit increased neoantigen burden, elevated IFNγ signatures, and enriched tumour-infiltrating T-cells, conditions that favour robust antitumour immunity upon checkpoint blockade (Hossain *et al.*, 2021; Ma *et al.*, 2016). In tumours where antigen load is high, and regulatory mechanisms are less pronounced, monotherapy often results in sustained objective responses with prolonged progression-free and overall survival. Conversely, malignancies with a highly immunosuppressive myeloid stroma, T-cell exclusion, or low baseline T-cell abundance may derive more benefit from combinatorial strategies (Baksh and Weber, 2015; Dyck and Mills, 2017). Biomarker assessments such as PDL1 expression by immunohistochemistry, although variable and subject to heterogeneity, are used to enrich patient selection; however, the correlation between PDL1 levels and clinical outcome is not absolute (Dyck and Mills, 2017; Goleva *et al.*, 2021). The interplay between tumour neoantigen load, IFNγ-driven immune activation, and the suppressive influence of myeloid and regulatory cell populations explains the heterogeneity observed in clinical efficacy across tumour

types, which points outs the value of precise mapping of TME. The alignment of these immunological features underpins the rationale for adopting biomarker-driven treatment paradigms and for combining PD1/PDL1 blockade with other agents in tumours that are inherently less responsive (Baksh and Weber, 2015; Dyck and Mills, 2017).

1.8.3 Biomarkers enrich responders but remain imperfect gatekeepers

Patient selection for PD1/PDL1 monotherapy is frequently informed by PDL1 immunohistochemistry using tumour percentage score (TPS) or combined positive score (CPS); nevertheless, quantitative assessment is marred by inter-assay variability, heterogeneous expression, and inconsistent thresholds (Ma *et al.*, 2016) (Baksh and Weber, 2015). In certain cancers, molecular biomarkers such as microsatellite instability and deficient mismatch repair status, as well as tumour mutational burden, provide valuable guidance for the use of immunotherapy, yet their predictive value can be limited by technical and biological factors (Dyck and Mills, 2017; Granier *et al.*, 2017). The density of CD8+ T-cells and expression of immune-related gene signatures, including those reflecting IFNγ signalling, have been shown to correlate with response and are increasingly integrated into composite biomarker panels (Ma *et al.*, 2016). Moreover, genetic alterations that impact antigen presentation, such as loss of HLA or mutations in JAK1/2, may undermine the efficacy of PD1/PDL1 blockade by obviating effective T-cell recognition of tumour antigens (Dyck and Mills, 2017; Hossain *et al.*, 2021). Pre-analytic variability, spatial heterogeneity within the tumour, and dynamic changes during treatment further complicate biomarker interpretation (Goleva *et al.*, 2021). A composite strategy that integrates immunohistochemical, genetic, and transcriptional markers has emerged as the preferred approach for improving patient stratification and predicting therapeutic response (Dyck and Mills, 2017; Granier *et al.*, 2017).

1.8.4 Resistance emerges through antigen loss, interferon pathway defects, and myeloid rewiring

Resistance to PD1/PDL1 monotherapy may manifest as primary non-response or as acquired resistance following an initial period of clinical benefit. Primary resistance frequently reflects low intrinsic immunogenicity, limited tumour neoantigen load, and an immunosuppressive microenvironment that precludes effective T-cell priming (Baksh and Weber, 2015; Hossain *et al.*, 2021). Acquired resistance has been linked to genetic alterations that impair antigen presentation, such as defects in beta-2 microglobulin and loss of HLA expression, as well as mutations in interferon pathway elements, including JAK1 and JAK2, that blunt downstream signalling and reduce T-cell responsiveness. Furthermore, alterations in the tumour microenvironment, such as the establishment of T-cell exclusion architectures and the rewiring of myeloid cell phenotypes, contribute to a suppressive milieu by increasing the activity of adenosine-producing enzymes, indoleamine 2,3-dioxygenase (IDO) and CSF1 receptor-dependent pathways (Hossain *et al.*, 2021; Willsmore *et al.*, 2021; Yin *et al.*, 2021). Rational combination strategies have been proposed to overcome these resistance mechanisms. Oncolytic viruses and radiotherapy can provide antigenic stimulation and enhance T-cell priming, while therapies targeting VEGF, CSF1R, or adenosine signalling may reprogramme the myeloid compartment to facilitate T-cell infiltration (Popovic *et al.*, 2018). The convergence of genetic, antigenic, and microenvironmental alterations underlines the complexity of resistance and emphasises the need for robust, multi-modality approaches to restore effective antitumour immunity (Willsmore *et al.*, 2021).

1.8.5 Toxicity is mechanism-linked and manageable with protocolised care

Immune-related adverse events associated with PD1/PDL1 monotherapies typically involve endocrine, hepatic, and pulmonary systems. Thyroiditis, mild hepatitis, and pneumonitis are among the most frequently observed toxicities, with onset generally later than the acute colitis or dermatological reactions seen with CTLA4-containing regimens (Chae *et al.*, 2018). PD1/PDL1 inhibitors tend to exhibit a more favourable safety profile due to their selective targeting of exhausted T-cells in peripheral tissues, thereby limiting the extent of systemic immune activation (Buchbinder and Hodi, 2015).

Established clinical guidelines advocate early recognition and grading of toxicities, with prompt initiation of corticosteroids when moderate to severe adverse events are identified. Re-challenge with immunotherapy after resolution of toxicity is guided by careful clinical assessment and may be supported by dose adjustments or alternative schedules; management protocols emphasise symptom alleviation, patient monitoring, and multidisciplinary collaboration (Buchbinder and Hodi, 2015; Goleva *et al.*, 2021). The mechanistic basis for toxicity differences is linked to the divergent roles of CTLA4 versus PD1 in T-cell regulation and the ancillary effects imparted by Fc receptor interactions; CTLA4 blockade, for example, may induce broader immune activation and depleting effects on regulatory T-cells, whereas PD1/PDL1 inhibitors tend to preserve a more circumscribed activity profile (Hong and Maleki Vareki, 2022). Optimised dosing strategies and Fc domain engineering represent key levers for balancing therapeutic efficacy against adverse events and enhancing overall risk-benefit outcomes (Goleva *et al.*, 2021).

1.8.6 Combination strategies expand benefit through complementary biology

The rationale for combining PD1 blockade with CTLA4 inhibition is grounded in the temporal complementarity between T-cell priming and effector restoration. CTLA4 blockade removes early inhibitory signals that limit CD28-mediated co-stimulation and broad T-cell activation, while PD1/PDL1 inhibitors reactivate exhausted T-cells within the TME (Baksh and Weber, 2015). This dual approach results in enhanced tumour antigen recognition and effector function, translating into improved antitumour responses in certain malignancies. In settings where chemotherapy or anti-VEGF agents are added, the increased antigen release and vascular normalisation further promote T-cell infiltration and function, supporting synergy with PD1/PDL1 blockade (Granier *et al.*, 2017). Emerging combinations involving PD1 blockade with LAG3 or TIGIT inhibitors address secondary inhibitory pathways that often co-exist with PD1 expression on exhausted lymphocytes (Kabut *et al.*, 2025). Although combinations may elevate the risk of immune-mediated toxicity, protocolised management and careful patient selection have rendered these approaches clinically feasible. PD1/PDL1 monotherapy remains the foundational comparator given its proven

efficacy and manageable safety profile, establishing a benchmark for next-generation formats that seek to integrate multiple checkpoints into a single therapeutic construct. The interplay of complementary immune mechanisms underscores the potential of carefully engineered combination regimens to expand clinical benefit across a broader array of tumour types (Granier *et al.*, 2017) (Baksh and Weber, 2015; Popovic *et al.*, 2018).

1.8.7 Future directions focus on next-generation targets and delivery

Advances in antibody engineering offer promising avenues to enhance the selectivity and safety of immune checkpoint inhibitors. Next-generation strategies are increasingly focusing on additional inhibitory receptors such as TIM3 and VISTA, which may extend the benefits observed with PD1/PDL1 blockade by targeting residual pathways of T-cell exhaustion (Popovic *et al.*, 2018). Fc-tuned and conditionally active antibodies, designed with modified Fc regions to mitigate off-target effects and optimise tissue localisation, further refine therapeutic specificity (Nguyen and Maynard, 2021). Intratumoural delivery of antibody constructs and bispecific formats that retain a PD1/PDL1 backbone while engaging a complementary immune effector, for example, cytokine fusion that boosts local T-cell activation, has also advanced in preclinical development (Granier *et al.*, 2017). These innovations seek to directly counteract resistance mechanisms such as antigen loss and myeloid reprogramming by focussing immune activation within the tumour milieu. Emerging modalities, including mesenchymal stem cell-delivered soluble PD1 (sPD1), offer conceptual frameworks for remodelling the TME to favour sustained antitumour immunity while minimising systemic toxicity (Popovic *et al.*, 2018). Continued exploration of these next-generation targets and delivery systems is expected to complement existing therapies, ultimately leading to more durable clinical responses and improved patient outcomes (Galli *et al.*, 2020).

Clinical benefit from PD1/PDL1 blockade is uneven and maps closely to the TME. Response depends on antigen load, T-cell presence, interferon signalling, and myeloid tone. Many solid tumours remain poorly responsive because dense stroma limits penetration, T-cells are excluded, or suppressive myeloid programmes dominate. Robust profiling of the TME, including precise T-cell markers, T-cell density and type

proportion, IFNγ-linked transcription, antigen presentation competence, and myeloid signatures, is therefore central to selecting patients and designing rational combinations.

Current antibodies maintain prolonged systemic exposure but can show restricted intratumoural coverage in fibrotic or poorly vascularised lesions. Biomarkers enrich but are imperfect, and resistance arises through antigen loss, defects in interferon pathways and myeloid rewiring. These constraints are as much about delivery, and distribution as they are about target biology.

High affinity sPD1 offers one route to stronger PDL1 engagement with potentially better tissue access. Using yeast surface display and surface plasmon resonance, Maute et al. identified a $PD1^{HAC}$ variant with roughly 35,000-fold higher affinity than $PD1^{WT}$ and a compact format compatible with tissue penetration (Maute *et al.*, 2015). Local availability of such a ligand living inside tumours could more effectively out-compete endogenous PD1 for PDL1 and support T-cell function in situ.

Key gaps remain. Whether sustained local release of high affinity sPD1 can remodel an immunosuppressive TME without excessive systemic exposure is untested. MSCs come forefront at this point not only as carriers for sustained PD1 and overcoming infiltration into solid tumours, but also their flexibility to carry more than one therapeutic and ability to further modulate TME. Engineered MSCs to deliver a sPD1 variant have not been inspected before. $sPD1^{HAC}$ expressed by MSCs and PDL1 engagement is still unclear both in vitro and in vivo.

1.9 MSCs and utilizing them as vectors for cancer therapeutics

Types and Sources of MSCs Mesenchymal stromal cells (MSCs) represent a heterogeneous group of multipotent progenitors that can be isolated from several tissue sources, with bone marrow (BM-MSCs), adipose tissue (AT-MSCs), and umbilical cord (UC-MSCs) being the most extensively explored for therapeutic use. These cells are defined by their ability to adhere to plastic under standard culture conditions, express a panel of characteristic surface markers (CD73, CD90 and CD105), and lack expression of haemopoietic and endothelial markers such as CD45, CD34 and CD14 (Almeida-Porada *et al.*, 2020; Bieback *et al.*, 2019). This minimal

definition, although useful for initial characterisation, does not fully address the inherent heterogeneity within MSC populations arising from donor variability, tissue of origin and differences in isolation and culture conditions (Baer, 2014; Camilleri *et al.*, 2016). Notably, BM-MSCs, historically the first to be described and most widely applied clinically, are collected via invasive procedures and represent only a rare population, whereas AT-MSCs provide a more abundant and accessible alternative with comparable multipotency (Baer, 2014; Mastrolia *et al.*, 2019). In addition, UC-MSCs derived from birth-associated tissues have emerged as a promising source given their rapid expansion capacity, primitive phenotype and reduced exposure to somatic mutations relative to adult MSCs (Bieback *et al.*, 2019; Mebarki *et al.*, 2021). Careful manufacturing strategies, including xeno-free culture systems and human platelet lysate supplementation, are employed to ensure reproducible expansion and preservation of cell functionality under Good Manufacturing Practice (GMP) conditions (Bieback *et al.*, 2019; Mastrolia *et al.*, 2019; Phinney and Galipeau, 2019). These considerations are central as they allow a consistent definition of MSC products that form the basis for subsequent therapeutic applications and comparative evaluations across pre-clinical and clinical studies.

MSCs are inherently equipped with the ability to home to sites of tissue injury and inflammation, a property that is exploited by solid tumours that generate chemokine gradients reminiscent of chronic, non-healing wounds (Dvorak, 2015; Kidd *et al.*, 2009). Recruitment of MSCs into the TME is mediated by factors such as VEGF, FGF, PDGF, interleukins and chemokines like CCL5 and IL-8, which act in concert to facilitate adhesion, migration and extravasation (Gil-Chinchilla *et al.*, 2024; Kangari *et al.*, 2024). Once localised within the TME, MSCs engage in complex crosstalk with tumour cells, immune cells and stromal constituents via direct cell contacts and a myriad of secreted cytokines, growth factors and extracellular vesicles. Although these interactions can lead to tumour suppression through the modulation of immunostimulatory pathways, they may also involve pro-tumour processes such as enhanced angiogenesis, immune suppression and support for cancer stem cell niches (Ebrahimi *et al.*, 2023; Gil-Chinchilla *et al.*, 2024). This bidirectional effect is context-dependent and is influenced by the specific inflammatory milieu, the differentiation state of the MSCs, and the local concentration of soluble mediators (Ebrahimi *et al.*, 2023). The result is a dynamic and plastic MSC phenotype that may either contribute

to tumour progression or, when appropriately manipulated, support tumour regression This phenomenon underpins their potential as therapeutic delivery vehicles in cancer (Gil-Chinchilla *et al.*, 2024; Mahhengam *et al.*, 2022).

The innate tumour tropism of MSCs offers a decisive advantage over conventional systemic approaches by enabling selective migration to and retention within the TME (Ebrahimi *et al.*, 2023; Marofi *et al.*, 2017). Pre-clinical models have demonstrated that MSCs can selectively home to solid tumours in various tissues, including brain, colon, liver and lung, thereby permitting a sustained release of therapeutic agents directly at the target site while minimising systemic exposure (Kangari *et al.*, 2024; Moreno, 2021). This localised delivery can result in a superior therapeutic index, as evidenced by studies in which BM-MSCs loaded with oncolytic adenoviruses produced an 8.1-fold improvement in antitumour efficacy compared with naked viruses in hepatocellular carcinoma models (Moreno, 2021). Furthermore, the relative immune evasiveness of MSCs, owing to low expression levels of MHC class I and lack of co-stimulatory molecules, facilitates allogeneic use, thereby overcoming donor-specific limitations and enabling off-the-shelf applications (Ebrahimi *et al.*, 2023; Marofi *et al.*, 2017). The sustained persistence of MSCs within the TME also allows continuous modulation of local immune responses through the secretion of factors that influence myeloid and T-cell compartments, This capacity for prolonged, site-specific delivery is a fundamental benefit when considering the limitations of systemic drug administration, particularly in the context of immune checkpoint blockade where off-target effects and immune-related adverse events remain a concern (Ebrahimi *et al.*, 2023; Garza Treviño *et al.*, 2024).

Despite the promising advantages, the application of MSCs as therapeutic vectors is hampered by several challenges and risks that necessitate careful mitigation. The inherent heterogeneity in MSC populations as, a reflection of differences in tissue origin, donor variability and culture protocols, raises concerns regarding consistency and reproducibility across batches intended for clinical use (Baer, 2014; Mendicino *et al.*, 2014; Viswanathan *et al.*, 2014). In addition, the pro-tumorigenic potential of MSCs, as evidenced by their ability to secrete factors that enhance tumour proliferation, angiogenesis and metastasis, constitutes a major safety concern (Ma *et al.*, 2023; Mahhengam *et al.*, 2022). Biodistribution studies have revealed that following systemic infusion, a significant portion of MSCs becomes entrapped in off-

target organs such as the lungs, liver and spleen, thereby complicating the assessment of their precise in vivo behaviour and therapeutic concentration within the tumour (Kangari *et al.*, 2024). Immunogenicity, particularly in the context of repeated administrations, remains a consideration despite the immune-evasive profile of MSCs; concerns over potential thromboembolic events and genetic instability during ex vivo expansion further compound these issues (Garza Treviño *et al.*, 2024; Neri, 2019; Sharma *et al.*, 2014). Regulatory hurdles also persist with respect to cell-based medicinal products, where the lack of universally accepted potency assays and standardised manufacturing protocols complicates clinical translation and quality control (Phinney and Galipeau, 2019; Robb *et al.*, 2019) (Wilson *et al.*, 2019). Collectively, these challenges underscore the need for rigorous donor screening, controlled expansion protocols under physiologic conditions (such as hypoxia) and the development of robust release criteria to ensure consistent therapeutic performance and safety.

Given the limitations inherent in systemic checkpoint inhibitor therapies, particularly those targeting PD1 and PDL1, exploration of alternative delivery modalities is warranted. Systemically administered PD1/PDL1 antibodies, while effective in certain contexts, often exhibit off-target immune activation and associated toxicities that restrict their therapeutic index (Gil-Chinchilla *et al.*, 2024; Phinney and Galipeau, 2019). MSC-mediated delivery of sPD1 fused to a hinge and antigen-targeting module (sPD1$^{\mathbf{HAC}}$) offers a targeted approach that elevates the tumour-homing capabilities of MSCs to concentrate checkpoint inhibition specifically within the TME. Pre-clinical insights suggest that localised release of sPD1$^{\mathbf{HAC}}$ can achieve effective checkpoint blockade with reduced systemic exposure, thereby mitigating adverse immunological events and enhancing the antitumour immune response (Ebrahimi *et al.*, 2023; Gil-Chinchilla *et al.*, 2024). This strategy also capitalises on the sustained presence of MSCs within the TME, providing a continuous source of checkpoint modulators that can be dynamically regulated by the local inflammatory milieu. As a result, the use of MSCs to deposit sPD1$^{\mathbf{HAC}}$ locally may yield a superior therapeutic index compared with conventional systemic antibody administration, particularly in solid tumours characterised by an immunosuppressive microenvironment (Gil-Chinchilla *et al.*, 2024). This approach represents a rational convergence of cell therapy and immunomodulation that is amenable to further bioengineering and assay optimisation.

A growing body of preclinical studies supports the feasibility of employing MSCs as vectors for antitumour therapeutics. In several solid tumour models, MSCs loaded with therapeutic payloads, including oncolytic viruses and immune-modulating factors, have demonstrated effective tumour homing, sustained retention and significant antitumour efficacy (Niess *et al.*, 2011). For instance, BM-MSCs loaded with an oncolytic adenovirus encoding a WNT inhibiting decoy receptor achieved an 8.1-fold improvement in therapeutic efficacy in hepatocellular carcinoma models when compared with administration of the naked virus (Moreno, 2021). These findings are corroborated by biodistribution studies that reveal extensive tumour colonisation by MSCs, as assessed through in vivo bioluminescent imaging and other tracking modalities (Gil-Chinchilla *et al.*, 2024). Early clinical trials have further established the safety profile of MSC-based therapies, with indications of minimal immunogenicity and manageable adverse events when MSCs are administered systemically (Ebrahimi *et al.*, 2023). Although the therapeutic efficacy in humans remains to be fully elucidated in larger, controlled trials, the preclinical data coupled with emerging clinical experience suggest that MSC vectors can provide a stable and effective delivery system for checkpoint inhibitors and other therapeutic agents. Importantly, the pharmacokinetic profile of MSC-delivered payloads indicates a shift towards sustained, localised exposure that may circumvent the rapid clearance and off-target effects typically observed with conventional antibody therapies (Garza Treviño *et al.*, 2024). Recent meta-analyses and controlled studies in solid tumours emphasise that the MSC-based approach not only enhances local drug concentration but may also modulate the TME in a manner that potentiates immune-mediated tumour cell killing (Ebrahimi *et al.*, 2023). Although precise effect sizes and confidence intervals vary among studies, the convergence of evidence from multiple primary research reports underlines the potential for MSC vectors to improve the therapeutic index in cancer treatment.

The collective evidence indicates that MSCs, whether derived from bone marrow, adipose tissue or umbilical cord, represent a versatile and promising platform for the targeted delivery of cancer therapeutics. Their well-defined phenotypic criteria and established manufacturing practices ensure a degree of consistency that permits reproducible clinical application, while their innate homing ability and immunomodulatory properties enable them to deliver therapeutic agents such as

sPD1^{HAC} directly into the TME. This inherent tumour tropism serves to concentrate the therapeutic payload at the intended target, potentially overcoming the limitations of systemic antibody therapies that are frequently associated with widespread immune activation and resultant toxicities. At the same time, challenges regarding MSC heterogeneity, protumour risk, biodistribution and regulatory complexities must be rigorously addressed through improved donor selection, enhanced expansion protocols and tailored gene-modification strategies. Therefore, the integration of MSC-based delivery with the checkpoint modulation offers a compelling strategy to enhance the therapeutic index in solid tumours. The preclinical and early clinical evidence bespeaks the potential for such an approach to achieve effective, sustained antitumour activity with reduced systemic toxicity (Almeida-Porada *et al.*, 2020; Garza Treviño *et al.*, 2024; Moreno, 2021).

1.9 Aims and objectives

Building on the clinical impact of ICB therapies, particularly those targeting the PD1/PDL1 axis, this study seeks to develop an innovative MSC-based therapeutic approach using a potent, non-antibody sPD1 variant. Specifically, HAC-V, as described by Maute et al., is selected for this study, which serves as the basis for our sPD1 variant, termed sPD1^{HAC}. While Maute's work established high-affinity binding through surface plasmon resonance, our research focuses on a different context: genetically engineering MSCs to deliver sPD1^{HAC} to the TME with high binding efficacy. This strategy aims to overcome some persistent challenges of ICB therapies, including poor tumour penetration, inefficient therapeutic delivery, and low-affinity, short-duration binding interactions in biological systems. Through integrated bioinformatic analyses, in vitro functional assays, and in vivo evaluations, this study aims to investigate the biological performance of MSC-delivered sPD1^{HAC}, assess its therapeutic potential, and establish its feasibility as a next-generation cell-based immunotherapy. The central hypothesis is that MSC-mediated delivery of sPD1^{HAC} will provide effective PD1/PDL1 inhibition in relevant models, translating into improved antitumour activity when compared with standard recombinant PD1 or with antibody-mediated blockade in defined in vitro contexts, and will show evidence of efficacy in vivo with acceptable safety.

The objectives of this research are designed to comprehensively address key questions surrounding the therapeutic modulation of the PD1/PDL1 axis in cancer immunotherapy. Initially, a systematic comparative bioinformatic investigation of The Cancer Genome Atlas (TCGA) Pan-Cancer Atlas datasets will be performed to evaluate correlations between PD1/PDL1 expression and key T-cell activation and exhaustion markers across diverse cancer types. This analysis aims to determine whether distinct cancer types can be accurately categorised into immunologically "hot," "intermediate," and "cold" tumour phenotypes by T-cell markers, providing critical insights into their potential responsiveness to immunotherapy.

Subsequently, an in-depth analysis will quantify correlations between PDL1 expression and mRNA expression profiles of selected immune-related genes, including T-cell activation/exhaustion markers, inflammatory cytokines, and significant TME biomarkers in major TCGA datasets. Identifying distinct immune phenotypes across multiple cancer types will facilitate therapeutic stratification and inform prognosis related to treatments targeting the PD1/PDL1 pathway.

Furthermore, experimental investigations will characterise baseline and interferon-gamma (IFNγ)-induced PDL1 expression across a panel of commonly utilised cancer cell lines, alongside profiling PD1 surface expression. These analyses aim to characterise variability in PDL1 cell surface expression patterns across cancer cell lines, both at baseline and following IFNγ stimulation. While PDL1 is a widely used biomarker for predicting responsiveness to ICB therapies targeting PDL1, its inducibility and constitutive expression differ markedly among tumour models. By systematically quantifying these differences, this study seeks to highlight the heterogeneity in PDL1 regulation, challenge the prevailing assumption of universal IFNγ-driven induction, and identify representative in vitro model systems that most explicitly portray the binding efficacy of PD1 variants.

In parallel, robust expression and secretion of the sPD1^{HAC} will be achieved utilising multiple cell expression systems, including Chinese hamster ovary (CHO) cells, human embryonic kidney (HEK293T) cells, and human adipose tissue-derived MSCs Subsequently, the competitive inhibition of PD1/PDL1 interactions by sPD1^{HAC} will be rigorously evaluated using diverse binding assays conducted on murine and human cancer cell lines.

Additionally, the inhibitory efficacy of the engineered sPD1^{HAC} variant will be quantitatively compared with the commercial anti-PDL1 monoclonal antibody Durvalumab, using comprehensive in vitro assays designed to evaluate both direct inhibition of Durvalumab binding and relative differences in their PD1/PDL1 blocking capacities. These assessments aim to establish the therapeutic potential and translational feasibility of sPD1^{HAC} as a novel immune checkpoint inhibitor.

Finally, preclinical studies utilising murine tumour models will assess the therapeutic efficacy and biological functionality of sPD1^{HAC} in vivo. These evaluations will specifically investigate the capacity of sPD1^{HAC} derived from MSCs to mediate blockade of the PD1/PDL1 axis and its consequent effects on tumour progression and enhanced immune responses, thus validating the clinical potential of MSC-derived sPD1^{HAC} immunotherapeutic strategies.

Chapter 2: Materials and Methods

2.1 Cell culture

The following human cancer cell lines were obtained from the American Type Culture Collection (ATCC, Manassas, VA, USA): pancreatic (PancTu1, BxPC3, Colo-357), colorectal (HCT116, LoVo, RKO), breast (MDA-MB-231, T-47D, MCF-7), myeloma (MM.1R, MM.1S, U266), prostate (PC-3, Du145, LNCaP), cervical (HeLa), lung adenocarcinoma (A549), and ovarian (A2780). Engineered cell lines including Chinese hamster ovary (CHO), human embryonic kidney (HEK293T), and human mesenchymal stem cells derived from bone marrow (BM-MSC), umbilical cord (UC-MSCs), and adipose tissue (AT-MSC) as well as murine lines such as Lewis lung carcinoma (LL/2-Luc), colon adenocarcinoma (MC38), multiple myeloma (5TGM1), and melanoma (B16.F10) were also purchased from ATCC.

CHO, HEK293T, MCF-7, MDA-MB-231, LoVo, Du145, HeLa, A549, LL/2-Luc, MC38, and B16.F10 cells were cultured in Dulbecco's Modified Eagle Medium (DMEM), while PancTu1, BxPC3, Colo-357, LNCaP, PC-3, MM.1R, MM.1S, U266, T-47D, A2780, and 5TGM1 cells were maintained in Roswell Park Memorial Institute 1640 (RPMI-1640) medium. RKO and HCT116 cells were grown in McCoy's 5A Modified Medium. MSCs in MesenPRO medium. All media were purchased from Thermo Fisher and supplemented with 10% fetal bovine serum (FBS; Thermo Fisher Scientific, Waltham, MA, USA), 100 IU/mL penicillin, and 100 µg/mL streptomycin. LL/2-Luc cells were additionally supplemented with 2 µg/mL blasticidin. Cells were maintained at 37 °C in a humidified incubator with 5% CO_2 and subcultured using trypsin-EDTA (Lonza, Basel, Switzerland). Cell types, cell sources, media can also be found in Table 1.

Table 2.1. Detailed medium composition for each cell line along with their source tissue or organ.

Cell Line	Source	Culture Medium	Supplement
CHO	Chinese hamster ovary	DMEM	+10% FBS +1%pen/Strep
HEK293T	Human embryonic kidney		
MCF7	Human breast cancer		
MDA-MB-231	Human breast cancer		
LoVo	Human colorectal cancer		
Du145	Human prostate cancer		
HeLa	Human cervical cancer		
A549	Human lung adenocarcinoma		
B16.F10	Murine melanoma		
MC38	Murine colon adenocarcinoma		
LL/2	Murine lewis lung carcinoma	DMEM	+10% FBS +1%pen/Strep +2 µg/mL blasticidin
MM1.R	Human myeloma cancer	RPMI-1640	+10% FBS +1%pen/Strep
MM1.S	Human myeloma cancer		
U266	Human myeloma cancer		
PancTu1	Human pancreatic cancer		
BxPC3	Human pancreatic cancer		
Colo-357	Human pancreatic cancer		
LnCap	Human prostate cancer		
PC-3	Human prostate cancer		
T47-D	Human breast cancer		
A2780	Human ovarian cancer		
5TGM1	Murine myeloma cancer		
RKO	Human colorectal cancer	McCoy's 5A	+10% FBS +1% pen/Strep
HCT116	Human colorectal cancer		
BM-MSC	Bone marrow	α-MEM	+10% FBS +1% pen/Strep
UC-MSC	Umbilical cord	α-MEM	+10% FBS +1% pen/Strep
AT-MSC	Human adipose tissue	α-MEM	+10% FBS +1% pen/Strep

2.2 Drugs and reagents

To assess PDL1 modulation, interferon-gamma (IFNγ; R&D Systems, Cat. No. 285-IF-100) was utilised at a final concentration of 100 ng/mL and the chemotherapeutic agents; gemcitabine (GEM; Selleckchem, Cat. No. S1714) at 10 μM and 5-fluorouracil (5FU) purchased from Sigma (St Louis, MO, USA). All reagents were stored at -20 °C according to the manufacturers' instructions and incubated with cells for 48 h under standard culture conditions unless otherwise stated.

In-house prepared reagents included phosphate-buffered saline (PBS), prepared using PBS tablets (Sigma-Aldrich, Cat. No. P4417-100TAB) dissolved in distilled water (final pH 7.2-7.4); wash buffer (0.05% Tween-20 in PBS), dilution buffer (1% BSA in PBS, 0.2 μm filtered), 1 M hydrochloric acid as stop solution, and 4% paraformaldehyde (PFA) in PBS for cell fixation.

2.3 Antibodies

PE-conjugated anti-human CD274 and CD279 antibodies (referred to as αhPDL1 and αhPD1, respectively; BioLegend, Cat. Nos. 329705 and 329905) were used for PDL1 and PD1 detection on cells and also for antibody binding competition assays. For murine samples, PE-conjugated anti-mouse PDL1 antibodies corresponding to MIH7, MIH6, and 10F.9G2 clones (Cat. Nos. 155403, 153611, and 124301, respectively) were also obtained from BioLegend and used for murine PDL1 detection and antibody binding competition assays. These antibodies are referred to by their clone's name or as αmPDL1. Additionally, PE conjugated anti PDL1 monoclonal antibody, durvalumab biosimilar (Dima Biotech, Cat. No. BME100153P) was also utilised as a main competitor in the antibody binding competition setting and referred to as DUR (PE). As isotype controls, PE-conjugated mouse IgG2b κ (BioLegend, Cat. No. 400311) was used for αhPDL1/αhPD1, PE-conjugated rat IgG2b κ (BioLegend, Cat. No. 400607) was used for 10F.9G2, PE-conjugated rat IgG2a κ (BioLegend, Cat. No. 400508) was used for MIH6 and MIH7 and PE-conjugated mouse IgG1κ (BD Pharmingen, Cat. No. 555749) was used for DUR (PE).

In cell-based competition assays, biotinylated recombinant human PD1 Fc-fusion protein (referred to as rhPD1 (Biotin); BioLegend, Cat. No. 799506) and

biotinylated recombinant mouse PD1 (referred to as rmPD1 (Biotin); Sino Biological, Cat. No. 50124-M08H-B) were utilised as the main competitors. rhPD1 (Biotin) was additionally used as the main competitor in the solid-phase competition assays. In these two assays, the commercial immunotherapeutic αPDL1 monoclonal antibody durvalumab (DUR; Selleckchem, Cat. No. A2013) was also used as a secondary competitor in parallel to sPD1 variants to compare their blocking efficiencies against rhPD1 (Biotin) and rmPD1 (Biotin). In solid-phase competitions, recombinant human PDL1 Fc chimera protein was utilised as the coating antibody (referred to as rhPDL1; R&D Systems; Cat. No. 156-B7-100). A comprehensive list of antibodies utilised were also given in a table with regarding their binding target and assay information (Table 2).

Table 2.2 Detailed information on antibodies used in this study, with corresponding clone name, binding target, catalogue number, supplier, and assay application.

Antibody/ Protein	Binding Target	Clone	Company / Cat. No.	Assays	Stock Concentration
αhPDL1 (PE)	Human PDL1	29E.2A3	BioLegend / 329705	Surface stain, Ab binding competition assays	400 µg/ml
αhPD1 (PE)	Human PD1	EH12.2H7	BioLegend / 329905	Surface stain, Ab binding competition assays	50 µg/ml
αmPDL1 (PE)	Mouse PDL1	MIH7	BioLegend / 155403	Surface stain, Ab binding competition assays	200 µg/ml
αmPDL1 (PE)	Mouse PDL1	MIH6	BioLegend / 153611	Surface stain, Ab binding competition assays	200 µg/ml
αmPDL1 (PE)	Mouse PDL1	10F.9G2	BioLegend / 124301	Surface stain, Ab binding competition assays	200 µg/ml
Isotype control (PE)	IgG2a κ (rat)	RTK2758	BioLegend /400508	Control for mouse MIH6 & MIH7 clones	200 µg/ml
Isotype control (PE)	IgG2b κ (mouse)	MPC-11	BioLegend / 400311	Control for αhPDL1 & αhPD1	200 µg/ml

Isotype control (PE)	IgG2b κ (rat)	RTK4530	BioLegend / 400607	Control for mouse 10F.9G2 clone	200 µg/ml
Isotype control (PE)	IgG1 κ (mouse)	MOPC-21	BD Pharmingen 555749	Control for DUR (PE)	Not disclosed by manufacturer, used 1 µl/test as recommended
DUR (PE)	Human PDL1	N/A (mAb biosimilar)	Dima Biotech BME100153P	Ab binding competition assays	Not disclosed by manufacturer, used 1 µl/test as recommended
DUR (unlabelled)	Human PDL1	N/A (mAb)	Selleckchem / A2013	Cell-based competition assay	5990 µg/ml
rhPD1 (Biotin)	Human PDL1	N/A (Fc chimera protein)	BioLegend / 799506	Solid-phase and cell-based competition assay	200 µg/ml
rmPD1 (Biotin)	Mouse PDL1	N/A (Fc chimera protein)	Sino Biological / 50124-M08H-B	Cell-based competition assay	250 µg/ml
rhPDL1-Fc chimera	ELISA plate coating	N/A (Fc chimera protein)	R&D Systems / 156-B7-100	Solid-phase competition assay (capture protein)	100 µg/ml
Streptavidin (PE)	Biotin detection	N/A (Labelled tetrameric protein)	BioLegend / 405203	Cell-based competition assay	200 µg/ml
Streptavidin (HRP)	Biotin detection	N/A (Labelled tetrameric protein)	R&D systems DY998	Solid-phase competition assay (detection antibody)	Not disclosed by manufacturer, used 1:40 in PBS as recommended

2.4 Generation of sPD1 and PDL1 constructs

Soluble PD1 (sPD1) and mouse PDL1 (mPDL1) constructs were generated by the Protein Structure & Mechanisms of Disease group at the University of Essex and were sequence-verified prior to application. These included: full-length mouse PDL1 mRNA for ligand overexpression on HEK293T cells, and multiple sPD1 variants. $sPD1^{WT}$ corresponded to the extracellular domain of human PD1 (amino acids 25-167, GenBank NM_005018.3) was synthesised by an external manufacturer (DC Bioscience, Dundee) using the full-length PD1 construct (288 aa), while $sPD1^{HAC}$ was a high-affinity consensus variant bearing 10 targeted point mutations (on aa positions; 64, 65, 66, 68, 70, 74, 78, 122, 125, and 132) as previously described (Maute *et al.*, 2015). Both were cloned into the pFUSE-hIgG1-Fc vector (InvivoGen, Cat. No. #pfuse-hg1fc1), downstream of a human fibrillin-1-derived signal peptide (SP) and a furin cleavage (FC) site to facilitate secretion. These constructs either included (stWT, stHAC) or excluded (WT, HAC) a stop codon between the hIgG1-Fc domain and the PD1 fragment to evaluate secretion efficiency with or without IgG1-Fc fusion. Adenoviral vector carrying $sPD1^{HAC}$ ($Ad.sPD1^{HAC}$) and a luciferase control (Ad.LUC) were also kindly provided by Dr. Andrea Mohr and utilised for MSC transduction.

2.5 Cell transfections and transductions

CHO and HEK293T cells (1×10^6 cells per well) were seeded in 6-well plates and transfected 24 h later with lipid transfection technique and using TurboFect transfection reagent (Thermo Fisher Scientific, Cat. No. R0533) according to the manufacturer's instructions (reagent-to-DNA ratio 3:1). For sPD1 constructs, supernatants were collected 48 h post-transfection and later analysed by an enzyme-linked immunosorbent assay. For mPDL1 expression, HEK293T cells were transfected in the same manner, harvested 24 h post-transfection, and analysed by flow cytometry for ligand surface expression Transfected cells were named as 'cell names' followed by a point and 'cloned DNA names' such as HEK293T.mPDL1.

MSCs were transduced with E1/E3-deleted adenoviral vectors encoding either $sPD1^{HAC}$ ($Ad.sPD1^{HAC}$) or luciferase (Ad.LUC, control) at varying multiplicities of infection (MOIs), as previously described by Yu et al. (2013), 48 h prior to downstream analysis. Cells were centrifuged at 800×g for 90 mins at 37°C to enhance viral

adsorption, incubated with virus for 6 hours in 2% FBS-containing medium, washed, and subsequently cultured under standard conditions, and harvested 48 hours later. The resulting transduced cells were named MSC.sPD1^{HAC} or MSC.LUC (Yu *et al.*, 2013).

2.6 Detection of PD1 secretion by enzyme-linked immunosorbent assay (ELISA)

PD1 protein secretion in the culture supernatants of transfected CHO and HEK293T cells, as well as transduced MSCs (48 h post-application), was quantified using a human PD1 DuoSet ELISA kit (R&D Systems/Bio-Techne, Cat. No. DY1086), following the manufacturer's instructions. Briefly, culture supernatants were collected, clarified by centrifugation, and appropriately diluted 1:100 (MSC and CHO cells) and 1: 1000 (HEK293T cells) for PD1 quantification by ELISA.

2.7 Cell viability assay

Transfected HEK293T and CHO cells as well as transduced MSCs were measured 48 h after the application to determine how modification affected the cell viability. This was done according to Nicoletti at al. (Nicoletti *et al.*, 1991). Cells were harvested and washed with PBS. They were resuspended in hypotonic fluorochrome solution containing 50 g/ml propidium iodide, 0.1% sodium citrate, and 0.1% Triton-X100 after pelleted and incubated at 4 °C for 2 h. Then cell viability was analysed by flow cytometry.

2.8 Cell surface staining and FACS analysis

To measure surface expression of PDL1 and PD1 of the cells, $4x10^5$ cells were harvested and pelleted by centrifugation. Then cells were treated with R-phycoerythrin (PE)-conjugated anti-mouse PDL1 or anti-human PDL1 or anti-human PD1 antibodies following the manufacturer's instructions. Matched isotype control antibodies were included to assess non-specific binding. After 25 mins incubation at 4°C cells were washed with PBS and fixed with 4% PFA and analysed by BD Accuri C6 flow

cytometer. Mean fluorescence intensity (MFI) ratios were calculated by dividing the MFI of specific antibody-stained samples by the MFI of their corresponding isotype controls.

2.9 Binding competition assays

To assess the affinity and specificity of the engineered sPD1 variants, competitive binding assays were performed. These assays measured the ability of sPD1 variants to out compete biotin labelled rhPD1, PE-conjugated αPDL1 antibodies, or PE-labelled Durvalumab which bind to PDL1 presented on either solid-phase surfaces or cell membranes. Three complementary assay formats were employed: solid-phase binding competition, cell-based binding competition, and antibody binding competition assays.

2.9.1 Solid-phase binding competition assay

96-well plates were coated overnight at 4°C with 50 ng/well of recombinant PD1 ligands rhPDL1 Fc chimaera, or rhPDL2 Fc chimaera. Then the next day, wells were washed three times, blocked with dilution reagent for 1 h at room temperature. Wells were subsequently incubated for 2 h with a mixture of rhPD1 (50 ng/well) and decreasing concentrations of competing sPD1 variant-containing supernatants (40 - 0.1 ng/ well) or a molar equivalent of DUR in PBS. Controls contained only biotin labelled rhPD1 and untreated supernatant. After incubation, the wells were washed and blocked for an additional 10 mins. Streptavidin-HRP (1:40) was added for 20 mins, followed by TMB staining, and the reaction was stopped with the stop solution. Optical density (OD) at 450 nm was measured, and the binding percentage of rhPD1 was calculated for each sample as: (OD sample / OD control) × 100.

2.9.2 Cell-based binding competition assay

Cell-based binding competition assays were performed on RKO cells or B16.F10 cells. 4×10^5 cells were incubated for 25 min on ice with a mixture of supernatant containing biotin labelled rhPD1 (used as the primary binding probe) and a second competitor;

either sPD1 variants (sPD1^{HAC} or sPD1^{WT} derived from HEK293T, CHO, or MSC) or molar-equivalent Durvalumab (DUR). On RKO cells, rhPD1 and sPD1 variants were mixed at a 5:1 mass ratio; for B16.F10 cells, rhPD1 and sPD1 variants were used molar equivalents (1:1 molar ratio). Negative controls included cells with the same volume of PBS (without rhPD1), and positive controls included cells with only rhPD1 in the same volume of PBS. Following incubation, cells were washed and stained with Streptavidin-PE (1:25 dilution in PBS) for 20 mins at 4 °C. The cells were fixed with 4% PFA after the wash, centrifugation, and aspiration steps and analysed by flow cytometry.

To normalise the data, background fluorescence (from cells treated with PBS and Streptavidin-PE only) was subtracted from all measurements. Binding in the absence of any competitor (rhPD1 only) was defined as 100%. The percentage of PD1 binding in the presence of each competitor was calculated as: [%] Binding = (MFI_sample - MFI_negative control) / (MFI_positive control - MFI_negative control) × 100.

2.9.3 Antibody binding competition assay

To assess the ability of sPD1^{HAC} to inhibit recombinant antibody-ligand interactions, antibody binding competition assays were performed on RKO, HEK293T.mPDL1, B16.F10, and 5TGM1 cells. Cells (4×10^5) were incubated for 25 mins on ice with a mixture of PE-conjugated αPDL1 antibody (including a DUR biosimilar, used as the primary binding probe) and either sPD1^{HAC} or sPD1^{WT} (used as the secondary competitor). sPD1 variants were applied at 0.8 µg per sample unless otherwise stated, and the amount of PE-conjugated αPDL1 was determined according to the manufacturer's instructions. Positive controls consisted of cells incubated with αPDL1 antibody alone in PBS, while negative controls were incubated with the corresponding isotype control.

Following incubation, cells were washed with PBS, fixed in 4% paraformaldehyde, and analysed by flow cytometry. MFI values were normalised and calculated in the same manner as described for the cell-based binding competition assays.

2.10 Animal studies

Ten-week-old C57BL/6 mice were housed in the University of East Anglia Norwich. All procedures complied with the Animals (Scientific Procedures) Act 1986 and EU Directive 2010/63/EU and were approved by the institutional ethics committee. On day 0, pulmonary metastases were established by tail vein injection of B16.F10 cells ($4x10^5$ cells in 100 µL PBS) to seed lung lesions. On the day 7, mice received either a single intravenous dose of MSC.sPD1^{HAC} ($4x10^5$ cells in 100 µL PBS) or control MSC.LUC (in PBS) at the same volume via lateral tail vein. Animals were monitored daily for clinical status. Euthanasia was performed on day 14, lungs were dissected, rinsed in PBS, fixed in 4% PFA, and photographed for surface nodule enumeration. Animals were randomised to MSC.sPD1^{HAC} and MSC.LUC groups, with 8 mice per group across two independent cohorts (total n = 16). Macroscopic surface nodule enumeration was performed by investigators blinded to treatment allocation; the full study schema and corresponding in vivo outcome are presented in Section 4.11 and Figure 4.19.

2.11 Tissue embedding and H&E staining

Dissected lung lobes were processed for histology through graded ethanol dehydration (70%, 90%, and 100%) for 1 h each, followed by three xylene washes for 1 h each, and were then embedded in a melted paraffin wax (Epredia, paraffin type 6, Cat. No. 8336). Paraffin blocks were sectioned at 5 µm from multiple planes across the lobes and mounted onto slides. Sections were deparaffinised in xylene (3 min), rehydrated through descending ethanol concentrations (100%, 90%, and 70%), stained with haematoxylin for 5 min and eosin for 3 min, dehydrated, cleared in xylene (2 min), and mounted with DPX mounting medium. Representative fields, including micronodules, were examined by microscopy and imaged using the EVOS M5000 imaging system.

2.12 Statistical analysis

Statistical analyses for the experimental datasets were performed using one-way ANOVA for comparisons involving multiple groups. Normality was visually inspected

where the structure of the dataset permitted, particularly for ELISA and solid-phase competition assay datasets. Formal post hoc multiple-comparison correction was not applied after ANOVA. Exact p-values are reported in the corresponding figures, and $p < 0.05$ was considered statistically significant. Quantitative data are presented as mean ± standard error (SE). Where applicable, the number of independent experiments is indicated in the relevant figure legends. Bioinformatic and correlation-based analyses of TCGA datasets were evaluated separately, as described in Sections 2.13 and 2.14.

2.13 Bioinformatic data thresholds and calculations

For bioinformatics data, TCGA PanCancer atlas data sets were benefitted for mRNA expression Z-scores through cBioPortal (https://www.cbioportal.org/). For bioinformatic analyses, two distinct TCGA PanCancer Atlas cohorts were used according to the aim of the analysis. For hot/cold classification, the seven cancer types with the largest sample sizes were selected. For the immune-related gene expression and PDL1 correlation heatmap analyses, all cancer types with a sample size greater than 150 were included, yielding 21 cohorts in total. Correlations were calculated by Pearson method. For all the heatmaps generated, Python programming language and seaborn library were used. Scripts and directory regarding bioinformatic analyses were given in detail in GitHub (https://github.com/serapgokcen/Tcellmarker_Heatmap_analysis).

Hot/cold classification in the T-cell activation analysis included several steps. For each sample, mRNA Z-scores of T-cell abundances (CD3D, CD3E, CD8A, PTPRC), activation (IFNG, ICOS, TNFRSF9, CD69, CD40LG, CD274), progenitor-exhausted (SLAMF6, TCF7, CCR7) and exhaustion (PDCD1, CTLA4, LAG3, TIGIT, HAVCR2, TOX, CXCL13) genes computed as separate panels. Each panel index was standardised across all samples using its median and median absolute deviation (MAD). The HotScore combined these standardised indices, and the contribution of the exhaustion panel was gated by T-cell abundance. When T-cell abundance was above the within-cancer mean, higher exhaustion was treated as a pro-hot signal and added to the total score. When T-cell abundance was below the mean, exhaustion was subtracted, indicating an immune-deserted ecosystem with terminally exhausted T-cells. A robust Z value of the HotScore was then computed across all samples, and

a gene-level consistency metric (p_consistency) was defined as the fraction of panel genes whose sign agreed with the hot direction (pro-hot genes > 0; gated exhaustion genes < 0). Samples were classified as hot (Z ≥ 1.0 and p_consistency ≥ 0.70), intermediate-hot (0.3 ≤ Z < 1.0 or 0.55 ≤ p_consistency < 0.70), intermediate-cold (−1.0 < Z ≤ −0.3 or 0.30 < p_consistency ≤ 0.30), or cold (Z ≤ −1.0 and p_consistency ≤ 0.30). Per-cancer summaries included the fraction in each group (Wilson 95% CI), Width of Hot Coverage (WHC = hot + 0.5×intermediate-hot), Hot Intensity (median Z among hot/intermediate-hot, bootstrap 95% CI), and the composite Hot Summary Score (HSS = min [1, WHC×HI/1.5]).

2.13.1 Panel indices

Let $z_{g,s}$be the provided z-score for gene "g" in sample “s”. For prespecified panels, T-cell abundance (T: CD3D, CD3E, CD8A, PTPRC), activation (A: IFNG, ICOS, TNFRSF9, CD69, CD40LG, CD274), progenitor-exhausted (P: TCF7, SLAMF6, CCR7), and terminal exhaustion (E: PDCD1, CTLA4, LAG3, TIGIT, HAVCR2, TOX, CXCL13), we formed sample-level means:

$$T_s = \frac{1}{|T|}\sum_{g\in T} z_{g,s} \quad A_s = \frac{1}{|A|}\sum_{g\in A} z_{g,s} \quad P_s = \frac{1}{|P|}\sum_{g\in P} z_{g,s} \quad E_s = \frac{1}{|E|}\sum_{g\in E} z_{g,s}$$

Each index was robustly standardized across all samples using median/MAD:

$$\tilde{X}_s = \frac{X_s - \mathrm{median}(X)}{\mathrm{MAD}(X)} \quad \text{with} \quad X\in\{T,A,P,E\}$$

2.13.2 TEX gating by abundance

Terminal exhaustion contributes with a sign that depends on T-cell abundance within cancer type. For sample s belonging to cancer c[s]:

$$w_s = \mathrm{sign}(T_s - \overline{T}_{c[s]})$$

Where $\overline{T}_c$ is the within cancer mean of T. Thus, TEX is pro-hot when abundance is high and anti-hot when abundance is low.

HotScore (with gated exhaustion), amplitude Z, and consistency

The per-sample HotScore averages the available standardized parts;

$$\mathrm{HotScore}_s = \mathrm{mean}\left(\tilde{T}_s \tilde{A}_s \tilde{P}_s w_s \tilde{E}_s\right)$$

Amplitude is a robust Z score across samples;

$$Z_s^{\mathrm{hot}} = \frac{\mathrm{HotScore}_s - \mathrm{median}(\mathrm{HotScore})}{\mathrm{MAD}(\mathrm{HotScore})}$$

"Consistency" quantifies gene-level agreement with the hot direction:

$p_{\mathrm{cons}_s} = \frac{1}{m_s} \sum_{g \in \mathcal{T} \cup \mathcal{A} \cup \mathcal{P} \cup \mathcal{E}} \mathbf{1}[\mathrm{align}_{g,s}]$,

With $\mathrm{align}_{g,s} = (z_{g,s} > 0)$ for $g \in \mathcal{T} \cup \mathcal{A} \cup \mathcal{P}$ and

$\mathrm{align}_{g,s} = (w_s z_{g,s} > 0)$ for $g \in \mathcal{E}$ is the number of non-missing genes.

2.13.3 Discrete label rules

Samples were classified using fixed thresholds (tuned a priori):

Hot: $Z_s^{\mathrm{hot}} \geq 1.0 \wedge p_{\mathrm{cons}_s} \geq 0.70$

Intermediate-hot: $0.3 \leq Z_s^{\mathrm{hot}} < 1.0$ or $0.55 \leq p_{\mathrm{cons}_s} < 0.70$

Intermediate-cold: $-1.0 < Z_s^{\mathrm{hot}} \geq -0.3$ or $0.30 < p_{\mathrm{cons}_s} \geq 0.35$

Cold: $Z_s^{\mathrm{hot}} \leq -1.0 \wedge p_{\mathrm{cons}_s} \leq 0.30$

(Edge cases fall to the nearest intermediate class)

2.13.4 Cohort summary metrics (per cancer type)

Per cancer type we report counts and fractions of the four classes with 95% Wilson binomial CIs; Hot Intensity (HI) = median Z^{hot} among the hot-side (hot ∪ intermediate-hot) with 95% bootstrap CIs (5,000 resamples; seed=42):

$$\mathrm{HI} = \mathrm{median}\{Z_s^{\mathrm{hot}} : s \in (\text{hot} \cup \text{intermediate-hot})\}$$

Width of Hot Coverage $(\mathrm{WHC}) = f_{\mathrm{hot}} + 0.5 f_{\mathrm{iHot}}$ and a bounded composite

Hot Summary Score (HSS): min (1, WHC × HI÷ 1.5)

2.14 Correlation analysis

Pairwise correlations between CD274 expression and each immune-related gene (detailed in the results section) were calculated using the Pearson product-moment correlation coefficient (Pearson-r), as implemented in the default pandas.Series.corr() function (Python). For each cancer dataset, gene-wise expression z-score normalised expression values were used as input. Correlation coefficients range from -1 (perfect negative linear association) to +1 (perfect positive linear association). In line with established conventions in transcriptomic studies, we considered correlations with r > 0.5 as indicative of a strong positive association with CD274 expression, while weaker correlations (r ≤ 0.5) were retained for visualisation but not prioritised for interpretation. Negative correlations were also recorded but were not the primary focus of this study.

CHAPTER 3: PD1 and PDL1 Expression on Cancer Cells and Their Relationship with Immune Related Markers

3.1 Major cancer types represent distinct immune profiles in terms of T-cell activation state and abundance

T-cell activation and exhaustion markers are discussed in the literature as the critical decisive part for the hot or cold phenotype of tumours. To elucidate overall T-cell presence and activation within a sample, markers such as CD3D, CD3E, CD8A, and PTPRC are used to assess T-cell abundance. In contrast, a set of activation/IFNγ axis markers, including IFNG, ICOS, TNFRSF9, CD69, CD40LG, and CD274, provides further insights into the functional state and recent activation of these T-cells. Because CD274 (encoding PDL1) is an IFNγ-inducible checkpoint on tumour and myeloid cells, its behaviour mechanistically links the activation axis to a negative-feedback brake; in inflamed samples, PDL1 is expected to scale with IFNγ and co-stimulatory signals. Although T-cell lineages dynamically change in the TME and markers for specific lineages have not been established clearly yet, there are some progenitor and terminally exhausted T-cell markers that are mostly agreed upon in recent studies. These core marker groups for terminally exhausted T-cells (TEX) are HAVCR2 (TIM-3), TOX, CXCL13, TIGIT, CTLA4, and LAG3, PDCD1, and for progenitor exhaustion (PEX) are TCF7, SLAMF6, and CCR7. For these marker expressions, mRNA Z-scores (threshold 2.0) were retrieved from cBioPortal regarding TCGA PanCancer Atlas studies and analysed in a clustered heatmap to delineate possible patient stratifications (Figure 3.1).

Across cancers, two dominant patterns emerge; first, several cohorts split cleanly into four sample groups. In breast cancer, a left-hand cluster shows the highest T-cell abundance with concordant high activation (dark reds), while the TEX panel is relatively suppressed (dark blue). The right-hand cluster inverses this relation (low abundance/activation with higher TEX). Although it is not immediately distinguishable in breast cancer, other cancer types have definable two more panels with high-leaning activation/low TEX and low-leaning activation/high TEX. Melanoma, colorectal, ovarian and lung display a similar stratification, abundance and activation track together and oppose TEX across much of the cohort. In these tumours, PEX is generally higher in the inflamed cluster, consistent with preserved stem-like memory within otherwise active infiltrates.

Melanoma

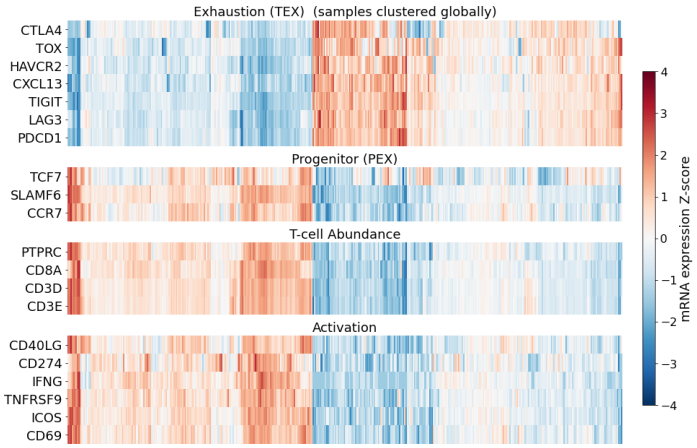

Breast

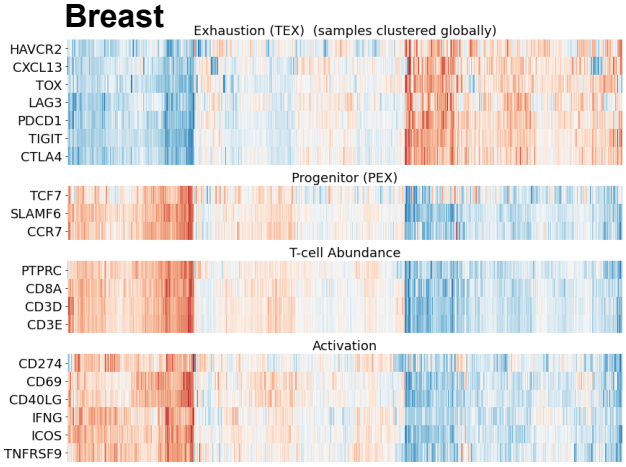

Lung

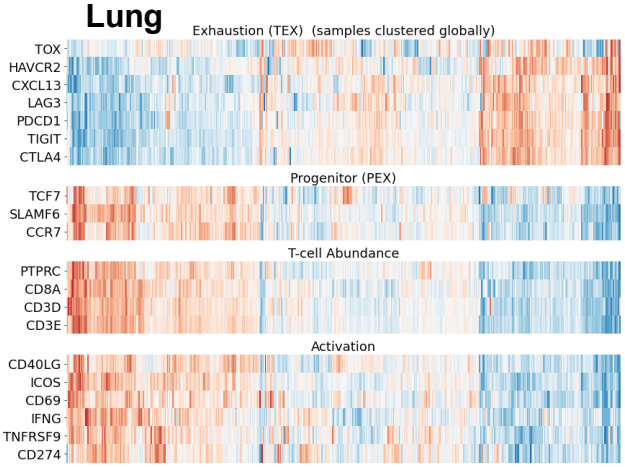

Pancreatic

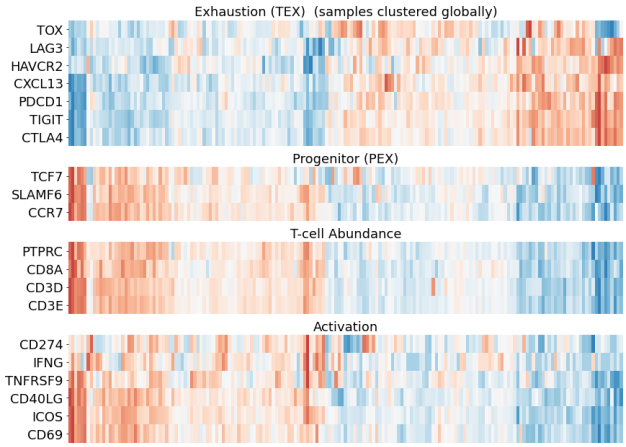

Prostate

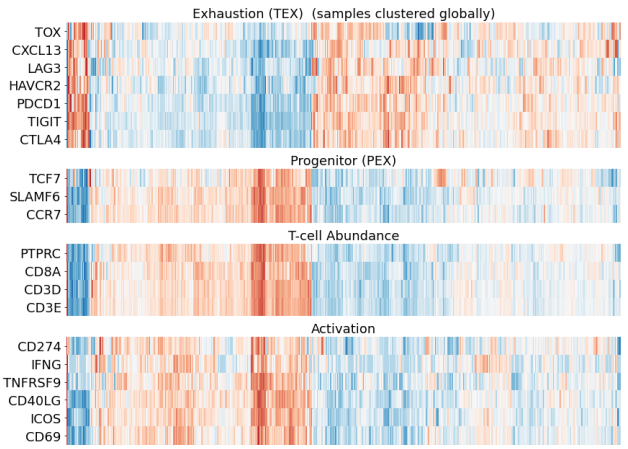

Colorectal

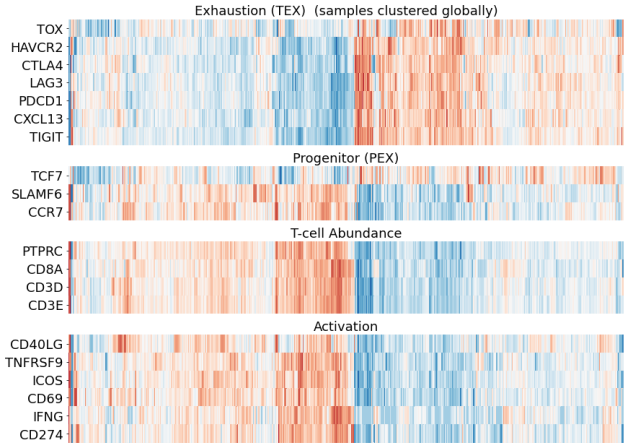

Ovarian

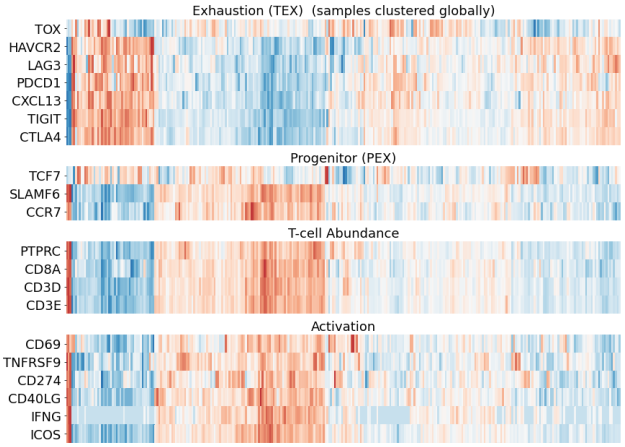

Figure 3.1 Pan-cancer heatmaps of T-cell abundance, activation, progenitor exhaustion and terminal exhaustion gene signatures. Heatmaps show mRNA Z-scores for selected immune gene panels across seven TCGA PanCancer Atlas cohorts. Columns represent tumour samples and rows represent genes grouped into T-cell abundance (CD3D, CD3E, CD8A, PTPRC), activation (IFNG, ICOS, TNFRSF9, CD69, CD40LG, CD274), terminal exhaustion (HAVCR2, TOX, CXCL13, TIGIT, CTLA4, LAG3, PDCD1), and progenitor exhaustion (TCF7, SLAMF6, CCR7). Samples within each cancer type were arranged by hierarchical clustering. Red indicates higher relative expression, and blue indicates lower relative expression on the mRNA Z-score scale.

Second, other cohorts show a heterogeneous or more banded structure. Ovarian and colorectal contain sample segments in which abundance, activation, and TEX are simultaneously elevated, consistent with a chronic inflammation phenotype in which interferon-driven activation coincides with checkpoint up-regulation. In these segments, PDL1 upregulation is a defining feature: it correlates with the IFNγ-high state and also co-occurs with TEX, rationalising why PD1/PDL1 blockade would be necessary, but in some cases, combination strategies that also reinvigorate exhausted T-cells might be needed as well. Outside these bands, signals are lower and patchier in some cancer types, such as colorectal and pancreatic. Pancreatic indicates a narrower inflamed subset (left-hand subgroup) with raised abundance and activation, along with broader low-signal regions and TEX rises toward the opposite flank, indicating a mixture of cold and TEX-dominant states. However, more precise statements require dedicated computational analysis, which has been undertaken and will be presented in a subsequent section.

At the colder end, prostate and colorectal are dominated by muted abundance and activation with TEX-dominant streaks. In colorectal, for example, TEX increases as abundance/activation decline across the panel, yielding a prolonged TEX-high/effector-low sector. This pattern helps explain the low aggregate hotness for these indications and argues against treating TEX as intrinsically “hot”. High exhaustion in the absence of infiltration or activation likely reflects dysfunctional or bystander populations rather than productive anti-tumour immunity.

Gene-wise, several consistent anchors are visible. Within activation, IFNG, TNFRSF9, and CD40LG rise in inflamed segments, with CD274 typically co-elevated and a pattern consistent with IFNγ-responsive PDL1 induction. Within TEX, CXCL13 and TOX/HAVCR2 often mark the TEX-high sectors most strongly, while PDCD1 and

CTLA4 are present but less uniformly intense. This pattern is consistent with reports associating CXCL13-positive T-cells with tertiary lymphoid/Tfh-like or late exhausted states (Lin *et al.*, 2024a; Oliveira and Wu, 2023). PEX tends to be highest where activation is also high (melanoma, lung, breast), and lowest in TEX-dominant cold zones, indicating that stem-like capacity concentrates in inflamed microenvironments.

Across cancer types, the heatmaps delineated degrees of immune 'hotness', but TCF7 and TOX behaved discordantly. Neither gene consistently tracked with the broader hot, cold, hot-leaning, or cold-leaning patterns, limiting their utility as pan-cancer indicators of inflamed versus immune-desert phenotypes. Notably, in ovarian, colorectal, and lung cohorts, TOX co-varied with T-cell activation/abundance and progenitor markers, consistent with a highly stimulated yet exhausted T-cell milieu and a potential resistance way to PD1/PDL1 therapy. These patterns suggest a context-specific interpretation of TCF7 and TOX, rather than using them as universal classifiers. TCF7 also correlated with TEX markers in colorectal and ovarian besides having a mixed expression pattern in others, indicating possible dual roles of it on T-cell lineage differentiation.

Taken together, the heatmaps delineate three reproducible microenvironmental states across cancers: hot (high abundance/activation/PEX with low-to-moderate TEX), TEX-dominant cold (high TEX with low abundance/activation/PEX), and hot/cold -leaning states (less expression and mostly still distinguishable hot or cold patterns). An adaptive-resistance group was also noticeable with co-elevated activation, CD274, and TEX in a subset, which was prominent in ovarian and present to a lesser extent in pancreatic. These visual patterns align with the summary metrics (higher hotness in melanoma, breast, and lung; lower in prostate and pancreatic) and justify the TEX-gating rule used downstream: treat TEX as pro-hot only when T-cell abundance is high, and discount or invert its contribution when abundance is low.

3.2 Quantitative analysis of hot and cold immune states across cancers confirmed the stratification finding visualised by heatmaps

To define hot-cold immune types and their coverage in the same data set, a comprehensive mRNA expression analysis of tumours' "hotness" (inflammation

degree but considering only T-cell activation state) was performed. For this, two main metrics were employed: the Hot Summary Score (HSS) on a 0-1 scale and the Hot Intensity (HI), representing the median Z-score of the hot side along with its 95% confidence interval (CI). Cancers were ranked by HSS in descending order, yielding the following order: melanoma 0.28, lung 0.24, breast 0.23, ovarian 0.21, pancreatic 0.21, prostate 0.18, and colorectal 0.17. Based on these HSS values, cancers were stratified into three categories: the high tier comprising melanoma and lung; the intermediate tier including breast, ovarian, and pancreatic; and the low tier represented by prostate and colorectal. This stratification employs a meaningful separation threshold of at least 0.03 in HSS differences, as exemplified by the 0.04 difference between melanoma and lung, among other pairwise comparisons across tiers. The width of hot coverage (WHC) was calculated by aggregating samples with the hot fraction and half of the hot-leaning samples' fraction.

Activation scores were derived from pooled-rank-normalized expression of canonical T-cell activation genes, TEX, PEX, and T-cell abundance markers. Samples were classified as hot / intermediate-hot (i_hot) / intermediate-cold (i_cold) / cold using amplitude (Z) and consistency (fraction of activation genes up), and per-cancer WHC, HI, and HSS were summarized (N: melanoma = 443; colorectal = 592; lung = 510; breast = 1082; pancreatic = 177; ovarian = 300; prostate = 493). The HI metric, with its accompanying 95% CI, provided an independent quantitative assessment of hot signal intensity.

For every cancer type, the CI was entirely above zero, confirming a non-zero hot signal across the dataset. In detail, melanoma exhibited the highest HI at 1.07 with a 95% CI of (0.94-1.19), followed by breast with an HI of 0.95 (0.86-1.05), lung with an HI of 0.89 (0.75-1.06), ovarian with an HI of 0.86 (0.65-0.96), pancreatic with an HI of 0.85 (0.62-1.10), prostate with an HI of 0.74 (0.63-0.90) and colorectal with an HI of 0.69 (0.62-0.79) . In terms of meaningful separation for HI differences, which was set at a threshold of ≥0.10, the difference between melanoma and colorectal cancers, at approximately 0.38, highlights a marked separation in hot signal intensity that is consistent with the HSS ranking (Figure 3.1b).

A)

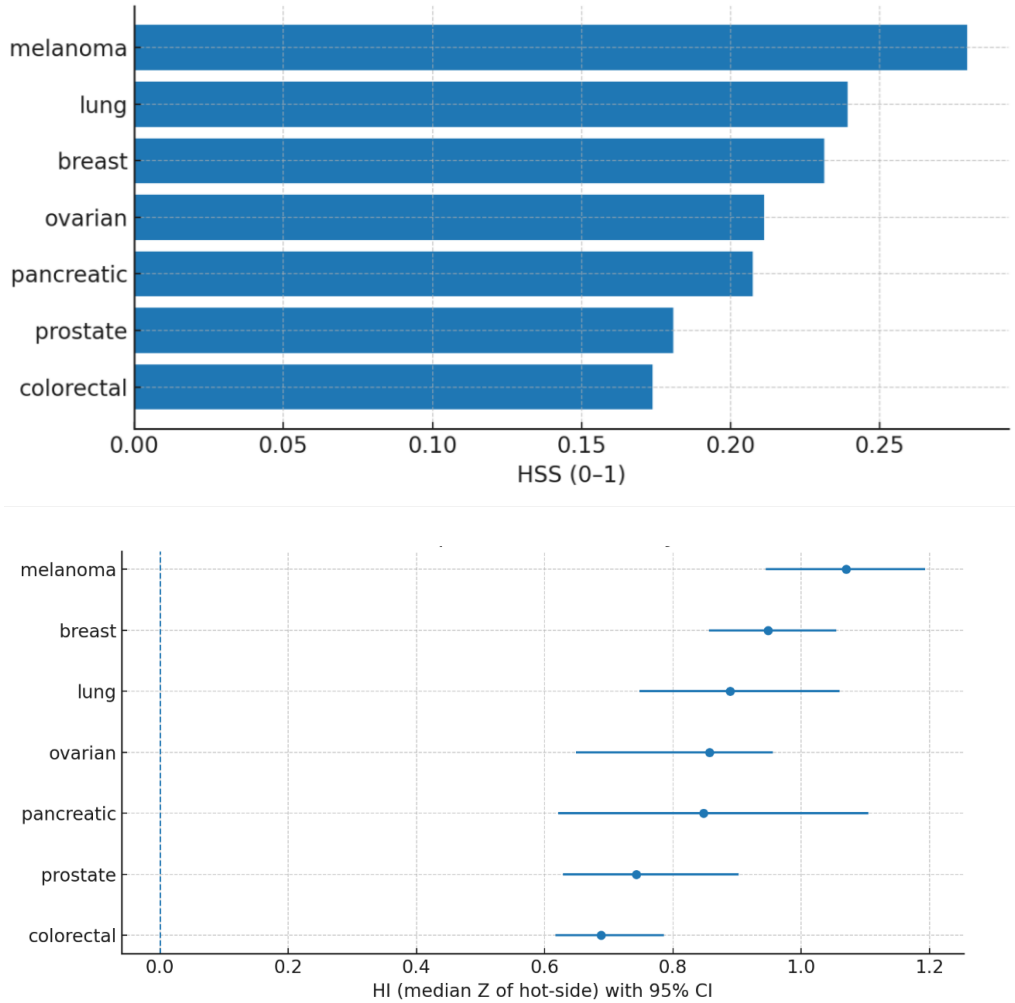

Figure 3.2 Summary metrics of T-cell-defined hotness across seven TCGA cancer cohorts. A) Hot Summary Score (HSS) by cancer type on a 0 to 1 scale. HSS integrates width of hot coverage and hot intensity as defined in the Methods section. **B)** Hot Intensity (HI), shown as the median standardised activation score among hot-side samples with 95% bootstrap confidence intervals; the dashed line indicates the pooled median across cohorts. Samples were assigned to hot-side or cold-side classes using predefined amplitude and consistency cut-offs described in Section 2.13.

Collectively, these data-bound results indicate that melanoma stands out as the most T-cell-inflamed “hot” cancer type, both in terms of its summarised hotness and signal intensity, while the precision of HI estimates varies considerably across cancers, particularly with notable uncertainty for pancreatic cancer (likely due to the sample size N:177). Together, these results indicate that several cancers (notably lung, melanoma, breast, and ovarian) harbor broad hot-leaning profiles with varying core intensity, whereas colorectal shows lower hot-side intensity despite similar coverage. These distributions quite matched the sample-wise patterns in the heatmap overview

Figure 3.1, where large intermediate-hot blocks accompanied smaller strictly hot segments.

These findings should be interpreted as cohort-level immune patterns rather than fully resolved representations of the heterogeneity within each cancer type. Although the seven-cancer TCGA analysis identifies broad differences in T-cell-defined hot and cold states, it does not account for several layers of clinicopathological variation that are likely to influence these patterns. As a result, the distributions shown in Figure 3.1 and summarised in Figure 3.2 should be understood as overall cohort behaviour, rather than as a uniform feature of all tumours within a given cancer type.

One important source of variation not resolved here is tumour subtype. In breast cancer, for example, luminal A, luminal B, HER2-positive, and triple-negative tumours differ substantially in immune infiltration, inflammatory signalling, and checkpoint-related biology. The breast cancer heatmap therefore represents a composite signal derived from biologically distinct subgroups, some of which would be expected to show hotter or colder immune profiles than others. A related issue applies to colorectal cancer, where proximal and distal tumours can differ in molecular background, inflammatory composition, and clinical behaviour. When such subgroups are analysed together, subtype- or location-specific immune states may be obscured, and this may contribute to the more heterogeneous patterns observed in some cohorts.

Tumour stage is another variable that was not separated in the present analysis. Stage I to IV disease may differ markedly in stromal organisation, immune exclusion, chronic interferon exposure, and the degree of T-cell dysfunction. Consequently, a cancer type that appears relatively cold at cohort level may still contain subsets with stronger inflammatory activity, while a generally hotter cohort may also include biologically distinct tumours with lower immune engagement. For this reason, these data should not be interpreted at patient level or taken to indicate that all tumours within a cancer category share the same immunological state.

This is also relevant because the hot and cold classification was performed only in the seven largest cohorts, whereas the later correlation analysis in this chapter was expanded to a broader 21 cancer framework. The present section should therefore be read as a comparative overview rather than a stratified within cancer analysis. Even so, the analysis remains informative in showing that recurrent T-cell related immune

states can be detected across major cancer types, while also indicating that further subdivision by subtype, anatomical location, and stage would be necessary for a more clinically refined interpretation.

3.3 PDL1 expression correlates with the maximum number of immune markers in melanoma

Next, the analysed gene set was expanded from specific T-cell activation genes to 323 other immune-related genes commonly referred to play crucial roles in T-cell regulation, inflamed TME, and hot profiles of tumours in recent literature. These genes were aggregated from 21 recent peer-reviewed papers, most of which are closely related to immunotherapy and T-cells 21 paper(Andreatta *et al.*, 2021; Ayers *et al.*, 2017; Bredel *et al.*, 2023; Buchholz and Busch, 2019; Chen *et al.*, 2019b; Hammerl *et al.*, 2021; Khan *et al.*, 2022; Kirschenbaum *et al.*, 2024; Liu *et al.*, 2021; Miragaia *et al.*, 2019; Prokhnevska *et al.*, 2023; Rade *et al.*, 2023; Shifrut *et al.*, 2018; Sousa *et al.*, 2019; Strazza *et al.*, 2021; Sun *et al.*, 2022; Szabo *et al.*, 2019; Tirosh *et al.*, 2016; van Elsas *et al.*, 2024; Wang *et al.*, 2022b; Wegrzyn *et al.*, 2023). Then they were systematically subdivided into 11 functional categories that represent long-standing and recent literature-based roles in tumour immunology and TME biology (Table 3.3). Cancer cohorts were also expanded from major cancer types to pan-cancer cohorts with a sample size higher than 150.

Table 3.3 Functional classification of predefined immune-related genes in a pan-cancer expression analysis.

Trans-criptional & Epigenetic Regulators	MSC & Immunosuppressive Mediators	Myeloid & Macrophage Immunosuppressive Markers	T-cell Activation & Effector Function	Signaling, Cell-Cycle & Apoptosis Effectors	Surface & Micro-environment Interactors
BACH2	TGFB1	CD163	CD3D	ATM	ADAM8
BATF	TGFB3	CSF1R	CD3E	CCND3	AIF1
BATF3	IL10	CSF1	CD4	CDKN1A	ANXA1/2
BCL6	IL10RA	ITGAM	CD8A	BCL2	APBB1
BHLHE40	IDO1	ITGAX	CD8B	BCL2L11	CD109
BCL2L11	CD200	AIF1	IL2RA	CAPN3	ITGA1
NFATC1	ARG1	FCGR1A	IL2RB	DUSP1	ITGA4
FOXO4		NLRP3	IL2RG	JUN	ITGAE
FOXP3		CEACAM8	GZMA	MDM4	ITGAL
GATA3			GZMB	MKI67	ITGB7
IKZF1/2			GZMH	ORC6	ITGAM
IRF4/7/8			GZMK	PYCARD	ITGAX
KLF2/6			GZMM	FAS	NCAM
LEF1			PRF1	FASLG	SELPLG
MAF			TBX21	TRADD	MS4A1
ZNF683			EOMES	P2RX7	CD226
R4A1/3					CD248
RORA					DPP4
ZBTB16					CD47/48
ZBTB32					CD58/59
ZBTB49					PTPRC
TBX21					TUBB
TCF7					SELL
RORC					LGALS1/3
RUNX1/2					TUBA1A/1B
PRDM1					TUBB4B
ZEB2					VIM
MYB					WARS1
STAT1/3/4					WHAMMP3
STAT5A/6					EZR
					CMKLR1
					COL10A1
					CORO1A

Co-stimulation & Immunological Synapse	T-cell Exhaustion & Dysfunction	T-cell Recruitment & Chemokine Signaling	Metabolic & Hypoxia-Related Suppression
CD28	CTLA4	CCL3	HIF1A
CD40	PDCD1	CCL4	VEGFA
CD40LG	LAG3	CCL5	PPARG
ICOS	TIGIT	CCL18	NT5E
CD27	TOX	CCL20	NOS2
TNFRSF4	TOX2	CXCL9	NOSIP
TNFRSF9	HAVCR2	CXCL10	AQP3
CD2	FOXP3	CXCL11	
		CXCL13	
		CCR2	
		CCR3	
		CCR4	
		CCR5	
		CCR6	
		CCR7	
		CCR10	

IFN Signaling & Antigen Presentation
IFNGR1
IFNAR1
IRF1
STAT1
HLA-DQA1
HLA-DRA
HLA-DRB1
HLA-E
CIITA

The first category, T-cell activation & effector function, includes genes that trigger and sustain T-cell receptor signalling, subsequent cytokine production and cytolytic activity. Representative genes from the list are the T-cell receptor components (CD3D, CD3E), lineage markers (CD4, CD8A, CD8B), and cytokine/effector molecules such as IL2 and its receptor subunits (IL2RA, IL2RB, IL2RG), alongside cytolytic effectors (GZMA, GZMB, GZMH, GZMK, GZMM, PRF1) and master regulators (TBX21, EOMES).

The second category was T-cell recruitment & chemokine signalling genes. In this group, members mediate chemotaxis and migration of T-cells into the tumour microenvironment. They include chemokine ligands such as CCL3, CCL4, CCL5, CCL18, CCL20 and chemokines of the CXCL family (CXCL9, CXCL10, CXCL11, CXCL13), as well as their receptors (CCR2, CCR3, CCR4, CCR5, CCR6, CCR7, CCR10) that help coordinate T-cell trafficking.

IFN signalling & antigen presentation as a third functional group comprises genes that are considered upregulated in highly “inflamed” tumours and contribute to both interferon signalling and antigen presentation. Key components include the effector cytokine IFNG and its receptors (IFNGR1, IFNAR1), transcriptional mediators such as IRF1 and STAT1, along with major histocompatibility complex genes (HLA-DQA1, HLA-DRA, HLA-DRB1, HLA-E) and their master regulator CIITA.

The other class, co-stimulation & immunological synapse genes, are mechanistically involved in providing co-stimulatory signals and forming the immunological synapse. This group included co-stimulatory receptors and ligands (CD28, CD40, CD40LG, ICOS, CD27) along with members of the TNF receptor superfamily such as TNFRSF4 and TNFRSF9, as well as other adhesion components like CD2.

T-cell exhaustion & dysfunction were the fifth functionally distinguishable group. This group is typically marked by inhibitory receptors and regulators. CTLA4, PDCD1, LAG3, TIGIT, TOX, TOX2, HAVCR2, and FOXP3 emerge as central mediators of exhaustion and regulatory T-cell-associated suppressive function.

The MSC & immunosuppressive mediators’ group was dedicated to soluble factors and cell-surface molecules largely responsible for immunosuppression, often linked to the mesenchymal or stromal compartment. Notable genes include the immunosuppressive cytokines TGFB1 and TGFB3, IL10, along with its receptor IL10RA, the enzyme IDO1, and the immune checkpoint molecule CD200. ARG1 is

also associated with myeloid-derived suppressor cell function, but is not included in every cancer type.

Myeloid & macrophage immunosuppressive markers, macrophage group members help the constitution of a suppressive TME through myeloid and macrophage cells. Key markers include CD163 and CSF1R, as well as CSF1 itself and additional myeloid effectors such as AIF1, FCGR1A, and NLRP3. Lastly, a neutrophil marker, CEACAM8 also considered in this category.

Metabolic & hypoxia-related suppression genes modulate the metabolic environment or mediate hypoxia-driven suppression fall into this category. HIF1A and VEGFA are prototypical factors, with PPARG, NT5E (encoding CD73), NOS2 and NOSIP also contributing to a metabolism-mediated immunosuppressive milieu. AQP3, as a water channel impacting cell physiology, may complement this group.

Transcriptional & epigenetic regulators comprise transcription factors and epigenetic modifiers that define immune cell identity and function. The list includes AHR, BACH2, BATF, BATF3, BCL6, BHLHE40, BCL2L11, as well as other nuclear regulators such as NFATC1, FOXO4, FOXP3, GATA3, IKZF1/2, IRF4/7/8, KLF2, KLF6, LEF1, MAF, MYB, NR4A1/3, RORA, RORC, RUNX1/2, STAT1/3/4/5A/6, TBX21, TCF7, PRDM1 and zinc finger proteins (ZBTB16, ZBTB32, ZBTB49, ZEB2, ZNF683).

Signalling, cell-cycle & apoptosis effectors genes that integrate stress, cell-cycle control, and apoptotic signals populate this class. Among these are ATM, CCND3, CDKN1A, BCL2 and its pro-apoptotic family member BCL2L11, as well as regulators such as CAPN3, DUSP1, JUN, MDM4, MKI67, ORC6, PYCARD, FAS and FASLG, TRADD and P2RX7.

The last group of surface & microenvironment interactors encompasses genes encoding receptors, adhesion molecules and extracellular proteins that interface directly with the TME. Notable examples include proteases and adhesion molecules ADAM8, ANXA1, ANXA2, APBB1, CD109, integrins (ITGAL, ITGAM, ITGAX, ITGA1, ITGA4, ITGAE, ITGB7), NCAM1, SELPLG, MS4A1, CD226, CD248, DPP4, CD47, CD48, CD58, CD59, PTPRC, CMKLR1, COL10A1, CORO1A, EZR, LGALS1/3, SELL, and cytoskeletal components (TUBA1A, TUBA1B, TUBB, TUBB4B, VIM, WARS1, WHAMMP3).

This comprehensive mapping not only facilitates downstream analyses of tumour immune phenotypes but also underpins immunogenomic deconvolution approaches that have been validated across numerous transcriptomic datasets in the past decade. Each category is grounded in robust literature that supports its specialised roles in TME regulation, patient prognosis, and immunotherapy response.

After grouping these genes, the mRNA expression data of them were retrieved from the TCGA PanCancer Atlas. This data was organised, and the expression of genes was represented as a cluster heatmap using hierarchical clustering with average linkage and Euclidean distance to reorder genes. A second heatmap (green hue) was then generated for PDL1 correlations (Figure 3.4). Each cancer type in the TCGA PanCancer atlas dataset with a sample size higher than 150 (a total of 21 types of cancer) was analysed. Although correlation and expression heatmaps of melanoma were given here as a reference, heatmaps of other cancer types were provided in the supplementary material since the data is large-scale (Supplementary Figure 1). Yet, the main reason for generating heatmaps was to make the correlations visually testable and to make the calculations relatively easier.

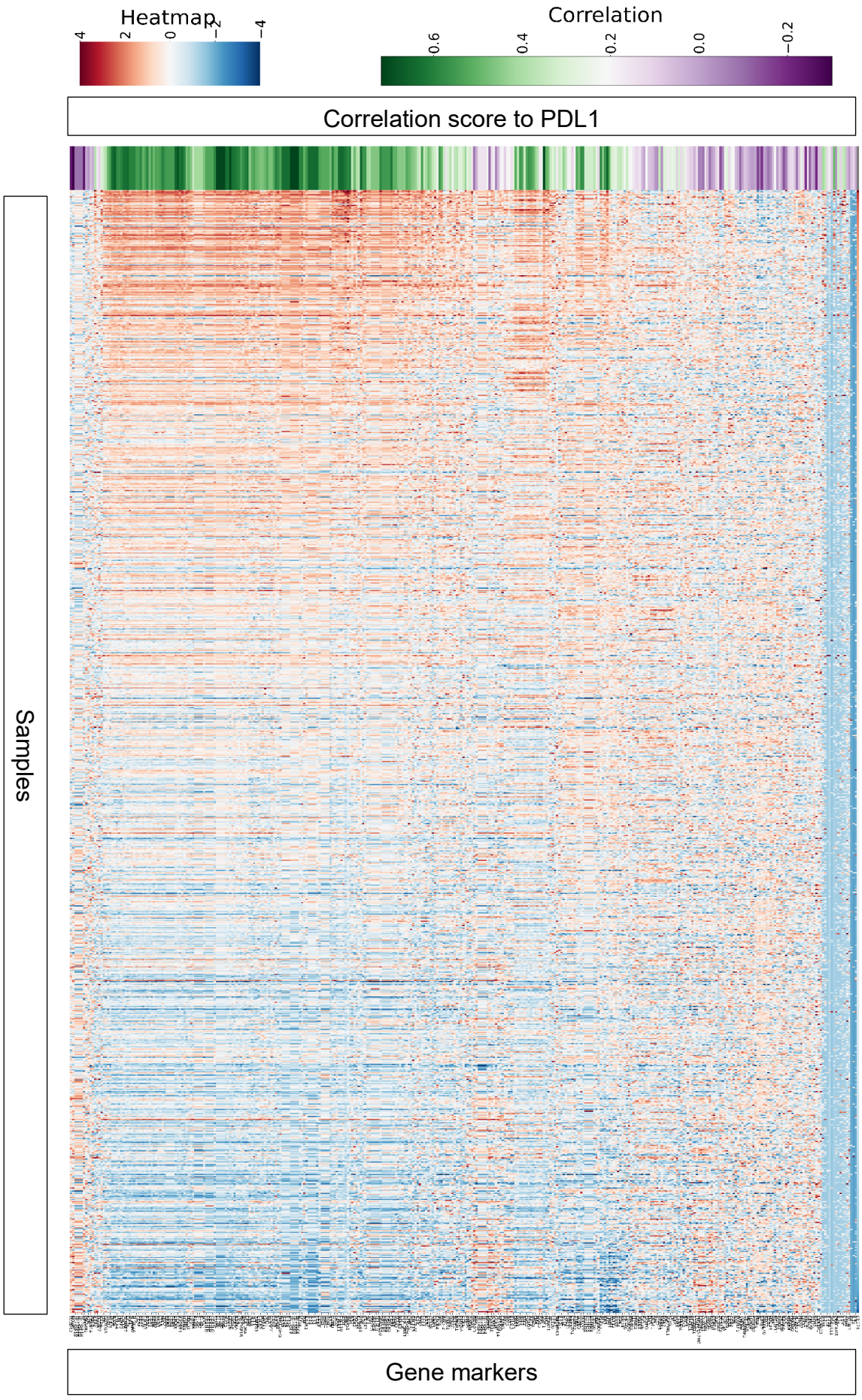
Heatmap
4
2
0
−2
−4
Correlation
0.6
0.4
0.2
0.0
−0.2
Correlation score to PDL1
Samples
Gene markers

Figure 3.4 Immune-related gene expression and PDL1 correlation heatmaps in the melanoma TCGA cohort. Rows represent predefined immune-related genes and columns represent melanoma tumour samples from the TCGA PanCancer Atlas. The analysed immune-related genes are listed in Table 3.3. Gene expression values are shown as dataset-provided mRNA Z-scores in the red/blue heatmap. Genes and samples were reordered by hierarchical clustering using average linkage and Euclidean distance. The accompanying green/purple heatmap shows Pearson correlation coefficients between each gene and PDL1 (CD274), with strong positive association defined as r > 0.5. Heatmaps for the remaining cancer types with sample size ≥150 are provided in Supplementary Figure 1.

3.4 No universal immune signature explains PDL1 expression across the 323-gene panel, but melanoma has its unique set of genes upregulated with PDL1

Pearson correlations (r) were computed between PDL1 and immune-related genes using z-score-normalised expression values. Correlations with r > 0.5 were considered strong positive associations, downloaded for each cancer type, and analysed. The aim was to define solid indicators of PDL1 expression as a biomarker prevalent in every cancer type and also to find out whether any cancer type has a signature gene group correlating to PDL1 expression. The outcome of correlation scores, as well as the strong positive correlations, was analysed. The genes with a higher correlation score than 0.5 were given as a table for each cancer type (Supplementary Table 1).

Melanoma showed the greatest breadth of positive association (n = 128 genes above the threshold, where n represents the number of co-expressed genes individually in that cancer type), followed by breast cancer (n = 101), colorectal cancer (n = 100), bladder cancer (n = 94), and ovarian cancer (n = 93). The number of genes co-expressed with PDL1 ubiquitously in these cancer types was 46. These communally displayed genes were related to T-cell abundance and activation (such as CD3E and CD8A), t-cell activation and effector functions (TAGAP, GZMA, PRF1, GNLY, NKG7, IL10, IL21, IL12, IL2 and its subunits), and the IFNγ-chemokine axis (IFNG with CXCL9/10/11 and CCL5), transcriptional factors such as (STAT1, STAT4, JAK2), and IRF1 and multiple checkpoints (PDCD1, IDO1, TIGIT, HAVCR2, ICOS) also tracked with PDL1, consistent with adaptive up-regulation in inflamed settings. Besides, B-cell and T-cell features, dendritic/NK markers KLRD1 were also represented, indicating a broadly coordinated immune contexture rather than a purely T-cell-restricted signal.

An intermediate group, prostate (n = 67), lung adenocarcinoma (n = 57), cervical (n = 54), stomach (n = 53), thyroid (n=52), head-and-neck squamous (n = 41), and pancreatic (n = 36), retained elements of this programme but with reduced coherence. The intersection across the five high-tier cancers and the intermediate group (excluding pancreatic and thyroid) was exclusively analysed here since it exhibited the greatest shared gene set in downstream analyses. This gene set was comprised of T-cell-related genes (CD8A, CD226, CCR5), interleukins and chemokines closely linked to the PDL1, such as CXCR6, IL2, and IL12, co-receptors such as TIGIT, ICOS, HAVCR2, as well as transcriptional factors (STAT1, JAK2). The insistent prevalence of these genes across 10 cancer types indicates their importance as biomarkers or as indicators of PDL1 expression.

By contrast, the “cold-leaning” group, sarcoma (n=23), brain lower-grade glioma (n = 22), liver hepatocellular carcinoma (n = 13), esophageal (n = 10), glioblastoma (n = 2), kidney clear-cell (n = 1), kidney papillary (n = 1) and lung squamous (n = 1), contained few genes strongly co-varying with PDL1. In these cohorts, IFNγ-linked chemokines and cytotoxic markers were rarely above threshold, and antigen-presentation genes showed weaker coupling to PDL1, indicating limited coordination of the canonical inflamed programme.

Together, these counts (number of genes with $r > 0.5$ versus PDL1) resolve cohort-level differences in relation to immune activation and PDL1. While melanoma, breast, colorectal, bladder, and ovarian form a clearly inflamed relation coordinated together with PDL1, prostate, lung adenocarcinoma, cervical, stomach, head-and-neck, and pancreatic more likely to have a hot-leaning inflammation with fewer genes that are still closely orchestrated with PDL1 expression. Lower-grade glioma, liver, oesophageal, glioblastoma, and renal/squamous cohorts, on the other hand, showed almost no relation of the analysed 323 genes to PDL1 expression, possibly indicating immune-deserted or cold-leaning tumour/tissue types.

These strata motivated further analyses aimed at defining the intersections of cancer types in terms of PDL1-correlated genes. To visualise the extent of overlap across cohorts, we employed an UpSet plot in Python for the downloaded high-correlation files for each cancer type from the expression heatmaps (Figure 3.5). The most striking observation on the UpSet plot was the first bar, representing 15 genes uniquely

associated with melanoma. In addition to the broad set of 128 immune-related genes correlated with PDL1 in this cohort, the presence of a melanoma-specific subset of 15 genes suggests additional molecular cues that may contribute to the well-established responsiveness of melanoma to PD1/PDL1-directed immunotherapies and namely they were CCR3, CD52, CD8B, CORO1A, CLEC9A, GATA3, IL12B, IL18, TOX2, JAML, KLRB1, NCR3, PTGER2, and ZBTB32. Bladder cancer and lower-grade glioma each displayed four unique PDL1-correlated genes, further distinguishing them from other tumour types. Another notable feature was the intersection of 11 leading cancer types (those with the highest numbers of co-expressed genes, top group), which collectively -and exclusively only to those- shared four genes, implying a central role for these genes in regulating PDL1 expression and sustaining an inflamed TME. Beyond these patterns, most cancer types shared only one or two correlated genes, highlighting the absence of a universal immune signature within the analysed 323-gene panel.

Distinctively, JAK2 was consistent across 18 cancer types analysed out of 21. Co-expression of it with PDL1 was not detected only in 3 cohorts: esophageal, kidney renal papillary, and glioblastoma, supporting recent literature that indicates JAK2 induction of PDL1 expression (Carreño-Tarragona *et al.*, 2025; Chen *et al.*, 2022). While JAK2 was found to correlate with PDL1 in 18 cancer types, other genes that followed with high frequency were STAT1 (15), IL2RA (12), IL2RB (13), and IFNG (10).

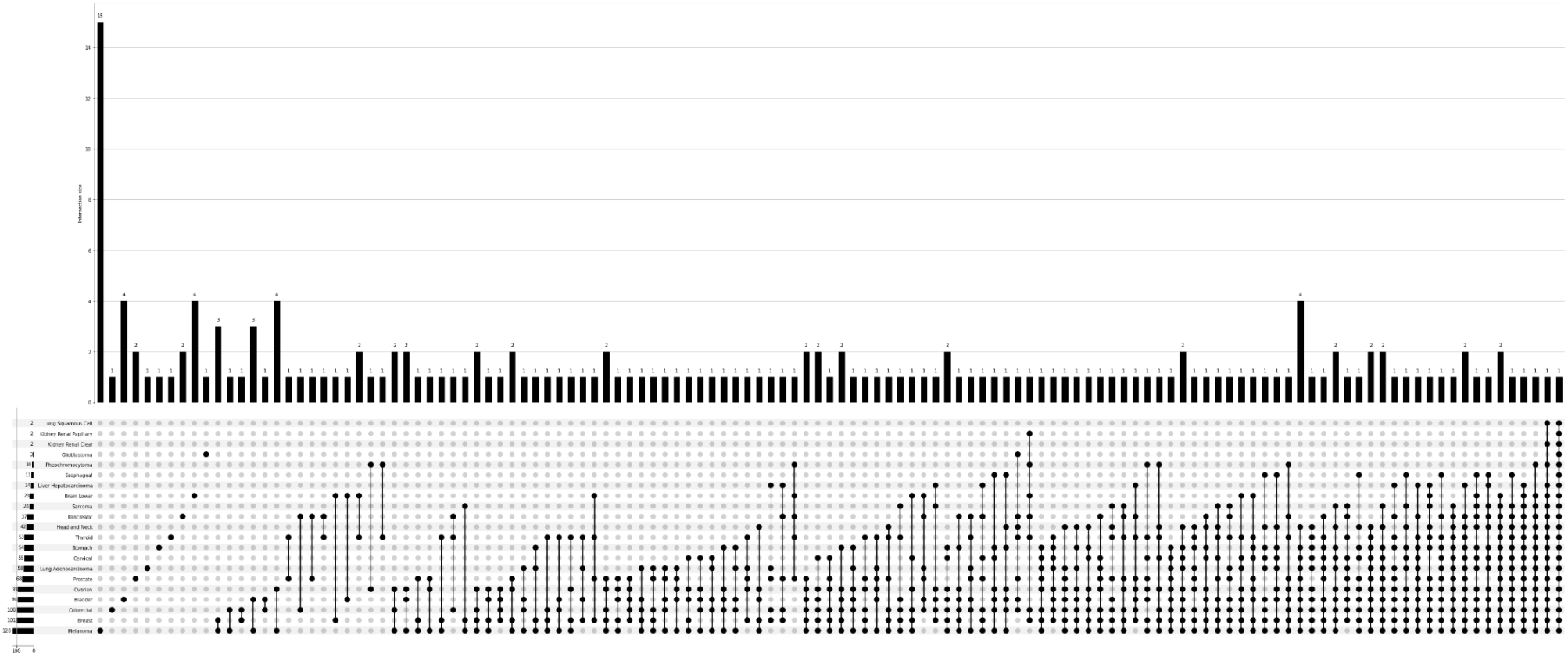

Figure 3.5 UpSet analysis of PDL1-associated gene overlap across 21 TCGA cancer cohorts. UpSet plot illustrating the extent of overlap among genes showing strong positive correlation with PDL1 (CD274) across 21 TCGA PanCancer Atlas cohorts. Correlations were calculated using Pearson correlation coefficients from mRNA z score normalised expression values, and a threshold of $r > 0.5$ was used to define strong positive association. Horizontal bars represent the number of correlated genes identified in each individual cohort, and vertical bars represent the number of genes shared across the cohort combinations indicated by the connected dot matrix below. Counts include PDL1 itself because self-correlation equals 1

3.5 IFNγ upregulates PDL1 expression significantly in assayed cancer cell lines

Co-variation of IFNG (encoding IFNγ) in many cancer types further led us to analyse cancer cell lines commonly used for cancer research. Using surface stain and FACS techniques, we quantified the IFNγ-induced modulation of PDL1 expression across 18 human cancer cell lines representing pancreatic (BxPC3, PancTu1, Colo357), colorectal (RKO, HCT116, LoVo), breast (MCF7, T47-D, MDA-MB-231), prostate (PC3, LNCaP,Du145) , myeloma (MM.1R, MM.1S, U266) and assorted group cancer types. 3 cancer cell lines were employed for each group, and the assorted group was comprised of lung adenocarcinoma (A549), cervical carcinoma (HeLa), and ovarian cancer (A2780) cancer types. For each cell line, triplicate measurements were taken from both anti-PDL1-stained samples and isotype-stained samples under 2 conditions: control and IFNγ-treated. MFI ratio was computed as MFI of the anti-PDL1-stained sample divided by the MFI of the isotype-stained sample.

Statistical analysis via one-way ANOVA revealed that 15 cell lines out of 18 exhibited significant IFNγ-induced PD1/PDL1 modulation, specifically BxPC3, PancTu1, Colo357, HCT116, LoVo, MCF-7, T47-D, PC-3, LnCap, MM.1R, MM.1S, U266, HeLa, A549, and A2780 (Figure 3.6B). Within this subset, the most significant PDL1 expression increase was observed in the colorectal cancer cell line HCT116 ($p < 9e-07$), and it was followed by another colorectal cell line LoVo ($p < 6e-06$) and a prostate cancer cell line PC-3 ($p < 2e-05$). In contrast, no significant changes were observed in the RKO, T47-D, and HeLa cell lines.

The lowest basal PDL1 expression was observed in the BxPC3 cell line, with a median MFI ratio of 0.33. Across all cell lines except the outliers (RKO and MDA-MB-231), the overall median MFI ratio was 1.34, with an interquartile range of 0.33 to 2.59 for control groups. Notably, RKO and MDA-MB-231 displayed markedly high basal PDL1 MFI ratio values (approximately 24.84 and 8.05, respectively), potentially diminishing the relative impact of IFNγ stimulation; however, MDA-MB-231 exhibited a modest increase with a p-value of 0.0039. To accommodate pronounced baseline values and p-values, the same data was also represented in a box plot orientation, denoting certain outliers with a graphical axis break introduced at 12, thereby enabling a comprehensive visual representation of the data (Figure 3.6B).

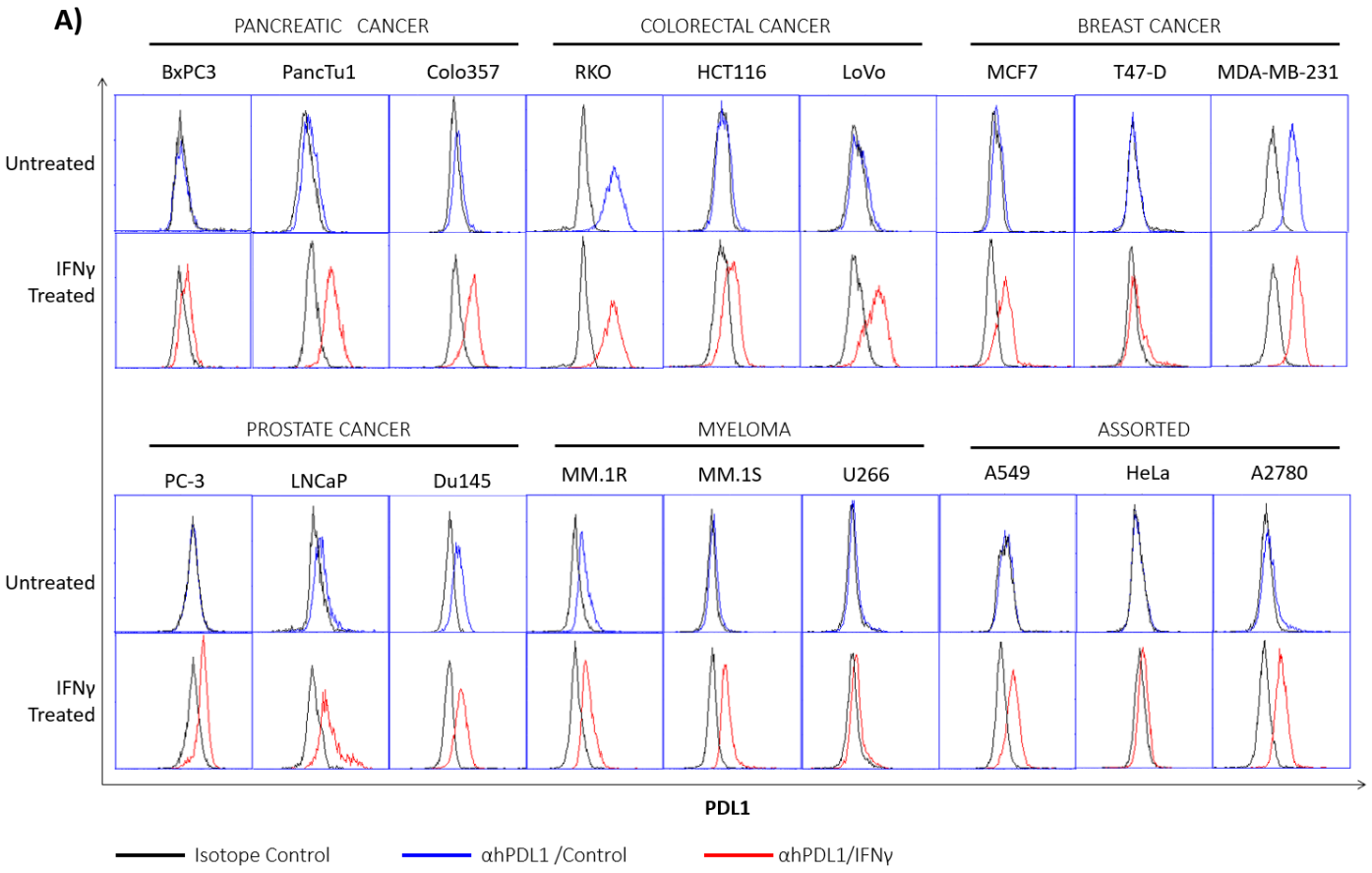
A)
PANCREATIC CANCER
COLORECTAL CANCER
BREAST CANCER
BxPC3
PancTu1
Colo357
RKO
HCT116
LoVo
MCF7
T47-D
MDA-MB-231
Untreated
IFNγ Treated
PROSTATE CANCER
MYELOMA
ASSORTED
PC-3
LNCaP
Du145
MM.1R
MM.1S
U266
A549
HeLa
A2780
PDL1
Isotope Control
αhPDL1 /Control
αhPDL1/IFNγ

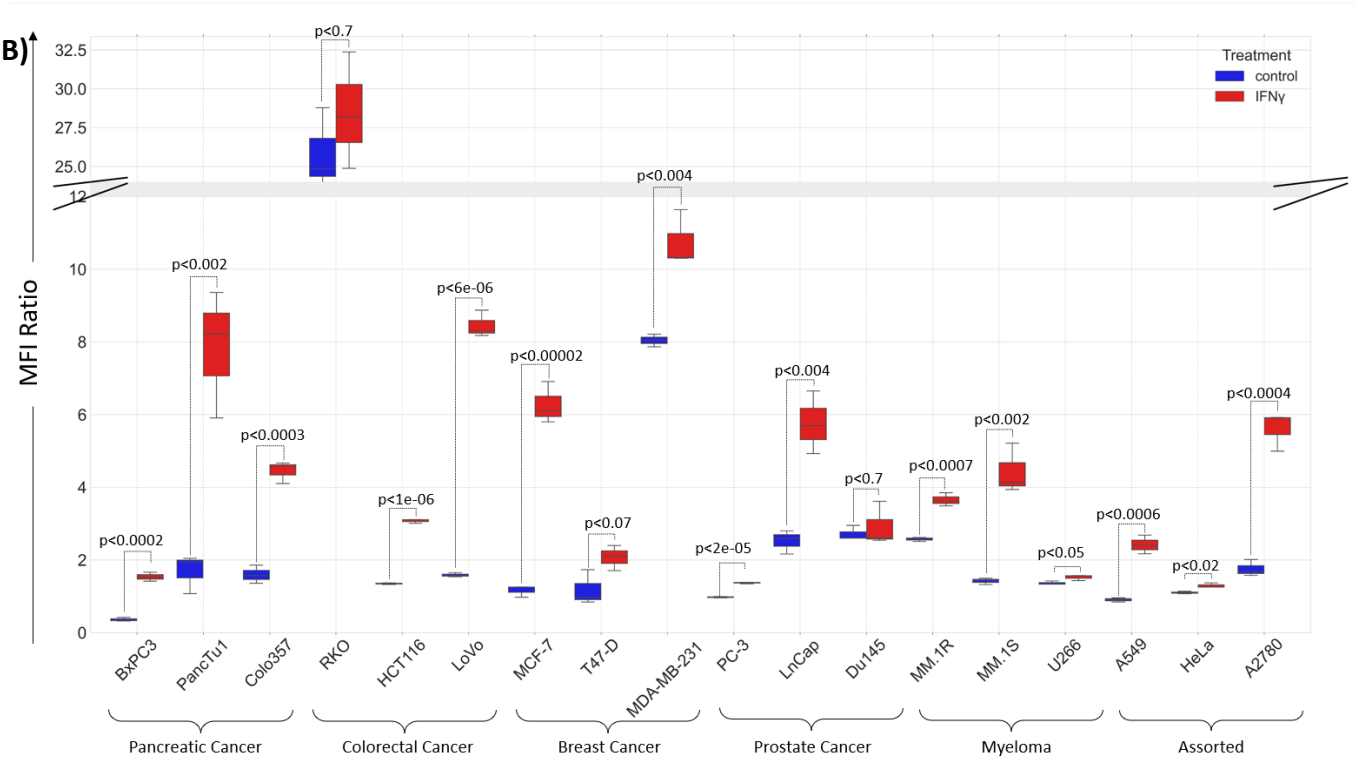
B)
MFI Ratio
Treatment
control
IFNγ
p<0.7
p<0.004
p<0.002
p<6e-06
p<0.00002
p<0.004
p<0.0003
p<0.0002
p<1e-06
p<0.07
p<2e-05
p<0.7
p<0.0007
p<0.002
p<0.0004
p<0.0006
p<0.05
p<0.02
BxPC3
PancTu1
Colo357
RKO
HCT116
LoVo
MCF-7
T47-D
MDA-MB-231
PC-3
LnCap
Du145
MM.1R
MM.1S
U266
A549
HeLa
A2780
Pancreatic Cancer
Colorectal Cancer
Breast Cancer
Prostate Cancer
Myeloma
Assorted

Figure 3.6 Surface PDL1 expression in human cancer cell lines under control and IFNγ treated conditions. Cell surface PDL1 expression was assessed by antibody staining and flow cytometric analysis across 18 human cancer cell lines. PDL1 expression is presented as MFI ratio, calculated as the MFI of anti-hPDL1-stained cells divided by that of isotype-stained cells, with n = 3 replicates per condition. Statistical analysis was performed by one-way ANOVA, with $p < 0.05$ considered significant. **A)** Representative histograms showing anti-hPDL1 and isotype control staining under untreated and IFNγ-treated conditions. **B)** Box plot quantifying the same experiment shown in panel A, allowing comparison of basal PDL1 expression and IFNγ-induced change across the analysed cell lines. This panel facilitates comparison of both basal PDL1 expression and IFNγ-induced change across the analysed cell lines. An axis break at 12 was applied to improve visualisation of high basal expression values.

3.6 Cancer cell lines do not exhibit PD1 on their surface

The transcription of PDCD1, the gene encoding PD1, has been observed in cancer cells, and it was also evidenced that PD1 expression in cancer cells is primarily intrinsic. Findings on clinical tumour specimens support this. and the increasing body of evidence that cancer cell-derived PD1 also plays a role in immune evasion and tumour progression (Hanamura et al., 2021; Wang et al., 2020). We wondered whether PD1 is also expressed on the surface of any cancer cell line that expresses PDL1. Consequently, the cell surface expression of PD1 was investigated on a panel of 18 cancer cell lines representing 9 different cancer types.

4×10^5 cells were harvested and stained either with PE-conjugated human anti-PD1 antibody to assess cell surface expression of PD1 or with its isotype antibody to assess nonspecific binding. Flow cytometry analysis revealed a lack of cell surface PD1 expression on the studied cancer cells (Figure 3.7).

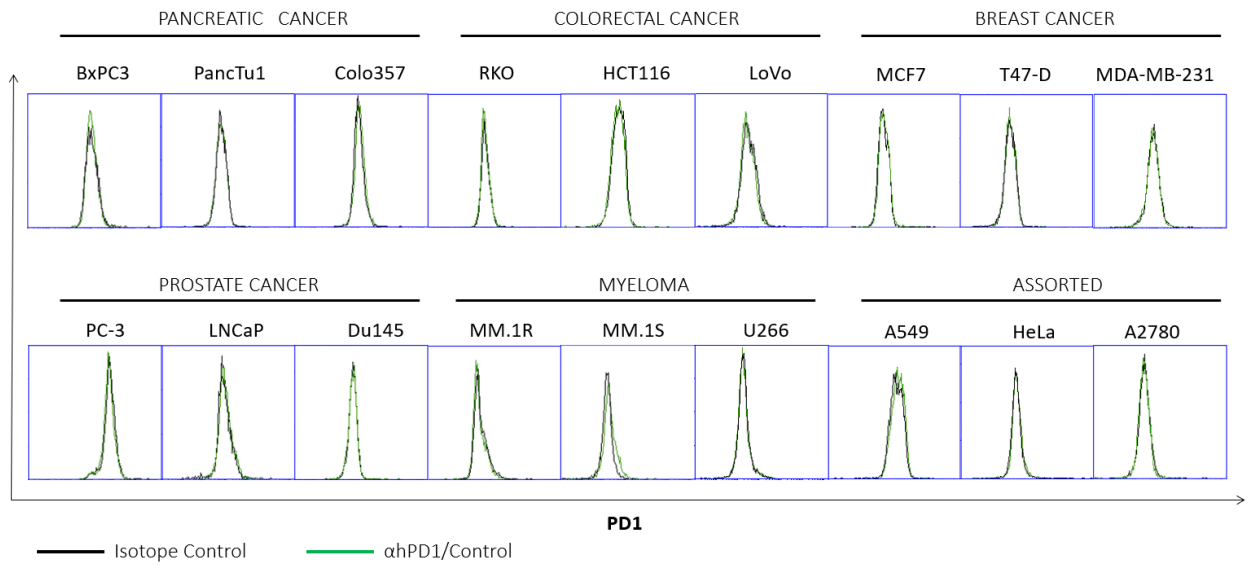

Figure 3.7 Surface PD1 staining in a panel of human cancer cell lines. Cell surface staining and flow cytometric analysis were used to assess PD1 expression across 18 human cancer cell lines representing nine cancer types. Cells were stained with PE-conjugated anti-hPD1 antibody or the corresponding isotype control. In the histograms, the green line represents anti-hPD1 staining and the black line represents the isotype control. Representative histograms for the analysed cell lines are shown.

Collectively, analyses of PD1/PDL1 expression across cancer types underscore the need for patient stratification by immune contexture when deploying anti-PD1/PDL1 therapies. Sensitivity is heterogeneous both between and within histology. Melanoma and subsets of colorectal and breast cancers tend to respond more readily when a pre-existing T-cell-inflamed microenvironment, intact IFNγ signalling, and preserved antigen-presentation machinery are present. Nevertheless, durable benefit remains limited for many patients owing to primary and acquired resistance mechanisms, including paucity of cytotoxic T-cell infiltration, defects in IFNγ-JAK/STAT or antigen-presentation pathways, compensatory checkpoints (such as LAG3, TIGIT), immunosuppressive myeloid and stromal programmes, and metabolic or hypoxic constraints. These observations argue for context-aware selection guided by composite biomarkers that integrate PDL1 protein levels with immune gene-expression signatures, spatial metrics, and genomic features, and for rational combinations tailored to tumour immune state.

In the subsequent chapter, an infiltration-ready refinement of anti-PDL1 therapy is proposed, elevating engineered MSCs to deliver a high-affinity soluble PD1 variant ($PD1^{HAC}$) to intensify local PD1/PDL1 blockade, which has the possibility to convert cold tumours toward an inflamed state with conditioned MSC infiltration and minimise systemic exposure to antibodies.

CHAPTER 4: MSC-Secreted sPD1^{HAC} Variant Blocks the PD1/PDL1 Pathway

Immune checkpoint therapies targeting the PD1/PDL1 pathway have transformed cancer treatment with effective results in various cancer types, yet important limitations persist, including tumour penetration, binding affinity, and barriers imposed by the TME. Additional challenges include immune-related adverse events and the emergence of resistance to ICB therapies. Multiple classes of PD1/PDL1 blockers have therefore been explored, ranging from PD1-derived peptides to small molecule inhibitors, bispecific antibodies, and engineered T-cells. Among non-antibody formats, the high-affinity consensus (HAC) variant, described by Maute and his colleagues, exhibits markedly increased PD1-PDL1 binding in surface plasmon resonance assays. This chapter carries that study further into a cell-based, biologically more relevant environment and evaluates whether HAC engineered as a soluble PD1 (sPD1^{HAC}) can be efficiently secreted by cells without compromising cell health, and whether sPD1^{HAC} (with a particular interest in the MSC-derived version) can block the PD1/PDL1 pathway in vitro and in vivo.

4.1 sPD1^{HAC}, constructed with a hIgG1-Fc domain and expressed into CHO/HEK293T cells, provides high secretion yield and stability

In the very first step of structuring a therapeutic PD1 cell therapy, the extracellular domain of human PD1 was utilised as a base to carry point mutations that the HAC variant acquires. Extracellular domain of PD1 inserted into pFUSE plasmid right after a signal peptide and furin cleavage site without mutations, representing our wild-type PD1, and with mutations, representing HAC variant. Then they were inserted into pFUSE, enabling cloning into CHO and HEK293T cells in two different ways (with or without a stop codon between hIgG1-Fc domain and PD1 ectodomain) to determine whether extension of hIgG1-Fc can alter the secretion or stability of the PD1 secretion.

4.1.1 sPD1^{HAC} constructs (+/− hIgG1) were successfully engineered.

The full-length PD1 is a type I membrane receptor consisting of 288 amino acids. Extracellular domain, including N-loop, Stalk region, and IgGV domain, was used for the generation of soluble wild-type and HAC variant (Figure 4.1A) since these parts have binding sites of the protein that interacts with PDL1 and PDL2. The goal was to

convert the PD1 protein to a form that can be secreted by cells rather than remaining membrane bound. To ensure that this truncated PD1 could be expressed and secreted effectively by cells, the signal peptide (SP) from the human Fibrillin protein (aa 1- aa 27) was introduced together with a Furin cleavage site (FC Site). Furin is a protease that processes proteins within the secretory pathway, facilitating the secretion of the modified PD1 protein. This modified construct was referred to as $sPD1^{WT}$ or WT in the text. To create the $sPD1^{HAC}$ variant, site-directed mutagenesis was performed on the $sPD1^{WT}$ construct. Specifically, 10-point mutations (in aa. positions of the 64,65,66,68,70,74,78,122,125,132) were introduced as described by Maute and his colleagues, which are known to enhance the binding capabilities of the PD1 protein (Figure 4.1A). The resulting construct, now referred to as $sPD1^{HAC}$ or HAC from here on, retains the extracellular domain but has enhanced binding properties due to the introduced mutations. By engineering the PD1 protein to be secreted and incorporating specific mutations to enhance its binding affinity, we have created a version of PD1 ($sPD1^{HAC}$) that can be evaluated for its therapeutic potential, particularly when carried by MSCs. This form is expected to be more convenient to inspect its binding capabilities to its targets in a biological context, thereby offering promising therapeutic applications.

To determine the optimal configuration for maximal secretion yield of our PD1 constructs, we investigated the necessity of linkage to the IgG1-Fc domain within the pFUSE vector. Specifically, we introduced a stop codon to our PD1 constructs, interfering truncated PD1 and hIgG1-Fc domain in the pFUSE to assess the stability and secretion efficiency of the protein without this domain, which was named pFUSE.stPD1 (stHAC and stWT in the secreted form). The IgG1-Fc fusion construct was named pFUSE.sPD1 (HAC and WT in the secreted form) for the following assays (Figure 4.1B).

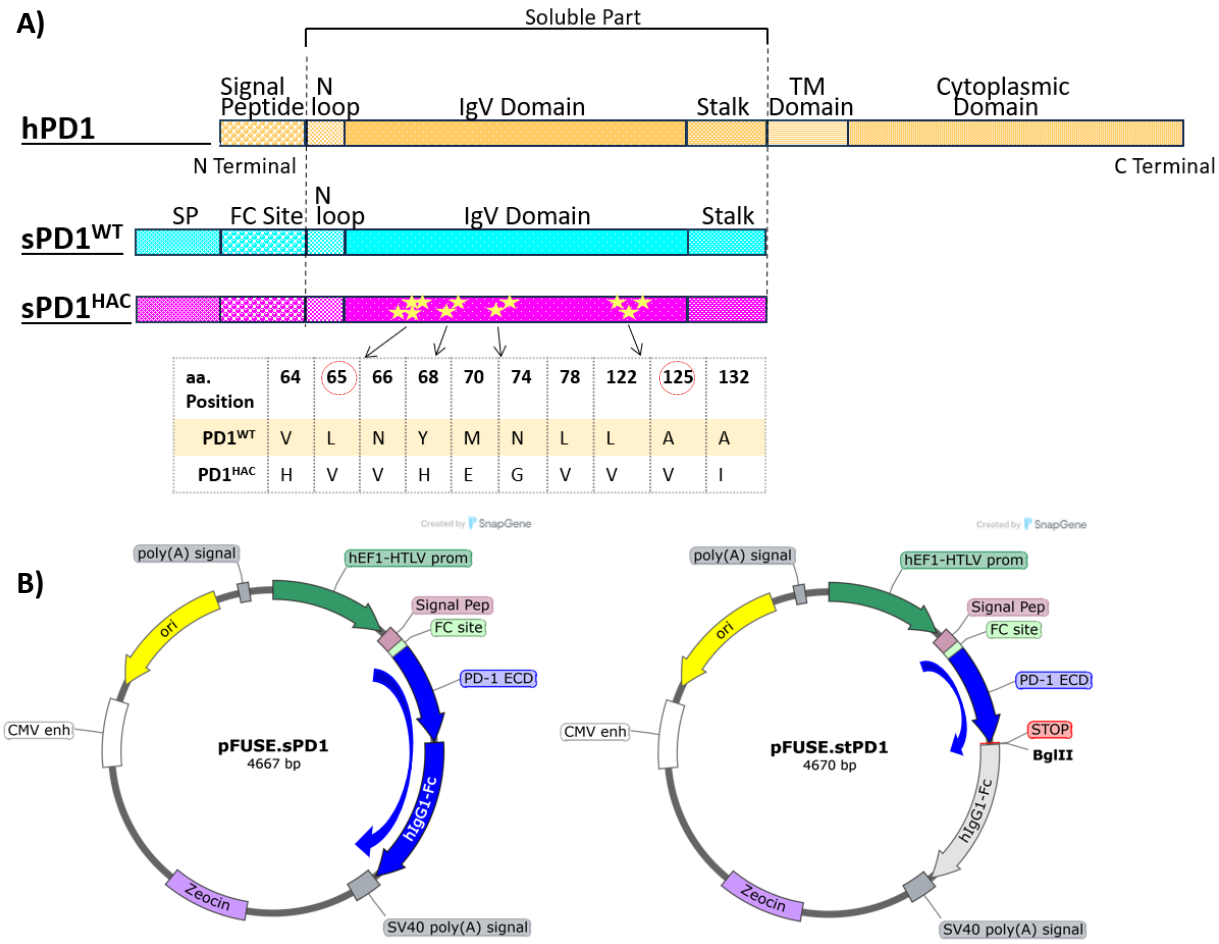

Figure 4.1 Design of sPD1^{WT} and PD1^{HAC} constructs with and without hIgG1-Fc fusion. A) Depiction of sPD1 constructs compared with the full-length human PD1 and 10-point mutation indicated by yellow stars on the PD1 extracellular domain. Below the sPD1^{HAC} construct, amino acid substitutions of the PD1^{HAC} were given together with the corresponding aa. residues on the wild-type PD1. Red-circled residues are core mutation residues, and remaining labelled residues indicate PDL1 interaction sites. **B)** pFUSE plasmid structures were depicted for pFUSE.sPD1 and pFUSE.stPD1, containing signal peptide (SP), Furin cleavage (FC) site, sPD1 constructs (PD1 ECD), and either stop codon or hIgG1-Fc domain.

4.1.2 IgG1-Fc fusion enhances sPD1^{HAC} secretion and stability.

Generated sPD1^{HAC} and sPD1^{WT} constructs with or without IgG1-Fc fusion were introduced into HEK293T and CHO cells by lipid transfection method, as in pFUSE plasmids, which facilitates the entry of the plasmid DNA into the cells (Figure 4.2A). Post-transfection, cells were cultured for 48 hours under standardized conditions, and supernatants were harvested for analysis. Secretion levels of the PD1 were quantified using human PD1 duo set ELISA and were given as secretion fold change between

groups, specifically, as a secretion ratio of IgG1 attached PD1s (HAC/WT) to the stop codon introduced PD1s (stHAC/stWT).

Quantitative analysis of the ELISA results revealed significantly high expression and secretion levels of both HAC and WT when they were linked to the IgG1 domain compared to their counterparts without IgG1 fusion (Figure 4.2B). Secretion of WT increased the PD1 yield significantly, by around 2-fold, either expressed by CHO or HEK293T cells ($p < 0.06$ and $p < 0.002$, respectively). HAC variant showed approximately 3.5-fold and 5.5-fold increases when expressed in CHO and HEK293T cells, with $p < 0.006$ and $p < 0.0004$, respectively.

Therefore, our results conclusively demonstrate that to achieve efficient production and maximal secretion of recombinant PD1 protein, the PD1 fragment must be positioned adjacent to the IgG1 domain within the pFUSE plasmid. This strategic placement likely facilitates more efficient trafficking and secretion of the PD1 protein, enhancing its yield and stability.

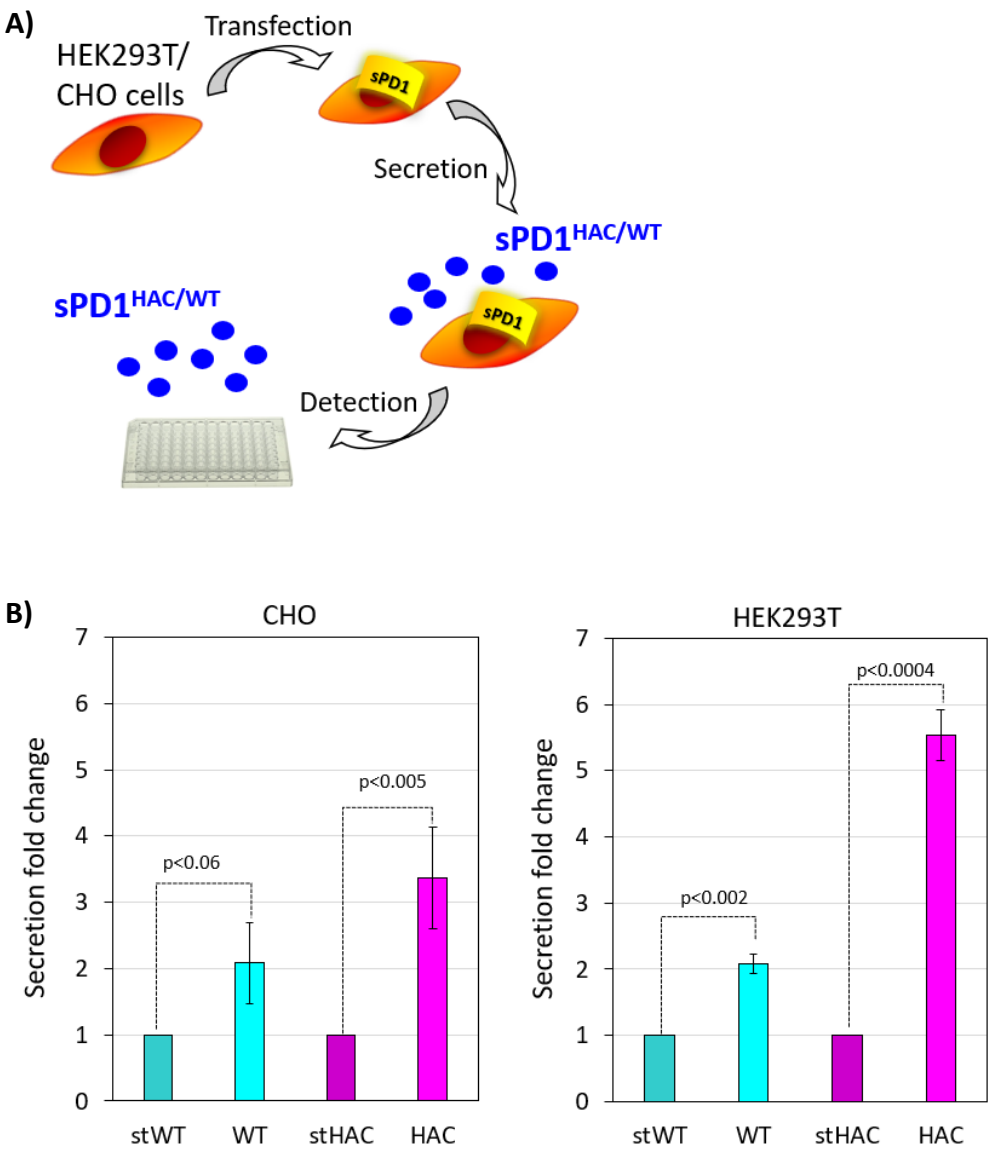

Figure 4.2 Secretion of IgG1-fused and non-fused sPD1 variants in HEK293T and CHO producer cell lines. A) Schematic overview of the transfection and secretion assay. HEK293T and CHO producer cell lines were transfected with pFUSE constructs encoding sPD1WT or sPD1^{HAC} either with hIgG1-Fc fusion (WT, HAC; light-coloured bars) or without hIgG1-Fc fusion through insertion of a stop codon (stWT, stHAC; dark-coloured bars). Secreted PD1 in conditioned supernatants was quantified by ELISA. **B)** Bar charts show secretion fold change relative to the corresponding non-IgG1 construct in HEK293T and CHO producer cell lines. Data are presented from three independent experiments (n = 3), and exact p-values are indicated on the figure.

4.1.3 Transient expression in CHO and HEK293T was robust without compromising viability.

To evaluate the capability of our construct to be inserted and expressed in cells, we initially cloned the constructs into CHO and HEK293T cells. These cell lines were chosen for their high transfection efficiency and common use in protein expression studies. Continuing with IgG1 fusion proteins, sPD1^{HAC} and sPD1^{WT} plasmids were inserted into these cell lines by lipid transfection. Then, PD1 secretion capabilities were evaluated by ELISA.

Supernatants were collected 48 hours post-transfection, and the presence of PD1 was assessed using a human PD1-specific ELISA. PD1 secretion was subsequently quantified by measuring absorbance at 450 nm with a microplate spectrophotometer. In HEK293T cells, sPD1^{HAC} was secreted at 8,143 ± 644 ng/mL compared with 6,940 ± 988 ng/mL for sPD1^{WT}. By contrast, secretion yields in CHO cells exhibited lower secretion levels, reaching 3,408 ± 219 ng/mL for sPD1^{HAC} and 2,789 ± 317 ng/mL for sPD1^{WT} **(**Figure 4.3A). This discrepancy may reflect differences between human (HEK293T) and murine (CHO) protein processing machinery, which can influence folding efficiency and secretion yields.

To exclude transfection-related cytotoxicity, cell viability was assessed using the Nicoletti DNA hypodiploidy assay, which detects the sub-G1 fraction generated by apoptotic DNA fragmentation. 48 hours post-transfection, CHO and HEK293T cultures expressing sPD1^{HAC} or sPD1^{WT} were harvested, stained with propidium iodide, and profiled by flow cytometry. Under these conditions, both producer lines retained high viability. In HEK293T cells, the viable (non-hypodiploid) population constituted 94.9 ± 2.8% for sPD1^{HAC} and 95.2 ± 2.8% for sPD1^{WT}, with small sub-G1 fractions (~2-3%); in CHO cells, viability was likewise high at 91.5 ± 1.3% and 90 ± 2.6 % for sPD1^{HAC} and sPD1^{WT}, respectively (Figure 4.3B). No material differences were observed between constructs or cell lines beyond minor variation typical of transfection procedures, indicating that expression of the sPD1 variants did not measurably compromise producer-cell viability over the assay window.

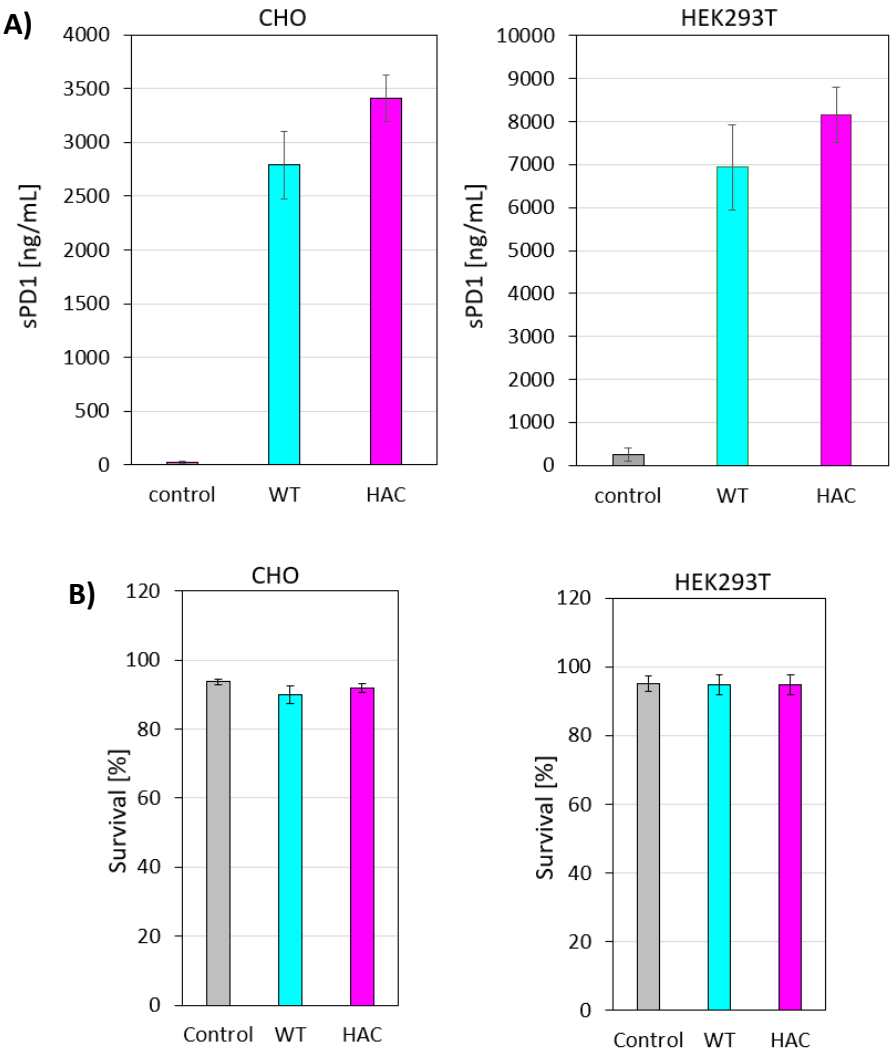

Figure 4.3 PD1 secretion and viability of transfected HEK293T and CHO producer cell lines. A) PD1 concentrations measured in supernatants collected from untransfected control, sPD1^{WT}-transfected, and sPD1^{HAC}-transfected HEK293T and CHO producer cell lines at 48 h post-transfection. **B)** Cell viability analysis of matched transfected HEK293T and CHO producer cell lines. Data are presented for control, sPD1^{WT}, and sPD1^{HAC} conditions from three independent experiments (n = 3).

4.2 sPD1^{HAC} inhibits rhPD1-PDL1 binding

The binding of rhPD1 to PDL1 was decreased 77-94% when it was competed with various concentrations of sPD1^{HAC} derived from CHO and HEK293T cells, except the smallest concentration of 0.1 ng/well (which corresponds to a 1:500 ratio of rhPD1). This reduction was consistent in both solid-phase and cell-based assays.

4.2.1 sPD1^{HAC} selectively engaged PDL1 but not PDL2 and blocked rhPD1-PDL1 binding in solid-phase assays

As transfection did not measurably compromise producer-cell viability (~95% viable by Nicoletti), conditioned supernatants were next evaluated in a solid-phase binding competition assay to determine whether sPD1 variants inhibit biotinylated rhPD1 binding to immobilised hPDL1-Fc or hPDL2-Fc. In this assay, rhPD1 was used at a fixed amount of 50 ng/well, whereas sPD1 variants derived from CHO or HEK293T producer cell lines were tested across titrations of 40, 20, 10, 5, 1, 0.5, and 0.1 ng/well. The assay workflow is shown in Figure 4.4A. Signals obtained in the presence of control (untransfected supernatant in equal volumes to the samples and 50ng rhPD1) were normalised to 100% binding and served as the reference for calculating percent inhibition across the titrations.

When the competition was done for the second ligand (immobilised hPDL2-Fc), neither HAC variant nor WT was able to compete against rhPD1 binding, showing equivalent signals to positive controls (Figure 4.4B). This effectiveness was observed for both CHO- and HEK293T-derived sPD1 variants. It is concluded that, likewise, sPD1^{WT}, sPD1^{HAC} had minimal or no effect on PDL2-rhPD1 binding in measured concentrations: 40, 20, 10, 5, and 1 ng.

In the case of immobilised hPDL1-Fc, the HEK293T-derived sPD1^{HAC} variant demonstrated a strong inhibitory effect on rhPD1 binding to PDL1, whereas sPD1^{WT} showed no measurable inhibition, with signals almost indistinguishable from the untransfected control across the titrations apart from small fluctuations attributable to assay noise. At a concentration of 40 ng rhPD1, the binding was reduced to approximately 8% of the control, signifying that 92% of PDL1 was effectively occupied by the sPD1^{HAC} variant.

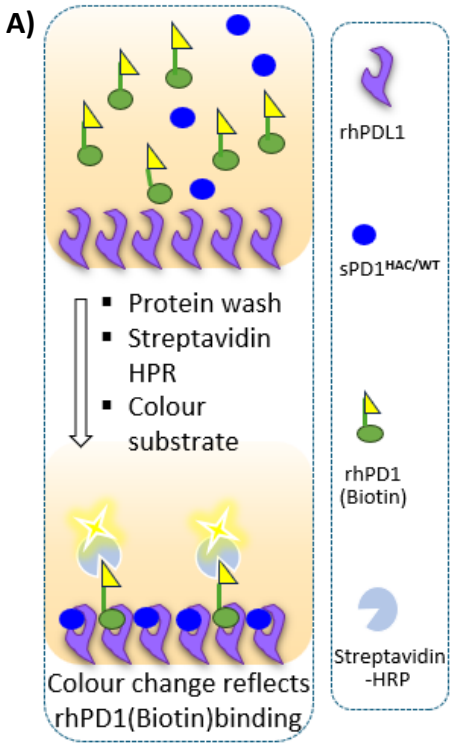

Figure 4.4 Solid-phase competition assay for rhPD1 interaction with immobilised PDL1 and PDL2 in the presence of sPD1 variants. Supernatants containing graded amounts of sPD1 variants (40, 20, 10, 5, 1, 0.5, and 0.1 ng per well) derived from CHO (upper bar charts) or HEK293T (lower bar charts) producer cell lines were tested in a solid-phase binding competition assay. sPD1^{HAC} is shown in magenta, sPD1^{WT} in cyan, and matched untransfected control in grey. **A)** Assay workflow. High-binding plates were coated with recombinant hPDL1-Fc or hPDL2-Fc (50 ng per well), incubated with biotinylated rhPD1 (50 ng per well) premixed with the indicated supernatants, and bound rhPD1 was detected using streptavidin-HRP with absorbance read at 450 nm. **B)** Competition assay using immobilised hPDL2-Fc. **C)** Competition assay using immobilised hPDL1-Fc. Binding was normalised to control wells containing rhPD1 with matched untransfected supernatant, defined as 100%. Exact p-values are indicated in the figures where applicable. Data are presented as mean ± SE from three independent experiments.

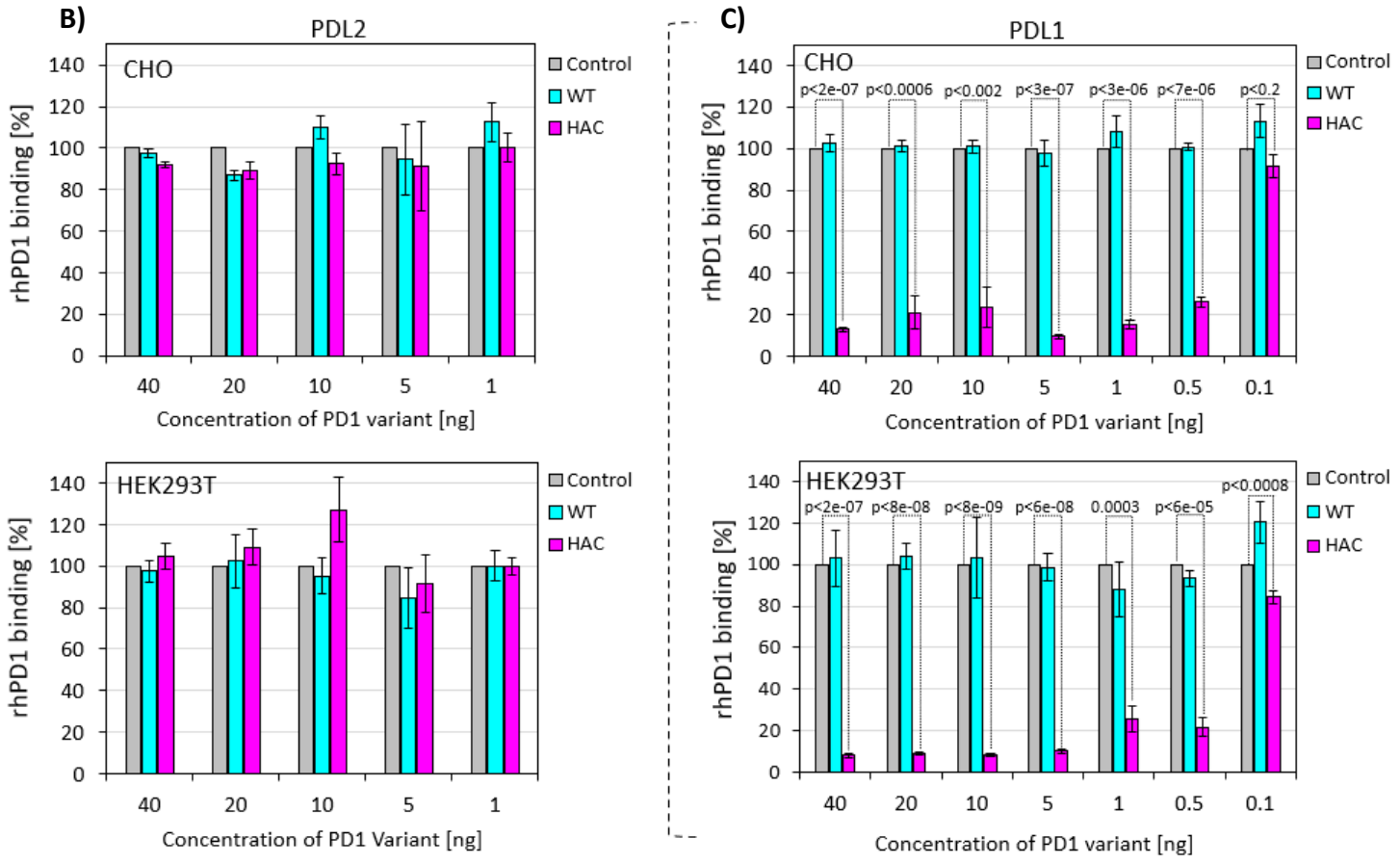

Lower concentrations, such as 20 ng, 10 ng, and 5 ng, exhibited similar binding reductions to 9%, 8.4%, and 10.2 % respectively. Even with 1 ng and 0.5 ng of $sPD1^{HAC}$ concentrations, rhPD1 binding was reduced to approximately 74% and 78%, respectively. All these decreases were statistically significant when compared to controls, highlighting the robust efficacy of the HEK293T-derived $sPD1^{HAC}$ variant in disrupting the PD1/PDL1 interaction (Figure 4.4C).

Although the extent of inhibition was relatively lower than observed in HEK293T supernatants, CHO-derived $sPD1^{HAC}$ significantly reduced rhPD1-PDL1 binding at all concentrations except 0.1 ng (Figure 4.4C). In the presence of $sPD1^{HAC}$, residual rhPD1 binding was approximately 17%, 20%, 22%, 10%, 18%, and 23% at 40, 20, 10, 5, 1, and 0.5 ng, respectively, corresponding to a consistent inhibition of 77-90%. Notably, this effect was maintained even when $sPD1^{HAC}$ was applied at a 100-fold lower concentration than rhPD1. By contrast, $sPD1^{WT}$ showed no measurable inhibition, yielding binding values comparable to the positive control irrespective of the producer cell line.

4.2.2 Cell-based binding competition assay was established utilising RKO cells and 4000 ng rhPD1

Whether derived from CHO or HEK293T, the HAC variant was approved to block the rhPD1-PDL1 pathway on cell-free assays. To investigate if it can show the same competitive binding for PDL1 on the surface of cancer cells, a cell-based assay was established. In this assay, a cancer cell line with high PDL1 expression (to ensure flow cytometric visibility of the binding) and the concentration of rhPD1 that can occupy all the ligands on this cancer cell line needed to be unveiled. For the cancer cell line determination, we referred to our PDL1 detection study on cancer cell lines, and RKO cells were the straightforward candidate with significantly high PDL1 expression without any interference. Therefore, RKO cells were chosen as they were expected to provide an extended interval from the isotype control signal to the bound biotinylated rhPD1 signal, thereby giving enough space for visualising the reduction.

To establish a saturating dose of rhPD1 for on-cell binding, the standard cell-based competition assay was run on RKO cells in the absence of any PD1 competitor. Cells

stained with streptavidin-PE alone served as the negative control. Biotinylated rhPD1 was titrated (50, 100, 250, 500, 1000, 2000, 3000, and 4000 ng per $4x10^5$ cells). Signal intensity increased monotonically with concentration up to ~3000 ng and then approached saturation (Figure 4.5). Signals at 3000 and 4000 ng were indistinguishable, indicating receptor saturation. Therefore, 4000 ng was selected as the saturating rhPD1 amount for subsequent RKO assays.

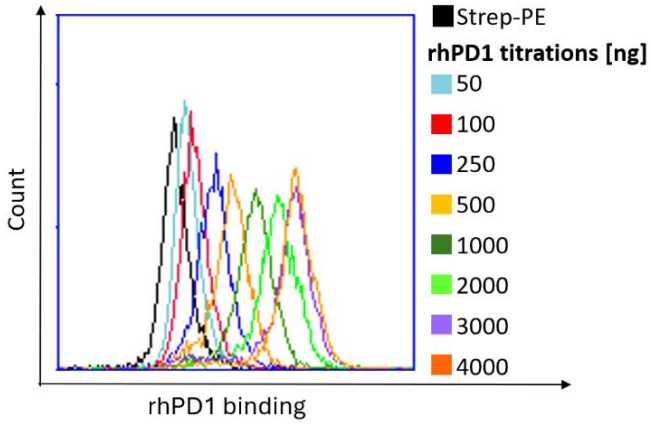

Figure 4.5 Titration of biotinylated rhPD1 binding to RKO cells for the cell-based competition assay. Overlaid PE histograms showing binding of biotinylated rhPD1 to $4x10^5$ RKO cells following titration of 50, 100, 250, 500, 1000, 2000, 3000, and 4000 ng rhPD1 per sample (100 µL). Streptavidin-PE only is shown in black as the negative control. Histograms represent streptavidin-PE fluorescence corresponding to bound biotinylated rhPD1 on the cell surface. This titration was used to define the rhPD1 input for subsequent cell-based competition assays on RKO cells.

4.2.3 HEK293T- and CHO- derived $sPD1^{HAC}$ outcompetes rhPD1 on the cell surface

To further substantiate the supremacy of $sPD1^{HAC}$ binding on rhPD1-PDL1 interaction, cell-based binding competition was designed. In brief, cell-based competition was quantified as the percentage of rhPD1 binding to membrane-bound PDL1 relative to the positive control. Test samples contained rhPD1 co-incubated with a competitor ($sPD1^{HAC}$ or $sPD1^{WT}$). The positive binding control contained rhPD1 without a competitor, and the negative control omitted biotinylated rhPD1 and sPD1 variants (streptavidin-PE only). Bound biotinylated rhPD1 4,000 was detected with streptavidin-PE. An overview of the experimental design is shown in Figure 4.6A.

In cell-based binding competitions, sPD1^{HAC} inhibited rhPD1 binding irrespective of the sourced cell line. In the flow cytometry histogram results, which display the single-cell distribution of streptavidin-PE fluorescence (x-axis, biotinylated rhPD1 bound to PDL1 on the RKO cells) against event count (y-axis), the magenta line (sPD1^{HAC} mixed sample) was overlapped with the black line (negative control, lack of PD1), indicating significant binding reduction. On the contrary, the cyan line (sPD1^{WT} mixed sample) overlapped with the blue line (positive control, only biotinylated rhPD1), indicating limited inhibition and retention of the majority of the binding signal. Binding was quantified across biological replicates as a percentage of rhPD1 binding (mean ± SE) after background subtraction. For each sample, the MFI value was first corrected by subtracting the negative-control MFI and then expressed relative to the background-subtracted positive control. In agreement with the histogram shifts, HEK293T- and CHO-derived HAC significantly reduced binding to 6% and 8% respectively, while WT reduced it to 90% and 86% respectively, as an average result of three independent experiments (Figure 4.6B and C).

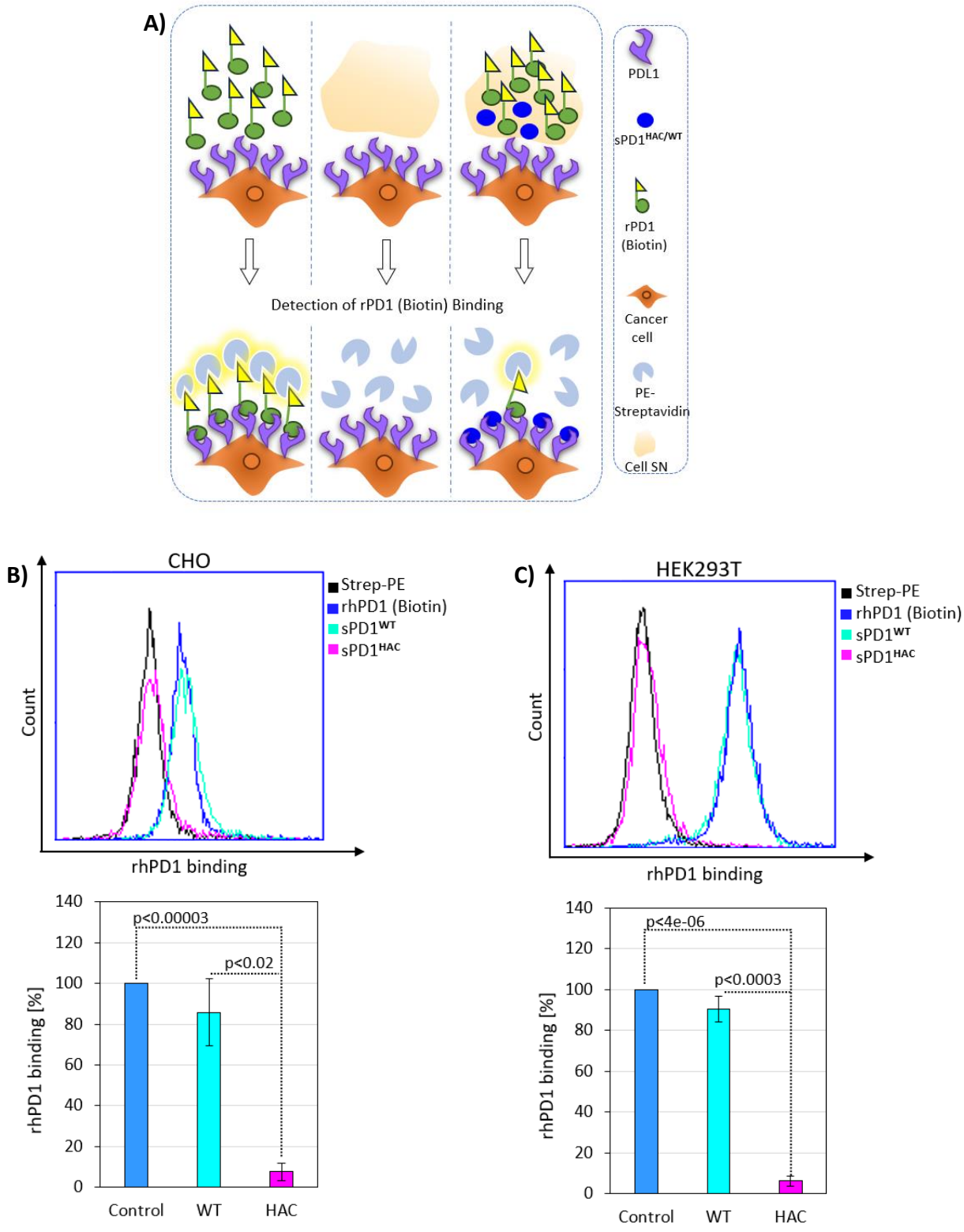

Figure 4.6 Cell-based binding competition assay for rhPD1 interaction with membrane-bound PDL1 on RKO cells in the presence of sPD1 variants derived from CHO and HEK293T cells. **A)** The illustration shows the experimental groups and workflow. PDL1 on the surface of RKO cells was targeted by biotinylated rhPD1 alone (positive control), together with sPD1^{HAC}, or together with sPD1^{WT}. The negative control group included only streptavidin-PE, which was used for biotin detection, and binding was measured by flow

cytometry. **B)** In the histogram, the addition of CHO-derived HAC variant (magenta) reduced the binding of rhPD1 from positive control (blue line) towards the negative control (black), whereas WT had minimal effect. Reductions were quantified as background-corrected rhPD1 binding, expressed as a percentage of the positive control**. C)** Similarly, HEK293T-derived $sPD1^{HAC}$ caused a leftward shift of the cell-surface binding histogram and, binding was quantified as background-corrected percentage of rhPD1 binding relative to the positive control. Values represent mean ± SE from three independent experiments. Only statistically significant p-values are indicated on the figure.

Overall, results of competitions against rhPD1 indicated that not $sPD1^{WT}$ but $sPD1^{HAC}$ variant was able to highly significantly inhibit rhPD1-PDL1 binding, whether on a solid-phase or on the cell surface.

4.3 $sPD1^{HAC}$ significantly inhibits anti-hPDL1 binding

Despite the fact that a cell-based binding competition assay is highly sensitive for hard-to-detect antibodies and, as an indirect immunofluorescence method due to signal amplification of the secondary antibody, another binding competition was constructed to ensure $sPD1^{HAC}$ exhibits the same binding capability across directly PE-conjugated anti-PDL1 antibodies. Although the indirect immunofluorescence method has its own advantages, direct immunofluorescence provides competition against monoclonal recombinant antibodies, lower background unspecific binding, and minimal human error with fewer steps for the assay. In this assay, instead of the rhPD1 protein, PE-conjugated anti-hPDL1 was mixed with sPD1 variants to treat RKO cells. The binding signal was detected directly after incubation with this mix (without a second incubation), representing the samples. While the negative control included cells treated with the corresponding isotype, the positive control included cells treated only with anti-hPDL1 (Figure 4.7A). Then PE fluorescence was measured by flow cytometry and recorded as MFI. For each condition, background was removed by subtracting the isotype-control MFI, and values were then expressed relative to the background-corrected positive control to yield percentage anti-hPDL1 binding. Data are presented as mean ± SE across three independent experiments, with statistical comparisons shown on the bar charts.

The overlaid histograms reveal a pronounced leftward displacement of the anti-hPDL1 trace in the presence of CHO-derived $sPD1^{HAC}$, bringing the distribution close to the

isotype-control baseline. This behaviour is consistent with robust competition at PDL1 on intact cells. In contrast, CHO-derived sPD1^{WT} produces a trace that remains near the positive-control position, indicating little or no inhibition. Quantification after background correction and normalisation shows that sPD1^{HAC} reduces anti-hPDL1 binding to in the region of 24%, whereas sPD1^{WT} retains around 108% of the positive-control signal. The slight elevation above 100% is readily explained by run-to-run variability inherent to cytometric measurements rather than any true increase in binding. The difference between the HAC variant and the controls is reflected in the statistics annotated on Figure 4.7B ($p < 0.0001$ versus the positive control; $p < 0.003$ versus WT).

A closely parallel pattern is observed when the variants are produced in HEK293T cells. HEK293T-derived sPD1^{HAC} shifts the histogram decisively towards the isotype trace, and, after normalisation, reduces anti-hPDL1 binding to about 8%. By comparison, HEK293T-derived sPD1^{WT} fails to achieve meaningful inhibition; across three independent experiments, the normalised values fluctuate at 73%, 96%, and 108% of the positive control, yielding an average close to 92% (Figure 4.7C). These findings are supported by the statistical annotations ($p = 0.001$ for HAC versus WT; $p = 6 \times 10^{-6}$ for HAC versus the positive control).

Together, these data show that sPD1^{HAC} robustly competes with a PE-labelled monoclonal anti-hPDL1 for access to RKO cell-surface PDL1, whereas sPD1^{WT} is largely ineffective; the effect is reproduced with CHO and HEK293T sources.

Up to this point, the PD1 constructs, their secretion by CHO/HEK293T cells, and their ability to block the PD1/PDL1 pathway had been verified. The next objective was to transduce MSCs to secrete sPD1^{HAC} and to evaluate whether the MSC-derived sPD1^{HAC} variant could compete across the various competition settings.

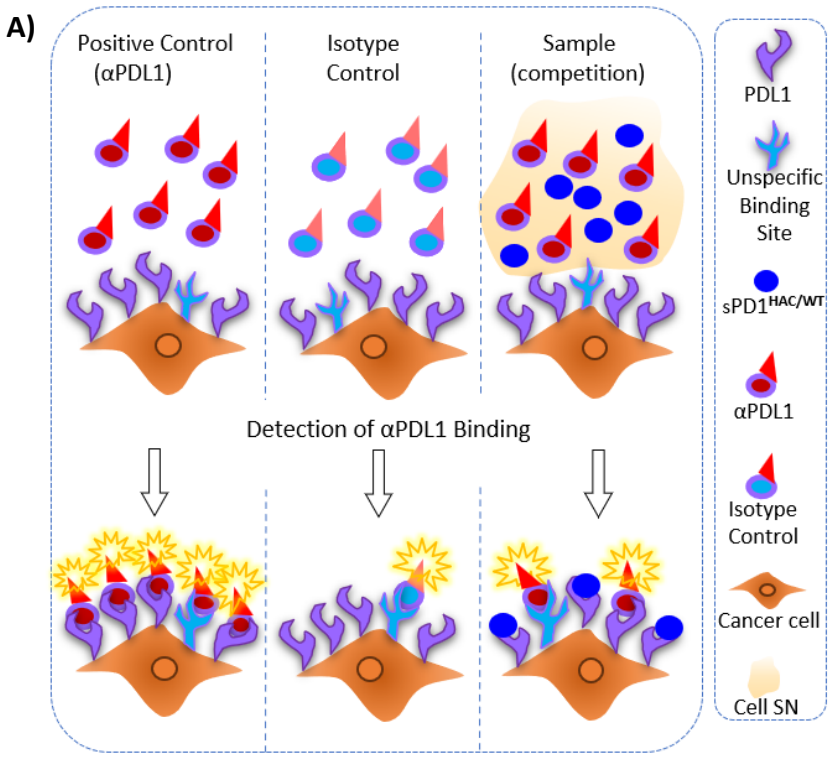
A)
Positive Control (αPDL1)
Isotype Control
Sample (competition)
Detection of αPDL1 Binding
PDL1
Unspecific Binding Site
sPD1HAC/WT
αPDL1
Isotype Control
Cancer cell
Cell SN

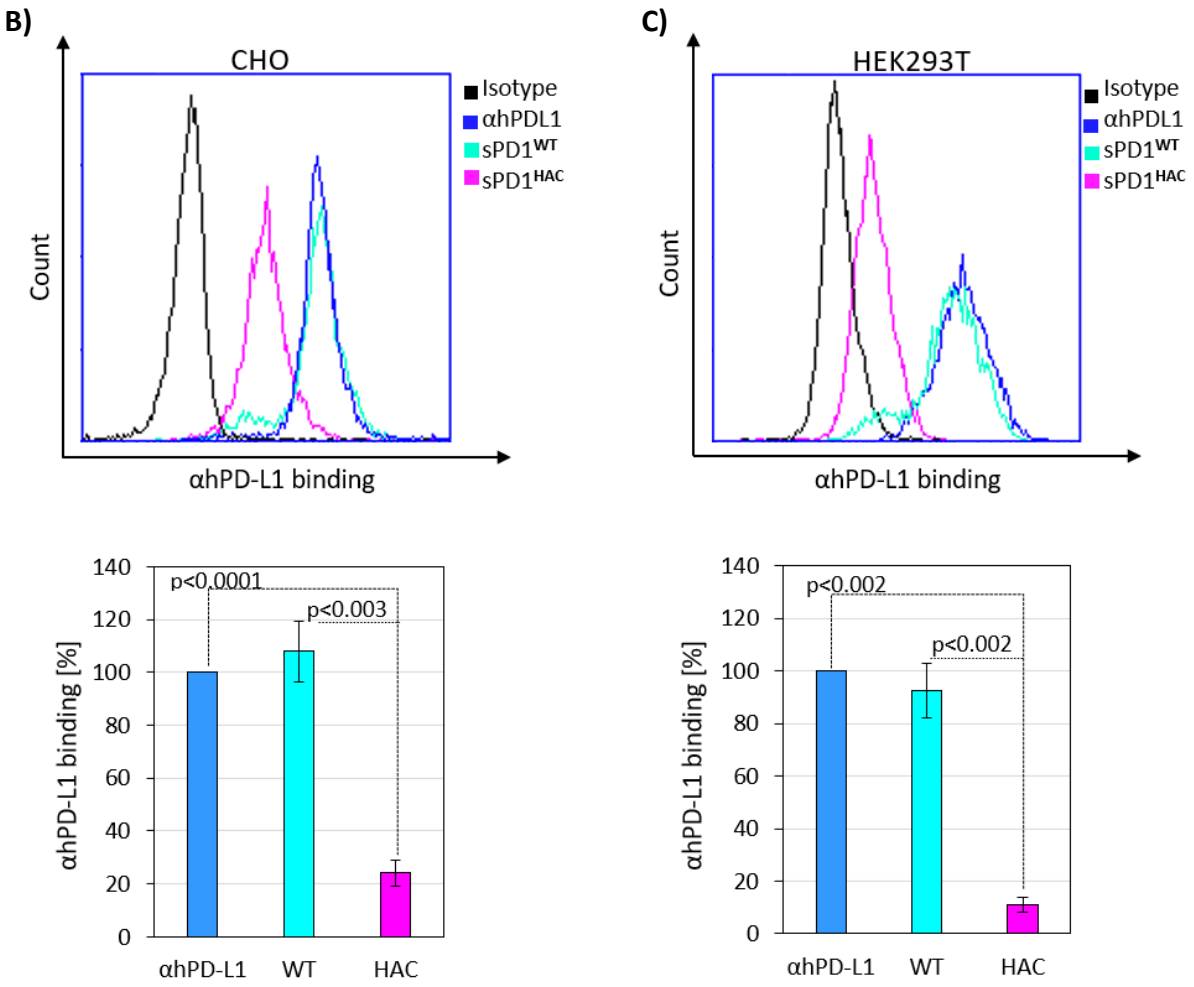
B)
CHO
Isotype
αhPDL1
sPD1WT
sPD1HAC
Count
αhPD-L1 binding
C)
HEK293T
Isotype
αhPDL1
sPD1WT
sPD1HAC
Count
αhPD-L1 binding
αhPD-L1 binding [%]
p<0.0001
p<0.003
αhPD-L1
WT
HAC
αhPD-L1 binding [%]
p<0.002
p<0.002
αhPD-L1
WT
HAC

Figure 4.7 Antibody binding competition assay against PE-conjugated anti-hPDL1 antibody in the presence of sPD1 variants. A) Antibody binding competition assay schematic. RKO cells were incubated with PE-conjugated anti-hPDL1 mixed with sPD1 variants (sample/competition). Controls were isotype only (negative) and anti-hPDL1 only (positive). For each condition, the isotype MFI was subtracted, and values were then normalised to the background-corrected positive control to yield percentage anti-hPDL1 binding. **B)** Representative histogram and quantification for CHO-derived sPD1 variants. **C)** Representative histogram and quantification for HEK293T-derived sPD1 variants. Data are shown as mean ± SE from three independent experiments; statistical comparisons are annotated on the bar charts. Key: isotype (black), anti-hPDL1 (blue), $sPD1^{WT}$ (cyan), $sPD1^{HAC}$ (magenta).

4.4 AT-MSCs emerged as the most suitable source after PD1/PDL1 screening

Having verified construct integrity, secretion from CHO/HEK293T producers, and robust blockade of the PD1/PDL1 axis, the next step was to nominate a clinically relevant stromal vehicle for delivery. Two MSC sources, adipose tissue (AT) and bone marrow (BM), were profiled by flow-cytometric surface staining at baseline and after IFNγ exposure for 48 hours (readouts expressed as an MFI ratio defined as the sample's MFI divided by the isotype's MFI) to minimise intrinsic pathway confounds and to favour a source compatible with high-yield PD1 secretion. In AT-MSCs, basal PDL1 staining (blue line) overlaps the isotype control (black), indicating little to no detectable surface PDL1 at rest and represented with a 1.2 MFI ratio. Following IFNγ exposure, the anti-hPDL1 histogram (red line) shows a rightward shift relative to untreated/isotype baselines, evidencing slightly inducible up-regulation of PDL1 with a 1.7 MFI ratio. The magnitude of induction was greater in BM-MSCs than in AT-MSCs evidenced by both histograms (Figure 4.8A) and the MFI ratio of 1.6 increased to 4.0 with IFNγ treatment.

Potential medium effects on PDL1 expression were also evaluated in AT-MSCs at baseline and after IFNγ by comparing αMEM and MesenPRO. PDL1 profiles were similar across media. For PDL1, mean MFI ratios in αMEM were 1.0 at baseline and 2.6 after IFNγ, and in MesenPRO were 1.2 at baseline and 3.4 after IFNγ, indicating no medium-dependent difference in the qualitative pattern of induction under the conditions used (Figure 4.8B).

In addition to commercial sources, MSCs from patients with myeloma (n=3) were assessed by the same surface-staining protocol. PD1 remained at isotype-control levels in all three donors, whereas PDL1 exhibited a rightward shift, consistent with cytokine exposure within the tumour microenvironment. This increase in PDL1 was consistent in each donor (Figure 4.4C). Mean PDL1 MFI ratios (sample/isotype) were as follows: patient 003, 0.8 at baseline and 3.2 after IFNγ; patient 006, 0.6 at baseline and 2.1 after IFNγ; patient 007, 1.0 at baseline and 3.5 after IFNγ.

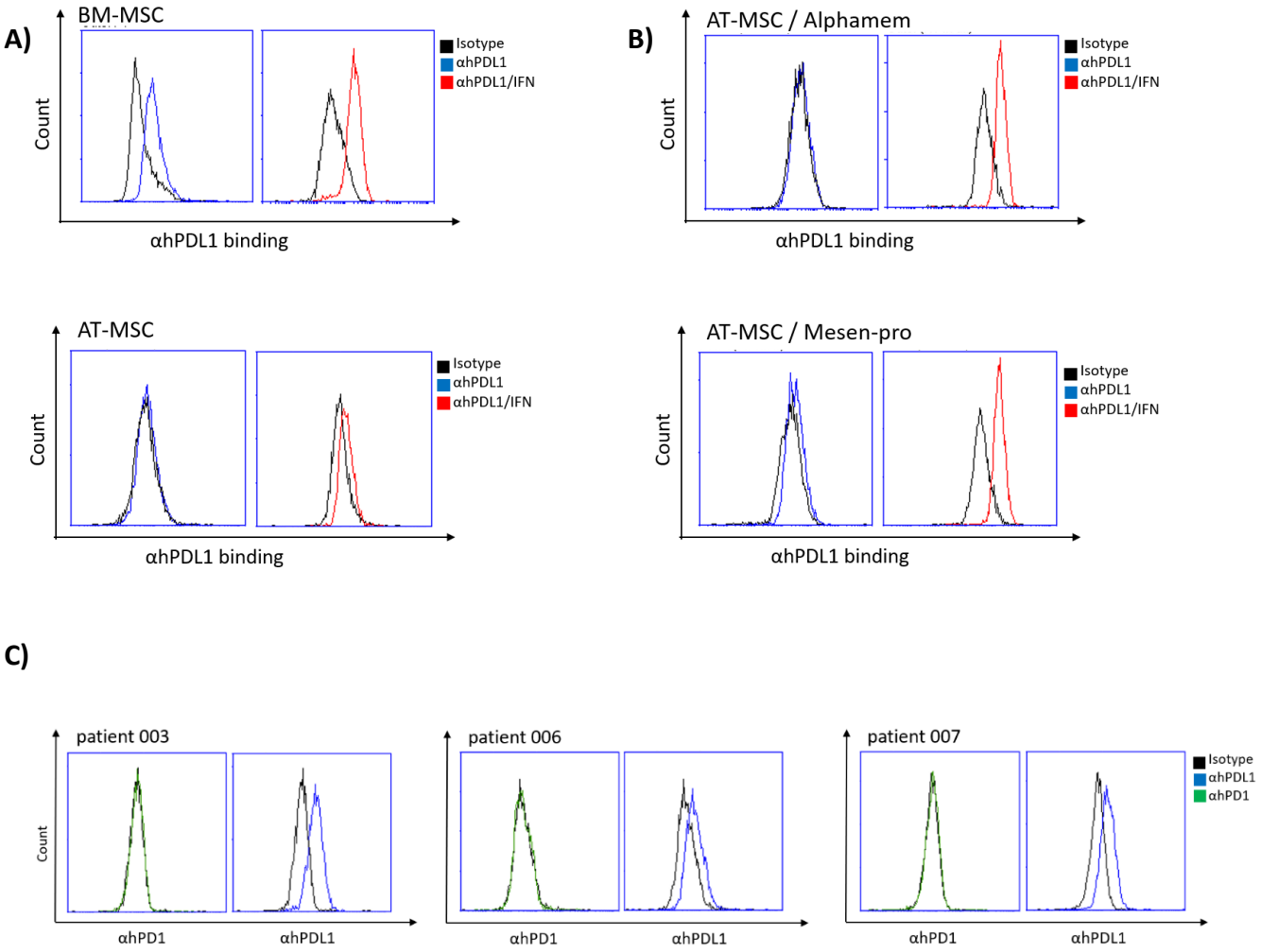

Figure 4.8 Commercial MSCs increase PDL1 expression upon IFNγ stimulation regardless of the medium utilised. Black traces indicate isotype control, blue indicates anti-hPDL1 at baseline, green indicates anti-hPD1 at baseline, and red indicates anti-hPDL1 following IFNγ treatment for 48 hours. **A)** Histograms depict surface PDL1 expression on MSCs derived from adipose tissue (AT) or bone marrow (BM) at baseline or with 48-hour IFNγ (100 ng/ml) treatment. Representative histograms are shown for AT-MSCs and BM-MSCs. **B)** AT-MSCs grown in αMEM and in MesenPRO display surface PDL1 staining profiles under

baseline and IFNγ-treated conditions. **C)** MSCs, derived from myeloma patients, exhibit surface PD1 and PDL1 staining profiles.

Taken together, this screen highlighted AT-MSCs as the most suitable candidate, combining negligible basal PD1/PDL1 with respectively slightly less IFNγ inducibility and practical advantages for production. Hereafter, "MSCs" refers to AT-MSCs, and MesenPRO was used for routine maintenance.

4.5 MSC transduction yielded stable sPD1^{HAC} expression without affecting viability or cytokines

Since MSCs' tissue origin and media were decided, attention then turned to the engineering step. MSCs were transduced for sPD1^{HAC} secretion while assessing the effects of transduction on cell viability and immunomodulatory state. Viability was quantified alongside routine culture performance by the cell viability assay (also called the Nicoletti assay), and the cytokine milieu was surveyed to detect any unintended activation or suppression relative to matched controls by employing a cytokine array. Together, these evaluations established both the choice of MSC source and the safety of the transduction procedure, setting the foundation for all subsequent competition assays using MSC-derived sPD1^{HAC}.

MSCs were transduced with an adenoviral vector carrying sPD1^{HAC} (Ad.sPD1^{HAC}) or Luciferase enzyme (Ad.LUC) as a control (Figure 4.9A). First, various multiplicities of infections (MOI) effects on transduction were examined, and then PD1 secretion of these cells was determined by human PD1 DuoSet ELISA. The sPD1^{HAC} cassette was successfully inserted into MSCs, and MSCs secreted adequate PD1 for future competition assays and for potential therapeutic purposes. The MOI providing the balance between cell viability and transduction efficiency was determined as 1000, and we achieved a secretion level of 1160 ng/ml for the sPD1^{HAC} variant at this MOI. Together with these expression levels, cell viability was checked on the same cells and found no considerable effect of PD1 transduction on MSCs with 90-93% cell viability (Figure 4.9B).

The effects of PD1 insert were also analysed by checking cytokine differentiation between MSC.HAC and MSC.LUC by C6 cytokine array and results reveal no

considerable differentiation in cytokine expression between control and MSC.HAC (Figure 4.9C).

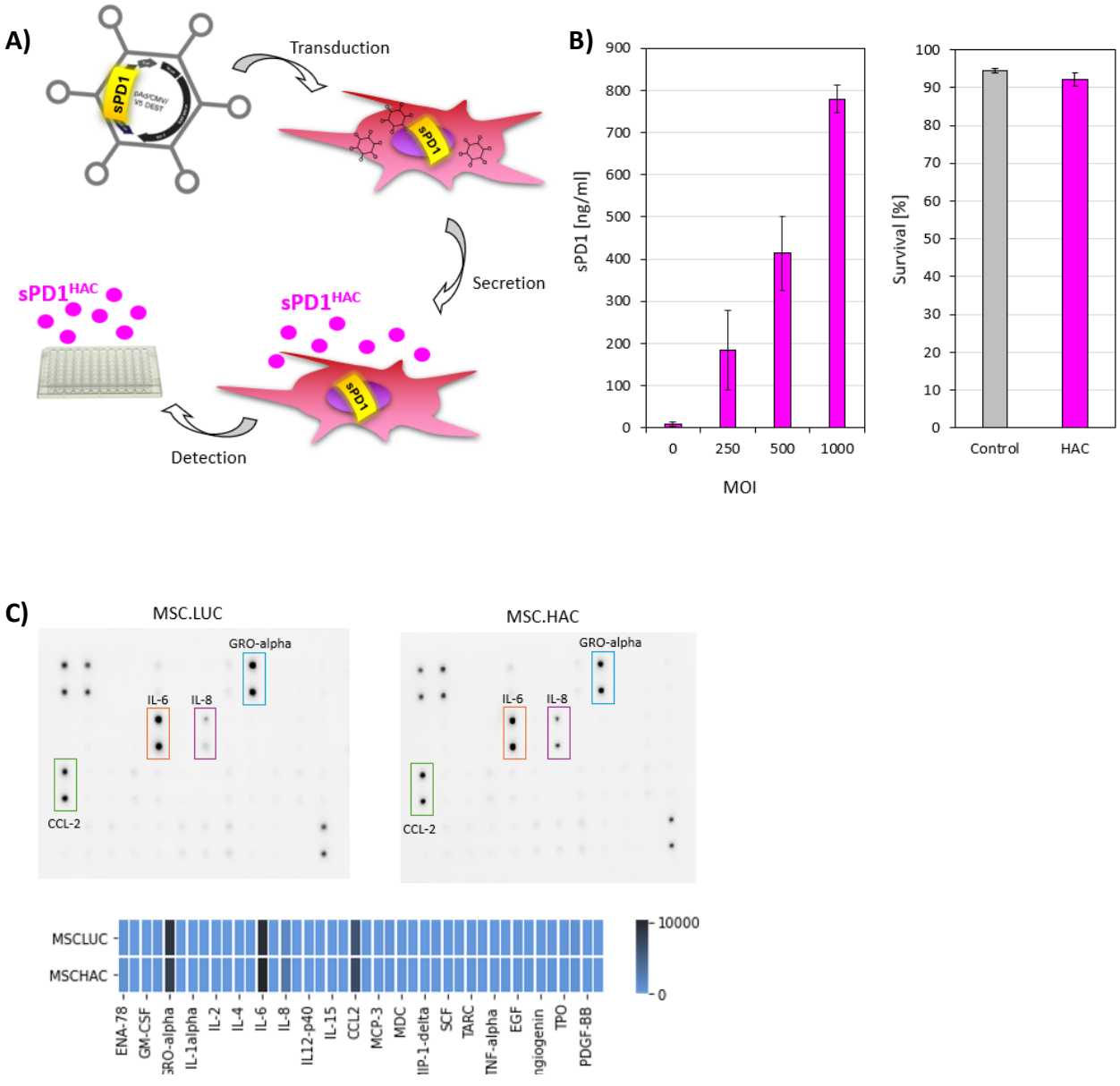

Figure 4.9 MSCs express and secrete sPD1^{HAC} following transduction with an adenoviral vector carrying the variant. A) The panel summarizes the workflow of MSC transduction, secretion, and detection steps. **B)** ELISA results show the PD1 secretion levels of engineered MSC.HAC and MSC.LUC relative to MOI. MSCs, transduced at 1000 MOI were analysed for PD1 secretion. Transduced MSCs were also analysed for apoptosis by the Nicoletti assay, and results are shown for MSC.HAC and MSC.LUC. **C)** C6 cytokine array was applied to the supernatants of these transduced MSC supernatants, and results are shown for MSC.HAC and MSC.LUC. The mean concentration of PD1 and viability were derived from three independent assays. Error bars represent the mean ± SEM.

4.6 MSC-derived sPD1^{HAC} reproduced strong competition in vitro

In solid-phase, cell-based, and antibody binding competition assays, sPD1^{HAC} leads to approximately 95% significant inhibition of the human PD1-PDL1 bindings in vitro when derived from MSC cells.

4.6.1 MSC-derived sPD1^{HAC} outcompetes with rhPD1

After priming MSCs to produce sPD1^{HAC,} the blocking capability of this variant was evaluated again in the form derived from MSCs. The first competition was for 50 ng/well immobilised hPDL1-Fc chimaera protein attached to a solid phase. sPD1^{HAC} concentrations ranging from 20 ng to 0.1ng against 50 ng of rhPD1 were utilised. Solid-phase binding competition protocol was followed as detailed in the methods. Positive control wells were incubated with rhPD1 mixed with MSC.LUC supernatants that were equal volume to the corresponding titrations and binding percentage normalised according to the positive control of each titration. When results were analysed, inhibition of MSC-derived sPD1^{HAC} was evident on rhPD1-PDL1 binding. It reduced the binding across all titrations significantly except for the 0.1 ng group of sPD1^{HAC} variant, which has a ratio of 1:500 to the rhPD1. In the presence of 20, 10, 0.8, and 0.6 ng sPD1^{HAC}, the binding ratios of rhPD1 were 13%, 18%, 35%, and 68% with p-values less than 8e-06, 0.0005, 0.008, and 0.05, respectively. This decrease in binding followed a steady trend with the decrease in sPD1^{HAC} concentration. However, when the sPD1^{HAC} concentration was dropped to very low levels, such as 0.1 ng across 50 ng of rhPD1, the blocking ability of sPD1^{HAC} lost its significance with giving an average of 80% binding to rhPD1 (Figure 4.10A).

The second binding competition with MSC-derived sPD1^{HAC} was on RKO cells for their endogenous PDL1. 4x10^5 RKO cells treated with MSC.HAC supernatant, which comprises 800 ng sPD1^{HAC} or the same volume of MSC.LUC supernatant. For the negative control cells, resuspended in PBS. Then 4000 ng rhPD1 was added to these cells (except the negative control) and incubated for 25 min, and biotin detection was provided via a second incubation with streptavidin-PE. For the positive control, rhPD1 was utilised alone in the first incubation, and this was defined as 100% rhPD1 binding in the analysis.

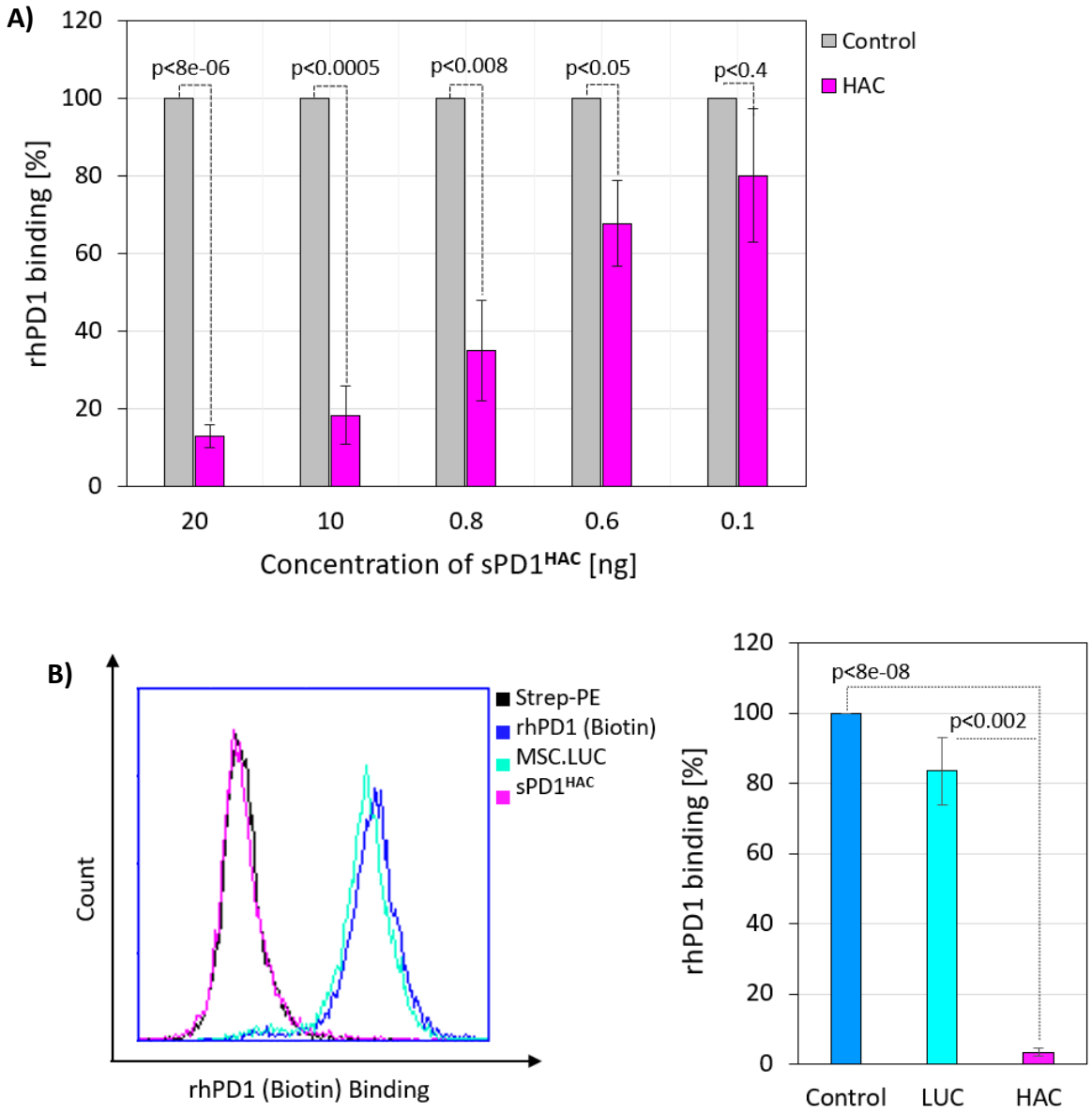

Figure 4.10 MSC-derived sPD1^{HAC} in solid-phase and in cell-based competition assays against rhPD1. A) Solid-phase competition assay using 50 ng of rhPD1 and varying amounts (20, 10, 0.8, 0.6, 0.1 ng) of MSC-derived sPD1^{HAC} against50 ng recombinant hPDL1 immobilised on an ELISA plate. **B)** Cell-based binding competition assay on 4x10^5 RKO cells using 4000 ng rhPD1 mixed with MSC-derived sPD1^{HAC} supernatant, containing 800 ng sPD1^{HAC}, or the same volume of MSC.LUC supernatant. The positive control indicates only rhPD1-treated cells, while the negative control indicates untreated RKO cells stained only with PE-conjugated Streptavidin. The histogram shows representative rhPD1 binding profiles under the indicated conditions. The statistical bar chart shows background-corrected percentage of rhPD1 binding relative to the positive control. Results were collected from three independent assays (n=3) and p-values are indicated on the figure.

Flow cytometry histograms showed overlapping lines of sPD1^{HAC}-mixed sample and negative control, indicating a strongly inhibited rhPD1 binding. Whereas the MSC.LUC-mixed sample was overlapping with the positive control, indicating a negligible effect (Figure 4.10B). Computational analysis of rhPD1 binding ratio was supported these findings with an average of 3.4% in the HAC variant added sample and 84% in the MSC.LUC added sample. Inhibition of rhPD1-PDL1 binding by the HAC variant was significant when compared to both normalization and MSC.LUC (Figure 4.10C).

Overall, the MSC-derived sPD1^{HAC} variant outcompetes rhPD1 for binding to PDL1, whether solid-surface attached or cell-surface attached. This inhibition was highly significant even in small concentrations across rhPD1, such as 1 in 83 in solid-phase competition, and 1 in 40 at cell surface competition.

4.6.2 MSC-derived sPD1^{HAC} outcompetes anti-hPDL1

To further substantiate the PD1-PDL1 pathway blocking ability of the MSC-derived HAC variant, antibody binding competition was set against PE-conjugated anti-hPDL1 on RKO cells. The antibody binding competition protocol was followed as detailed in the methods section. Positive controls included cells incubated only with anti-hPDL1 (800 ng), negative controls included cells with the corresponding isotype (200 ng), and samples included anti-hPDL1 (800 ng) mixed with MSC.HAC supernatant containing 800 ng of sPD1^{HAC} or the same volume of MSC.LUC supernatant. After washing and fixation, cells were analysed by flow cytometer.

MSC-derived sPD1^{HAC} demonstrated similar inhibition capabilities against PE-conjugated anti-hPDL1 antibody by significantly reducing its binding to 13%. Histogram also portrayed this inhibition with a leftward-shifted PE signal in the presence of the sPD1^{HAC} variant compared to the positive control. Contrarily signal of MSC.LUC supernatant added samples were overlapping with the positive control, proving the reliability of the assay. In the analysis binding ratio of anti-hPDL1 in MSC.LUC added samples were averagely at 91% (Figure 4.11).

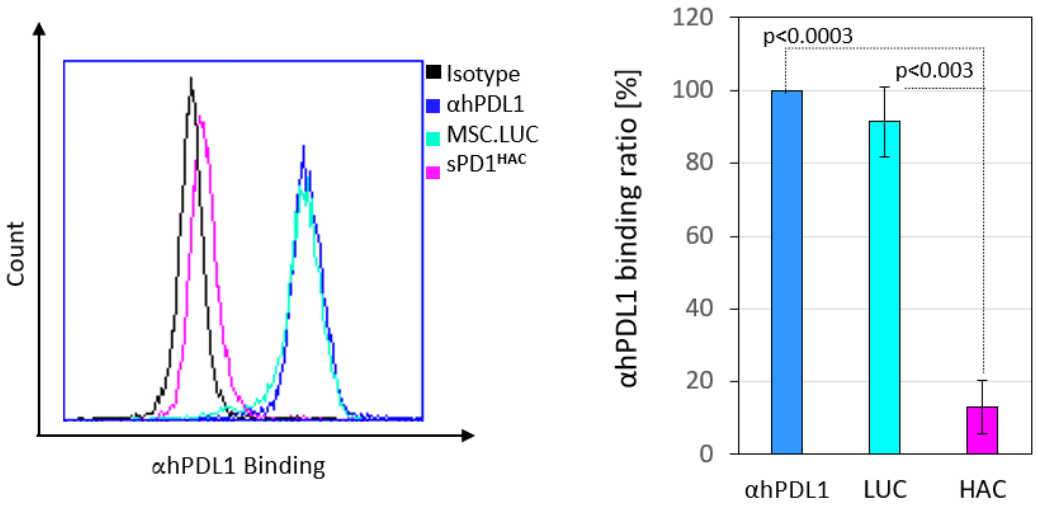

Figure 4.11 Antibody binding competition assay on RKO cells using MSC-derived sPD1^{HAC} and PE-conjugated anti-hPDL1. RKO cells were treated with PE-conjugated anti-hPDL1 (positive control), anti-hPDL1 mixed with either MSC.HAC (containing 800 ng sPD1^{HAC}) or MSC.LUC supernatants (samples), and with the corresponding isotype (negative control). After washing and fixation PE signal was measured by flow cytometry. The blue line on the histogram represents positive control, the black line the negative control, the magenta line the MSC.HAC condition, and the cyan line the MSC.LUC condition. For the analysis of anti-hPDL1 binding, background was corrected by subtracting MFI value of the negative control from the MFI value of the positive control and accepted as 100% binding. The bar chart shows background-corrected anti-hPDL1 binding under each condition. Results were collected from three independent assays (n=3) and p-values are indicated on the figure.

4.7 Durvalumab demonstrates similar or less inhibition than the HAC variant

To indirectly compare them, the blocking capability of DUR was evaluated next to sPD1^{HAC} in the solid-phase and cell-based competition assays. Firstly, they competed with rhPD1 for immobilised rhPDL1-Fc attached to a high-binding microplate. Either untransfected supernatant, HEK293T-derived sPD1^{HAC}, or equimolar DUR in PBS, all in the same volume, were added to hPDL1 (50 ng/well) attached wells. Then biotinylated rhPD1 (50 ng/well) was added to cells, and this was incubated before streptavidin-HRP and TMB treatment. After adding the stop solution, the binding signal was detected by a microplate reader at 450 nm. and the rhPD1 binding ratio was calculated by setting untransfected supernatant-added samples to 100%.

Solid-phase binding competition results represented that sPD1^{HAC} and DUR inhibited rhPD1 binding similarly when they were utilised in high concentrations, such as 40 (2.4 pmol), 20 (1.2 pmol), 10 (0.6 pmol), and 5 ng (0.3 pmol) HAC variant and equivalent molar of DUR. However, in smaller concentrations such as 0.06 (1 ng HAC), 0.03 (0.5 ng HAC), and 0.006 (0.1 ng HAC) pmol blocking efficacy of DUR drops losing its significance against rhPD1. On the contrary, sPD1^{HAC} can still block rhPD1 binding significantly in these concentrations (Figure 4.12A).

Similarly, DUR represented less inhibition of rhPD1-PDL1 binding on RKO cells. Cell-based binding competition protocol was followed as outlined in the methods section with either 800 ng HAC variant or equimolar DUR against 4000 ng rhPD1. Although both HAC and DUR reduced the binding, while the signal of rhPD1 binding was regressed to the negative control (background signal) levels in the presence of sPD1^{HAC}, DUR was not able to shift this binding signal as much as the HAC variant, whether produced by HEK293T or MSC cells (Figure 4.12B). Computational analysis of MFI values (normalised as in other cell-based assays) was also consistent with this observation. Both HEK293T- and MSC-derived sPD1^{HAC} decreased the binding of rhPD1 to 8% and 5% respectively. On the other hand, DUR reduced it to approximately 38-40% levels. Nevertheless, the reduction of both DUR and sPD1^{HAC} was significant when compared to the positive control. Interestingly, while the binding reduction of HEK293T-derived HAC variant was significantly different than DUR, the MSC-derived HAC variant was not able to catch this significant difference (Figure 4.12C).

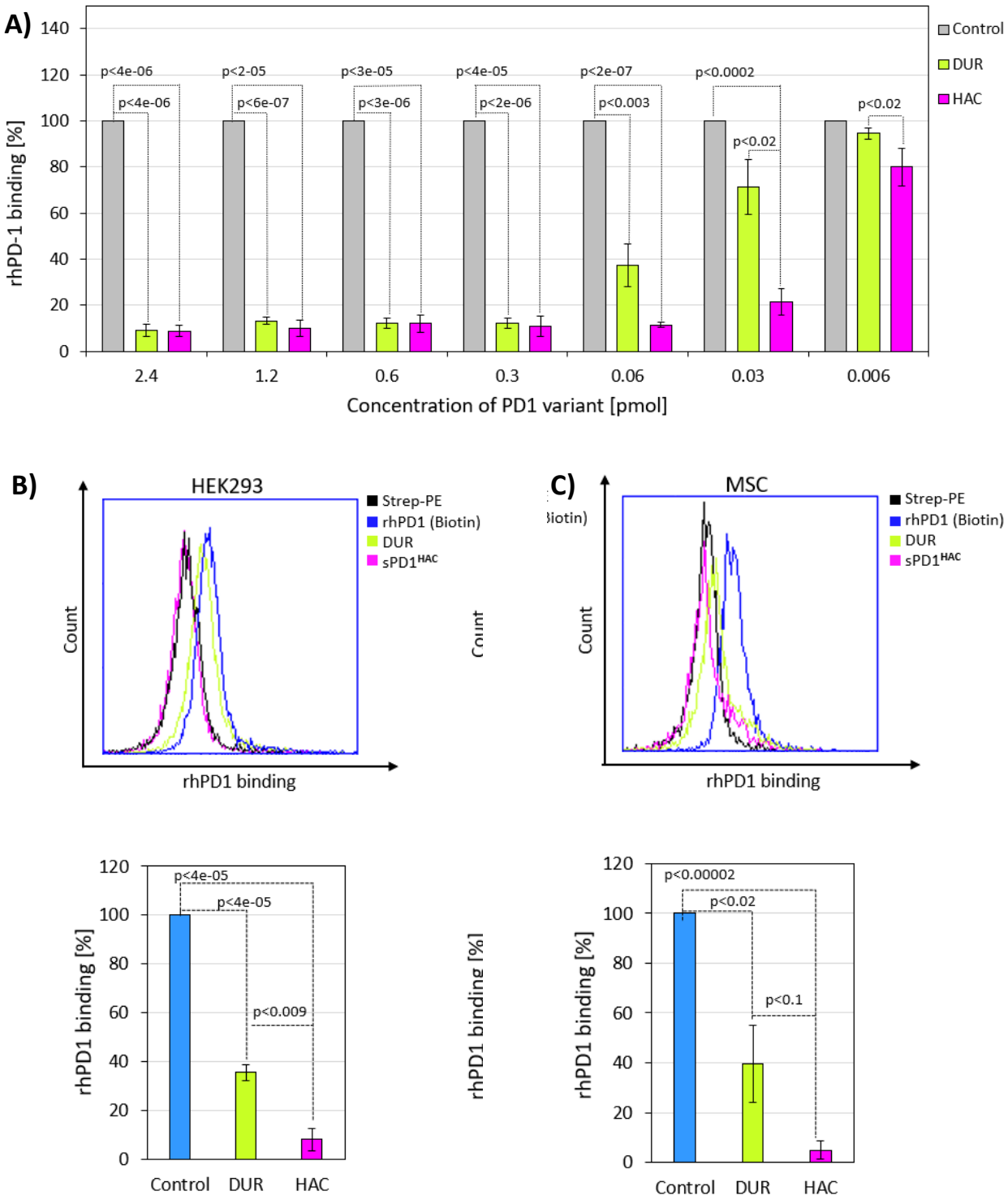

Figure 4.12 Comparison of durvalumab and sPD1^{HAC} in solid-phase and cell-based rhPD1 binding competition assays. A) Solid-phase binding competition assay using immobilised hPDL1 and biotinylated rhPD1 in the presence of HEK293T-derived sPD1^{HAC} or equimolar durvalumab (DUR), as indicated in pmol., and the binding of rhPD1 was detected with streptavidin-PE/HRP. Increasingly dilute competitors, DUR or sPD1^{HAC}, were pre-incubated with the coated antigen as indicated (pmol). rhPD1 binding was normalised to samples receiving the same volume of untransfected supernatant, defined as 100%. **B-C)**

Cell-based competition by flow cytometry on RKO cells using either HEK293T-derived sPD1^{HAC}, MSC-derived sPD1^{HAC}, or equimolar DUR against biotinylated rhPD1. Overlaid histograms show percentage of rhPD1 binding for each condition, and bar charts show background-corrected percentage of rhPD1 binding. Data represented as mean ± SE from three independent experiments and p-values are indicated on the figure.

4.8 sPD1^{HAC} inhibits DUR (PE) binding to PDL1 on RKO cells

The effects of DUR and HAC on PD1-PDL1 were compared before, as in separate sample tubes, and when they both competed against rhPD1, which led us to wonder how they would compete against each other. For this reason, a PE-conjugated durvalumab biosimilar monoclonal antibody, DUR (PE), was utilised in an antibody binding competition setting. Again, 800 ng/ per 4x10^5 cells sPD1^{HAC} produced in HEK293T and MSCs was used in a mix with DUR (PE) following the manufacturer's instructions. Positive controls included cells only with DUR (PE), and negative controls included cells with the corresponding isotype. Cells were incubated for 25 min on ICE before washing and fixation. PE fluorescence was quantified by flow cytometry as MFI. Background from the negative control was subtracted from all samples. The background-corrected positive control was defined as 100% binding, and sample signals were expressed as a percentage of this reference.

When competed directly against DUR (PE), sPD1^{HAC} caused a pronounced inhibition. Histograms showing MSC- and HEK293T-derived HAC variant competitions both revealed that the assay effectively caught the PE signal of DUR (PE) as it is seen in the positive control (purple), but sPD1^{HAC} addition to this sample shifts the binding towards the left, down to the negative control. By contrast, overlapping WT and positive control signals indicate sPD1^{WT} cannot affect DUR (PE) binding (Figure 4.13A). Analysis of these signals shows inhibition of DUR (PE) binding by HEK293T-derived sPD1^{HAC} to an average of 26%, which was significant compared to the positive control with a p-value less than 0.003, although sPD1^{WT} inhibits it to an average of 88%. In the same way, MSC-derived HAC variant curtained the DUR (PE) binding ratio by repressing it to 6% ($p < 7e-06$), while WT scaled it down to 90% (Figure 4.13B).

Therefore, it was established that sPD1^{HAC} was a competent high-binding blocker for the PD1-hPDL1 pathway, even sufficient to dampen a commercial monoclonal antibody, Durvalumab, binding on RKO cells as well as on a solid-phase.

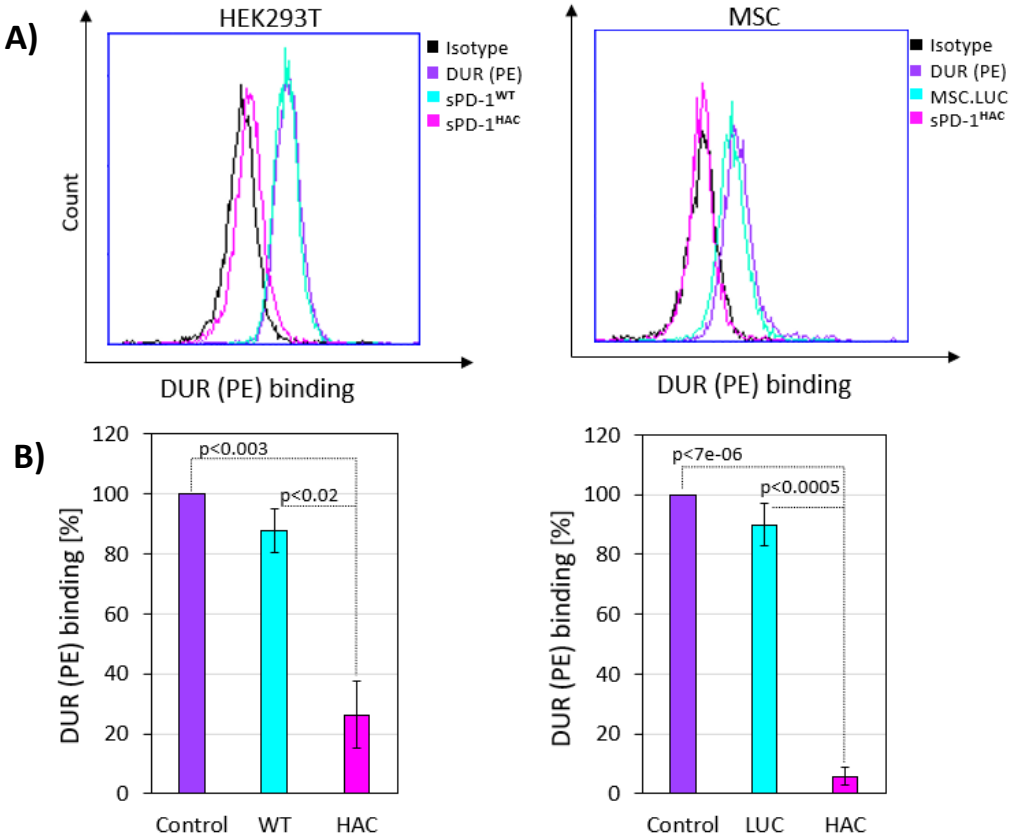

Figure 4.13 Antibody binding competition assay between sPD1 variants and PE-conjugated durvalumab on RKO cells. An antibody competition assay performed on RKO cells using PE-conjugated durvalumab biosimilar, DUR (PE), as the binding probe. HEK293T-derived or MSC-derived sPD1^{HAC} and sPD1^{WT} were mixed with DUR (PE) before incubation with 4x10^{5} RKO cells. The positive control consisted of cells treated with DUR (PE) alone, and the negative control consisted of cells treated with the corresponding isotype control. After incubation, PE fluorescence was measured by flow cytometric analysis as MFI. Background from the negative control was subtracted from all samples, and the background-corrected positive control was defined as 100% DUR (PE) binding. Sample signals were expressed as background-corrected percentage of DUR (PE) binding relative to the positive control. **A)** Representative histograms for HEK293T- and MSC-derived sPD1^{HAC} competition against DUR(PE). **B)** Quantification of the competitions. Results were collected from three independent experiments (n = 3), and significant p-values are indicated on the figure.

\

4.9 Murine PDL1-PD1 bindings were blocked by sPD1^{HAC}

Although sPD1^{HAC} was successful at blocking human PDL1-PD1 bindings, as a therapeutic, it is crucial that it has similar inhibition capabilities in murine cell lines. Interestingly, in vivo experiments regarding the blocking ability of monoclonal anti-

PD1/PDL1 therapies were not available in the literature. Particularly, in vivo examinations were skipped in the very first trials of Durvalumab. The binding evaluation of these agents is primarily based on clinical trial data and immunohistochemical assays performed on human tumour biopsies. Although monoclonal anti-PD1/PDL1 therapies were engineered for human targets, this gap in the literature may also suggest that testing PD1/PDL1 blockers on murine cells may not be feasible or quite suitable due to the differences in binding properties, protein packing, and/or protein structure itself between species. Since there is no concrete evidence of these suspicions, the blocking ability of sPD1^{HAC} on mouse PDL1 was examined in a stepwise manner. Before levelling up to in vivo assays, mPDL1 and murine cancer cell lines were inspected in terms of sPD1^{HAC}-mPDL1 binding.

4.9.1 HAC variant has various blocking effects on various anti-mPDL1 antibodies

HEK293T cells were initially utilised as an mPDL1 source. These cells were transfected with full-length mouse PDL1 and stained with three different anti-mPDL1 monoclonal antibodies, namely, MIH6, MIH7, and 10F.9G2 clones. For this, pFUSE.mPDL1 was transfected into the HEK293T cell line, and expression of mPDL1 was confirmed by the surface staining method and flow cytometry. Despite optimisation and titration efforts of the anti-mPDL1 concentrations in these experiments, the staining always resulted in two mPDL1 signal peaks for all three antibody clones (Figure 4.14A). These findings suggest that overexpression produces at least two surface-displayed forms of mPDL1, likely differing in the extent of post-translational modification.

After establishing mPDL1-overexpressing cells, antibody binding competition assays were conducted on these cells with all three antibodies. Although the PD1/PDL1 blocking efficacy of sPD1^{HAC} cannot be observed when it competes against recombinant anti-mouse PDL1, clone MIH6, it represented stronger blocking ability in competitions with MIH7 and 10F.9G2 clones.

Firstly, clone MIH6 was utilized as PE-conjugated recombinant anti-mPDL1, which is a competitor for sPD1^{HAC}. HEK293T.mPDL1 cells (4x10^5 cells per sample) were

treated with supernatant from sPD1^{HAC}-transfected or untransfected HEK293T cells as duplicates, and samples were incubated for 25 mins at room temperature. Then the samples were stained with either PE-conjugated recombinant anti-mPDL1 (clone MIH6), or its isotype, and incubated for 25 mins more on ice. After that, cells were washed, fixed, and analysed by flow cytometry. Results revealed that the sPD1^{HAC} variant is not able to block murine PDL1 on transfected HEK293T cells when it competes against MIH6. Further, this diminish in blocking efficacy of sPD1^{HAC} was inspected to find whether it is dependent on the recombinant anti-mPDL1 mAb clone. For this, competition against MIH6 was repeated, and the same competition was conducted on mPDL1-transfected HEK293T cells against two other mouse anti-PDL1 clones: MIH7 and 10F.9G2. Surprisingly, the sPD1^{HAC} variant showed various binding blocking efficacy for mPDL1 across different clones. While the sPD1^{HAC} variant mildly but still significantly reduced MIH7 binding (approximately 40%), it inhibited 10F.9G2 binding to an average of 5%, similarly to human PDL1 blocking experiments (Figure 4.14B).

Another critical observation in this assay was the binding variance between these three recombinants, anti-mPDL1 monoclonal antibodies. When the detection signals for mPDL1 obtained from the same transfection of HEK293T cells were compared, a wide range of signal intensities was observed among the three antibody clones. While MIH6 indicates the highest number of expressed mPDL1, followed by the 10F.9G2 clone, MIH7 shows the lowest number of mPDL1 (Figure 4.14C). These results likely reflect distinct epitope usage, with partial overlap between the MIH7 and 10F.9G2 epitopes and the sPD1^{HAC} contact surface, and no such overlap for MIH6. Collectively, the data indicate that sPD1^{HAC} can block antibody binding to mPDL1 when an epitope overlap exists. Nevertheless, our variant was verified for interfering with mPDL1 and PD1 interactions in the experimental cell line, HEK293T.

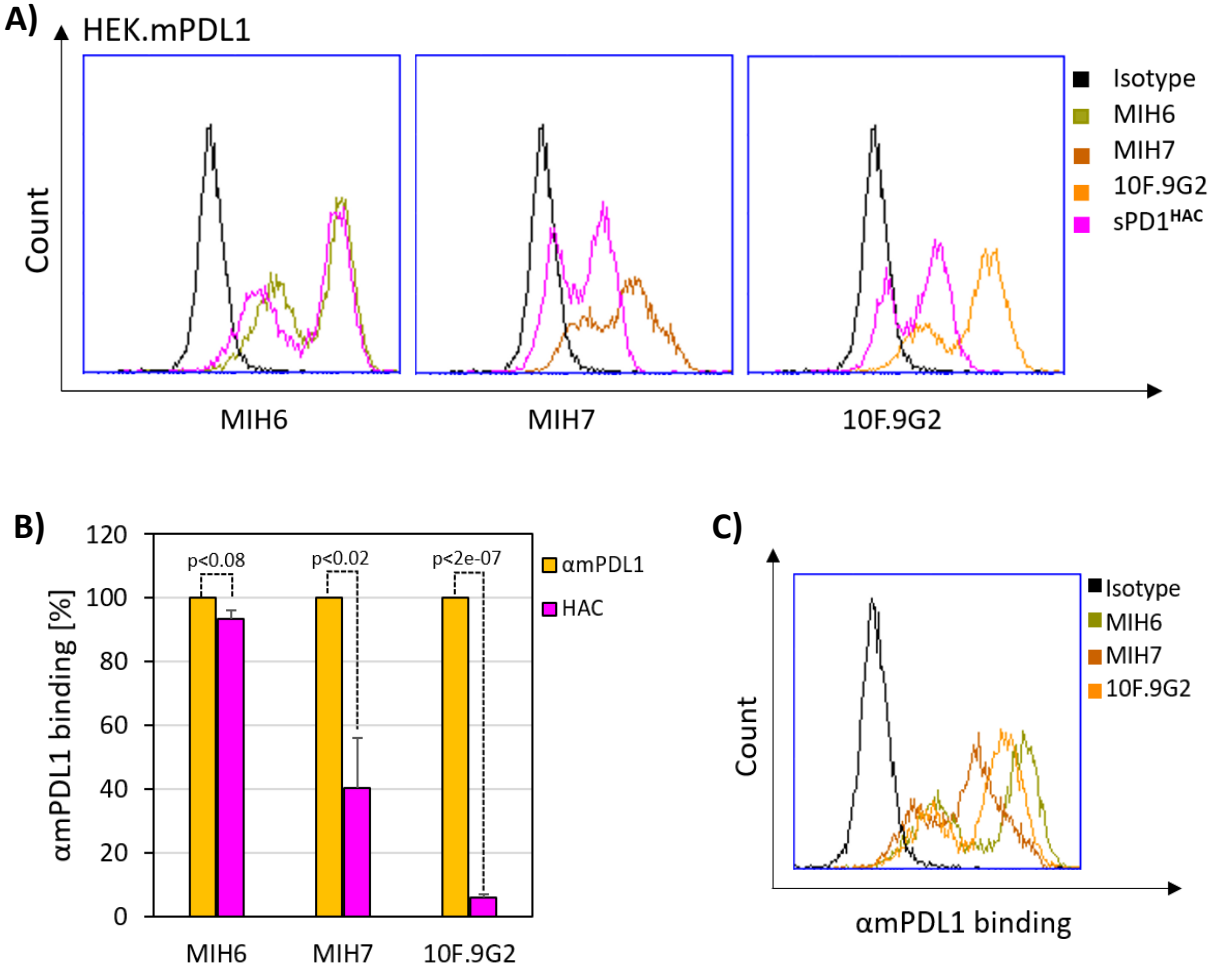

Figure 4.14 Interaction of sPD1^{HAC} with murine PDL1 on HEK293T.mPDL1 cells assessed using anti-mPDL1 clones. Antibody binding competition assays were conducted on HEK293T.mPDL1 cells, between each PE-conjugated anti-mPDL1 mAb clone (MIH6, MIH7, and 10F.9G2) and HEK293T-derived HAC variant. Cells treated only with PE-conjugated anti-mPDL1 mAb clone were utilised as a positive control, and cells treated only with isotype utilized as a negative control. The binding ratio was calculated by subtracting the negative controls' MFI from all samples' MFI and setting the corrected positive control's MFI to 100%. **A)** Related histograms of each competition. **B)** Computational analyses of background-corrected percentage anti-mPDL1 binding for each clone in the presence of sPD1^{HAC}. **C)** Representative overlaid histograms showing the positive-control staining profiles of MIH6, MIH7, and 10F.9G2 on HEK293T.mPDL1 cells to allow comparison of clone-specific binding signals. Results were collected from three independent experiments (n = 3), and p-values are indicated on the figure.

4.9.2 LL/2 and MC38 cells are not convenient for binding competition assays

Next, murine cancer cell lines were evaluated for their cell surface PDL1 expression. Since binding competition assays require high cell surface PDL1 expression for a sensitive competition and clear representation of the PD1-PDL1 inhibition activities, it is beneficial to detect a cell line with high mPDL1 expression. Specifically, Lewis Lung carcinoma (LL/2), colorectal carcinoma (MC38), melanoma (B16.F10), and myeloma (5TGM1) cell lines were stained with anti-mPDL1 mAb (clone 10F.9G2) to measure endogenous PDL1 expression levels. Flow cytometric analysis shows that not LL/2 and MC38 but B16.F10 and 5TGM1 cells have distinct cell-membrane PDL1 expression without stimulation (Figure 4.15). Then these cell lines were treated either with IFNγ (100 ng/ml) or chemotherapeutic drug gemcitabine (GEM, 10nM) for 48 hours to induce PDL1 expression. Surface staining with the 10F.9G2 clone, assessed by flow cytometry, indicated a modest increase in mPDL1 surface expression on LL/2 and MC38 cells following IFNγ treatment, although this was not significant by MFI ratio. By contrast, a significant increase was observed in B16.F10 cells treated with GEM and in 5TGM1 cells treated with IFNγ.

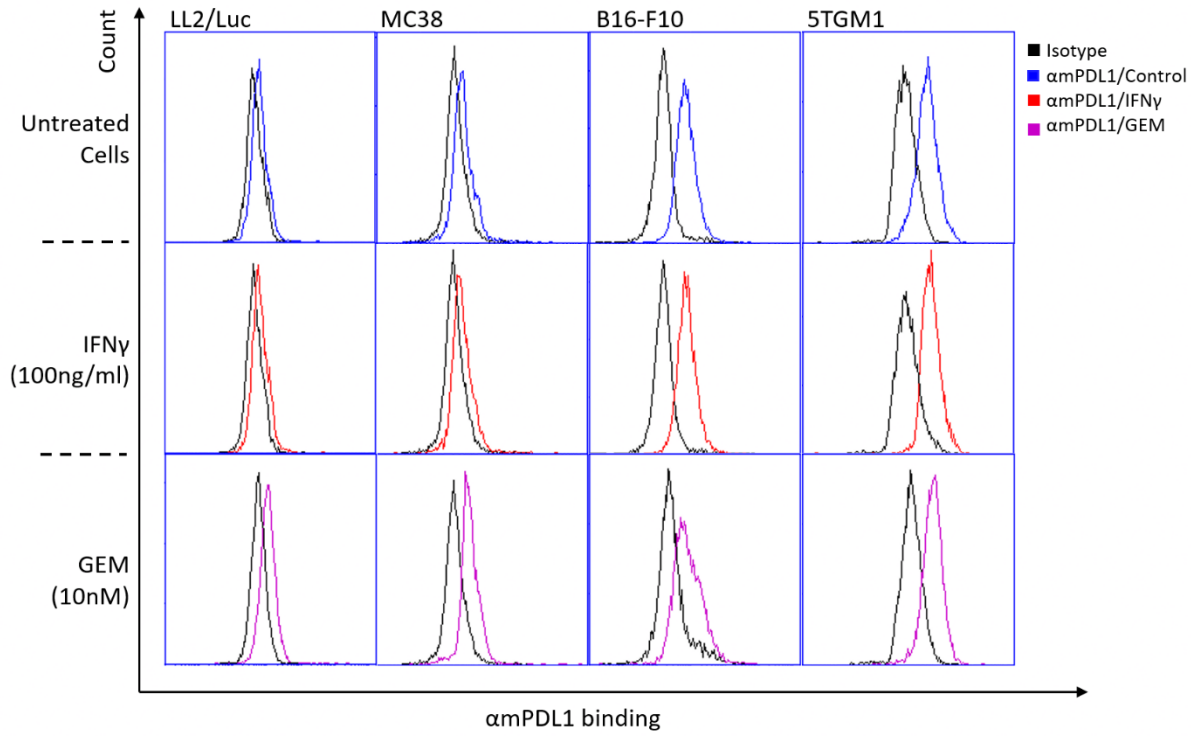

Figure 4.15 Surface mPDL1 staining in murine cancer cell lines at baseline and after IFNγ or gemcitabine treatment. Cell surface staining and flow cytometric analysis were used to assess mPDL1 expression in LL/2, MC38, B16.F10, and 5TGM1 cells under baseline conditions and after treatment with gemcitabine (10 nM, 48 h) or IFNγ (100 ng/ml, 48h) Black traces indicate isotype control, blue indicates anti-mPDL1 at baseline, purple indicates anti-mPDL1 following GEM treatment, and red indicates anti-mPDL1 following IFNγ treatment. Representative histograms are shown for each cell line.

4.9.3 Abundancy of sPD1^{HAC} does not lead stronger inhibition of mPDL1 binding on 5TGM1 cells on the analysed scale

After establishing 5TGM1 and B16.F10 cells as experimental models due to their endogenous mPDL1 cell surface expression levels, the possible effect of sPD1^{HAC} concentration on the binding inhibition was investigated. For this antibody competition on 5TGM1 cells were set using the 10F.9G2 clone and various concentrations of HEK293T-derived sPD1^{HAC}.

Basically, 4x10^5 cells/per sample were treated with 0.6, 0.8, 1, 1.2, and 1.5 ng of sPD1^{HAC}, or sPD1^{WT}. Then, cells were either stained with anti-mPDL1 (clone 10F.9G2) or the corresponding isotype. Positive control was cells treated only with anti-mPDL1, and negative control was cells treated only with the isotype control. Anti-mPDL1 binding ratio was calculated the same way as before in antibody binding competitions. In the concentration array we examined, 0.6 ng and 0.8 ng of sPD1^{HAC} blocked approximately 60% and 50% mPDL1 binding, and these inhibitions were significant with p-values lower than 0.004 and 0.03, respectively (Figure 4.16). Although all concentrations caused inhibition of this pathway, higher concentrations, such as 1 and 1.5 ng, did not lead to higher inhibition levels, which represented 70% and 90% anti-mPDL1 binding. sPD1^{WT}, on the other hand, represented an interesting inhibition at 0.8 ng concentration.

Subsequently, a 0.8 ng concentration, which was already utilised before for human cancer cells, was found to be feasible to continue, since higher inhibitions could not be achieved.

These results indicated that the 800ng concentration of sPD1^{HAC} that was used before was feasible to continue with. However, HAC variant inhibition on other anti-mPDL1

clones, as well as their ability to detect mPDL1 surface expression was, still a question to be answered in the next step.

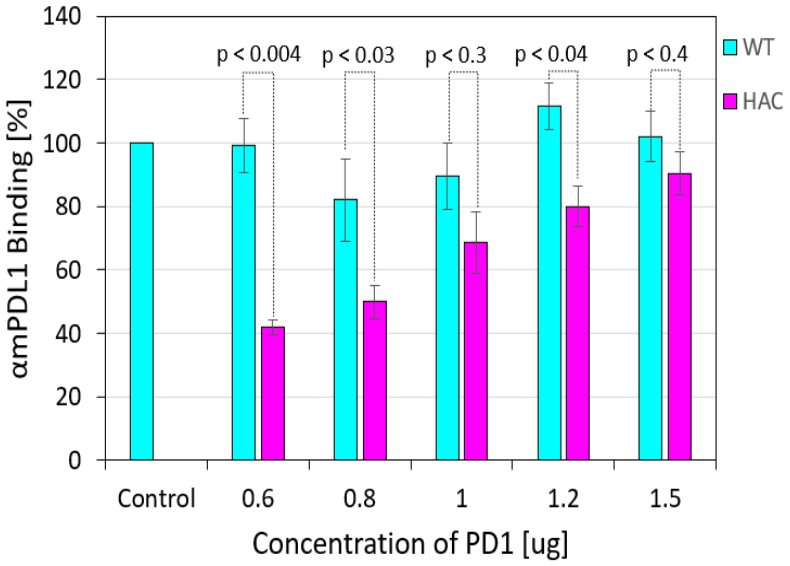

Figure 4.16 Effect of sPD1^{HAC} concentration on anti-mPDL1 binding to 5TGM1 cells. 4x10^{5} 5TGM1 cells per sample treated with either various concentrations of sPD1^{HAC}, sPD1^{WT}, or PBS (for controls). Then, sPD1 added samples were stained with PE-conjugated anti-mPDL1 (10F.9G2) and PBS-added cells were stained with PE-conjugated anti-mPDL1 (for positive control) or corresponding isotype (for negative control). MFI values were corrected by subtracting background (negative control), and the corrected positive control was accepted as 100% anti-mPDL1 binding. Results were collected from three independent experiments (n = 3), and p-values are indicated on the figure.

4.9.4 MSC-derived sPD1^{HAC} inhibitory effect on 10F.9G2 binding was evident on 5TGM1 and B16.F10 cells.

To further validate the differences between the binding of anti-mPDL1 clones and the inhibition effect of sPD1^{HAC} on these bindings MSC-derived HAC variant was used on 5TGM1 and B16.F10 cells. The same experimental setup of antibody binding competition, which was used for mPDL1 overexpressing HEK293T cells (section 4.9.1), was utilized.

On 5TGM1 cells HAC variant inhibited 10F.9G2 and MIF7 binding, but it was not able to interfere with the binding of MIH6. In the histograms, it was evident that sPD1^{HAC}

shifted the 10F.9G2 binding signal towards the negative control; MIH7 binding could not move that much, and MIH6 binding almost did not change (Figure 4.17A). Although fairly lower endogenous mPDL1 expression levels than RKO and HEK293T.mPDL1 present a clear representation of $sPD1^{HAC}$ inhibition on histograms, anti-mPDL1 binding ratio analysis confirmed these histograms with 15, 65, and 92% binding in that order, for 10F.9G2, MIH7, and MIH6, in the presence of HAC variant. Inhibitions of MIH7 and 10F.9G2 bindings were significant with p-values lower than 0.00005 and 0.003, respectively (Figure 4.17B).

In terms of anti-mPDL1 clones' bindings in the absence of a competitor, similar results were observed on 5TGM1 and HEK293T.mPDL1 cells. MIH6 was giving the highest signal indicating high mPDL1 expression, followed by 10F.9G2; however, MIH7 was able to detect less mPDL1 than these clones. This comparison was represented by giving the positive control signals of all three clones on 5TGM1 cells in a histogram (Figure 4.17C).

On B16.F10 cells, the HAC variant produced leftward shifts in the histograms for all three anti-mPDL1 clones. The pattern matched 5TGM1, with 10F.9G2 showing the largest shift, MIH7 intermediate, and MIH6 the smallest; shifts for MIH6 and MIH7 were marginally larger on B16.F10 than on 5TGM1 (Figure 4.17D). Anti-mPDL1 binding ratios were 87%, 58%, and 21% for MIH6, MIH7, and 10F.9G2 clones with p-values less than 0.2, 0.08, and 0.0003, respectively (Figure 4.17E). When only positive controls were compared, B16.F10 cells showed slightly higher binding by 10F.9G2 than by MIH6, in contrast to 5TGM1 and HEK293T.mPDL1, while MIH7 remained the lowest binder to mPDL1 (Figure 4.17F).

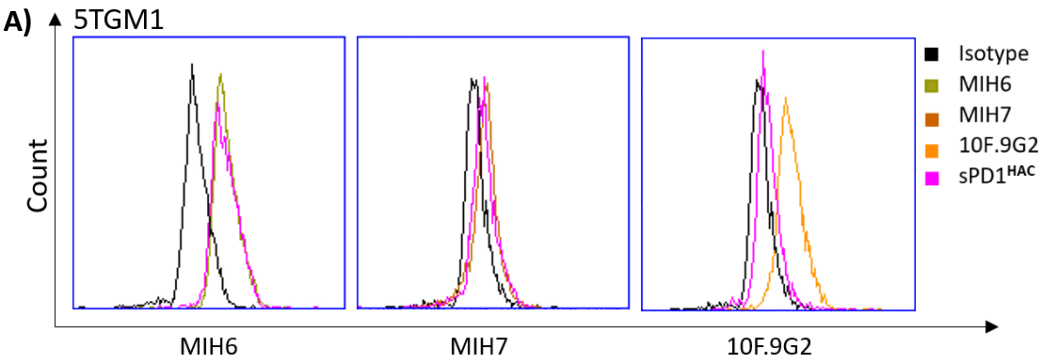
A)
5TGM1
Count
MIH6
MIH7
10F.9G2
Isotype
MIH6
MIH7
10F.9G2
sPD1HAC

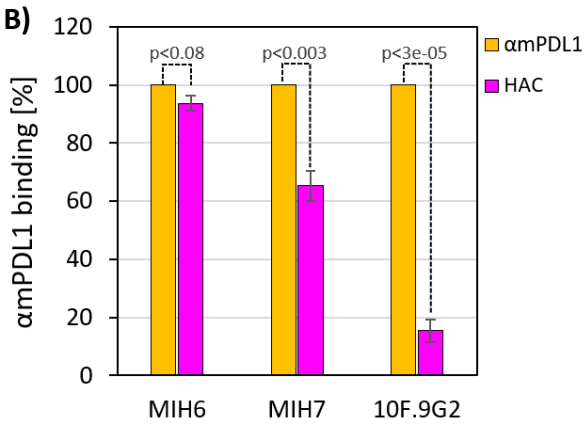
B)
αmPDL1 binding [%]
120
100
80
60
40
20
0
p<0.08
p<0.003
p<3e-05
αmPDL1
HAC
MIH6
MIH7
10F.9G2

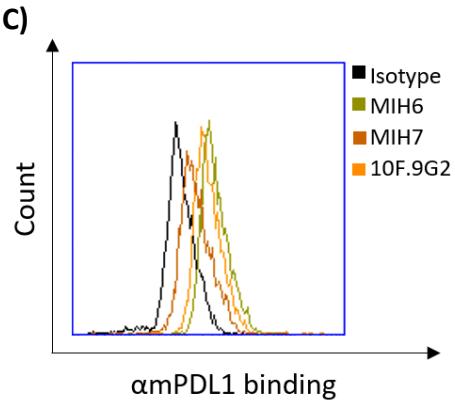
C)
Count
αmPDL1 binding
Isotype
MIH6
MIH7
10F.9G2

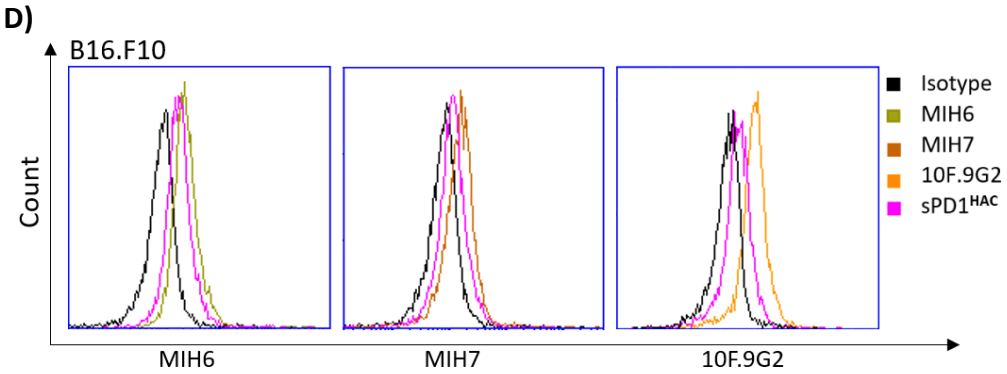
D)
B16.F10
Count
MIH6
MIH7
10F.9G2
Isotype
MIH6
MIH7
10F.9G2
sPD1HAC

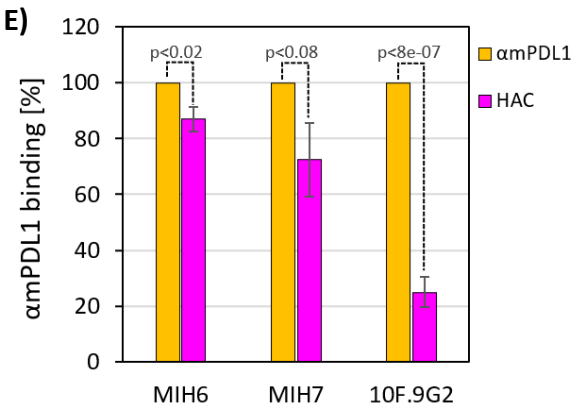
E)
αmPDL1 binding [%]
120
100
80
60
40
20
0
p<0.02
p<0.08
p<8e-07
αmPDL1
HAC
MIH6
MIH7
10F.9G2

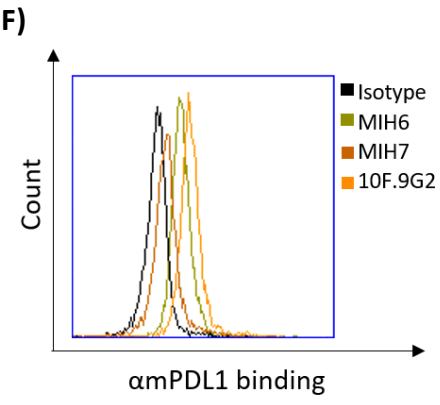
F)
Count
αmPDL1 binding
Isotype
MIH6
MIH7
10F.9G2

Figure 4.17 sPD1^{HAC} blocking effect on anti-mPDL1 clones binding to mPDL1 on both 5TGM1 and B16.F10. Antibody binding competition assays were applied as described before on 5TGM1 and B16.F10 cells between MSC-derived sPD1^{HAC} and mPDL1 clones (MIH6, MIH7, 10F.9G2), and normalisation and analysis of data were applied as outlined for antibody binding assays before. **A)** Histograms of antibody competitions against MIH6, MIH7, and 10F.9G2 clones of mPDL1 on 5TGM1 cells are shown. **B)** mPDL1 binding ratios are shown for MIH6, MIH7, and 10F.9G2 antibodies in the presence of HAC variant**. C)** Positive controls of competitions were represented in one histogram for binding comparison of these clones. **D)** Histograms of antibody competition on B16.F10 cells with these clones are shown. **E)** Data analysis shows 21%, 58%, and 87% binding ratios, respectively. **F)** Comparison histograms show the highest binding for the 10F.9G2 clone on B16.F10 cells, followed by MIH6 and MIH7. Results were collected from three independent experiments (n = 3), and p-values are indicated on the figures.

Consequently, B16.F10 cells were identified as a feasible candidate to explore the therapeutic effect of MSC-derived sPD1^{HAC} in *in vivo* experimental settings, due to strong inhibition of HAC variant on these cells within other murine cancer cell lines analysed.

4.10 Binding of mPDL1 on B16.F10 to Durvalumab monoclonal antibody was significantly inhibited by sPD1^{HAC}

To confirm the strong blocking capability of the HAC variant and to confirm the murine cancer cell line that will be used in vivo, lastly, binding reductions of HAC and Durvalumab monoclonal anti-PDL1 therapeutic antibody were compared on B16.F10 cells. Two different competitions were conducted with this aim: a cell-based binding assay, in which DUR and HAC, each, competes against biotinylated rmPD1 (the main competitor), and an antibody binding assay, in which HAC variant competes against PE-conjugated Durvalumab, DUR (PE), utilised as a main competitor. While antibody binding competition provides direct competition of these two blockers, cell-based provides in direct comparison by giving the inhibition effect of both on biotinylated rmPD1.

B16.F10 cells incubated with 800 ng/per sample sPD1^{HAC} (either derived from HEK293T or MSC) or molar equivalent DUR mixed with biotinylated rmPD1 (4000 ng/per sample) for 25 min. Positive controls were incubated only with rmPD1, and negative controls were incubated only with PBS in this step. Then they were treated

with streptavidin-PE for another 25 min for the detection of rmPD1 binding. Lastly, cells were cleared and fixed for PE detection on flow cytometry. The rmPD1 binding ratio was calculated by taking the background-corrected positive control as 100% binding. Results show that both DUR and HEK293T-derived sPD1^{HAC} inhibit the mPDL1-rmPD1 binding on B16.F10 cells, letting 37% and 5% rmPD1 bind, respectively, but sPD1^{HAC} inhibition was significantly stronger than DUR ($p < 0.0003$). Similarly, MSC-derived sPD1^{HAC} caused highly inhibited rmPD1 binding with 7%, while DUR could only reach approximately 63% rmPD1 binding in this assay (Figure 4.18A). Still, both of these binding reductions were significant compared to the positive control, and sPD1^{HAC} inhibition was still substantially higher than the DUR ($p < 0.0002$).

In antibody binding competition, here we used DUR (PE) as a main competitor and binding probe, which consequently directly competes against sPD1 variants. Briefly, B16.F10 cells were treated with one of the HEK293T-derived sPD1 variants (sPD1^{HAC}/ sPD1^{WT}), MSC.LUC, or MSC-derived sPD1^{HAC}. Then DUR (PE) was added to the samples following the manufacturer's instructions, and cells were incubated with these mixes for 25 min. For positive control, cells were treated with only DUR (PE), and for negative control, they were treated with the corresponding isotype.

After flow cytometric analysis, HEK293T-derived sPD1^{HAC} was revealed as a strong inhibitor of mPDL1-DUR (PE) binding. The histogram shows a wide leftward shift in the presence of sPD1^{HAC}, indicating inhibited DUR (PE) binding, while the addition of sPD1^{WT} was able to shift the signal moderately (Figure 4.18B). However, this inhibition of sPD1^{WT} was particularly interesting due to its strength, since sPD1^{WT} has not been able to cause this much inhibition on any of the main competitors (rhPD1, rmPD1, anti-mPDL1, or ahPDL1) before.

sPD1^{HAC} produced in MSCs was capable of reducing mPDL1-DUR (PE) binding. This was evidenced on the histogram by the leftward shifting signal from positive control to negative in the presence of sPD1^{HAC} (Figure 4.18B). Analysis of MFI ratios indicated that MSC-derived HAC variant significantly ($p < 0.0004$) inhibited DUR (PE) binding to 18%, while MSC.LUC was not effective on it (Figure 4.18C).

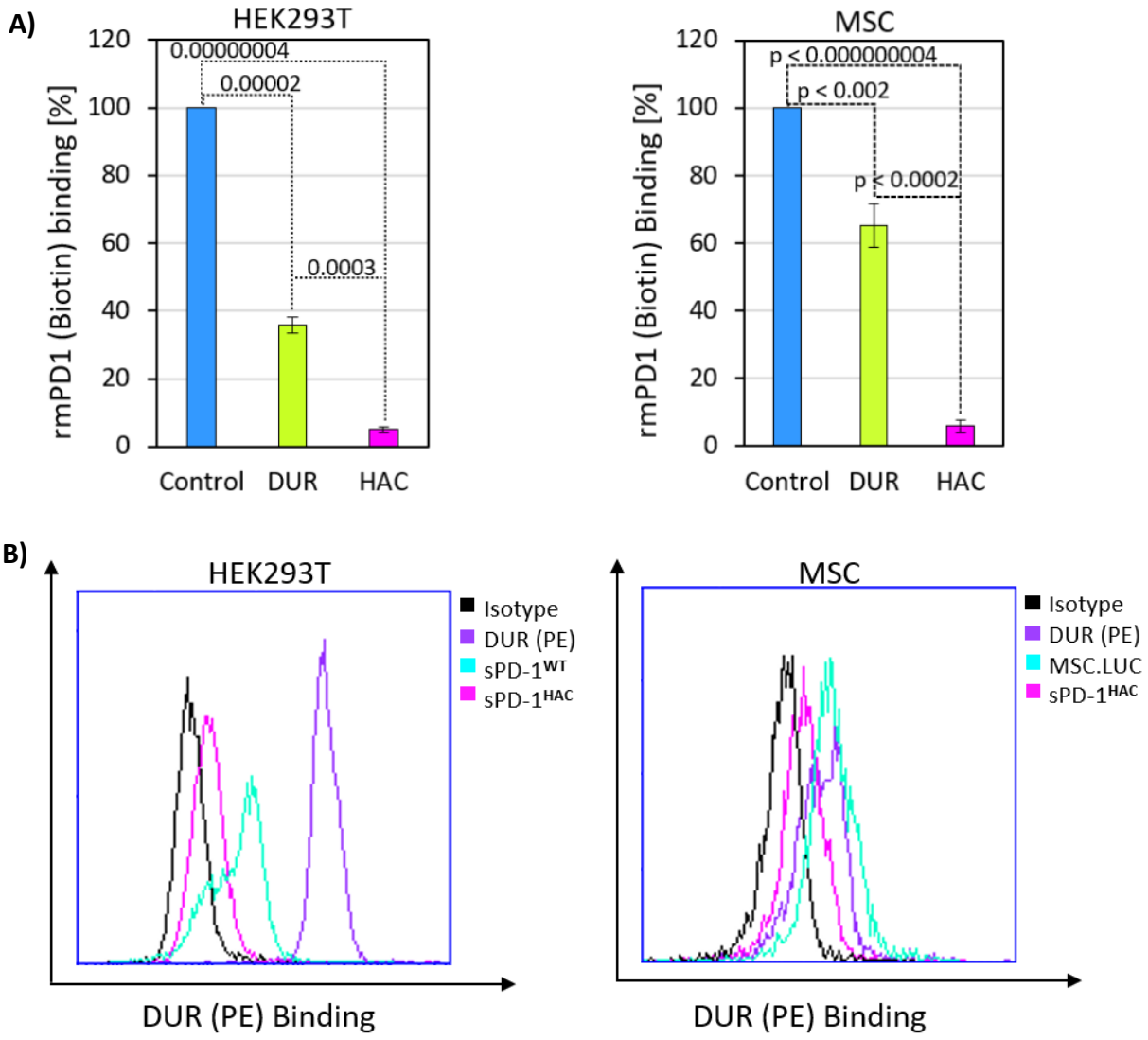
A)
HEK293T
rmPD1 (Biotin) binding [%]
0.00000004
0.00002
0.0003
Control
DUR
HAC
MSC
rmPD1 (Biotin) Binding [%]
p < 0.000000004
p < 0.002
p < 0.0002
B)
HEK293T
Isotype
DUR (PE)
sPD-1WT
sPD-1HAC
DUR (PE) Binding
MSC
Isotype
DUR (PE)
MSC.LUC
sPD-1HAC
DUR (PE) Binding
C)
DUR (PE) Binding [%]
p < 0.002
p < 0.3
Control
WT
HAC
p < 0.0004
p < 0.0005
Control
LUC
HAC

Figure 4.18 sPD1^{HAC} and DUR competition for PDL1 on B16.F10 cells. A) Cell-based binding competition assay was utilised with the same parameters as detailed before on B16.F10 cells and utilising biotinylated recombinant mouse PD1 (rmPD1). The binding of rmPD1 was accepted as 100% by subtracting the MFI of the negative control from the MFI of the positive control. DUR, MSC-derived sPD1^{HAC}, and HEK293T-derived sPD1^{HAC} competed against rmPD1 for the PDL1 on B16.F10 cells. **B)** To establish the competition between DUR and sPD1^{HAC} directly, PE-conjugated DUR was used as the main binding probe in the antibody binding competition setting. 4x10^5 B16.F10 cells treated with sPD1^{HAC} or PBS (positive control), then stained with DUR (PE) or its isotype (negative control). Corrected MFI of the positive control was accepted as 100% DUR (PE) binding. **C)** Analysis of the antibody competition on B16.F10 cells shows the percentage of background-corrected PE-conjugated DUR binding in the presence of sPD1 variants or MSC.LUC. Results were collected from three independent experiments (n = 3), and p-values are indicated on the figure.

Consequently, it was established that the HAC variant was significantly effective at blocking not only human PD1-hPDL1 bindings but also on murine PD1-mPDL1 bindings, as well as the cross-species bindings of this pathway (mPDL1-DUR). Particularly, in the presence of sPD1^{HAC} derived from MSCs, more than 72% of all explored PD1-PDL1 reactions were inhibited significantly. The fact that these therapeutics (DUR or HAC) were not generated for murine cells, the HAC variant was found effective even on murine cancer cells by reducing mPDL1 bindings significantly to approximately a 10% range. Besides, MSCs have proven themselves as a feasible therapeutic carrier with the lowest endogenous PDL1 expression, high yields of sPD1, and no change in cytokine secretion after the sPD1 gene insertion. All these odds taken together, the next step was found viable, and in vivo experiments were set to see the inhibition ability of the HAC variant on mice.

4.11 MSC-delivered sPD1^{HAC} reduces pulmonary metastatic burden in a syngeneic melanoma model

Having established that sPD1^{HAC}, specifically the MSC-secreted version of it, blocks PD1-PDL1 engagement and reduces binding of selected recombinant anti-PDL1 antibodies as well as recombinant PD1 proteins both in human and murine systems, in vivo efficacy was next evaluated in an immune-competent setting. The B16.F10 model was selected because intravenous inoculation yields reproducible pulmonary

metastases in C57BL/6 mice within a short interval, and it is widely used to assess checkpoint-directed interventions (Sitnik *et al.*, 2020; Tata *et al.*, 2021)

C57BL/6 mice were randomised to treatment and control groups (8 per group; two independent cohorts, total=16). On day 0, B16.F10 cells were administered by tail vein injection at $4x10^5$ cells in 100 µL PBS to seed lung lesions. Seven days later, mice received a single intravenous dose of MSC.sPD1^{HAC} $4x10^5$ cells in 100 µL PBS or control MSC.LUC in PBS at the same volume. Macroscopic lesion counts were conducted by investigators blinded to treatment assignment. Animals were euthanised on day 14, lungs were dissected and fixed in 4% PFA, photographed for surface nodule enumeration, and processed for histology (Figure 4.19A). The primary endpoint was the number of surface metastases per lung.

At day 14, control lungs (MSC.LUC) displayed numerous black metastatic nodules consistent with B16.F10 growth, whereas MSC.sPD1^{HAC}-treated lungs showed visibly fewer and smaller nodules (Figure 4.19B). Quantitatively, median surface nodule counts were reduced approximately six-fold in the MSC.sPD1^{HAC} group relative to MSC.LUC (median 215 vs 35 nodules per lung). This magnitude of reduction was replicated across independent cohorts with comparable variance ($p < 0.008$), supporting the robustness of the effect. Representative gross images illustrate the qualitative difference in metastatic load (Figure 4.19C).

Macroscopic lung nodules in the sections were enumerated by visual inspection using a millimetre ruler for size reference after embedding lung lobes in paraffin blocks and sectioning them through various dimensions. Counts were then stratified by diameter (1-0.5 mm and ≤0.5 mm) and recorded under a microscope at 4x. Section nodule size and count inspection revealed a parallel decrease in mean nodule number. Mean number of nodules with a diameter size of 1 mm to 0.5 mm decreased on averagely from 3.7 to 0.6 with MSC.sPD1^{HAC} treatment, and nodules with a diameter size of 0.5 mm or smaller decreased from 127 to 43 (Figure 4.19D).

Treatment with MSC.sPD1^{HAC} consistently reduced pulmonary metastatic burden in the B16.F10 model across macroscopic counts and quantitative section-based metrics (Figure 4.19A-D). The magnitude of effect was notable given the cross-species context, as sPD1^{HAC} was engineered for human PDL1 yet demonstrated activity in a murine system in which partial cross-reactivity had been observed in vitro. These

results indicate that sustained delivery of sPD1^{HAC} from MSCs can produce a therapeutically meaningful reduction in tumour load within a short dosing window.

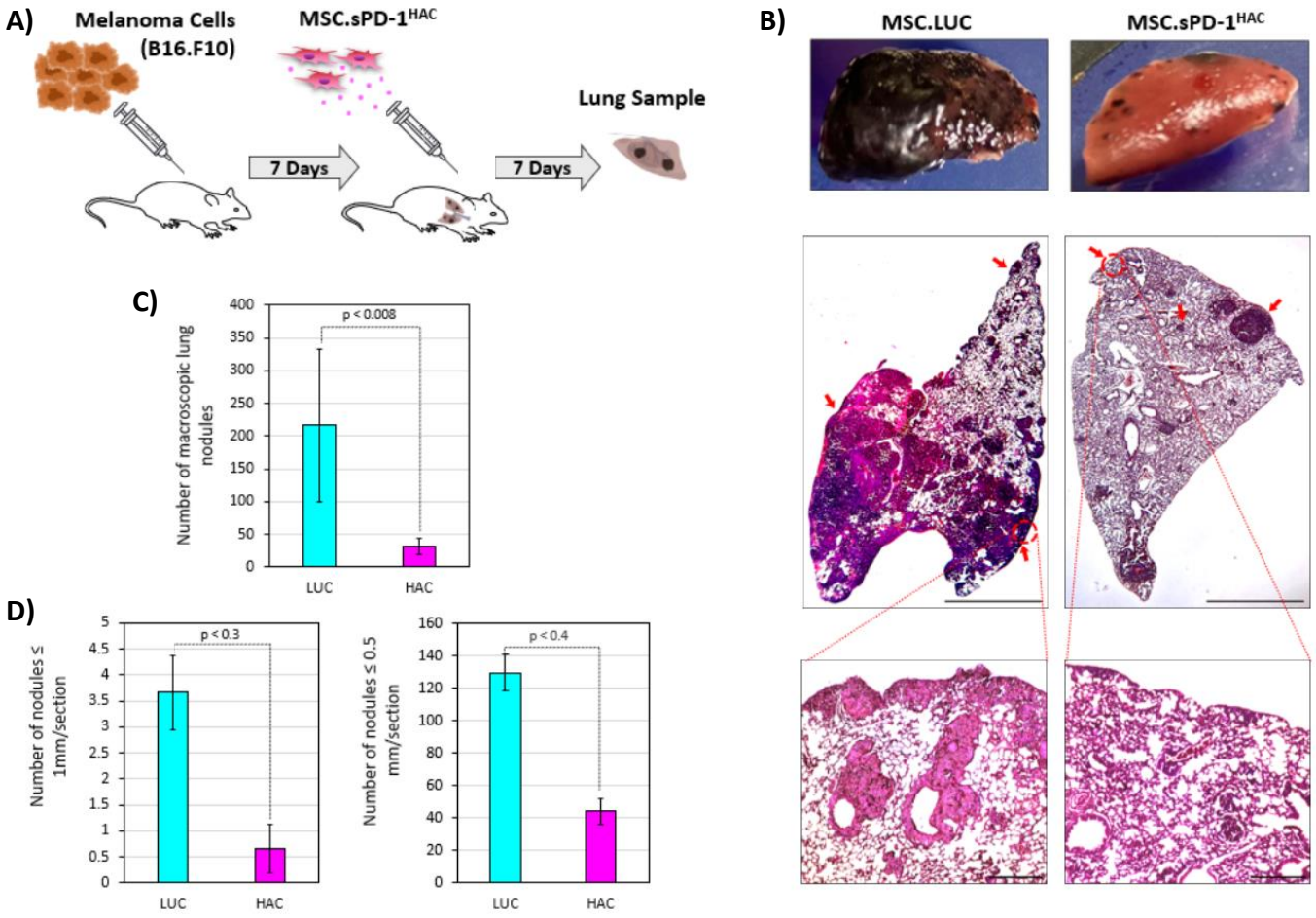

Figure 4.19 In vivo effects of PD1/PDL1 blocking by MSC-delivered sPD1^{HAC} in a syngeneic B16.F10 model. A) Study schema. C57BL/6 mice received B16.F10 cells (4×10^5 cells, i.v., day 0), followed on day 7 by a single i.v. dose of MSCs secreting sPD1^{HAC} (MSC.sPD1^{HAC}, 4×10^5 cells) or control luciferase-expressing MSCs (MSC.LUC, 4×10^5 cells). Lungs were collected on day 14 for macroscopic counting and histology assessment. **B)** Representative gross lung images from MSC.LUC and MSC.sPD1^{HAC}-treated mice. Lung lobes were embedded in paraffin wax, sectioned at 5 µm from multiple planes across the lung lobes and stained with H&E. Microscopic images of the representative sections are shown, with metastatic foci indicated by arrows (scale bar: 3mm). Lower panels show corresponding 10x magnification views with a scale bar of 300 µm. **C)** Analysis of macroscopic surface nodule counts of randomised lungs. D) Quantification of metastatic nodules in lung sections stratified by diameter. Results are shown as mean ± SE, and p-values indicated on the figure.

The current study was designed as a short-term metastasis-burden read-out rather than a survival study; durability of response and optimal dosing frequency, therefore, remain to be defined. Additional studies will evaluate alternative schedules (for example, dosing on days 7 and 10), dose-response of MSC numbers, and biodistribution of infused MSCs. Orthogonal read-outs such as ex vivo cytotoxic T-cell activity, cytokine profiling, and longitudinal imaging are expected to strengthen mechanistic attribution. Given the efficacy signal and acceptable tolerability observed here, escalation to survival endpoints in subcutaneous or orthotopic models is warranted.

Chapter 5: Discussion

5. Discussion

Collectively, these data show that sPD1^{HAC}, when delivered via MSCs, inhibits PD1-PDL1 interactions both in vitro and in vivo, resulting in a marked reduction of metastatic burden in a syngeneic C57BL/6 highly aggressive melanoma model. Unlike other cell therapies, this MSC-based novel approach addresses the central barriers of delivery, infiltration, and durability by exploiting the MSC homing ability for targeted delivery and employing a non-antibody sPD1^{HAC}, which has a high PDL1 affinity exceeding that of commercial anti-PDL1 antibodies, including durvalumab.

Additionally, although hot-cold tumour phenotypes are defined by not only T-cells but overall inflammation and cell type composition of TME, we found that T-cell markers alone can stratify patients into hot/cold phenotypes which was then indicate melanoma as the most susceptible to PD1 therapies, followed by lung adenocarcinoma and breast invasive carcinoma consistently with the responsive cancer types to these therapies in the literature (Cormedi *et al.*, 2021). Colorectal cancer was not found in the top three of inflamed cancer types, probably due to the mix of samples with or without mismatch repair deficiency (Mao *et al.*, 2023). Therefore, it shows PD1 therapies are tightly dependent on developmental lineage and the presence of T-cells, as well as inflamed TME and genomic factors such as high tumour mutational burden, dMMR, and high microsatellite instability (Ribas, 2025). Second analysis of cancer types for PDL1 co-expression profiles showed that, particularly in skin cutaneous melanoma, PDL1 expression significantly correlated with 128 other immune-related genes, followed by breast invasive (101) and colorectal cancer (100). In contrast, 16 other cancer types cannot reach a total of 58 correlated genes, further explaining the response rates to monoclonal therapy in these cancer types.

Engineering of CHO, HEK293T, and MSC cells showed that sPD1^{HAC} can be secreted efficiently from these producer cells. Secretion was approximately 3.5-5.5 fold higher with IgG1-Fc fusion and was achieved in all cell types, with CHO reaching approximately 3µg /ml for sPD1^{HAC}, HEK293T reaching 8µg /ml, and MSC reaching 1.2µg/ml at 48 h, without compromising producer-cell viability, thereby supporting scale-up potential for bioactive payload provision in vitro and in vivo. The IgG1-Fc domain confers advantageous pharmacokinetic and effector properties to fusion proteins. Fusion to Fc increases the hydrodynamic size and reduces renal clearance.

At the same time, engagement of the neonatal Fc receptor (FcRn) in a pH-dependent recycling pathway protects the protein from endosomal degradation and thereby extends plasma half-life (Ward *et al.*, 2015). In immune effector terms, Fc ligation of Fcγ receptors (FcγRs) on leukocytes can elicit antibody-dependent cellular cytotoxicity, with target-cell killing mediated by perforin, granzymes and tumour necrosis factor (Nimmerjahn *et al.*, 2015). Among human IgG subclasses, IgG1 exhibits the highest overall affinity for activating FcγRs and is correspondingly one of the most potent in recruiting cytotoxic effector pathways (Cohen Saban *et al.*, 2023). These features render the IgG1-Fc scaffold attractive in oncology applications that require selective elimination of tumour cells and, when appropriately configured, enhance the therapeutic performance of sPD1^{HAC}.

Cell-based, solid-phase and antibody-based competition assays supported this approach and cumulatively demonstrated that MSC-derived sPD1^{HAC} inhibited rhPD1 binding to PDL1 by approximately 77-92% across titrations as low as 0.5-1 ng sPD1^{HAC} against 50 ng rhPD1 in solid-phase assays, while showing no measurable inhibition of rhPD1-PDL2 binding, indicating maintained ligand selectivity. Relative to a clinically used anti-PDL1 antibody, durvalumab, sPD1^{HAC} achieved similar or greater inhibition. It retained this activity by inhibiting the binding of rPD1 and anti-PD1 antibodies, including Durvalumab, approximately 80-94% on melanoma, colorectal, and myeloma cancer cell lines.

Aligning with this evidence, intravenous injection of MSC.sPD1^{HAC} to B16.F10 bearing mice resulted in a marked reduction of metastatic burden in a syngeneic C57BL/6 melanoma model. Together, the data support a model in which local ligand interception within the tumour bed, provided continuously by homing MSCs, can restore cytotoxic function where PDL1 is abundant and T-cell tone is sufficient. These sections interpret the mechanistic basis for this effect, situate the findings within the context of prior literature on checkpoint modulation and MSC vectors, delineate limitations, and outline testable predictions and translational steps.

5.1 Melanoma is the most susceptible cancer type to PD1 therapies due to inflamed and PDL1-related expression networks

PD1-PDL1 monoclonal therapies were the first to gain recognition by demonstrating durable responses in metastatic melanoma. Since then, several cancer types have been treated, showing promising results, such as renal cancer, non-small lung cancer, and triple-negative breast cancer (Balar and Weber, 2017; Brahmer *et al.*, 2010). However, the response rate was higher in melanoma patients (Eroglu *et al.*, 2018), and the reason behind this hold-back in monoclonal therapies has been rigorously studied to date, with the aim of finding a patient group that can benefit from these therapies. Several studies indicate that patients with dMMR, MSI-H, or high tumour mutational burden exhibit higher response rates to PD1 therapy (Darvin *et al.*, 2018). An inflamed, T-cell-rich TME is likewise associated with improved benefit (Homet Moreno *et al.*, 2015). Nevertheless, the mechanistic basis for melanoma's apparent susceptibility to PD1 blockade remains incompletely defined.

5.1.1 Pan-cancer immune landscapes rationalise where a PDL1-focused strategy should work

In this study, the TCGA Pan-Cancer Atlas studies were inspected from two perspectives: T-cell markers and 323 other immune-related genes. According to T-cell marker analysis, "hot" and TEX-dominant "cold" states, with melanoma, lung and breast cancer, are harbouring broader and more intense hot sample numbers across 7 cancer types. Although this study was limited to a predetermined gene group and specific cancer types, melanoma yielded the highest results in both studies, with a hot intensity of 1.2 (95% CI), a hot summary score of 0.28, and 128 out of 323 genes correlating with PDL1 expression. This inflamed TME and dense connections to PDL1 expression may underlie comparatively high response rates in melanoma (Eroglu *et al.*, 2018). Prospective stratification across larger, multi-tumour cohorts, analysed alongside treatment outcomes, will be needed to clarify this relationship and optimise patient selection.

In 2021, it was found that the IFNγ expression loop, which leads to anti-PD1 immunotherapy resistance, is caused by a downstream effector, yes-associated

protein (Du *et al.;* Yu *et al.*, 2021). Based on this finding, we can say that there are narrow adaptive-resistance subgroups within several cancer types, characterised by the co-elevation of activation markers, PDL1, and TEX features, consistent with IFN-γ-driven negative feedback. This pattern also predicts that local interception of PDL1 should be most productive where pre-existing activation is measurable and ligand is induced. Therefore, targeting this phenotype with combinational MSC-cell therapy that harbours $sPD1^{HAC}$ and a YAP inducer may be the next strategy to overcome resistance.

5.1.2 PDL1 tracks IFNγ-linked activation yet lacks a universal regulatory signature, implying indication-specific biomarkers.

Expansion from a narrow T-cell activation panel to a 323-gene immune-related gene panel reveals that PDL1 lacks a single pan-cancer correlational fingerprint applicable to all cancer types. Melanoma exhibits the strongest association with PDL1 among immune markers, whereas other cancer types display mixed or tissue-specific associations. This argues against a one-size-fits-all biomarker approach and supports tumour type-specific cut-offs or composite scores that integrate abundance, activation, and immune context. Overall, the cancer types in which PDL1 expression correlated with more immune-related genes were the representative cancer types where PD1 monoclonal therapies are recommended the most, including melanoma, breast and colorectal cancer. This may suggest that certain cancer types and tissues are more likely to utilise PDL1 as an escape mechanism.

In the present study, the preclinical focus on melanoma and colorectal cancer systems is consistent with the bioinformatic expectation that PDL1-centric interventions will perform the best where hotness and IFNγ-induced PDL1 are present. The dataset also cautions that immune-desert tissues or TEX-dominant cold states without abundance are less likely to benefit without priming or recruitment strategies that raise T-cell tone. Spatial context is also critical, since PDL1 confined to stromal myeloid cells without T-cell ingress may be less informative than tumour cell proximal ligand within inflamed nests. Accordingly, thresholds should be calibrated per indication and platform, and composite predictors should be prospectively validated with harmonised assays to reduce false negatives and enable cross-trial comparability.

5.1.3 The biology of IFNγ-PDL1 induction and PD1 expression on target cells clarifies the scope and boundary conditions

IFNγ robustly induces PDL1 on several tumour lines, whereas PD1 is absent from tumour cell surfaces in this panel. Across assayed cancer cell lines, IFNγ increased PDL1 significantly on 15 cell lines out of 18, aligning with the expectation of adaptive resistance in hot microenvironments. It was stated before that tumour intrinsic PD1 promotes tumorigenesis in many cancer types (Chen *et al.*, 2023). Starting with this knowledge, we wondered whether they have PD1 attached to their cell membranes. No detectable PD1 was found on tumour surfaces, reducing concern that tumour-cell PD1 might sequester $sPD1^{HAC}$. These observations support a ligand-interception mechanism that does not involve significant off-target scavenging by cancer cells themselves. Although the inducing ability of IFNγ on PDL1 expression has been well-studied, these studies were limited to 1 to 4 cancer types or focused on downstream pathways of the induction mechanism (Garcia-Diaz *et al.*, 2017; Iwasa *et al.*, 2019). This leaves a gap in the literature, as it is not determined how cancer cell lines respond to IFNγ induction, particularly those commonly utilised in cancer research. Ultimately, this knowledge informs future project designs to utilise the most suitable cell line.

The combination of inducible PDL1 and absent tumour PD1 provides favourable pharmacology for an MSC-delivered soluble PD1. In such contexts, $sPD1^{HAC}$ competes primarily at the intended

ligand, with minimal diversion to tumour PD1 sinks.

5.2 $sPD1^{HAC}$ variant blocks the PD1-PDL1 pathway both in vitro and in vivo

IgG1-Fc fusion of $sPD1^{HAC}$ enabled high-yield secretion without producer toxicity while preserving selectivity for PDL1. Across orthogonal solid-phase and cell-based assays, $sPD1^{HAC}$ consistently displaced rhPD1 from PDL1 more effectively than $sPD1^{WT}$ and DUR, with negligible activity on PDL2; when delivered by MSCs, this translated into a reduced pulmonary metastatic burden in a B16.F10 model, supporting ligand

interception as the operative mechanism and motivating studies of durability, Fc silencing, and functional co-culture readout.

5.2.1 Molecular engineering choices enabled high-yield secretion without imposing producer toxicity

IgG1-Fc fusion increased secretion by approximately threefold and fivefold, and stabilised the payload in both human and hamster producer lines, respectively. Expression from pFUSE with sPD1 binding to IgG1-Fc yielded higher secretion than sPD1 variants in both CHO and HEK293T. The increase for $sPD1^{HAC}$ was significant in both lines, with a more substantial effect in HEK293T, while $sPD1^{WT}$ exhibited a significant increase in HEK293T and a non-significant trend in CHO. These gains, together with viability preservation measured by Nicoletti hypodiploidy assays, indicate that Fc fusion improved trafficking and secretion without evident cytotoxic cost at 48 h. This has two mechanistic consequences. First, Fc fusion likely contributes to avidity and half-life in conditioned media and in the pericellular milieu of MSCs, which may increase functional occupancy of PDL1 at a given secretion rate. Second, a stable Fc-bearing scaffold supports consistent competition readouts across assays.

The signal peptide and furin site ensured entry into and processing through the secretory pathway, while the $sPD1^{HAC}$ mutational constellation encoded at residues 64, 65, 66, 68, 70, 74, 78, 122, 125 and 132 enhanced affinity to PDL1. Interestingly, it is suggested that the most flexible T59, N74, P89 and key contributors of binding N33, Q75, T76, R104, K131, and K135 residues were more suitable to perform multi-site mutagenesis by Du et al. $sPD1^{HAC}$ variant argues this by representing competitive and high binding abilities in vitro and in vivo. In the same study, Du et al. identified that K135 changes the affinity of the protein. However, it is not in the contact area, indicating that structural proteomic techniques require coupling with biological context assays to determine high affinity (Du *et al.*, 2018). Additionally, the absence of measurable binding interference to PDL2 across tested concentrations indicates that the affinity optimisation preserved selectivity in the context of this fusion and assay configuration.

Although 48 h secretion and viability look favourable, longer secretion windows and stress assays were not reported here and will be needed to define durability. Glycosylation and Fcγ receptor engagement were not profiled; while the Fc is used primarily for secretion and stability, inadvertent engagement could modulate local myeloid tone in vivo. An Fc-silenced or non-effector variant would clarify whether any Fc-dependent biology contributes to efficacy.

5.2.2 sPD1^{HAC} exhibited robust PDL1-selective competition in solid-phase formats

Solid-phase competition demonstrated profound, selective inhibition of rhPD1-PDL1 binding, with a negligible effect on PDL2. Across titrations as low as 0.5-1 ng of sPD1^{HAC} against a fixed 50 ng rhPD1, residual PD1 binding to PDL1 was 8-23% depending on producer line and concentration, while sPD1^{WT} remained near control levels. By contrast, neither variant altered rhPD1-PDL2 binding under identical conditions. These data isolate ligand-centric interference and exclude a generalised artefact of biotinylated PD1 handling. This antibody binding competition is also a novel approach, with one exception. Ji Yeon Ha et al. have used a similar protocol to compare PD1 bindings in 2023, but their study focused on Glycan-controlled PD1 variants. For the competitions, they utilised the same or higher concentrations of PD1 variants than the ligand (Ha *et al.*, 2023). Other than this study, the binding abilities of a PD1 variant and its ability to re-establish PD1-PDL1 binding have been studied through biochemical and proteomic assays such as surface plasmon resonance, phage display screening and affinity tests (Li *et al.*, 2018; Maute *et al.*, 2015; Pascolutti *et al.*, 2016) however, this technique allow PD1 variants to compete for the limited source of ligand, thereby imitating biological environment they would be in as a therapeutic.

5.2.3 Cell-based competition on RKO cells confirmed on-cell displacement of rhPD1

A saturating dose of rhPD1 was established at approximately 4,000 ng per 4 × 10^5 RKO cells. Under these conditions, conditioned media containing 5-fold less sPD1^{HAC}

reduced detectable rhPD1 occupancy on PDL1 and outcompeted rhPD1 in multiple assays, determined by flow cytometric readouts with streptavidin-PE detection. sPD1^{HAC} variant blocked almost all ligands leaving 7.6%, 6%, and 3.4% residual rhPD1 binding when derived from CHO, HEK293T, and MSC cells, respectively. While sPD1^{WT} retained 86-90% rhPD1 binding. It is also noteworthy that the blocking ability of CHO-derived sPD1^{HAC} was the lowest among these producer cell lines, which may indicate differences in the glycosylation step between human and animal cells. Overall, the direction and relative magnitudes were consistent with the solid-phase results, and a clear separation was observed between sPD1^{HAC} and sPD1^{WT}.

Lázár-Molnár et al. also developed a high-affinity PD1 variant. Although they studied it in a protein structure-guided method, they utilised a fairly similar binding method on the cell surface. They used PD1 variants as a base together with the producer cells and added ligands on these cells. Then they measured bound ligands for each condition, and detection was provided through APC-conjugated IgG and anti-hPDL1 antibodies. However, this assay differs from the usage of endogenous PDL1 expressed on the surface of colorectal cancer cells, providing a more physiologically relevant model.

5.2.4 sPD1^{HAC} has higher blocking ability than DUR, particularly in smaller concentrations

sPD1^{HAC} achieved similar or stronger competition than DUR in solid-phase competition for hPDL1-Fc on high-binding plates. Notably, smaller concentrations, 0.03 and 0.006 pmol of sPD1^{HAC} and DUR, which were respectively 100-fold and 500-fold smaller than rPD1 that they competed for, sPD1^{HAC} continuously showed inhibition, while DUR lost its ability to displace rPD1. The difference between them was significant ($p < 0.02$ for both concentrations). Although DUR, as a commercial anti-PDL1 monoclonal antibody, achieved high response rates in many studies, particularly in a non-small lung cancer cohort with 473 patients, the 24-month overall survival rate was 66.3% (Antonia *et al.*, 2018), sPD1^{HAC} holds more potential in lower doses. Considering that the approved dose is 10 mg/kg every 3-4 weeks for up to 12 months (Alvarez-Argote and Dasanu, 2019), an MSC. sPD1^{HAC} therapy would perform better, secreting less PD1 without

frequent patient visits and possibly decreasing dose-dependent adverse effects that have been linked to the high doses (Colard-Thomas *et al.*, 2023).

The second competition platform was the cell surface; sPD1^{HAC} and DUR competed with rPD1 for RKO cell surface attached PDL1, in which sPD1^{HAC} again showed higher inhibition. While DUR inhibits, on average, 60% of the sPD1-PDL1 binding, MSC-derived sPD1^{HAC} caused approximately 95% binding reduction.

To be confident about the blocking superiority of sPD1^{HAC} over DUR, we designed another competition where they can compete against each other. For this, we utilised PE-conjugated DUR, which may negatively affect DUR binding performance due to the increased mass of the PE tag; however, this effect was negligible as the assay followed the manufacturer's recommended doses. This final direct competition indicated 94% binding reduction of DUR (PE) in the presence of sPD1^{HAC}, suggesting high-affinity and epitope-advantaged occupancy by sPD1^{HAC} on the native ligand. Antibodies provide systemic exposure and Fc-dependent mechanisms that may contribute to in vivo effects. By contrast, MSC-derived sPD1^{HAC} emphasises spatially concentrated ligand sequestration at tumour sites, potentially resulting in reduced systemic exposure. This difference may translate to distinct safety and efficacy trade-offs, particularly in immune-desert or myeloid-dominated tumours, where Fc-enabled myeloid modulation may be advantageous for antibodies, but where distribution limits can hamper their access. Conversely, in dense, inflamed lesions, local interception may better sustain effective occupancy.

sPD1^{HAC} overcompeted not only DUR but also other recombinant anti-PDL1 antibodies specifically designed to bind PDL1. CHO-, HEK293T-, and MSC-derived sPD1^{HAC} reduced anti-hPDL1 binding to 24%, 8% and 13%, respectively. Its blocking efficacy was consistent even in cross-species settings by reducing all three anti-mPDL1 clones on the surface of both B16.F10 and 5TGM1 cells, suggesting that sPD1^{HAC} can rival a full-length monoclonal in a ligand-occupancy context, particularly when delivered by MSCs. However, specific monoclonal antibodies and sPD1^{HAC} include different Fc-mediated mechanisms that may operate differently in vivo and may not be captured by binding competition alone.

In murine systems, sPD1^{HAC} blocked mPDL1-PD1 binding and inhibited multiple anti-mPDL1 clones with varying magnitudes. B16.F10 and 5TGM1 systems were

informative, whereas LL/2 and MC38 proved suboptimal for competition formats. The absence of a monotonic relationship between increasing sPD1^{HAC} concentration and inhibition of 5TGM1 within the analysed range suggests that surface presentation, local concentration, or epitope overlap can limit functional inhibition before mass action saturates the system or reaches the limits of sPD1^{HAC} blocking ability on murine cancer cells. Nevertheless, binding competition does not equate to functional antagonism in all contexts. While ligand occupancy is a prerequisite, signalling outcomes depend on spatial organisation, cis versus trans interactions, and local cytokine and myeloid states. Future assays should therefore include functional readouts such as phospho-signalling in T-cells, cytokine rescue, or killing assays to couple occupancy to function in co-culture.

5.2.5 MSCs are credible vehicles for sPD1^{HAC} delivery, with AT-MSCs offering a favourable baseline

MSC source screening identified AT-MSCs as operationally optimal for the vector role. Baseline PD1/PDL1 expression in MSC sources was low and inducible by IFNγ. AT-MSCs emerged as the best candidate as the least affected type of MSCs from IFNγ treatment, balancing transducibility, stability (no viability lost after transduction), and neutral cytokine output at baseline and after engineering (no change observed in cytokine array), which reduces confounding paracrine effects unrelated to the sPD1 payload.

Stable transduction produced durable secretion without affecting viability or cytokine profiles. Engineered MSCs sustained sPD1^{HAC} expression with preserved viability and without a detectable shift in cytokine secretion within the measured panel, supporting their use as a delivery vehicle that is mechanistically clean with respect to the endpoints studied.

In vivo, MSC tropism to inflamed or remodelling tissues positions the secreted sPD1^{HAC} in proximity to PDL1-bearing tumour and myeloid cells. Continuous local production may partially overcome challenges that limit bolus antibody delivery in dense stroma and may maintain higher effective occupancy during IFNγ-driven adaptive resistance, where PDL1 is dynamically upregulated.

MSCs can adopt immunoregulatory phenotypes in response to specific contexts. Although cytokine output did not change in the measured conditions, in vivo polarisation by tumour factors could theoretically attenuate efficacy or, conversely, enhance it by providing additional chemokine gradients that recruit effector cells. Biodistribution and persistence studies, with lineage tracing and quantitative proteomics of sPD1^{HAC} in situ, will be necessary.

5.2.6 In vivo efficacy in a melanoma lung metastasis model demonstrates the functional consequence of ligand interception

Single-dose MSC.sPD1^{HAC} reduced the pulmonary metastatic burden compared to MSC.LUC controls. In C57BL/6 mice bearing B16.F10 pulmonary metastases initiated on day 0 and treated on day 7 with a single intravenous dose of engineered MSCs, lungs harvested on day 14 exhibited visibly fewer and smaller macroscopic lesions in the sPD1^{HAC} group. Quantitative measures of nodule count showed that macroscopic lesions were reduced 7-fold, and nodules smaller than 0.5 mm/section were reduced 3-fold by MSC.sPD1^{HAC}, with visual and descriptive endpoints indicating a marked reduction.

The efficacy is consistent with the in vitro selectivity profile and with the melanoma bioinformatics that identify a robust inflamed subset with adaptive resistance signatures. The reduction in metastatic burden following a single dose suggests that even transient occupancy can tip cytotoxic balance in hot lesions. Durability and dose response remain to be defined.

The syngeneic B16.F10 model, while stringent for lung colonisation, differs from orthotopic or spontaneous models in vascular access, stromal composition, and myeloid tone. A single dose and a 7-day window provide a conservative estimate of benefit; repeated dosing, earlier administration, or combination with priming agents could increase effect sizes but will require careful safety evaluation. Blinded histology and IHC quantifying CD8, PDL1, and Treg markers would tie efficacy to the predicted immune mechanism. Mularz et all who studied on mouse versus human PDL1 bindings on MC38 induced C57BL/6 mice and found that Durvalumab and small molecule inhibitors were found to be ineffective in blocking mPDL1 interactions (Magiera-Mularz *et al.*, 2021). Our study updates this opinion by blocking mPDL1 as a small molecule inhibitor.

The present work agrees with prior evidence that IFNγ induces PDL1, that ligand occupancy can relieve PD1-mediated inhibition, and that MSCs can deliver functional proteins to pathological tissues. The decoy approach is conceptually aligned with efforts to present PD1 domains as engineered ligands or trap constructs to neutralise PDL1.

Reports emphasising MSC-associated immunosuppression often involve alternative contexts, including different tissue sources, activation states, or cargoes. Here, AT-MSCs were selected following PD1/PDL1 screening and showed stable sPD1^{HAC} expression without shifts in cytokine profiles, which may explain the absence of overt suppression in the studied assays. Outcome differences across platforms can arise from differential Fc engagement, epitope geometry/valency, species constraints, or distribution dynamics, which are not captured by binding competition alone (Van Der Horst *et al.*, 2020).

The bioinformatic analyses indicate that the benefit is conditional on pre-existing T-cell abundance and activation, as well as IFNγ-inducible PDL1. In immune-desert states, ligand interception alone is unlikely to suffice, as increasingly evidenced across recent studies (Chen *et al.*, 2021; Ouyang *et al.*, 2024). Because the determinants of PDL1 expression vary across cancers and are not as favourable as in melanoma, ligand occupancy alone is unlikely to suffice universally, which may explain reduced benefit in some settings and the need for priming strategies.

5.3 Scope and next steps

The present work prioritised binding-competition readouts in vitro and a single-dose evaluation in one syngeneic model, establishing proof-of-principle. Binding competition assays demonstrate ligand interception at the tumour cell surface, including displacement of rhPD1 or anti PDL1 reagents, but they remain surrogate readouts of pathway blockade. Ligand occupancy alone does not confirm relief of PD1 mediated suppression or restoration of T-cell function, including T-cell reactivation, cytokine release, or restored tumour cell cytotoxicity, even though these outcomes have been demonstrated for checkpoint blockade in the wider literature. Demonstration of functional rescue, therefore, requires additional assays, ideally tumour and T-cell co-culture systems in which activation markers, effector cytokines,

and target cell killing are quantified under conditions that maintain PD1 and PDL1 engagement.

For the in vivo evaluation, the IgG1-Fc was used to enhance secretion and stability, while detailed characterisation of Fc-dependent effector pathways was outside the scope. Likewise, quantitative biodistribution, persistence, and in situ concentrations after MSC delivery to the murine model were not measured. These aspects are readily addressable through antigen-specific co-culture/killing assays to directly quantify functional restoration, alongside multi-dose orthotopic studies with blinded pathology, Fc-tuned comparators, and pharmacokinetic analyses (e.g., tagged sPD1^{HAC} or mass spectrometry) in tumour and normal tissues, strengthening translational implications and testable predictions.

The integrated dataset suggests a biomarker strategy centred on PDL1 levels and T-cell abundance, ideally integrating a composite score that reflects activation and excludes TEX-dominant cold states if abundance is low. The predictive metrics for inflamed T-cells applied here, including Hot Summary Score and Hot Intensity, can be adapted as a preclinical filter to prioritise indications such as melanoma and subsets of lung and breast cancers where adaptive resistance is likely to be operative. In immune-desert lesions, priming agents that increase T-cell infiltration and antigen presentation will be required. In myeloid-dominant tumours, agents that reduce suppressive tone may be necessary to complement PDL1 interception. Where PDL1 is abundant but T-cells are terminally exhausted, coupling sPD1^{HAC} with co-stimulatory agonists may be advantageous.

The single-dose in vivo design suggests that transient occupancy can be beneficial; however, the kinetics of MSC localisation and secretion argue for schedules that sustain local sPD1^{HAC} above an empirically defined occupancy threshold. A dose-finding study measuring lung and tumour sPD1^{HAC} concentrations versus inhibition of ex vivo DUR(PE) binding would directly link pharmacokinetics to pharmacodynamics.

Ligand interception localised by MSCs may reduce systemic immune perturbation relative to systemic antibodies, but ectopic deposition in inflamed non-tumour tissues could still occur. Off-tumour on-target risks can be evaluated by profiling sPD1^{HAC} in secondary lymphoid tissues and by monitoring T-cell activation markers systemically.

5.4 Concluding remarks

Taken together, the evidence supports a tractable model in which MSC-delivered sPD1^{HAC} achieves local ligand interception at PDL1, preserves selectivity over PDL2, and meaningfully reduces metastatic burden in an aggressive melanoma setting. Concordant bioinformatic signals indicate that benefit is most likely where hotness and IFNγ-inducible PDL1 coincide, with melanoma showing the most substantial alignment, while immune-desert or TEX-dominant states are less likely to respond without priming. The secretion gains conferred by the IgG1-Fc scaffold, the absence of producer toxicity, and superior low-dose competition versus a clinical monoclonal together position sPD1^{HAC} as a credible payload for spatially concentrated checkpoint interception.

Translationally, these findings motivate the development of a composite, indication-specific biomarker that integrates PDL1 levels, T-cell abundance, and activation, with prospective calibration of thresholds across platforms. Following these experiments, occupancy should be coupled to function in antigen-specific co-cultures, pharmacokinetics, and in situ concentrations after MSC delivery should be defined, and repeated dosing and orthotopic models with blinded pathology should be tested. Fc-tuned or Fc-silent comparators, YAP-axis or priming combinations in feedback-adapted niches, and biodistribution and safety studies will refine scope and boundary conditions. If validated, MSC-directed sPD1^{HAC} offers a practical route to sustain effective PDL1 occupancy in inflamed lesions, while potentially reducing systemic exposure, providing a clear rationale for staged progression from preclinical to early clinical trials.

Chapter 6: References

6. References

Adam, K., Butler, S. C., Workman, C. J. and Vignali, D. A. A. (2025) Advances in LAG3 cancer immunotherapeutics. *Trends in Cancer,* **11**, 37-48.

Agata, Y., Kawasaki, A., Nishimura, H., Ishida, Y., Tsubat, T., Yagita, H. and Honjo, T. (1996) Expression of the PD-1 antigen on the surface of stimulated mouse T and B lymphocytes. *International immunology,* **8**, 765-772.

Ahmadnia, A., Mohammadi, S., Yamchi, A., Kalani, M. R., Farazmandfar, T., Khosravi, A. and Memarian, A. (2024) Augmenting the Antitumor Efficacy of Natural Killer Cells via SynNotch Receptor Engineering for Targeted IL-12 Secretion. *Current Issues in Molecular Biology,* **46**, 2931-2945.

Ajina, A. and Maher, J. (2017) Prospects for combined use of oncolytic viruses and CAR T-cells. *Journal for ImmunoTherapy of Cancer,* **5**.

Allison, J. P., McIntyre, B. W. and Bloch, D. (1982) Tumor-specific antigen of murine T-lymphoma defined with monoclonal antibody. *J Immunol,* **129**, 2293-300.

Almeida-Porada, G., Atala, A. J. and Porada, C. D. (2020) Therapeutic Mesenchymal Stromal Cells for Immunotherapy and for Gene and Drug Delivery. *Mol Ther Methods Clin Dev,* **16**, 204-224.

Alvarez-Argote, J. and Dasanu, C. A. (2019) Durvalumab in cancer medicine: a comprehensive review. *Expert Opinion on Biological Therapy,* **19**, 927-935.

Amarnath, S., Mangus, C. W., Wang, J. C. M., Wei, F., He, A., Kapoor, V., Foley, J. E., Massey, P. R., Felizardo, T. C., Riley, J. L., Levine, B. L., June, C. H., Medin, J. A. and Fowler, D. H. (2011) The PDL1-PD1 Axis Converts Human TH1 Cells into Regulatory T Cells. *Science Translational Medicine,* **3**, 111ra120-111ra120.

Andreatta, M., Corria-Osorio, J., Müller, S., Cubas, R., Coukos, G. and Carmona, S. J. (2021) Interpretation of T cell states from single-cell transcriptomics data using reference atlases. *Nature Communications,* **12**.

Ansell, S. M., Lesokhin, A. M., Borrello, I., Halwani, A., Scott, E. C., Gutierrez, M., Schuster, S. J., Millenson, M. M., Cattry, D., Freeman, G. J., Rodig, S. J., Chapuy, B., Ligon, A. H., Zhu, L., Grosso, J. F., Kim, S. Y., Timmerman, J. M., Shipp, M. A. and Armand, P. (2015) PD-1 Blockade with Nivolumab in Relapsed or Refractory Hodgkin's Lymphoma. *New England Journal of Medicine,* **372**, 311-319.

Antonia, S. J., Villegas, A., Daniel, D., Vicente, D., Murakami, S., Hui, R., Kurata, T., Chiappori, A., Lee, K. H., Wit, M. d., Cho, B. C., Bourhaba, M., Quantin, X., Tokito, T., Mekhail, T., Planchard, D., Kim, Y.-C., Karapetis, C. S., Hiret, S., Ostoros, G., Kubota, K., Gray, J. E., Paz-Ares, L., Carpeño, J. d. C., Faivre-Finn, C., Reck, M., Vansteenkiste, J., Spigel, D. R., Wadsworth, C., Melillo, G., Taboada, M., Dennis, P. A. and Özgüroğlu, M. (2018) Overall Survival with Durvalumab after Chemoradiotherapy in Stage III NSCLC. *New England Journal of Medicine,* **379**, 2342-2350.

Audsley, K. M., Mcdonnell, A. M. and Waithman, J. (2020) Cross-Presenting XCR1+ Dendritic Cells as Targets for Cancer Immunotherapy. *Cells,* **9**, 565.

Augustin, R. C., Bao, R. and Luke, J. J. (2023) Targeting Cbl-b in cancer immunotherapy. *Journal for ImmunoTherapy of Cancer,* **11**, e006007.

Ayers, M., Lunceford, J., Nebozhyn, M., Murphy, E., Loboda, A., Kaufman, D. R., Albright, A., Cheng, J. D., Kang, S. P., Shankaran, V., Piha-Paul, S. A., Yearley, J., Seiwert, T. Y., Ribas, A. and Mcclanahan, T. K. (2017) IFN-γ–related mRNA profile predicts clinical response to PD-1 blockade. *Journal of Clinical Investigation,* **127**, 2930-2940.

Azeez, S. S., Yashooa, R. K., Smail, S. W., Salihi, A., Ali, A. S., Mamand, S. and Janson, C. (2025) Advancing CAR-based cell therapies for solid tumours: challenges, therapeutic strategies, and perspectives. *Molecular Cancer,* **24**, 191.

Baer, P. C. (2014) Adipose-derived mesenchymal stromal/stem cells: An update on their phenotype in vivo and in vitro. *World J Stem Cells,* **6**, 256-65.

Bai, R. and Cui, J. (2022) Burgeoning Exploration of the Role of Natural Killer Cells in Anti-PD-1/PD-L1 Therapy. *Frontiers in Immunology,* **Volume 13 - 2022**.

Bailey, S. R., Bartee, E., Daniels, K. G., Heery, C. R., Kaumaya, P., Lesinski, G. B., Lowinger, T. B., Nelson, M. H., Rubinstein, M. P., Wittling, M. C., Paulos, C. M. and Posey, A. D. (2025) Constructing the cure: engineering the next wave of antibody and cellular immune therapies. *Journal for ImmunoTherapy of Cancer,* **13**, e011761.

Baksh, K. and Weber, J. (2015) Immune Checkpoint Protein Inhibition for Cancer: Preclinical Justification for CTLA-4 and PD-1 Blockade and New Combinations. *Seminars in Oncology,* **42**, 363-377.

Balar, A. V. and Weber, J. S. (2017) PD-1 and PD-L1 antibodies in cancer: current status and future directions. *Cancer Immunology, Immunotherapy,* **66**, 551-564.

Ball, K., Dovedi, S. J., Vajjah, P. and Phipps, A. (2023) Strategies for clinical dose optimization of T cell-engaging therapies in oncology. *mAbs,* **15**.

Bardhan, K., Anagnostou, T. and Boussiotis, V. A. (2016) The PD1:PD-L1/2 Pathway from Discovery to Clinical Implementation. *Frontiers in Immunology,* **7**.

Beavis, P. A., Henderson, M. A., Giuffrida, L., Davenport, A. J., Petley, E. V., House, I. G., Lai, J., Sek, K., Milenkovski, N., John, L. B., Mardiana, S., Slaney, C. Y., Trapani, J. A., Loi, S., Kershaw, M. H., Haynes, N. M. and Darcy, P. K. (2018) Dual PD-1 and CTLA-4 Checkpoint Blockade Promotes Antitumor Immune Responses through CD4+Foxp3− Cell–Mediated Modulation of CD103+ Dendritic Cells. *Cancer Immunology Research,* **6**, 1069-1081.

Bergamaschi, C., Gaspar, M., Ciucci, T., Sitnikova, S. I., Cayatte, C., Pica, M. and Dovedi, S. J. (2025) Innovative strategies for T cell engagers for cancer immunotherapy. *mAbs,* **17**.

Berraondo, P., Sanmamed, M. F., Ochoa, M. C., Etxeberria, I., Aznar, M. A., Pérez-Gracia, J. L., Rodríguez-Ruiz, M. E., Ponz-Sarvise, M., Castañón, E. and Melero, I. (2019) Cytokines in clinical cancer immunotherapy. *British Journal of Cancer,* **120**, 6-15.

Bieback, K., Kuçi, S. and Schäfer, R. (2019) Production and quality testing of multipotent mesenchymal stromal cell therapeutics for clinical use. *Transfusion,* **59**, 2164-2173.

Brahmer, J. R., Drake, C. G., Wollner, I., Powderly, J. D., Picus, J., Sharfman, W. H., Stankevich, E., Pons, A., Salay, T. M., Mcmiller, T. L., Gilson, M. M., Wang, C., Selby, M., Taube, J. M., Anders, R., Chen, L., Korman, A. J., Pardoll, D. M., Lowy, I. and Topalian, S. L. (2010) Phase I Study of Single-Agent Anti–Programmed Death-1 (MDX-1106) in Refractory Solid Tumors: Safety, Clinical Activity, Pharmacodynamics, and Immunologic Correlates. *Journal of Clinical Oncology,* **28**, 3167-3175.

Bredel, D., Tihic, E., Mouraud, S., Danlos, F.-X., Susini, S., Aglave, M., Alfaro, A., Mohamed-Djalim, C., Rouanne, M., Halse, H., Bigorgne, A., Tselikas, L., Dalle, S., Hartl, D. M., Baudin, E., Guettier, C., Vibert, E., Rosmorduc, O., Robert, C., Ferlicot, S., Parier, B., Albiges, L., De Montpreville, V. T., Besse, B., Mercier, O., Even, C., Breuskin, I., Classe, M., Radulescu, C., Lebret, T., Pautier, P., Gouy, S., Scoazec, J.-Y., Zitvogel, L., Marabelle, A. and Bonvalet, M. (2023) Immune checkpoints are predominantly co-expressed by clonally expanded CD4+FoxP3+ intratumoral T-cells in primary human cancers. *Journal of Experimental & Clinical Cancer Research,* **42**.

Brentville, V. A., Atabani, S., Cook, K. and Durrant, L. G. (2018) Novel tumour antigens and the development of optimal vaccine design. *Therapeutic Advances in Vaccines and Immunotherapy,* **6**, 31-47.

Briukhovetska, D., Dörr, J., Endres, S., Libby, P., Dinarello, C. A. and Kobold, S. (2021) Interleukins in cancer: from biology to therapy. *Nature Reviews Cancer,* **21**, 481-499.

Brunell, A. E., Lahesmaa, R., Autio, A. and Thotakura, A. K. (2023) Exhausted T cells hijacking the cancer-immunity cycle: Assets and liabilities. *Frontiers in Immunology,* **14**.

Bu, M. T., Yuan, L., Klee, A. N. and Freeman, G. J. (2022) A Comparison of Murine PD-1 and PD-L1 Monoclonal Antibodies. *Monoclonal Antibodies in Immunodiagnosis and Immunotherapy,* **41**, 202-209.

Buchbinder, E. and Hodi, F. S. (2015) Cytotoxic T lymphocyte antigen-4 and immune checkpoint blockade. *Journal of Clinical Investigation,* **125**, 3377-3383.

Buchbinder, E. I. and Desai, A. (2016) CTLA-4 and PD-1 Pathways: Similarities, Differences, and Implications of Their Inhibition. *American Journal of Clinical Oncology,* **39**.

Buchholz, V. R. and Busch, D. H. (2019) Back to the Future: Effector Fate during T Cell Exhaustion. *Immunity,* **51**, 970-972.

Buckle, I. and Guillerey, C. (2021) Inhibitory Receptors and Immune Checkpoints Regulating Natural Killer Cell Responses to Cancer. *Cancers,* **13**, 4263.

Burova, E., Hermann, A., Waite, J., Potocky, T., Lai, V., Hong, S., Liu, M., Allbritton, O., Woodruff, A., Wu, Q., D'Orvilliers, A., Garnova, E., Rafique, A., Poueymirou, W., Martin, J., Huang, T., Skokos, D., Kantrowitz, J., Popke, J., Mohrs, M., Macdonald, D., Ioffe, E., Olson, W., Lowy, I., Murphy, A. and Thurston, G. (2017) Characterization of the Anti–PD-1 Antibody REGN2810 and Its Antitumor Activity in HumanPD-1Knock-In Mice. *Molecular Cancer Therapeutics,* **16**, 861-870.

Butterfield, L. H. and Najjar, Y. G. (2024) Immunotherapy combination approaches: mechanisms, biomarkers and clinical observations. *Nature Reviews Immunology,* **24**, 399-416.

Cameron, F., Whiteside, G. and Perry, C. (2011) Ipilimumab. *Drugs,* **71**, 1093-1104.

Camilleri, E. T., Gustafson, M. P., Dudakovic, A., Riester, S. M., Garces, C. G., Paradise, C. R., Takai, H., Karperien, M., Cool, S., Sampen, H.-J. I., Larson, A. N., Qu, W., Smith, J., Dietz, A. B. and Van Wijnen, A. J. (2016) Identification and validation of multiple cell surface markers of clinical-grade adipose-derived mesenchymal stromal cells as novel release criteria for good manufacturing practice-compliant production. *Stem Cell Research & Therapy,* **7**.

Camus, M., Tosolini, M., Mlecnik, B., PagèS, F., Kirilovsky, A., Berger, A., Costes, A., Bindea, G., Charoentong, P., Bruneval, P., Trajanoski, Z., Fridman, W.-H. and Galon, J. R. M. (2009) Coordination of Intratumoral Immune Reaction and Human Colorectal Cancer Recurrence. *Cancer Research,* **69**, 2685-2693.

Carreño-Tarragona, G., Tiana, M., Rouco, R., Leivas, A., Victorino, J., García-Vicente, R., Chase, A. J., Maidana, A., Tapper, W. J., Ayala, R., Cross, N. C. P., Martínez-López, J. and Manzanares, M. (2025) The JAK2 46/1 haplotype influences PD-L1 expression. *Blood,* **145**, 2196-2201.

Castiello, L., Santodonato, L., Napolitano, M., Carlei, D., Montefiore, E., Monque, D. M., D'Agostino, G. and Aricò, E. (2022) Chimeric Antigen Receptor Immunotherapy for Solid Tumors: Choosing the Right Ingredients for the Perfect Recipe. *Cancers,* **14**, 5351.

Cercek, A., Lumish, M., Sinopoli, J., Weiss, J., Shia, J., Lamendola-Essel, M., El Dika, I. H., Segal, N., Shcherba, M., Sugarman, R., Stadler, Z., Yaeger, R., Smith, J. J., Rousseau, B., Argiles, G., Patel, M., Desai, A., Saltz, L. B., Widmar, M., Iyer, K., Zhang, J., Gianino, N., Crane, C., Romesser, P. B., Pappou, E. P., Paty, P., Garcia-Aguilar, J., Gonen, M., Gollub, M., Weiser, M. R., Schalper, K. A. and Diaz, L. A. (2022) PD-1 Blockade in Mismatch Repair–Deficient, Locally Advanced Rectal Cancer. *New England Journal of Medicine*.

Cha, J.-H., Chan, L.-C., Li, C.-W., Hsu, J. L. and Hung, M.-C. (2019) Mechanisms Controlling PD-L1 Expression in Cancer. *Molecular Cell,* **76**, 359-370.

Chae, Y. K., Arya, A., Iams, W., Cruz, M. R., Chandra, S., Choi, J. and Giles, F. (2018) Current landscape and future of dual anti-CTLA4 and PD-1/PD-L1 blockade immunotherapy in cancer; lessons learned from clinical trials with melanoma and non-small cell lung cancer (NSCLC). *Journal for ImmunoTherapy of Cancer,* **6**.

Chakravarthy, A., Furness, A., Joshi, K., Ghorani, E., Ford, K., Ward, M. J., King, E. V., Lechner, M., Marafioti, T., Quezada, S. A., Thomas, G. J., Feber, A. and Fenton, T. R. (2018) Pan-cancer deconvolution of tumour composition using DNA methylation. *Nature Communications,* **9**.

Chauhan, A., Khan, T. and Omri, A. (2021) Design and Encapsulation of Immunomodulators onto Gold Nanoparticles in Cancer Immunotherapy. *International Journal of Molecular Sciences,* **22**, 8037.

Chen, B., Hu, J., Hu, X., Chen, H., Bao, R., Zhou, Y., Ye, Y., Zhan, M., Cai, W., Li, H. and Li, H.-B. (2022) DENR controls JAK2 translation to induce PD-L1 expression for tumor immune evasion. *Nature Communications,* **13**.

Chen, C.-Y., Hutzen, B., Wedekind, M. F. and Cripe, T. P. (2018a) Oncolytic virus and PD-1/PD-L1 blockade combination therapy. *Oncolytic Virotherapy,* **Volume 7**, 65-77.

Chen, G., Huang, A. C., Zhang, W., Zhang, G., Wu, M., Xu, W., Yu, Z., Yang, J., Wang, B., Sun, H., Xia, H., Man, Q., Zhong, W., Antelo, L. F., Wu, B., Xiong, X., Liu, X., Guan, L., Li, T., Liu, S., Yang, R., Lu, Y., Dong, L., McGettigan, S., Somasundaram, R., Radhakrishnan, R., Mills, G., Lu, Y., Kim, J., Chen, Y. H., Dong, H., Zhao, Y., Karakousis, G. C., Mitchell, T. C., Schuchter, L. M., Herlyn, M., Wherry, E. J., Xu, X. and Guo, W. (2018b) Exosomal PD-L1 contributes to immunosuppression and is associated with anti-PD-1 response. *Nature,* **560**, 382-386.

Chen, L., Deng, H., Cui, H., Fang, J., Zuo, Z., Deng, J., Li, Y., Wang, X. and Zhao, L. (2018c) Inflammatory responses and inflammation-associated diseases in organs. *Oncotarget,* **9**, 7204-7218.

Chen, M., Bie, L. and Ying, J. (2023) Cancer cell-intrinsic PD-1: Its role in malignant progression and immunotherapy. *Biomedicine & Pharmacotherapy,* **167**, 115514.

Chen, R., Zinzani, P. L., Lee, H. J., Armand, P., Johnson, N. A., Brice, P., Radford, J., Ribrag, V., Molin, D., Vassilakopoulos, T. P., Tomita, A., Von Tresckow, B., Shipp, M. A., Lin, J., Kim, E., Nahar, A., Balakumaran, A. and Moskowitz, C. H. (2019a) Pembrolizumab in relapsed or refractory Hodgkin lymphoma: 2-year follow-up of KEYNOTE-087. *Blood,* **134**, 1144-1153.

Chen, S., Zhang, Z., Zheng, X., Tao, H., Zhang, S., Ma, J., Liu, Z., Wang, J., Qian, Y., Cui, P., Huang, D., Huang, Z., Wu, Z. and Hu, Y. (2021) Response Efficacy of PD-1 and PD-L1 Inhibitors in Clinical Trials: A Systematic Review and Meta-Analysis. *Frontiers in Oncology,* **11**.

Chen, Z., Ji, Z., Ngiow, S. F., Manne, S., Cai, Z., Huang, A. C., Johnson, J., Staupe, R. P., Bengsch, B., Xu, C., Yu, S., Kurachi, M., Herati, R. S., Vella, L. A., Baxter, A. E., Wu, J. E., Khan, O., Beltra, J.-C., Giles, J. R., Stelekati, E., Mclane, L. M., Lau, C. W., Yang, X., Berger, S. L., Vahedi, G., Ji, H. and Wherry, E. J. (2019b) TCF-1-Centered Transcriptional Network Drives an Effector versus Exhausted CD8 T Cell-Fate Decision. *Immunity,* **51**, 840-855.e5.

Cheng, X., Veverka, V., Radhakrishnan, A., Waters, L. C., Muskett, F. W., Morgan, S. H., Huo, J., Yu, C., Evans, E. J., Leslie, A. J., Griffiths, M., Stubberfield, C., Griffin, R., Henry, A. J., Jansson, A., Ladbury, J. E., Ikemizu, S., Carr, M. D. and Davis, S. J. (2013) Structure and Interactions of the Human Programmed Cell Death 1 Receptor*. *Journal of Biological Chemistry,* **288**, 11771-11785.

Chi, W.-Y., Hu, Y., Huang, H.-C., Kuo, H.-H., Lin, S.-H., Kuo, C.-T. J., Tao, J., Fan, D., Huang, Y.-M., Wu, A. A., Hung, C.-F. and Wu, T.-C. (2024) Molecular targets and strategies in the development of nucleic acid cancer vaccines: from shared to personalized antigens. *Journal of Biomedical Science,* **31**.

Clynes, R. A. and Desjarlais, J. R. (2019) Redirected T Cell Cytotoxicity in Cancer Therapy. *Annual Review of Medicine,* **70**, 437-450.

Cohen Saban, N., Yalin, A., Landsberger, T., Salomon, R., Alva, A., Feferman, T., Amit, I. and Dahan, R. (2023) Fc glycoengineering of a PD-L1 antibody harnesses Fcγ receptors for increased antitumor efficacy. *Sci Immunol,* **8**, eadd8005.

Colard-Thomas, J., Manceron, C., Duflos, C., Herman, F., Simon, M., Maria, A. T. J., Faillie, J. L., Viala, M. and Palassin, P. (2023) Comparison of clinical safety between standard versus extended interval dosing of immune checkpoint inhibitors: a real-world retrospective cohort study. *ESMO Open,* **8**, 102070.

Cormedi, M. C. V., Van Allen, E. M. and Colli, L. M. (2021) Predicting immunotherapy response through genomics. *Current Opinion in Genetics & Development,* **66**, 1-9.

Cotton, A. D., Nguyen, D. P., Gramespacher, J. A., Seiple, I. B. and Wells, J. A. (2021) Development of Antibody-Based PROTACs for the Degradation of the Cell-Surface

Immune Checkpoint Protein PD-L1. *Journal of the American Chemical Society,* **143**, 593-598.
Crimini, E., Boscolo Bielo, L., Berton Giachetti, P. P. M., Pellizzari, G., Antonarelli, G., Taurelli Salimbeni, B., Repetto, M., Belli, C. and Curigliano, G. (2024) Beyond PD(L)-1 Blockade in Microsatellite-Instable Cancers: Current Landscape of Immune Co-Inhibitory Receptor Targeting. *Cancers,* **16**, 281.
Crowther, M. D., Svane, I. M. and Met, Ö. (2020) T-Cell Gene Therapy in Cancer Immunotherapy: Why It Is No Longer Just CARs on The Road. *Cells,* **9**, 1588.
Cui, H., Hamad, M. and Elkord, E. (2025) TIGIT in cancer: from mechanism of action to promising immunotherapeutic strategies. *Cell Death & Disease,* **16**.
D'Angelo, S. P., Lebbé, C., Mortier, L., Brohl, A. S., Fazio, N., Grob, J.-J., Prinzi, N., Hanna, G. J., Hassel, J. C., Kiecker, F., Georges, S., Ellers-Lenz, B., Shah, P., Güzel, G. and Nghiem, P. (2021) First-line avelumab in a cohort of 116 patients with metastatic Merkel cell carcinoma (JAVELIN Merkel 200): primary and biomarker analyses of a phase II study. *Journal for ImmunoTherapy of Cancer,* **9**, e002646.
D L Mueller, M K Jenkins, a. and Schwartz, R. H. (1989) Clonal Expansion Versus Functional Clonal Inactivation: A Costimulatory Signalling Pathway Determines the Outcome of T Cell Antigen Receptor Occupancy. *Annual Review of Immunology,* **7**, 445-480.
Dahlén, E., Veitonmäki, N. and Norlén, P. (2018) Bispecific antibodies in cancer immunotherapy. *Therapeutic Advances in Vaccines and Immunotherapy,* **6**, 3-17.
Dai, M., Liu, M., Yang, H., Küçük, C. and You, H. (2022) New insights into epigenetic regulation of resistance to PD-1/PD-L1 blockade cancer immunotherapy: mechanisms and therapeutic opportunities. *Experimental Hematology & Oncology,* **11**.
Darvin, P., Toor, S. M., Sasidharan Nair, V. and Elkord, E. (2018) Immune checkpoint inhibitors: recent progress and potential biomarkers. *Experimental & Molecular Medicine,* **50**, 1-11.
DePeaux, K. and Delgoffe, G. M. (2024) Integrating innate and adaptive immunity in oncolytic virus therapy. *Trends in Cancer,* **10**, 135-146.
Disis, M. L., Adams, S. F., Bajpai, J., Butler, M. O., Curiel, T., Dodt, S. A., Doherty, L., Emens, L. A., Friedman, C. F., Gatti-Mays, M., Geller, M. A., Jazaeri, A., John, V. S., Kurnit, K. C., Liao, J. B., Mahdi, H., Mills, A., Zsiros, E. and Odunsi, K. (2023) Society for Immunotherapy of Cancer (SITC) clinical practice guideline on immunotherapy for the treatment of gynecologic cancer. *Journal for ImmunoTherapy of Cancer,* **11**, e006624.
Dong, W., Wu, X., Ma, S., Wang, Y., Nalin, A. P., Zhu, Z., Zhang, J., Benson, D. M., He, K., Caligiuri, M. A. and Yu, J. (2019) The Mechanism of Anti–PD-L1 Antibody Efficacy against PD-L1–Negative Tumors Identifies NK Cells Expressing PD-L1 as a Cytolytic Effector. *Cancer Discovery,* **9**, 1422-1437.
Du, J., Qin, Y., Wu, Y., Zhao, W., Zhai, W., Qi, Y., Wang, C. and Gao, Y. (2018) The design of high affinity human PD-1 mutants by using molecular dynamics simulations (MD). *Cell Communication and Signaling,* **16**.
Dvorak, H. F. (2015) Tumors: Wounds That Do Not Heal—Redux. *Cancer Immunology Research,* **3**, 1-11.
Dyck, L. and Mills, K. H. G. (2017) Immune checkpoints and their inhibition in cancer and infectious diseases. *European Journal of Immunology,* **47**, 765-779.
Ebbing, E. A., van der Zalm, A. P., Steins, A., Creemers, A., Hermsen, S., Rentenaar, R., Klein, M., Waasdorp, C., Hooijer, G. K. J., Meijer, S. L., Krishnadath, K. K., Punt, C. J. A., van Berge Henegouwen, M. I., Gisbertz, S. S., van Delden, O. M., Hulshof, M. C. C. M., Medema, J. P., van Laarhoven, H. W. M. and Bijlsma, M. F. (2019) Stromal-derived interleukin 6 drives epithelial-to-mesenchymal transition and therapy resistance in esophageal adenocarcinoma. *Proceedings of the National Academy of Sciences,* **116**, 2237-2242.
Ebrahimi, A., Vakilzadeh, G., Izadi, M., Jalali Kondori, B., Raei, M., Farzanehpour, M. and Esmaeili Gouvrchin Ghaleh, H. (2023) Mesenchymal Stem Cell Carriers for Newcastle Oncolytic Viruses: The New Era in Colorectal Cancer treatment. *International Journal of Medical Reviews,* **10**, 553-564.

Efremova, M., Rieder, D., Klepsch, V., Charoentong, P., Finotello, F., Hackl, H., Hermann-Kleiter, N., Löwer, M., Baier, G., Krogsdam, A. and Trajanoski, Z. (2018) Targeting immune checkpoints potentiates immunoediting and changes the dynamics of tumor evolution. *Nature Communications,* **9**.

Elmusrati, A., Wang, J. and Wang, C.-Y. (2021) Tumor microenvironment and immune evasion in head and neck squamous cell carcinoma. *International Journal of Oral Science,* **13**.

Epstein, A. L. and Rabkin, S. D. (2024) Safety of non-replicative and oncolytic replication-selective HSV vectors. *Trends in Molecular Medicine,* **30**, 781-794.

Eroglu, Z., Zaretsky, J. M., Hu-Lieskovan, S., Kim, D. W., Algazi, A., Johnson, D. B., Liniker, E., Ben, K., Munhoz, R., Rapisuwon, S., Gherardini, P. F., Chmielowski, B., Wang, X., Shintaku, I. P., Wei, C., Sosman, J. A., Joseph, R. W., Postow, M. A., Carlino, M. S., Hwu, W.-J., Scolyer, R. A., Messina, J., Cochran, A. J., Long, G. V. and Ribas, A. (2018) High response rate to PD-1 blockade in desmoplastic melanomas. *Nature,* **553**, 347-350.

Esprit, A., de Mey, W., Bahadur Shahi, R., Thielemans, K., Franceschini, L. and Breckpot, K. (2020) Neo-Antigen mRNA Vaccines. *Vaccines,* **8**, 776.

Fabian, K. P., Malamas, A. S., Padget, M. R., Solocinski, K., Wolfson, B., Fujii, R., Abdul Sater, H., Schlom, J. and Hodge, J. W. (2021) Therapy of Established Tumors with Rationally Designed Multiple Agents Targeting Diverse Immune–Tumor Interactions: Engage, Expand, Enable. *Cancer Immunology Research,* **9**, 239-252.

Faget, J., Peters, S., Quantin, X., Meylan, E. and Bonnefoy, N. (2021) Neutrophils in the era of immune checkpoint blockade. *Journal for ImmunoTherapy of Cancer,* **9**, e002242.

Fan, T., Zhang, M., Yang, J., Zhu, Z., Cao, W. and Dong, C. (2023) Therapeutic cancer vaccines: advancements, challenges and prospects. *Signal Transduction and Targeted Therapy,* **8**.

Fishbein, A., Hammock, B. D., Serhan, C. N. and Panigrahy, D. (2021) Carcinogenesis: Failure of resolution of inflammation? *Pharmacology & Therapeutics,* **218**, 107670.

Foster, L. H. and Lum, L. G. (2019) Treatment of hematological malignancies with T cell redirected bispecific antibodies: current status and future needs. *Expert Opinion on Biological Therapy,* **19**, 707-720.

Francisco, L. M., Sage, P. T. and Sharpe, A. H. (2010) The PD-1 pathway in tolerance and autoimmunity. *Immunological Reviews,* **236**, 219-242.

Fu, J., Yu, A., Tang, J., He, B. and Chen, W. (2020) Adoptive CD8(+) T cell therapy generates immunological memory to inhibit melanoma metastasis. *Am J Transl Res,* **12**, 7262-7274.

Galli, F., Aguilera, J. V., Palermo, B., Markovic, S. N., Nisticò, P. and Signore, A. (2020) Relevance of immune cell and tumor microenvironment imaging in the new era of immunotherapy. *Journal of Experimental & Clinical Cancer Research,* **39**.

Galon, J. and Bruni, D. (2019) Approaches to treat immune hot, altered and cold tumours with combination immunotherapies. *Nature Reviews Drug Discovery,* **18**, 197-218.

Garcia-Diaz, A., Shin, D. S., Moreno, B. H., Saco, J., Escuin-Ordinas, H., Rodriguez, G. A., Zaretsky, J. M., Sun, L., Hugo, W., Wang, X., Parisi, G., Saus, C. P., Torrejon, D. Y., Graeber, T. G., Comin-Anduix, B., Hu-Lieskovan, S., Damoiseaux, R., Lo, R. S. and Ribas, A. (2017) Interferon Receptor Signaling Pathways Regulating PD-L1 and PD-L2 Expression. *Cell Reports,* **19**, 1189-1201.

Garza Treviño, E. N., Quiroz Reyes, A. G., Delgado Gonzalez, P., Rojas Murillo, J. A., Islas, J. F., Alonso, S. S. and Gonzalez Villarreal, C. A. (2024) Applications of Modified Mesenchymal Stem Cells as Targeted Systems against Tumor Cells. *International Journal of Molecular Sciences,* **25**, 7791.

Gatalica, Z., Snyder, C., Maney, T., Ghazalpour, A., Holterman, D. A., Xiao, N., Overberg, P., Rose, I., Basu, G. D., Vranic, S., Lynch, H. T., Von Hoff, D. D. and Hamid, O. (2014) Programmed Cell Death 1 (PD-1) and Its Ligand (PD-L1) in Common Cancers and Their Correlation with Molecular Cancer Type. *Cancer Epidemiology, Biomarkers & Prevention,* **23**, 2965-2970.

Gil-Chinchilla, J. I., Zapata, A. G., Moraleda, J. M. and García-Bernal, D. (2024) Bioengineered Mesenchymal Stem/Stromal Cells in Anti-Cancer Therapy: Current Trends and Future Prospects. *Biomolecules,* **14**, 734.

Girard, P., Sosa Cuevas, E., Ponsard, B., Mouret, S., Gil, H., Col, E., De Fraipont, F., Sturm, N., Charles, J., Manches, O., Chaperot, L. and Aspord, C. (2021) Dysfunctional BTN3A together with deregulated immune checkpoints and type I/II IFN dictate defective interplay between pDCs and γδ T cells in melanoma patients, which impacts clinical outcomes. *Clinical & Translational Immunology,* **10**.

Gitto, S., Natalini, A., Antonangeli, F. and Di Rosa, F. (2021) The Emerging Interplay Between Recirculating and Tissue-Resident Memory T Cells in Cancer Immunity: Lessons Learned From PD-1/PD-L1 Blockade Therapy and Remaining Gaps. *Frontiers in Immunology,* **12**.

Glorioso, J. C., Cohen, J. B., Goins, W. F., Hall, B., Jackson, J. W., Kohanbash, G., Amankulor, N., Kaur, B., Caligiuri, M. A., Chiocca, E. A., Holland, E. C. and Quéva, C. (2021) Oncolytic HSV Vectors and Anti-Tumor Immunity. *Curr Issues Mol Biol,* **41**, 381-468.

Goebeler, M.-E., Stuhler, G. and Bargou, R. (2024) Bispecific and multispecific antibodies in oncology: opportunities and challenges. *Nature Reviews Clinical Oncology,* **21**, 539-560.

Gogesch, P., Dudek, S., Van Zandbergen, G., Waibler, Z. and Anzaghe, M. (2021) The Role of Fc Receptors on the Effectiveness of Therapeutic Monoclonal Antibodies. *International Journal of Molecular Sciences,* **22**, 8947.

Goleva, E., Lyubchenko, T., Kraehenbuehl, L., Lacouture, M. E., Leung, D. Y. M. and Kern, J. A. (2021) Our current understanding of checkpoint inhibitor therapy in cancer immunotherapy. *Annals of Allergy, Asthma & Immunology,* **126**, 630-638.

Granier, C., De Guillebon, E., Blanc, C., Roussel, H., Badoual, C., Colin, E., Saldmann, A., Gey, A., Oudard, S. and Tartour, E. (2017) Mechanisms of action and rationale for the use of checkpoint inhibitors in cancer. *ESMO Open,* **2**, e000213.

Grippin, A. J., Dyson, K. A., Qdaisat, S., Mcguiness, J., Wummer, B., Mitchell, D. A., Mendez-Gomez, H. R. and Sayour, E. J. (2021) Nanoparticles as immunomodulators and translational agents in brain tumors. *Journal of Neuro-Oncology,* **151**, 29-39.

Grywalska, E., Pasiarski, M., Góźdź, S. and Roliński, J. (2018) Immune-checkpoint inhibitors for combating T-cell dysfunction in cancer. *OncoTargets and Therapy,* **Volume 11**, 6505-6524.

Gundersen, R. A., Chu, T., Abolfathi, K., Gokcen Dogan, S., Blair, P. E., Nago, N., Hamblin, M., Brooke, G. N., Zwacka, R. M., Kafash Hoshiar, A. and Mohr, A. (2023) Generation of magnetic biohybrid microrobots based on MSC.sTRAIL for targeted stem cell delivery and treatment of cancer. *Cancer Nanotechnology,* **14**.

Guo, L., Li, W., Zhu, X., Ling, Y., Qiu, T., Dong, L., Fang, Y., Yang, H. and Ying, J. (2016) PD-L1 expression and CD274 gene alteration in triple-negative breast cancer: implication for prognostic biomarker. *SpringerPlus,* **5**.

Guo, M., Liu, M. Y. R. and Brooks, D. G. (2024) Regulation and impact of tumor-specific CD4⁺ T cells in cancer and immunotherapy. *Trends in Immunology,* **45**, 303-313.

Gwadera, J., Grajewski, M., Chowaniec, H., Gucia, K., Michoń, J., Mikulicz, Z., Knast, M., Pujanek, P., Tołkacz, A., Murawa, A. and Dobosz, P. (2025) Can We Use CAR-T Cells to Overcome Immunosuppression in Solid Tumours? *Biology,* **14**, 1035.

Ha, J. Y., Chun, K.-J., Ko, S., Lee, H. W., Hwang, O. K., Lim, C. S., Ha, K., Ko, B. J. and Jung, S. T. (2023) Glycan-Controlled Human PD-1 Variants Displaying Broad-Spectrum High Binding to PD-1 Ligands Potentiate T Cell. *Molecular Pharmaceutics,* **20**, 2170-2180.

Hammerl, D., Martens, J. W. M., Timmermans, M., Smid, M., Trapman-Jansen, A. M., Foekens, R., Isaeva, O. I., Voorwerk, L., Balcioglu, H. E., Wijers, R., Nederlof, I., Salgado, R., Horlings, H., Kok, M. and Debets, R. (2021) Spatial immunophenotypes predict response to anti-PD1 treatment and capture distinct paths of T cell evasion in triple negative breast cancer. *Nature Communications,* **12**.

Hargadon, K. M. (2023) Genetic dysregulation of immunologic and oncogenic signaling pathways associated with tumor-intrinsic immune resistance: a molecular basis for combination targeted therapy-immunotherapy for cancer. *Cellular and Molecular Life Sciences,* **80**.

Hmadcha, A., Martin-Montalvo, A., Gauthier, B. R., Soria, B. and Capilla-Gonzalez, V. (2020) Therapeutic Potential of Mesenchymal Stem Cells for Cancer Therapy. *Frontiers in bioengineering and biotechnology,* **8**, 43-43.

Hnisz, D., Schuijers, J., Li, C. and Young, R. (2018) Regulation and Dysregulation of Chromosome Structure in Cancer. *Annual Review of Cancer Biology,* **2**.

Homet Moreno, B., Parisi, G., Robert, L. and Ribas, A. (2015) Anti–PD-1 Therapy in Melanoma. *Seminars in Oncology,* **42**, 466-473.

Hong, M. M. Y. and Maleki Vareki, S. (2022) Addressing the Elephant in the Immunotherapy Room: Effector T-Cell Priming versus Depletion of Regulatory T-Cells by Anti-CTLA-4 Therapy. *Cancers,* **14**, 1580.

Hossain, M. A., Liu, G., Dai, B., Si, Y., Yang, Q., Wazir, J., Birnbaumer, L. and Yang, Y. (2021) Reinvigorating exhausted CD8⁺ cytotoxic T lymphocytes in the tumor microenvironment and current strategies in cancer immunotherapy. *Medicinal Research Reviews,* **41**, 156-201.

Hu, Z., Ott, P. A. and Wu, C. J. (2018) Towards personalized, tumour-specific, therapeutic vaccines for cancer. *Nature Reviews Immunology,* **18**, 168-182.

Hübbe, M. L., Jæhger, D. E., Andresen, T. L. and Andersen, M. H. (2020) Leveraging Endogenous Dendritic Cells to Enhance the Therapeutic Efficacy of Adoptive T-Cell Therapy and Checkpoint Blockade. *Frontiers in Immunology,* **11**.

Ishida, Y., Agata, Y., Shibahara, K. and Honjo, T. (1992) Induced expression of PD-1, a novel member of the immunoglobulin gene superfamily, upon programmed cell death. *The EMBO Journal,* **11**, 3887-3895.

Iwasa, M., Harada, T., Oda, A., Bat-Erdene, A., Teramachi, J., Tenshin, H., Ashtar, M., Oura, M., Sogabe, K., Udaka, K., Fujii, S., Nakamura, S., Miki, H., Kagawa, K., Ozaki, S. and Abe, M. (2019) PD-L1 upregulation in myeloma cells by panobinostat in combination with interferon-γ. *Oncotarget,* **10**, 1903-1917.

Jeong, S., Park, E., Kim, H.-D., Sung, E., Kim, H., Jeon, J., Kim, Y., Jung, U.-J., Son, Y.-G., Hong, Y., Lee, H., Lee, S., Lim, Y., Won, J., Jeon, M., Hwang, S., Fang, L., Jiang, W., Wang, Z., Shin, E.-C., Park, S.-H. and Jung, J. (2021) Novel anti-4-1BB×PD-L1 bispecific antibody augments anti-tumor immunity through tumor-directed T-cell activation and checkpoint blockade. *Journal for ImmunoTherapy of Cancer,* **9**, e002428.

Jiang, N., Yang, Z., Miao, H., Xing, S., Wang, S. and Li, N. (2025) Recent advances in universal chimeric antigen receptor T cell therapy. *Journal of Hematology & Oncology,* **18**.

Jiao, S., Subudhi, S. K., Aparicio, A., Ge, Z., Guan, B., Miura, Y. and Sharma, P. (2019) Differences in Tumor Microenvironment Dictate T Helper Lineage Polarization and Response to Immune Checkpoint Therapy. *Cell,* **179**, 1177-1190.e13.

Jin, J., Wu, X., Yin, J., Li, M., Shen, J., Li, J., Zhao, Y., Zhao, Q., Wu, J., Wen, Q., Cho, C. H., Yi, T., Xiao, Z. and Qu, L. (2019) Identification of Genetic Mutations in Cancer: Challenge and Opportunity in the New Era of Targeted Therapy. *Frontiers in Oncology,* **9**.

Johnson, D. B., Bordeaux, J. M., Kim, J.-Y., Vaupel, C. A., Rimm, D. L., Ho, T. H., Joseph, R. W., Daud, A. I., Conry, R. M., Gaughan, E. M., Hernandez-Aya, L. F., Dimou, A., Funchain, P., Smithy, J. W., Witte, J. S., Mckee, S. B., Ko, J., Wrangle, J., Dabbas, B., Tangri, S., Lameh, J., Hall, J. M., Markowitz, J., Balko, J. M. and Dakappagari, N. K. (2018) Quantitative Spatial Profiling of PD-1/PD-L1 Interaction and HLA-DR/IDO-1 Predicts Improved Outcomes of anti-PD-1 Therapies in Metastatic Melanoma. *Clinical Cancer Research*, clincanres.0309.

June, C. H., Ledbetter, J. A., Gillespie, M. M., Lindsten, T. and Thompson, C. B. (1987) T-cell proliferation involving the CD28 pathway is associated with cyclosporine-resistant interleukin 2 gene expression. *Molecular and Cellular Biology,* **7**, 4472-4481.

Kabut, J., Gorzelak-Magiera, A. and Gisterek-Grocholska, I. (2025) New Therapeutic Targets TIGIT, LAG-3 and TIM-3 in the Treatment of Advanced, Non-Small-Cell Lung Cancer. *International Journal of Molecular Sciences,* **26**, 4096.

Kalbasi, A. and Ribas, A. (2020) Tumour-intrinsic resistance to immune checkpoint blockade. *Nature Reviews Immunology,* **20**, 25-39.

Kandra, P., Nandigama, R., Eul, B., Huber, M., Kobold, S., Seeger, W., Grimminger, F. and Savai, R. (2022) Utility and Drawbacks of Chimeric Antigen Receptor T Cell (CAR-T) Therapy in Lung Cancer. *Frontiers in Immunology,* **13**.

Kangari, P., Salahlou, R. and Vandghanooni, S. (2024) Harnessing the Therapeutic Potential of Mesenchymal Stem Cells in Cancer Treatment. *Advanced pharmaceutical bulletin,* **14**, 574-590.

Kaufman, H., Goldufsky, J., Sivendran, Harcharik, S., Pan, M., Bernardo, S., Stern, R. H., Friedlander, P., Ruby, C. and Saenger, Y. (2013) Oncolytic virus therapy for cancer. *Oncolytic Virotherapy*, 31.

Keir, M. E., Butte, M. J., Freeman, G. J. and Sharpe, A. H. (2008) PD-1 and Its Ligands in Tolerance and Immunity. *Annual Review of Immunology,* **26**, 677-704.

Khan, S. M., Desai, R., Coxon, A., Livingstone, A., Dunn, G. P., Petti, A. and Johanns, T. M. (2022) Impact of CD4 T cells on intratumoral CD8 T-cell exhaustion and responsiveness to PD-1 blockade therapy in mouse brain tumors. *Journal for ImmunoTherapy of Cancer,* **10**, e005293.

Kidd, S., Spaeth, E., Dembinski, J. L., Dietrich, M., Watson, K., Klopp, A., Battula, V. L., Weil, M., Andreeff, M. and Marini, F. C. (2009) Direct Evidence of Mesenchymal Stem Cell Tropism for Tumor and Wounding Microenvironments Using In Vivo Bioluminescent Imaging. *STEM CELLS,* **27**, 2614-2623.

Kim, Y., Clements, D., Sterea, A., Jang, H., Gujar, S. and Lee, P. (2015) Dendritic Cells in Oncolytic Virus-Based Anti-Cancer Therapy. *Viruses,* **7**, 6506-6525.

Kirschenbaum, D., Xie, K., Ingelfinger, F., Katzenelenbogen, Y., Abadie, K., Look, T., Sheban, F., Phan, T. S., Li, B., Zwicky, P., Yofe, I., David, E., Mazuz, K., Hou, J., Chen, Y., Shaim, H., Shanley, M., Becker, S., Qian, J., Colonna, M., Ginhoux, F., Rezvani, K., Theis, F. J., Yosef, N., Weiss, T., Weiner, A. and Amit, I. (2024) Time-resolved single-cell transcriptomics defines immune trajectories in glioblastoma. *Cell,* **187**, 149-165.e23.

Kluger, H. M., Zito, C. R., Turcu, G., Baine, M. K., Zhang, H., Adeniran, A., Sznol, M., Rimm, D. L., Kluger, Y., Chen, L., Cohen, J. V. and Jilaveanu, L. B. (2017) PD-L1 Studies Across Tumor Types, Its Differential Expression and Predictive Value in Patients Treated with Immune Checkpoint Inhibitors. *Clinical Cancer Research,* **23**, 4270-4279.

Koh, J., Kim, S., Woo, Y. D., Song, S. G., Yim, J., Han, B., Lim, S., Ahn, H. K., Mun, S., Kim, J. S., Keam, B., Kim, Y. A., Lee, S.-H., Jeon, Y. K. and Chung, D. H. (2022) TCF1+PD-1+ tumour-infiltrating lymphocytes predict a favorable response and prolonged survival after immune checkpoint inhibitor therapy for non-small-cell lung cancer. *European Journal of Cancer,* **174**, 10-20.

Köhnke, T., Krupka, C., Tischer, J., Knösel, T. and Subklewe, M. (2015) Increase of PD-L1 expressing B-precursor ALL cells in a patient resistant to the CD19/CD3-bispecific T cell engager antibody blinatumomab. *Journal of Hematology & Oncology,* **8**.

Kumar, P., Bhattacharya, P. and Prabhakar, B. S. (2018) A comprehensive review on the role of co-signaling receptors and Treg homeostasis in autoimmunity and tumor immunity. *Journal of Autoimmunity,* **95**, 77-99.

Lan, T., Luo, M. and Wei, X. (2021) Mesenchymal stem/stromal cells in cancer therapy. *Journal of Hematology & Oncology,* **14**.

Landskron, G., De La Fuente, M., Thuwajit, P., Thuwajit, C. and Hermoso, M. A. (2014) Chronic Inflammation and Cytokines in the Tumor Microenvironment. *Journal of Immunology Research,* **2014**, 1-19.

Latchman, Y., Wood, C. R., Chernova, T., Chaudhary, D., Borde, M., Chernova, I., Iwai, Y., Long, A. J., Brown, J. A., Nunes, R., Greenfield, E. A., Bourque, K., Boussiotis, V. A., Carter, L. L., Carreno, B. M., Malenkovich, N., Nishimura, H., Okazaki, T., Honjo, T., Sharpe, A. H. and Freeman, G. J. (2001) PD-L2 is a second ligand for PD-1 and inhibits T cell activation. *Nature Immunology,* **2**, 261-268.

Lee, H. T., Lee, J. Y., Lim, H., Lee, S. H., Moon, Y. J., Pyo, H. J., Ryu, S. E., Shin, W. and Heo, Y.-S. (2017) Molecular mechanism of PD-1/PD-L1 blockade via anti-PD-L1 antibodies atezolizumab and durvalumab. *Scientific Reports,* **7**.

Lei, X., De Groot, D. C., Welters, M. J. P., De Wit, T., Schrama, E., Van Eenennaam, H., Santegoets, S. J., Oosenbrug, T., Van Der Veen, A., Vos, J. L., Zuur, C. L., De Miranda, N. F. C. C., Jacobs, H., Van Der Burg, S. H., Borst, J. and Xiao, Y. (2024) CD4+ T cells produce IFN-I to license cDC1s for induction of cytotoxic T-cell activity in human tumors. *Cellular & Molecular Immunology,* **21**, 374-392.

Li, M. O. and Rudensky, A. Y. (2016) T cell receptor signalling in the control of regulatory T cell differentiation and function. *Nature Reviews Immunology,* **16**, 220-233.

Li, X., You, J., Hong, L., Liu, W., Guo, P. and Hao, X. (2023) Neoantigen cancer vaccines: a new star on the horizon. *Cancer Biology & Medicine*, 1-38.

Li, Y., Liang, Z., Tian, Y., Cai, W., Weng, Z., Chen, L., Zhang, H., Bao, Y., Zheng, H., Zeng, S., Bei, C. and Li, Y. (2018) High-affinity PD-1 molecules deliver improved interaction with PD-L1 and PD-L2. *Cancer Science,* **109**, 2435-2445.

Li, Y., Liu, J., Gao, L., Liu, Y., Meng, F., Li, X. and Qin, F. X.-F. (2020) Targeting the tumor microenvironment to overcome immune checkpoint blockade therapy resistance. *Immunology Letters,* **220**, 88-96.

Lin, W.-P., Li, H. and Sun, Z.-J. (2024a) T cell exhaustion initiates tertiary lymphoid structures and turbocharges cancer-immunity cycle. *EBioMedicine,* **104**, 105154.

Lin, X., Kang, K., Chen, P., Zeng, Z., Li, G., Xiong, W., Yi, M. and Xiang, B. (2024b) Regulatory mechanisms of PD-1/PD-L1 in cancers. *Molecular Cancer,* **23**.

Lin, Y., Song, Y., Zhang, Y., Li, X., Kan, L. and Han, S. (2025) New insights on anti-tumor immunity of CD8+ T cells: cancer stem cells, tumor immune microenvironment and immunotherapy. *Journal of Translational Medicine,* **23**.

Liu, C., Lan, Y., Liu, B., Zhang, H. and Hu, H. (2021) T Cell Development: Old Tales Retold By Single-Cell RNA Sequencing. *Trends in Immunology,* **42**, 165-175.

Liu, J.-N., Kong, X.-S., Huang, T., Wang, R., Li, W. and Chen, Q.-F. (2020) Clinical Implications of Aberrant PD-1 and CTLA4 Expression for Cancer Immunity and Prognosis: A Pan-Cancer Study. *Frontiers in Immunology,* **11**.

Liu, Y.-T. and Sun, Z.-J. (2021) Turning cold tumors into hot tumors by improving T-cell infiltration. *Theranostics,* **11**, 5365-5386.

Ma, W., Gilligan, B. M., Yuan, J. and Li, T. (2016) Current status and perspectives in translational biomarker research for PD-1/PD-L1 immune checkpoint blockade therapy. *Journal of Hematology & Oncology,* **9**.

Ma, Z., Hua, J., Liu, J., Zhang, B., Wang, W., Yu, X. and Xu, J. (2023) Mesenchymal Stromal Cell-Based Targeted Therapy Pancreatic Cancer: Progress and Challenges. *International Journal of Molecular Sciences,* **24**, 3559.

Magiera-Mularz, K., Kocik, J., Musielak, B., Plewka, J., Sala, D., Machula, M., Grudnik, P., Hajduk, M., Czepiel, M., Siedlar, M., Holak, T. A. and Skalniak, L. (2021) Human and mouse PD-L1: similar molecular structure, but different druggability profiles. *iScience,* **24**.

Mahalingam, D., Wilkinson, G. A., Eng, K. H., Fields, P., Raber, P., Moseley, J. L., Cheetham, K., Coffey, M., Nuovo, G., Kalinski, P., Zhang, B., Arora, S. P. and Fountzilas, C. (2020) Pembrolizumab in Combination with the Oncolytic Virus Pelareorep and Chemotherapy in Patients with Advanced Pancreatic Adenocarcinoma: A Phase Ib Study. *Clinical Cancer Research,* **26**, 71-81.

Mahhengam, N., Kazemnezhad, K., Setia Budi, H., Ansari, M. J., Olegovich Bokov, D., Suksatan, W., Thangavelu, L. and Siahmansouri, H. (2022) Targeted therapy of tumour

microenvironment by gold nanoparticles as a new therapeutic approach. *Journal of Drug Targeting,* **30**, 494-510.
Mani, N., Andrews, D. and Obeng, R. C. (2023) Modulation of T cell function and survival by the tumor microenvironment. *Frontiers in cell and developmental biology,* **11**.
Mao, Y., Xie, H., Lv, M., Yang, Q., Shuang, Z., Gao, F., Li, S., Zhu, L. and Wang, W. (2023) The landscape of objective response rate of anti-PD-1/L1 monotherapy across 31 types of cancer: a system review and novel biomarker investigating. *Cancer Immunology, Immunotherapy,* **72**, 2483-2498.
Marei, H. E., Hasan, A., Pozzoli, G. and Cenciarelli, C. (2023) Cancer immunotherapy with immune checkpoint inhibitors (ICIs): potential, mechanisms of resistance, and strategies for reinvigorating T cell responsiveness when resistance is acquired. *Cancer Cell International,* **23**.
Marin-Acevedo, J. A., Kimbrough, E. O. and Lou, Y. (2021) Next generation of immune checkpoint inhibitors and beyond. *Journal of Hematology & Oncology,* **14**.
Marofi, F., Motavalli, R., Safonov, V. A., Thangavelu, L., Yumashev, A. V., Alexander, M., Shomali, N., Chartrand, M. S., Pathak, Y., Jarahian, M., Izadi, S., Hassanzadeh, A., Shirafkan, N., Tahmasebi, S. and Khiavi, F. M. (2021) CAR T cells in solid tumors: challenges and opportunities. *Stem Cell Research & Therapy,* **12**.
Marofi, F., Vahedi, G., Biglari, A., Esmaeilzadeh, A. and Athari, S. S. (2017) Mesenchymal Stromal/Stem Cells: A New Era in the Cell-Based Targeted Gene Therapy of Cancer. *Frontiers in Immunology,* **8**.
Mastrolia, I., Foppiani, E. M., Murgia, A., Candini, O., Samarelli, A. V., Grisendi, G., Veronesi, E., Horwitz, E. M. and Dominici, M. (2019) Challenges in Clinical Development of Mesenchymal Stromal/Stem Cells: Concise Review. *Stem Cells Translational Medicine,* **8**, 1135-1148.
Maute, R. L., Gordon, S. R., Mayer, A. T., Mccracken, M. N., Natarajan, A., Ring, N. G., Kimura, R., Tsai, J. M., Manglik, A., Kruse, A. C., Gambhir, S. S., Weissman, I. L. and Ring, A. M. (2015) Engineering high-affinity PD-1 variants for optimized immunotherapy and immuno-PET imaging. *Proceedings of the National Academy of Sciences,* **112**, E6506-E6514.
Mazzoccoli, L. and Liu, B. (2024) Dendritic Cells in Shaping Anti-Tumor T Cell Response. *Cancers,* **16**, 2211.
Mebarki, M., Abadie, C., Larghero, J. and Cras, A. (2021) Human umbilical cord-derived mesenchymal stem/stromal cells: a promising candidate for the development of advanced therapy medicinal products. *Stem Cell Research & Therapy,* **12**.
Mendicino, M., Bailey, M., Alexander, Wonnacott, K., Puri, K., Raj and Bauer, R., Steven (2014) MSC-Based Product Characterization for Clinical Trials: An FDA Perspective. *Cell Stem Cell,* **14**, 141-145.
Met, Ö., Jensen, K. M., Chamberlain, C. A., Donia, M. and Svane, I. M. (2019) Principles of adoptive T cell therapy in cancer. *Seminars in Immunopathology,* **41**, 49-58.
Middelburg, J., Kemper, K., Engelberts, P., Labrijn, A. F., Schuurman, J. and Van Hall, T. (2021) Overcoming Challenges for CD3-Bispecific Antibody Therapy in Solid Tumors. *Cancers,* **13**, 287.
Miragaia, R. J., Gomes, T., Chomka, A., Jardine, L., Riedel, A., Hegazy, A. N., Whibley, N., Tucci, A., Chen, X., Lindeman, I., Emerton, G., Krausgruber, T., Shields, J., Haniffa, M., Powrie, F. and Teichmann, S. A. (2019) Single-Cell Transcriptomics of Regulatory T Cells Reveals Trajectories of Tissue Adaptation. *Immunity,* **50**, 493-504.e7.
Mishra, A. and Verma, M. (2018) Epigenetic and Genetic Regulation of PDCD1 Gene in Cancer Immunology. *Methods in Molecular Biology.* Springer New York.
Mistarz, A., Komorowski, M. P., Graczyk, M. A., Gil, M., Jiang, A., Opyrchal, M., Rokita, H., Odunsi, K. O. and Kozbor, D. (2019) Recruitment of Intratumoral CD103+ Dendritic Cells by a CXCR4 Antagonist-Armed Virotherapy Enhances Antitumor Immunity. *Molecular Therapy - Oncolytics,* **14**, 233-245.

Mittal, D., Gubin, M. M., Schreiber, R. D. and Smyth, M. J. (2014) New insights into cancer immunoediting and its three component phases—elimination, equilibrium and escape. *Current Opinion in Immunology,* **27**, 16-25.

Moloudizargari, M., Govahi, A., Fallah, M., Rezvanfar, M. A., Asghari, M. H. and Abdollahi, M. (2021) The mechanisms of cellular crosstalk between mesenchymal stem cells and natural killer cells: Therapeutic implications. *Journal of Cellular Physiology,* **236**, 2413-2429.

Mondino, A. and Manzo, T. (2020) To Remember or to Forget: The Role of Good and Bad Memories in Adoptive T Cell Therapy for Tumors. *Frontiers in Immunology,* **11**.

Moreno, R. (2021) Mesenchymal stem cells and oncolytic viruses: joining forces against cancer. *Journal for ImmunoTherapy of Cancer,* **9**, e001684.

Moriya, T., Kitagawa, K., Hayakawa, Y., Hemmi, H., Kaisho, T., Ueha, S., Ikebuchi, R., Yasuda, I., Nakanishi, Y., Honda, T., Matsushima, K., Kabashima, K., Ueda, M., Kusumoto, Y., Chtanova, T. and Tomura, M. (2021) Immunogenic tumor cell death promotes dendritic cell migration and inhibits tumor growth via enhanced T cell immunity. *iScience,* **24**, 102424.

Mortezaee, K. and Majidpoor, J. (2022) Extracellular vesicle-based checkpoint regulation and immune state in cancer. *Medical Oncology,* **39**.

Moseman, J. E., Rastogi, I., Jeon, D. and Mcneel, D. G. (2025) PD-1 blockade employed at the time CD8+ T cells are activated enhances their antitumor efficacy. *Journal for ImmunoTherapy of Cancer,* **13**, e011145.

Motzer, R. J., Rini, B. I., Mcdermott, D. F., Redman, B. G., Kuzel, T. M., Harrison, M. R., Vaishampayan, U. N., Drabkin, H. A., George, S., Logan, T. F., Margolin, K. A., Plimack, E. R., Lambert, A. M., Waxman, I. M. and Hammers, H. J. (2015) Nivolumab for Metastatic Renal Cell Carcinoma: Results of a Randomized Phase II Trial. *Journal of Clinical Oncology,* **33**, 1430-1437.

Nagasaki, J., Inozume, T., Sax, N., Ariyasu, R., Ishikawa, M., Yamashita, K., Kawazu, M., Ueno, T., Irie, T., Tanji, E., Morinaga, T., Honobe, A., Ohnuma, T., Yoshino, M., Iwata, T., Kawase, K., Sasaki, K., Hanazawa, T., Kochin, V., Kawamura, T., Matsue, H., Hino, M., Mano, H., Suzuki, Y., Nishikawa, H. and Togashi, Y. (2022) PD-1 blockade therapy promotes infiltration of tumor-attacking exhausted T cell clonotypes. *Cell Reports,* **38**, 110331.

Nair, R., Somasundaram, V., Kuriakose, A., Krishn, S. R., Raben, D., Salazar, R. and Nair, P. (2025) Deciphering T-cell exhaustion in the tumor microenvironment: paving the way for innovative solid tumor therapies. *Frontiers in Immunology,* **16**.

Neri, S. (2019) Genetic Stability of Mesenchymal Stromal Cells for Regenerative Medicine Applications: A Fundamental Biosafety Aspect. *International Journal of Molecular Sciences,* **20**, 2406.

Nghiem, P. T., Bhatia, S., Lipson, E. J., Kudchadkar, R. R., Miller, N. J., Annamalai, L., Berry, S., Chartash, E. K., Daud, A., Fling, S. P., Friedlander, P. A., Kluger, H. M., Kohrt, H. E., Lundgren, L., Margolin, K., Mitchell, A., Olencki, T., Pardoll, D. M., Reddy, S. A., Shantha, E. M., Sharfman, W. H., Sharon, E., Shemanski, L. R., Shinohara, M. M., Sunshine, J. C., Taube, J. M., Thompson, J. A., Townson, S. M., Yearley, J. H., Topalian, S. L. and Cheever, M. A. (2016) PD-1 Blockade with Pembrolizumab in Advanced Merkel-Cell Carcinoma. *New England Journal of Medicine,* **374**, 2542-2552.

Nguyen, A. W. and Maynard, J. A. (2021) Engineering Antibody-Based Therapeutics: Progress and Opportunities. *Protein Engineering.*

Nguyen, T. M., Bertolus, C., Giraud, P., Burgun, A., Saintigny, P., Bibault, J.-E. and Foy, J.-P. (2023) A Radiomics Approach to Identify Immunologically Active Tumor in Patients with Head and Neck Squamous Cell Carcinomas. *Cancers,* **15**, 5369.

Nicoletti, I., Migliorati, G., Pagliacci, M. C., Grignani, F. and Riccardi, C. (1991) A rapid and simple method for measuring thymocyte apoptosis by propidium iodide staining and flow cytometry. *J Immunol Methods,* **139**, 271-9.

Niess, H., Bao, Q., Conrad, C., Zischek, C., Notohamiprodjo, M., Schwab, F., Schwarz, B., Huss, R., Jauch, K. W., Nelson, P. J. and Bruns, C. J. (2011) Selective targeting of

genetically engineered mesenchymal stem cells to tumor stroma microenvironments using tissue-specific suicide gene expression suppresses growth of hepatocellular carcinoma. *Ann Surg,* **254**, 767-74; discussion 774-5.

Nimmerjahn, F., Gordan, S. and Lux, A. (2015) FcγR dependent mechanisms of cytotoxic, agonistic, and neutralizing antibody activities. *Trends in Immunology,* **36**, 325-336.

O'Malley, D. M., Bariani, G. M., Cassier, P. A., Marabelle, A., Hansen, A. R., De Jesus Acosta, A., Miller, W. H., Safra, T., Italiano, A., Mileshkin, L., Xu, L., Jin, F., Norwood, K. and Maio, M. (2022) Pembrolizumab in Patients With Microsatellite Instability–High Advanced Endometrial Cancer: Results From the KEYNOTE-158 Study. *Journal of Clinical Oncology,* **40**, 752-761.

Obeid, J. M., Erdag, G., Smolkin, M. E., Deacon, D. H., Patterson, J. W., Chen, L., Bullock, T. N. and Slingluff, C. L. (2016) PD-L1, PD-L2 and PD-1 expression in metastatic melanoma: Correlation with tumor-infiltrating immune cells and clinical outcome. *OncoImmunology,* **5**, e1235107.

Ohaegbulam, K. C., Assal, A., Lazar-Molnar, E., Yao, Y. and Zang, X. (2015) Human cancer immunotherapy with antibodies to the PD-1 and PD-L1 pathway. *Trends in Molecular Medicine,* **21**, 24-33.

Oliveira, G. and Wu, C. J. (2023) Dynamics and specificities of T cells in cancer immunotherapy. *Nature Reviews Cancer,* **23**, 295-316.

Oppermans, N., Kueberuwa, G., Hawkins, R. E. and Bridgeman, J. S. (2020) Transgenic T-cell receptor immunotherapy for cancer: building on clinical success. *Therapeutic Advances in Vaccines and Immunotherapy,* **8**, 251513552093350.

Ouyang, P., Wang, L., Wu, J., Tian, Y., Chen, C., Li, D., Yao, Z., Chen, R., Xiang, G., Gong, J. and Bao, Z. (2024) Overcoming cold tumors: a combination strategy of immune checkpoint inhibitors. *Frontiers in Immunology,* **15**.

Pansy, K., Uhl, B., Krstic, J., Szmyra, M., Fechter, K., Santiso, A., Thüminger, L., Greinix, H., Kargl, J., Prochazka, K., Feichtinger, J. and Deutsch, A. J. (2021) Immune Regulatory Processes of the Tumor Microenvironment under Malignant Conditions. *International Journal of Molecular Sciences,* **22**, 13311.

Pascolutti, R., Sun, X., Kao, J., Maute, L., Roy, Ring, M., Aaron, Bowman, R., Gregory and Kruse, C., Andrew (2016) Structure and Dynamics of PD-L1 and an Ultra-High-Affinity PD-1 Receptor Mutant. *Structure (London, England : 1993),* **24**, 1719-1728.

Pasero, C. and Olive, D. (2013) Interfering with coinhibitory molecules: BTLA/HVEM as new targets to enhance anti-tumor immunity. *Immunology Letters,* **151**, 71-75.

Pattu, V., Krause, E., Chang, H.-F., Rettig, J. and Li, X. (2025) IFNγ Expression Correlates with Enhanced Cytotoxicity in CD8+ T Cells. *International Journal of Molecular Sciences,* **26**, 7024.

Peña-Romero, A. C. and Orenes-Piñero, E. (2022) Dual Effect of Immune Cells within Tumour Microenvironment: Pro- and Anti-Tumour Effects and Their Triggers. *Cancers,* **14**, 1681.

Peng, K., Zhao, X., Fu, Y.-X. and Liang, Y. (2025) Eliciting antitumor immunity via therapeutic cancer vaccines. *Cellular & Molecular Immunology,* **22**, 840-868.

Perez, C. R. and De Palma, M. (2019) Engineering dendritic cell vaccines to improve cancer immunotherapy. *Nat Commun,* **10**, 5408.

Phinney, D. G. and Galipeau, J. (2019) Manufacturing mesenchymal stromal cells for clinical applications: A survey of Good Manufacturing Practices at U.S. academic centers. *Cytotherapy,* **21**, 782-792.

Pittet, M. J., Di Pilato, M., Garris, C. and Mempel, T. R. (2023) Dendritic cells as shepherds of T cell immunity in cancer. *Immunity,* **56**, 2218-2230.

Poole, R. M. (2014) Pembrolizumab: First Global Approval. *Drugs,* **74**, 1973-1981.

Popovic, A., Jaffee, E. M. and Zaidi, N. (2018) Emerging strategies for combination checkpoint modulators in cancer immunotherapy. *Journal of Clinical Investigation,* **128**, 3209-3218.

Prokhnevska, N., Cardenas, M. A., Valanparambil, R. M., Sobierajska, E., Barwick, B. G., Jansen, C., Reyes Moon, A., Gregorova, P., delBalzo, L., Greenwald, R., Bilen, M. A., Alemozaffar, M., Joshi, S., Cimmino, C., Larsen, C., Master, V., Sanda, M. and Kissick, H. (2023) CD8⁺ T cell activation in cancer comprises an initial activation phase in lymph nodes followed by effector differentiation within the tumor. *Immunity,* **56**, 107-124.e5.

Pu, J., Liu, T., Zhou, Y., Chen, M., Fu, X., Wan, Y., Wang, J., Chen, B., Sharma, A., Lukacs-Kornek, V., Schmidt-Wolf, I. G. H. and Hou, J. (2025) T cells in cancer: mechanistic insights and therapeutic advances. *Biomarker Research,* **13**, 97.

Rade, M., Böhlen, S., Neuhaus, V., Löffler, D., Blumert, C., Merz, M., Köhl, U., Dehmel, S., Sewald, K. and Reiche, K. (2023) A time-resolved meta-analysis of consensus gene expression profiles during human T-cell activation. *Genome Biology,* **24**.

Reading, J. L., Gálvez-Cancino, F., Swanton, C., Lladser, A., Peggs, K. S. and Quezada, S. A. (2018) The function and dysfunction of memory <scp>CD</scp>8⁺ T cells in tumor immunity. *Immunological Reviews,* **283**, 194-212.

Ribas, A. (2025) Basic rules to respond to PD-1 blockade cancer immunotherapy. *Journal for ImmunoTherapy of Cancer,* **13**, e012096.

Ribas, A., Dummer, R., Puzanov, I., Vanderwalde, A., Andtbacka, R. H. I., Michielin, O., Olszanski, A. J., Malvehy, J., Cebon, J., Fernandez, E., Kirkwood, J. M., Gajewski, T. F., Chen, L., Gorski, K. S., Anderson, A. A., Diede, S. J., Lassman, M. E., Gansert, J., Hodi, F. S. and Long, G. V. (2017) Oncolytic Virotherapy Promotes Intratumoral T Cell Infiltration and Improves Anti-PD-1 Immunotherapy. *Cell,* **170**, 1109-1119.e10.

Robb, K. P., Fitzgerald, J. C., Barry, F. and Viswanathan, S. (2019) Mesenchymal stromal cell therapy: progress in manufacturing and assessments of potency. *Cytotherapy,* **21**, 289-306.

Robilotti, E., Zeitouni, N. C. and Orloff, M. (2023) Biosafety and biohazard considerations of HSV-1–based oncolytic viral immunotherapy. *Frontiers in Molecular Biosciences,* **10**.

Rose-John, S. (2021) Therapeutic targeting of IL-6 trans-signaling. *Cytokine,* **144**, 155577.

Rosenberg, J. E., Hoffman-Censits, J., Powles, T., van der Heijden, M. S., Balar, A. V., Necchi, A., Dawson, N., O'Donnell, P. H., Balmanoukian, A., Loriot, Y., Srinivas, S., Retz, M. M., Grivas, P., Joseph, R. W., Galsky, M. D., Fleming, M. T., Petrylak, D. P., Perez-Gracia, J. L., Burris, H. A., Castellano, D., Canil, C., Bellmunt, J., Bajorin, D., Nickles, D., Bourgon, R., Frampton, G. M., Cui, N., Mariathasan, S., Abidoye, O., Fine, G. D. and Dreicer, R. (2016) Atezolizumab in patients with locally advanced and metastatic urothelial carcinoma who have progressed following treatment with platinum-based chemotherapy: a single-arm, multicentre, phase 2 trial. *The Lancet,* **387**, 1909-1920.

Rowshanravan, B., Halliday, N. and Sansom, D. M. (2018) CTLA-4: a moving target in immunotherapy. *Blood,* **131**, 58-67.

Sabatier, R., Finetti, P., Mamessier, E., Adelaide, J., Chaffanet, M., Ali, H. R., Viens, P., Caldas, C., Birnbaum, D. and Bertucci, F. (2015) Prognostic and predictive value of PDL1 expression in breast cancer. *Oncotarget,* **6**, 5449-5464.

Sakai, S. A., Oyoshi, H., Nakamura, M., Taki, T., Nomura, K., Hojo, H., Hirata, H., Motegi, A., Nakamura, Y., Zenkoh, J., Aokage, K., Hamada, A., Kojima, M., Kuwata, T., Tsuchihara, K., Akimoto, T., Soh, J., Mitsudomi, T., Tsuboi, M., Ishii, G., Suzuki, Y., Suzuki, A., Yamashita, R. and Kageyama, S.-I. (2025) Single-cell spatial analysis with Xenium reveals anti-tumour responses of CXCL13 + T and CXCL9+ cells after radiotherapy combined with anti-PD-L1 therapy. *British Journal of Cancer*.

Saleh, R., Toor, S. M., Sasidharan Nair, V. and Elkord, E. (2020) Role of Epigenetic Modifications in Inhibitory Immune Checkpoints in Cancer Development and Progression. *Frontiers in Immunology,* **11**.

Santos Apolonio, J., Lima De Souza Gonçalves, V., Cordeiro Santos, M. L., Silva Luz, M., Silva Souza, J. V., Rocha Pinheiro, S. L., De Souza, W. R., Sande Loureiro, M. and De Melo, F. F. (2021) Oncolytic virus therapy in cancer: A current review. *World Journal of Virology,* **10**, 229-255.

Saxena, M., Van Der Burg, S. H., Melief, C. J. M. and Bhardwaj, N. (2021) Therapeutic cancer vaccines. *Nature Reviews Cancer,* **21**, 360-378.

Serratì, S., Guida, M., Di Fonte, R., De Summa, S., Strippoli, S., Iacobazzi, R. M., Quarta, A., De Risi, I., Guida, G., Paradiso, A., Porcelli, L. and Azzariti, A. (2022) Circulating extracellular vesicles expressing PD1 and PD-L1 predict response and mediate resistance to checkpoint inhibitors immunotherapy in metastatic melanoma. *Molecular Cancer,* **21**.

Seyed-Khorrami, S.-M., Soleimanjahi, H., Soudi, S. and Habibian, A. (2021) MSCs loaded with oncolytic reovirus: migration and in vivo virus delivery potential for evaluating anti-cancer effect in tumor-bearing C57BL/6 mice. *Cancer Cell International,* **21**.

Seymour, L. W. and Fisher, K. D. (2016) Oncolytic viruses: finally delivering. *British Journal of Cancer,* **114**, 357-361.

Sharma, P. and Allison, J. P. (2015) The future of immune checkpoint therapy. *Science,* **348**, 56-61.

Sharma, P., Hu-Lieskovan, S., Wargo, J. A. and Ribas, A. (2017) Primary, Adaptive, and Acquired Resistance to Cancer Immunotherapy. *Cell,* **168**, 707-723.

Sharma, R. R., Pollock, K., Hubel, A. and Mckenna, D. (2014) Mesenchymal stem or stromal cells: a review of clinical applications and manufacturing practices. *Transfusion,* **54**, 1418-1437.

Sharpe, A. H. and Pauken, K. E. (2018) The diverse functions of the PD1 inhibitory pathway. *Nature Reviews Immunology,* **18**, 153-167.

Shifrut, E., Carnevale, J., Tobin, V., Roth, T. L., Woo, J. M., Bui, C. T., Li, P. J., Diolaiti, M. E., Ashworth, A. and Marson, A. (2018) Genome-wide CRISPR Screens in Primary Human T Cells Reveal Key Regulators of Immune Function. *Cell,* **175**, 1958-1971.e15.

Shulgin, B., Kosinsky, Y., Omelchenko, A., Chu, L., Mugundu, G., Aksenov, S., Pimentel, R., Deyulia, G., Kim, G., Peskov, K. and Helmlinger, G. (2020) Dose dependence of treatment-related adverse events for immune checkpoint inhibitor therapies: a model-based meta-analysis. *OncoImmunology,* **9**, 1748982.

Simpson, T. R., Li, F., Montalvo-Ortiz, W., Sepulveda, M. A., Bergerhoff, K., Arce, F., Roddie, C., Henry, J. Y., Yagita, H., Wolchok, J. D., Peggs, K. S., Ravetch, J. V., Allison, J. P. and Quezada, S. A. (2013) Fc-dependent depletion of tumor-infiltrating regulatory T cells co-defines the efficacy of anti–CTLA-4 therapy against melanoma. *Journal of Experimental Medicine,* **210**, 1695-1710.

Singh, A., Dees, S. and Grewal, I. S. (2021) Overcoming the challenges associated with CD3+ T-cell redirection in cancer. *British Journal of Cancer,* **124**, 1037-1048.

Sitnik, S., Masemann, D., Leite Dantas, R., Wixler, V. and Ludwig, S. (2020) PD-1 IC Inhibition Synergistically Improves Influenza A Virus-Mediated Oncolysis of Metastatic Pulmonary Melanoma. *Molecular Therapy - Oncolytics,* **17**, 190-204.

Soliman, H., Khalil, F. and Antonia, S. (2014) PD-L1 Expression Is Increased in a Subset of Basal Type Breast Cancer Cells. *PLOS ONE,* **9**, e88557.

Sousa, I. G., Simi, K. C. R., Do Almo, M. M., Bezerra, M. A. G., Doose, G., Raiol, T., Stadler, P. F., Hoffmann, S., Maranhão, A. Q. and Brigido, M. M. (2019) Gene expression profile of human T cells following a single stimulation of peripheral blood mononuclear cells with anti-CD3 antibodies. *BMC Genomics,* **20**.

Stovgaard, E. S., Dyhl-Polk, A., Roslind, A., Balslev, E. and Nielsen, D. (2019) PD-L1 expression in breast cancer: expression in subtypes and prognostic significance: a systematic review. *Breast Cancer Research and Treatment,* **174**, 571-584.

Strazza, M., Bukhari, S., Tocheva, A. S. and Mor, A. (2021) PD-1-induced proliferating T cells exhibit a distinct transcriptional signature. *Immunology,* **164**, 555-568.

Su, Y., Tsagkozis, P., Papakonstantinou, A., Tobin, N. P., Gultekin, O., Malmerfelt, A., Ingelshed, K., Neo, S. Y., Lundquist, J., Chaabane, W., Nisancioglu, M. H., Leiss, L. W., Östman, A., Bergh, J., Sedimbi, S., Lehti, K., Lundqvist, A., Stragliotto, C. L., Haglund, F. and Ehnman, M. (2021) CD11c-CD8 Spatial Cross Presentation: A Novel Approach to Link Immune Surveillance and Patient Survival in Soft Tissue Sarcoma. *Cancers,* **13**, 1175.

Sun, J., Corradini, S., Azab, F., Shokeen, M., Muz, B., Miari, K. E., Maksimos, M., Diedrich, C., Asare, O., Alhallak, K., Park, C., Lubben, B., Chen, Y., Adebayo, O., Bash, H., Kelley, S., Fiala, M., Bender, D. E., Zhou, H., Wang, S., Vij, R., Williams, M. T. S. and Azab, A. K. (2024) IL-10R inhibition reprograms tumor-associated macrophages and reverses drug resistance in multiple myeloma. *Leukemia,* **38**, 2355-2365.

Sun, K., Xu, R., Ma, F., Yang, N., Li, Y., Sun, X., Jin, P., Kang, W., Jia, L., Xiong, J., Hu, H., Tian, Y. and Lan, X. (2022) scRNA-seq of gastric tumor shows complex intercellular interaction with an alternative T cell exhaustion trajectory. *Nature Communications,* **13**.

Swann, J. B. and Smyth, M. J. (2007) Immune surveillance of tumors. *Journal of Clinical Investigation,* **117**, 1137-1146.

Szabo, P. A., Levitin, H. M., Miron, M., Snyder, M. E., Senda, T., Yuan, J., Cheng, Y. L., Bush, E. C., Dogra, P., Thapa, P., Farber, D. L. and Sims, P. A. (2019) Single-cell transcriptomics of human T cells reveals tissue and activation signatures in health and disease. *Nature Communications,* **10**, 4706.

Tai, X., Van Laethem, F., Pobezinsky, L., Guinter, T., Sharrow, S. O., Adams, A., Granger, L., Kruhlak, M., Lindsten, T., Thompson, C. B., Feigenbaum, L. and Singer, A. (2012) Basis of CTLA-4 function in regulatory and conventional CD4+ T cells. *Blood,* **119**, 5155-5163.

Talay, O., Shen, C.-H., Chen, L. and Chen, J. (2009) B7-H1 (PD-L1) on T cells is required for T-cell-mediated conditioning of dendritic cell maturation. *Proceedings of the National Academy of Sciences,* **106**, 2741-2746.

Tan, S., Chen, D., Liu, K., He, M., Song, H., Shi, Y., Liu, J., Zhang, C. W.-H., Qi, J., Yan, J., Gao, S. and Gao, G. F. (2016) Crystal clear: visualizing the intervention mechanism of the PD-1/PD-L1 interaction by two cancer therapeutic monoclonal antibodies. *Protein & Cell,* **7**, 866-877.

Tata, A., Dodard, G., Fugère, C., Leget, C., Ors, M., Rossi, B., Vivier, E. and Brossay, L. (2021) Combination blockade of KLRG1 and PD-1 promotes immune control of local and disseminated cancers. *OncoImmunology,* **10**, 1933808.

Tawbi, H. A., Schadendorf, D., Lipson, E. J., Ascierto, P. A., Matamala, L., Castillo Gutiérrez, E., Rutkowski, P., Gogas, H. J., Lao, C. D., De Menezes, J. J., Dalle, S., Arance, A., Grob, J.-J., Srivastava, S., Abaskharoun, M., Hamilton, M., Keidel, S., Simonsen, K. L., Sobiesk, A. M., Li, B., Hodi, F. S. and Long, G. V. (2022) Relatlimab and Nivolumab versus Nivolumab in Untreated Advanced Melanoma. *New England Journal of Medicine,* **386**, 24-34.

Theodoraki, M.-N., Yerneni, S. S., Hoffmann, T. K., Gooding, W. E. and Whiteside, T. L. (2018) Clinical Significance of PD-L1+ Exosomes in Plasma of Head and Neck Cancer Patients. *Clinical Cancer Research,* **24**, 896-905.

Thoreau, F. and Chudasama, V. (2022) Enabling the next steps in cancer immunotherapy: from antibody-based bispecifics to multispecifics, with an evolving role for bioconjugation chemistry. *RSC Chemical Biology,* **3**, 140-169.

Tirosh, I., Izar, B., Prakadan, S. M., Wadsworth, M. H., Treacy, D., Trombetta, J. J., Rotem, A., Rodman, C., Lian, C., Murphy, G., Fallahi-Sichani, M., Dutton-Regester, K., Lin, J.-R., Cohen, O., Shah, P., Lu, D., Genshaft, A. S., Hughes, T. K., Ziegler, C. G. K., Kazer, S. W., Gaillard, A., Kolb, K. E., Villani, A.-C., Johannessen, C. M., Andreev, A. Y., Van Allen, E. M., Bertagnolli, M., Sorger, P. K., Sullivan, R. J., Flaherty, K. T., Frederick, D. T., Jané-Valbuena, J., Yoon, C. H., Rozenblatt-Rosen, O., Shalek, A. K., Regev, A. and Garraway, L. A. (2016) Dissecting the multicellular ecosystem of metastatic melanoma by single-cell RNA-seq. *Science,* **352**, 189-196.

Tokunaga, R., Zhang, W., Naseem, M., Puccini, A., Berger, M. D., Soni, S., McSkane, M., Baba, H. and Lenz, H. J. (2018) CXCL9, CXCL10, CXCL11/CXCR3 axis for immune activation - A target for novel cancer therapy. *Cancer Treat Rev,* **63**, 40-47.

Tseng, S.-Y., Otsuji, M., Gorski, K., Huang, X., Slansky, J. E., Pai, S. I., Shalabi, A., Shin, T., Pardoll, D. M. and Tsuchiya, H. (2001) B7-Dc, a New Dendritic Cell Molecule with Potent Costimulatory Properties for T Cells. *Journal of Experimental Medicine,* **193**, 839-846.

Upadhaya, S., Yu, J. X., Shah, M., Correa, D., Partridge, T. and Campbell, J. (2021) The clinical pipeline for cancer cell therapies. *Nat Rev Drug Discov,* **20**, 503-504.

Van Der Horst, H. J., Nijhof, I. S., Mutis, T. and Chamuleau, M. E. D. (2020) Fc-Engineered Antibodies with Enhanced Fc-Effector Function for the Treatment of B-Cell Malignancies. *Cancers,* **12**, 3041.

van Elsas, M. J., Middelburg, J., Labrie, C., Roelands, J., Schaap, G., Sluijter, M., Tonea, R., Ovcinnikovs, V., Lloyd, K., Schuurman, J., Riesenfeld, S. J., Gajewski, T. F., de Miranda, N. F. C. C., van Hall, T. and van der Burg, S. H. (2024) Immunotherapy-activated T cells recruit and skew late-stage activated M1-like macrophages that are critical for therapeutic efficacy. *Cancer Cell,* **42**, 1032-1050.e10.

Vishnoi, K., Kumar, S., Ke, R., Rana, A. and Rana, B. (2022) Dysregulation of immune checkpoint proteins in hepatocellular carcinoma: Impact on metabolic reprogramming. *Curr Opin Pharmacol,* **64**, 102232.

Viswanathan, S., Keating, A., Deans, R., Hematti, P., Prockop, D., Stroncek, D. F., Stacey, G., Weiss, D. J., Mason, C. and Rao, M. S. (2014) Soliciting Strategies for Developing Cell-Based Reference Materials to Advance Mesenchymal Stromal Cell Research and Clinical Translation. *Stem Cells and Development,* **23**, 1157-1167.

Wang, C., Chen, L., Fu, D., Liu, W., Puri, A., Kellis, M. and Yang, J. (2024a) Antigen presenting cells in cancer immunity and mediation of immune checkpoint blockade. *Clinical & Experimental Metastasis,* **41**, 333-349.

Wang, D., Fang, J., Wen, S., Li, Q., Wang, J., Yang, L., Dai, W., Lu, H., Guo, J., Shan, Z., Xie, W., Liu, X., Wen, L., Shen, J., Wang, A., Chen, Q. and Wang, Z. (2022a) A comprehensive profile of TCF1+ progenitor and TCF1− terminally exhausted PD-1+CD8+ T cells in head and neck squamous cell carcinoma: implications for prognosis and immunotherapy. *International Journal of Oral Science,* **14**.

Wang, L., Geng, H., Liu, Y., Liu, L., Chen, Y., Wu, F., Liu, Z., Ling, S., Wang, Y. and Zhou, L. (2023) Hot and cold tumors: Immunological features and the therapeutic strategies. *MedComm,* **4**.

Wang, M., Chen, S., He, X., Yuan, Y. and Wei, X. (2024b) Targeting inflammation as cancer therapy. *Journal of Hematology & Oncology,* **17**.

Wang, X., Shen, X., Chen, S., Liu, H., Hong, N., Zhong, H., Chen, X. and Jin, W. (2022b) Reinvestigation of Classic T Cell Subsets and Identification of Novel Cell Subpopulations by Single-Cell RNA Sequencing. *The Journal of Immunology,* **208**, 396-406.

Wang, Y.-N., Lee, H.-H., Hsu, J. L., Yu, D. and Hung, M.-C. (2020) The impact of PD-L1 N-linked glycosylation on cancer therapy and clinical diagnosis. *Journal of Biomedical Science,* **27**.

Wang, Y., Zhang, H., Liu, C., Wang, Z., Wu, W., Zhang, N., Zhang, L., Hu, J., Luo, P., Zhang, J., Liu, Z., Peng, Y., Liu, Z., Tang, L. and Cheng, Q. (2022c) Immune checkpoint modulators in cancer immunotherapy: recent advances and emerging concepts. *Journal of Hematology & Oncology,* **15**.

Ward, E. S., Devanaboyina, S. C. and Ober, R. J. (2015) Targeting FcRn for the modulation of antibody dynamics. *Molecular Immunology,* **67**, 131-141.

Wegrzyn, A. S., Kedzierska, A. E. and Obojski, A. (2023) Identification and classification of distinct surface markers of T regulatory cells. *Frontiers in Immunology,* **13**.

Williams, M. J., Werner, B., Barnes, C. P., Graham, T. A. and Sottoriva, A. (2016) Identification of neutral tumor evolution across cancer types. *Nature Genetics,* **48**, 238-244.

Willsmore, Z. N., Coumbe, B. G. T., Crescioli, S., Reci, S., Gupta, A., Harris, R. J., Chenoweth, A., Chauhan, J., Bax, H. J., Mccraw, A., Cheung, A., Osborn, G., Hoffmann, R. M., Nakamura, M., Laddach, R., Geh, J. L. C., Mackenzie-Ross, A., Healy, C., Tsoka, S., Spicer, J. F., Josephs, D. H., Papa, S., Lacy, K. E. and Karagiannis, S. N. (2021) Combined anti-PD-1 and anti-CTLA-4 checkpoint blockade: Treatment of melanoma and immune mechanisms of action. *European Journal of Immunology,* **51**, 544-556.

Wilson, A., Hodgson-Garms, M., Frith, J. E. and Genever, P. (2019) Multiplicity of Mesenchymal Stromal Cells: Finding the Right Route to Therapy. *Frontiers in Immunology,* **10**.

Wu, K., Yi, M., Qin, S., Chu, Q., Zheng, X. and Wu, K. (2019) The efficacy and safety of combination of PD-1 and CTLA-4 inhibitors: a meta-analysis. *Experimental Hematology & Oncology,* **8**.

Xin Yu, J., Hubbard-Lucey, V. M. and Tang, J. (2019a) Immuno-oncology drug development goes global. *Nat Rev Drug Discov,* **18**, 899-900.

Xin Yu, J., Hubbard-Lucey, V. M. and Tang, J. (2019b) Immuno-oncology drug development goes global. *Nature Reviews Drug Discovery,* **18**, 899-900.

Yang, J., Riella, L. V., Chock, S., Liu, T., Zhao, X., Yuan, X., Paterson, A. M., Watanabe, T., Vanguri, V., Yagita, H., Azuma, M., Blazar, B. R., Freeman, G. J., Rodig, S. J., Sharpe, A. H., Chandraker, A. and Sayegh, M. H. (2011) The Novel Costimulatory Programmed Death Ligand 1/B7.1 Pathway Is Functional in Inhibiting Alloimmune Responses In Vivo. *The Journal of Immunology,* **187**, 1113-1119.

Yin, Z., Yu, M., Ma, T., Zhang, C., Huang, S., Karimzadeh, M. R., Momtazi-Borojeni, A. A. and Chen, S. (2021) Mechanisms underlying low-clinical responses to PD-1/PD-L1 blocking antibodies in immunotherapy of cancer: a key role of exosomal PD-L1. *Journal for ImmunoTherapy of Cancer,* **9**, e001698.

Yu, H., Boyle, T. A., Zhou, C., Rimm, D. L. and Hirsch, F. R. (2016a) PD-L1 Expression in Lung Cancer. *Journal of Thoracic Oncology,* **11**, 964-975.

Yu, J., Wang, X., Teng, F. and Kong, L. (2016b) PD-L1 expression in human cancers and its association with clinical outcomes. *OncoTargets and Therapy,* **Volume 9**, 5023-5039.

Yu, M., Peng, Z., Qin, M., Liu, Y., Wang, J., Zhang, C., Lin, J., Dong, T., Wang, L., Li, S., Yang, Y., Xu, S., Guo, W., Zhang, X., Shi, M., Peng, H., Luo, X., Zhang, H., Zhang, L., Li, Y., Yang, X.-P. and Sun, S. (2021) Interferon-γ induces tumor resistance to anti-PD-1 immunotherapy by promoting YAP phase separation. *Molecular Cell,* **81**, 1216-1230.e9.

Yu, R., Deedigan, L., Albarenque, S. M., Mohr, A. and Zwacka, R. M. (2013) Delivery of sTRAIL variants by MSCs in combination with cytotoxic drug treatment leads to p53-independent enhanced antitumor effects. *Cell Death & Disease,* **4**, e503-e503.

Zamarin, D., Holmgaard, R. B., Ricca, J., Plitt, T., Palese, P., Sharma, P., Merghoub, T., Wolchok, J. D. and Allison, J. P. (2017) Intratumoral modulation of the inducible co-stimulator ICOS by recombinant oncolytic virus promotes systemic anti-tumour immunity. *Nature Communications,* **8**, 14340.

Zhang, G., Bai, M., Du, H., Yuan, Y., Wang, Y., Fan, W., Zhu, H., Wu, D., He, P. and Xue, B. (2025) Current Advances and Challenges in CAR-T Therapy for Hematological and Solid Tumors. *ImmunoTargets and Therapy,* **Volume 14**, 655-680.

Zhang, J., Lyu, T., Cao, Y. and Feng, H. (2021) Role of TCF-1 in differentiation, exhaustion, and memory of CD8+ T cells: A review. *The FASEB Journal,* **35**, e21549.

Zhang, Y.-C., Zhang, Y.-T., Wang, Y., Zhao, Y. and He, L.-J. (2023) What role does PDL1 play in EMT changes in tumors and fibrosis? *Frontiers in Immunology,* **14**.

Zhao, H., Wu, L., Yan, G., Chen, Y., Zhou, M., Wu, Y. and Li, Y. (2021) Inflammation and tumor progression: signaling pathways and targeted intervention. *Signal Transduction and Targeted Therapy,* **6**.

Zhao, K.-N., Zhang, L. and Qu, J. (2017) Dr. Jian Zhou: The great inventor of cervical cancer vaccine. *Protein & Cell,* **8**.

Zheng, M., Huang, J., Tong, A. and Yang, H. (2019) Oncolytic Viruses for Cancer Therapy: Barriers and Recent Advances. *Molecular Therapy - Oncolytics,* **15**, 234-247.

Zhou, F., Gao, J., Tang, Y., Zou, Z., Jiao, S., Zhou, Z., Xu, H., Xu, Z. P., Yu, H. and Xu, Z. (2021) Engineering Chameleon Prodrug Nanovesicles to Increase Antigen Presentation and Inhibit PD-L1 Expression for Circumventing Immune Resistance of Cancer. *Advanced Materials,* **33**, 2102668.

Zhu, Y., Yao, S. and Chen, L. (2011) Cell Surface Signaling Molecules in the Control of Immune Responses: A Tide Model. *Immunity,* **34**, 466-478.

Supplementary of

Development of an MSC-Based Immune Checkpoint Inhibiting Cell Therapy

Serap GOKCEN

Supplementary Document of

a thesis will be submitted for the degree of Doctor of Philosophy

in Molecular Medicine

School of Life Science

University of Essex

Date of the First Submission October 2025

Supplementary Figure 1. The heatmaps cancer types (n>150) in TCGA PanCancer atlas studies, showing the correlation between mRNA Z-scores of PDL1 and 323 immune-related gene markers. Rows are genes (y-axis) and columns are tumour samples (x-axis). mRNA expression for the predefined immune-related genes was retrieved from the cBioPortal and plotted using the dataset-provided values. Genes and samples were reordered by hierarchical clustering (average linkage; Euclidean distance). A companion analysis computes Pearson correlations between each gene and PDL1 (Green hue, strong positive association defined as r > 0.5). Cancer type is denoted on the bottom left of the figures.

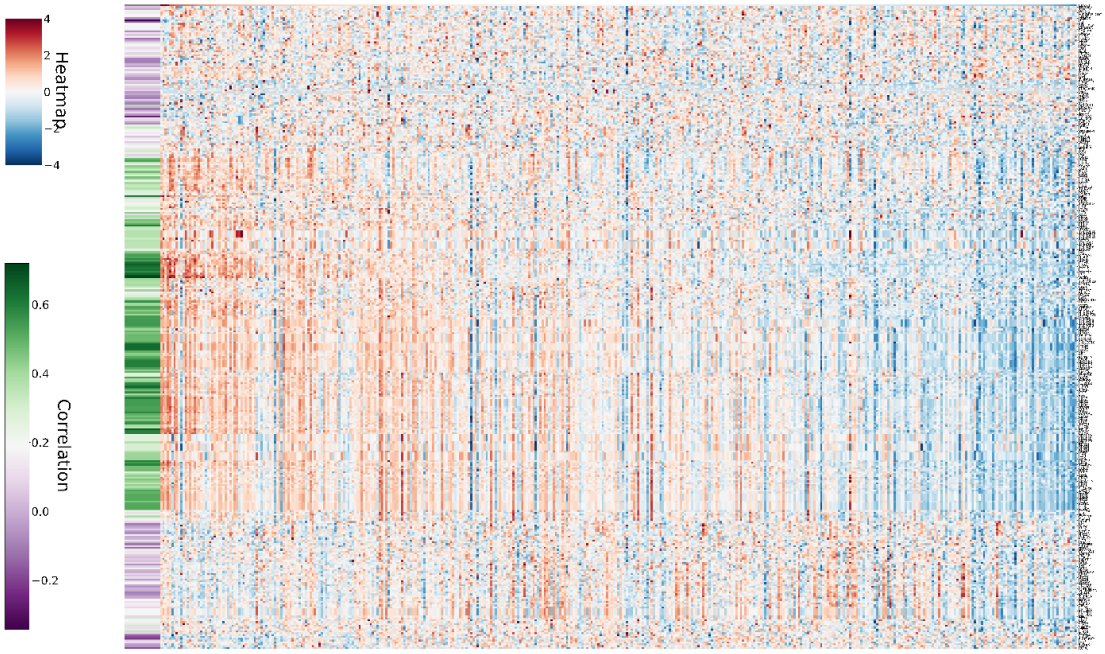

Stomach Adenocarcinoma

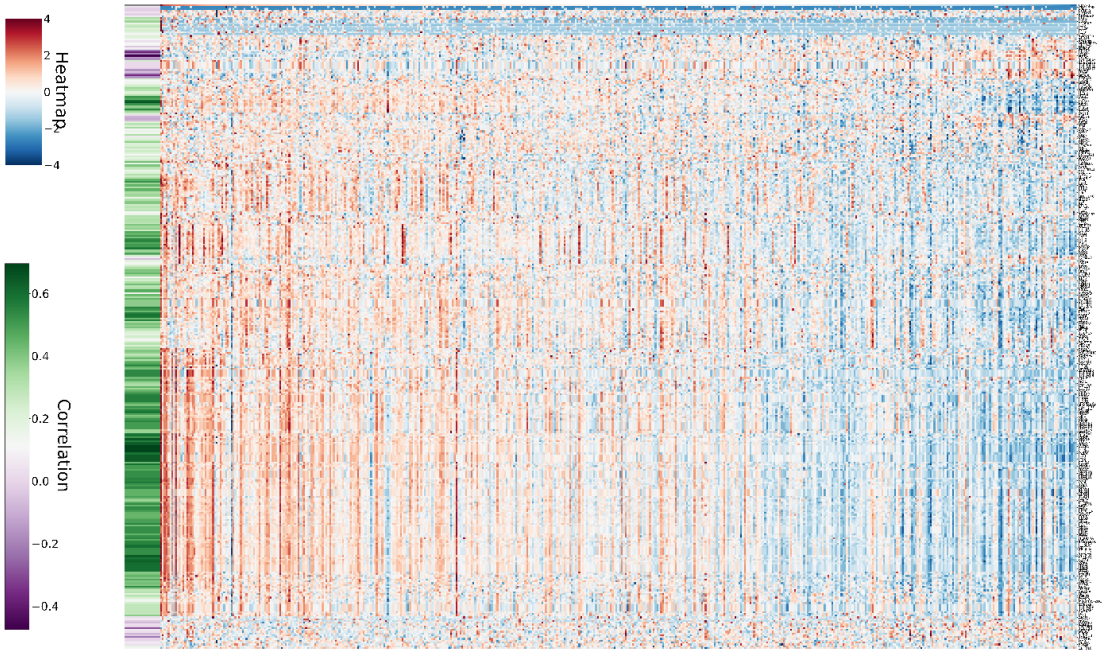

Prostate Adenocarcinoma

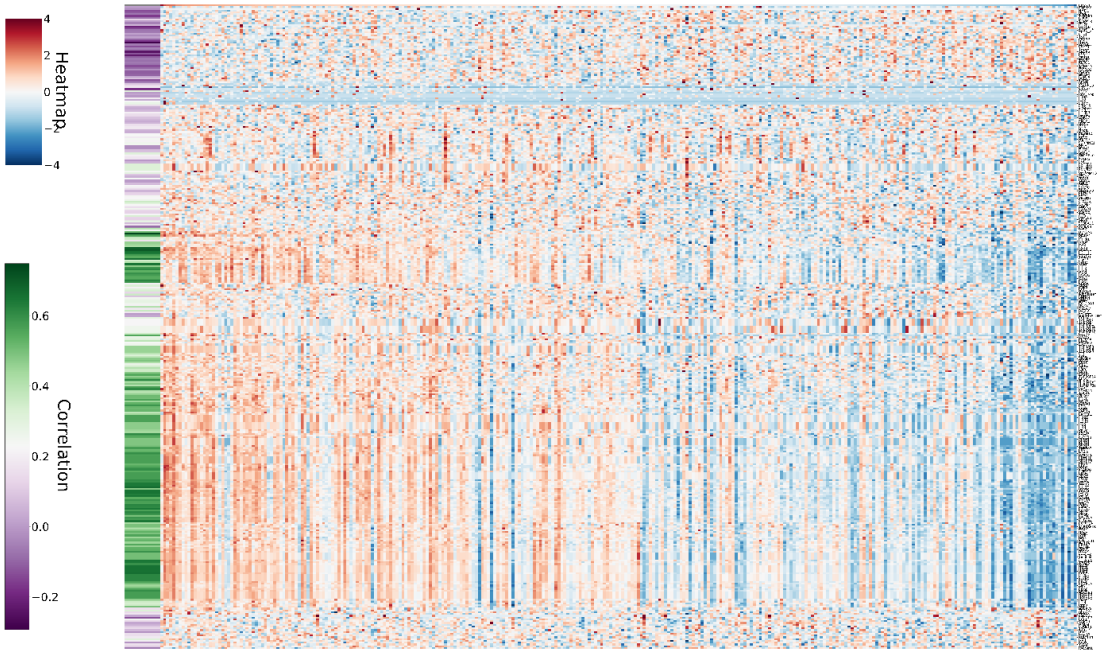

Ovarian Cancer

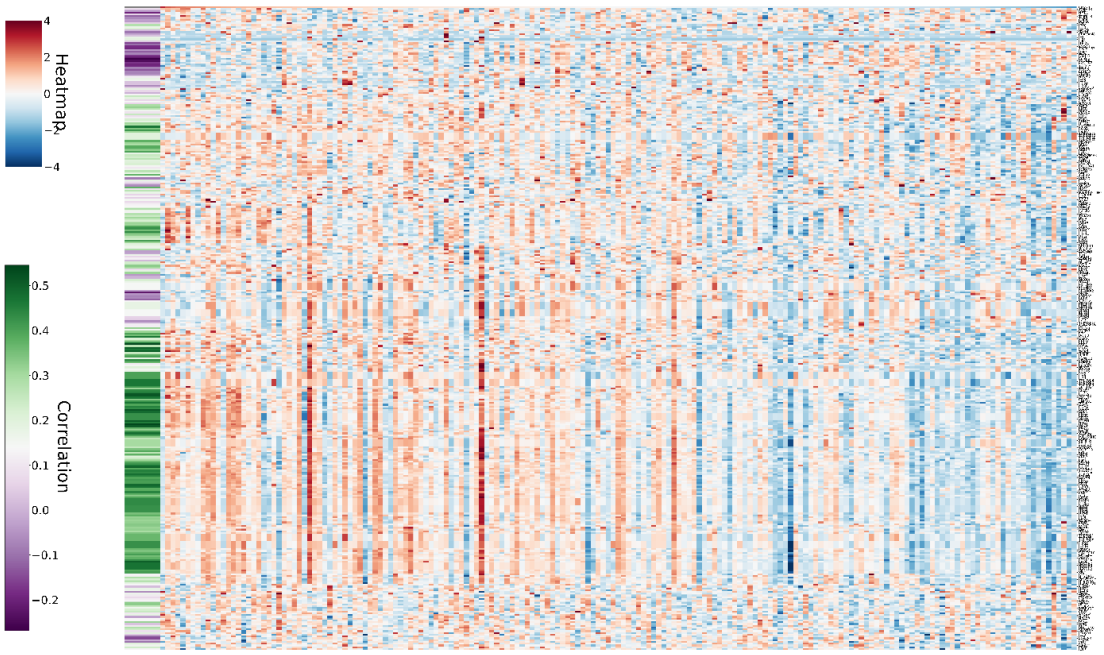

Esophageal Adenocarcinoma

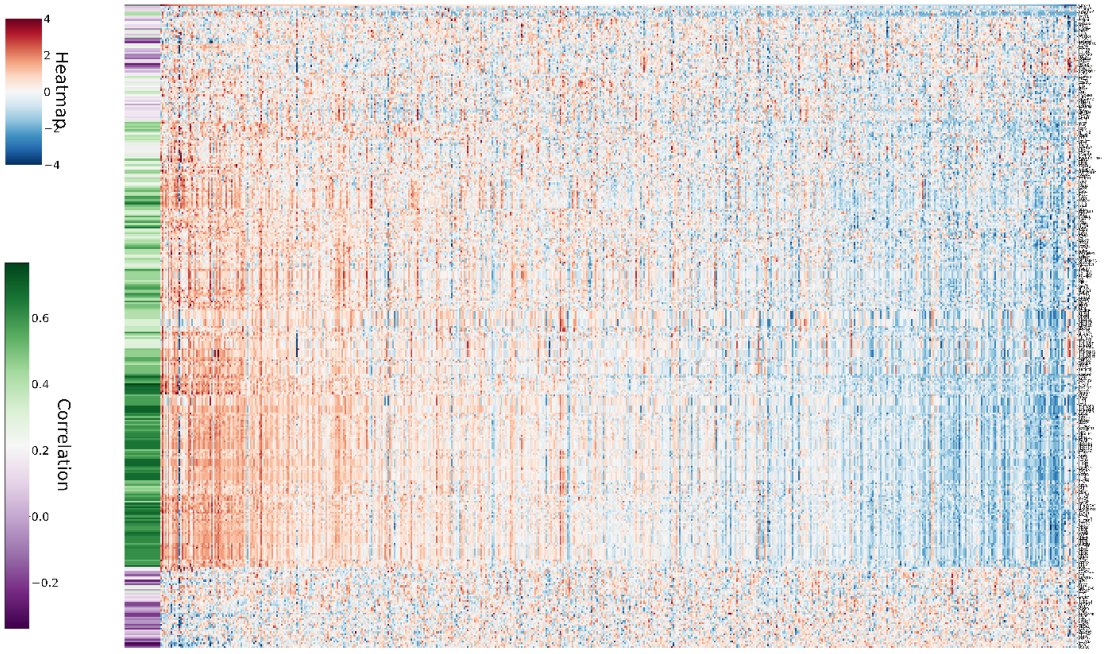

Colorectal Cancer

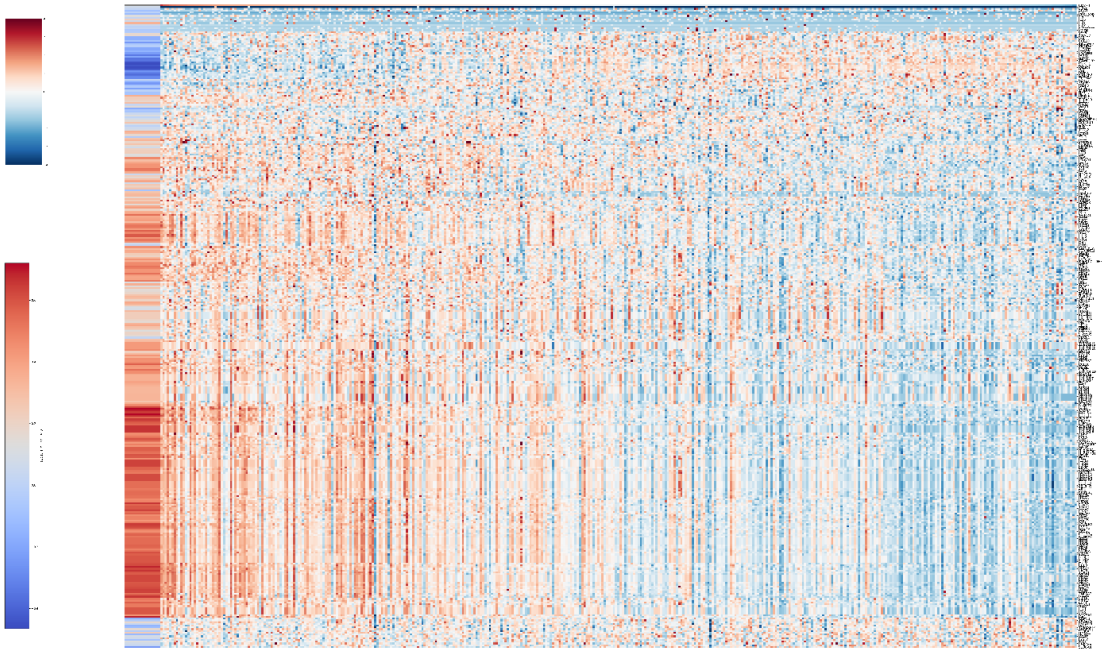

Bladder Cancer

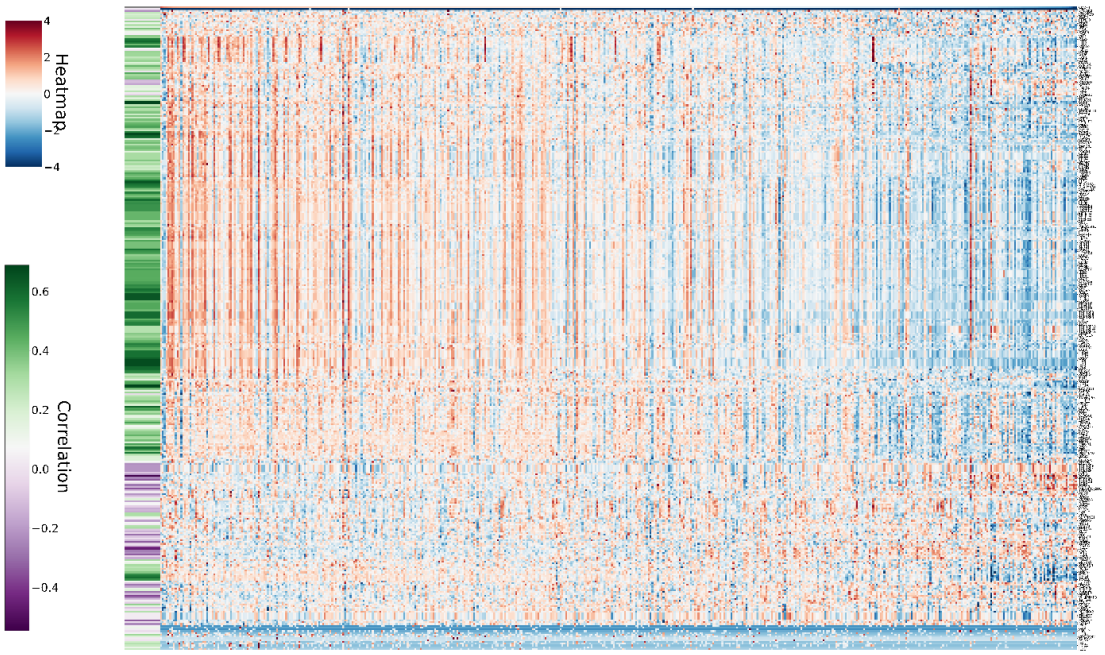

Thyroid Cancer

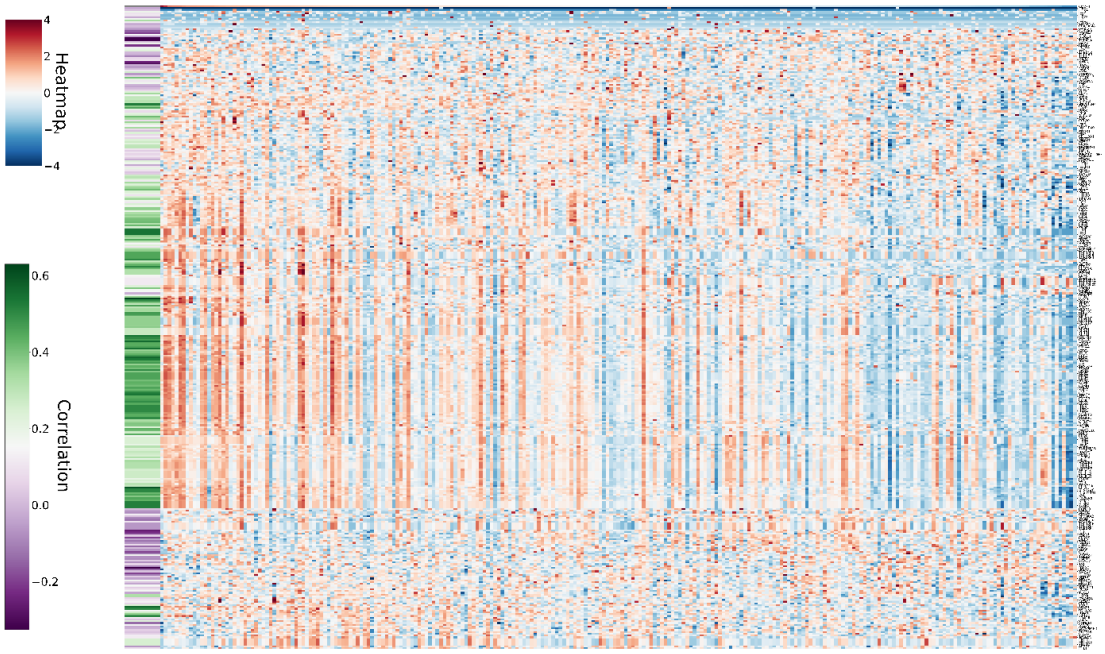

Sarcoma

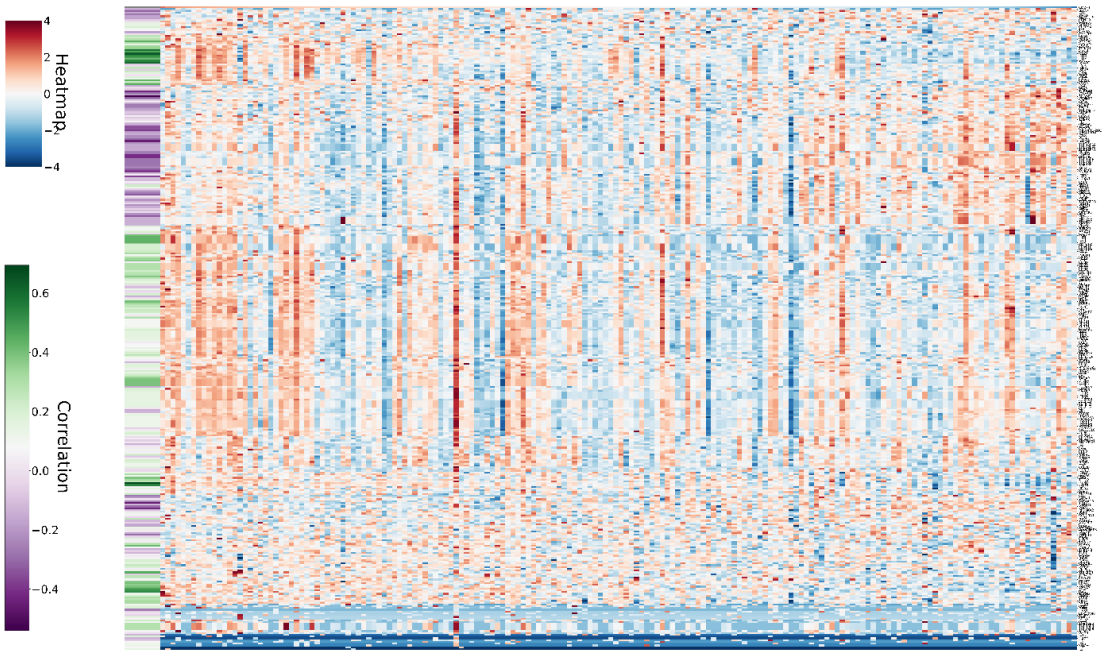

Pheochromocytoma and Paraganglioma

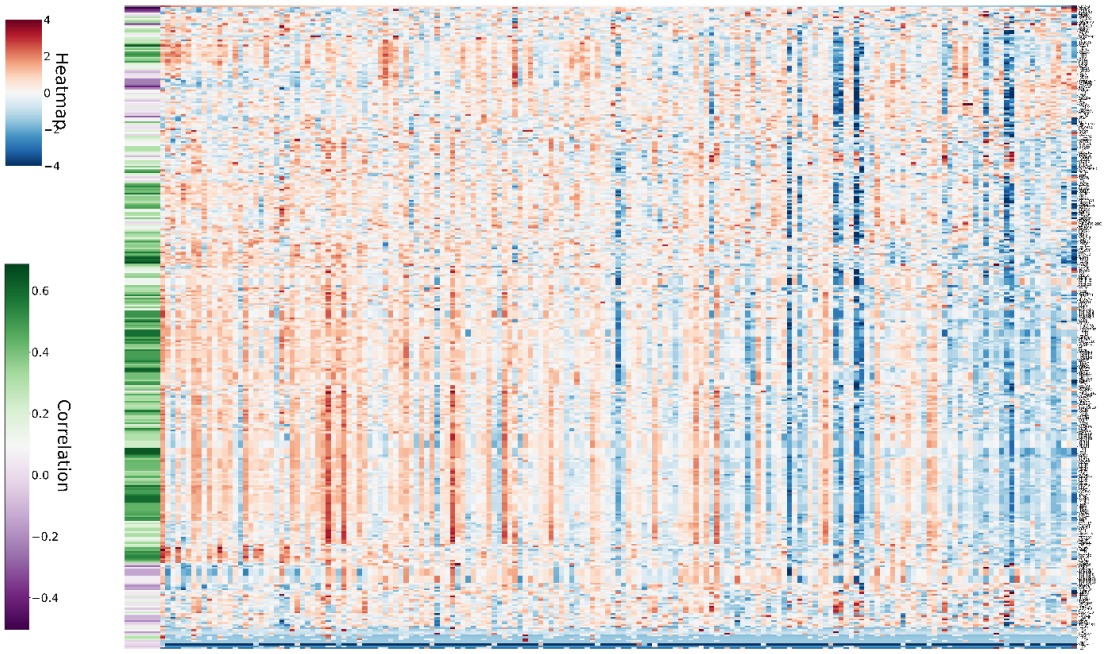

Pancreatic Adenocarcinoma

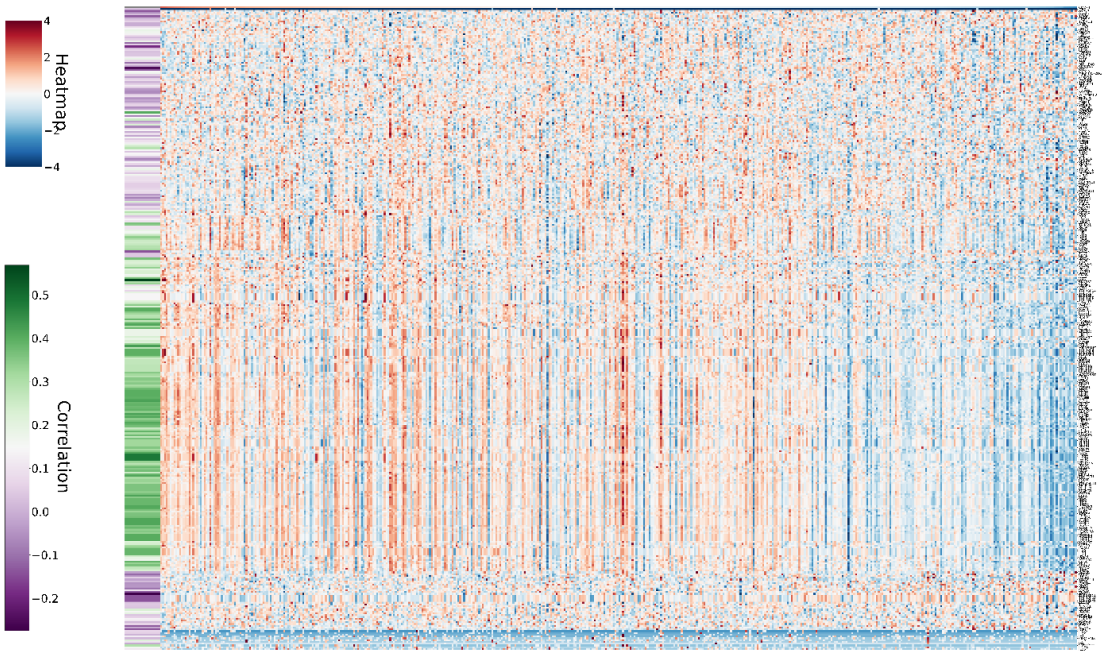

Lung Squamous Carcinoma

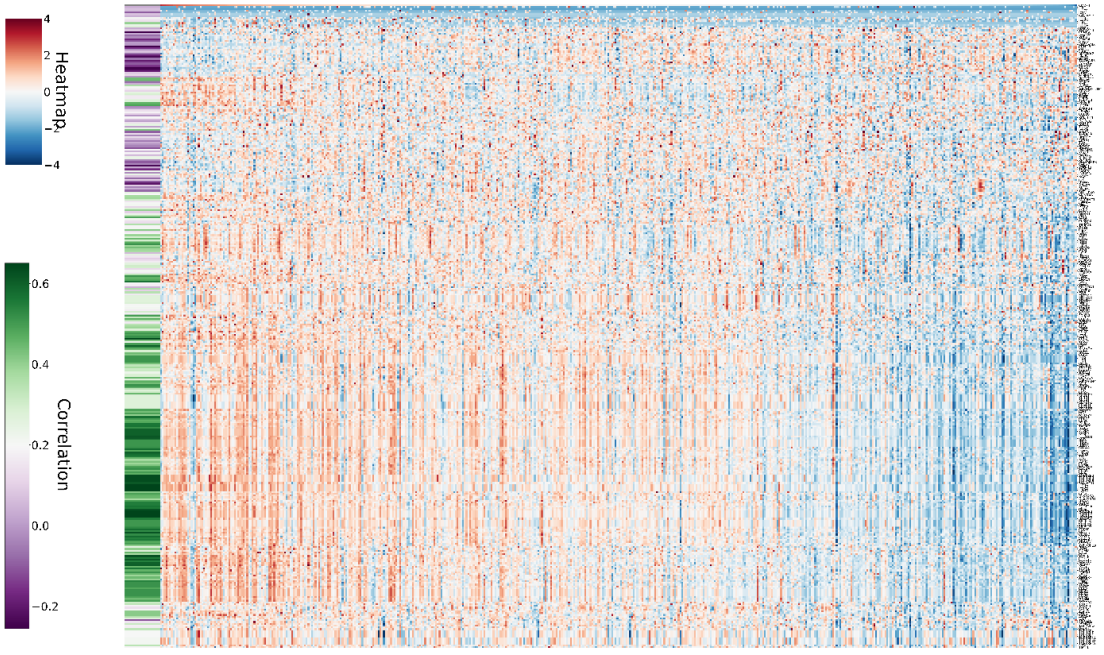

Lung Adenocarcinoma

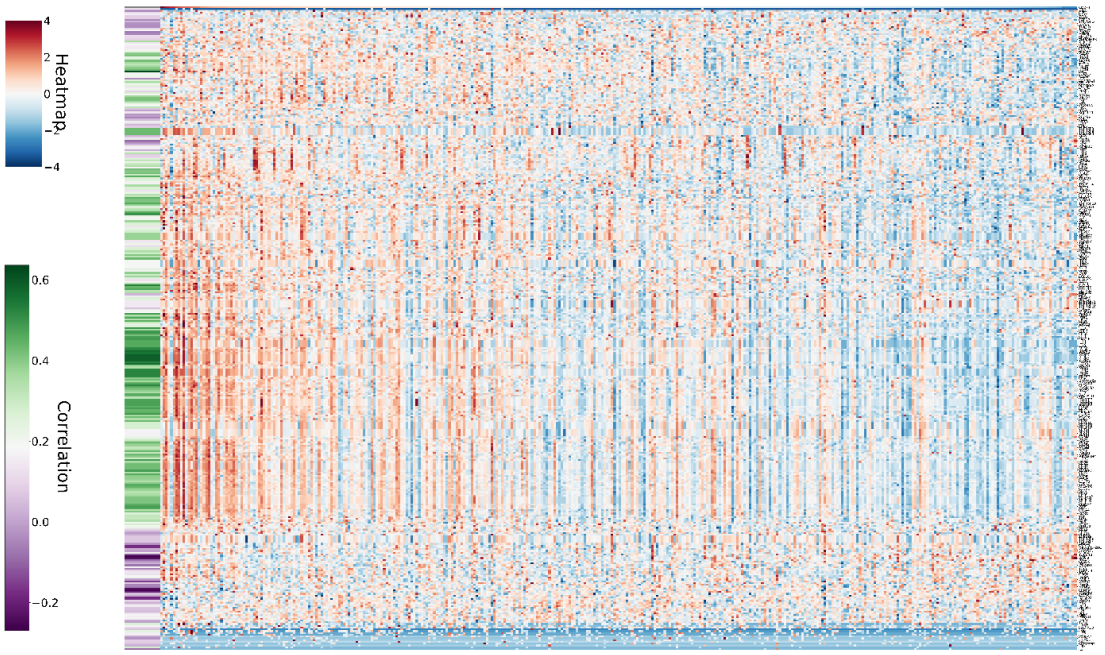

Liver Hepatocarcinoma

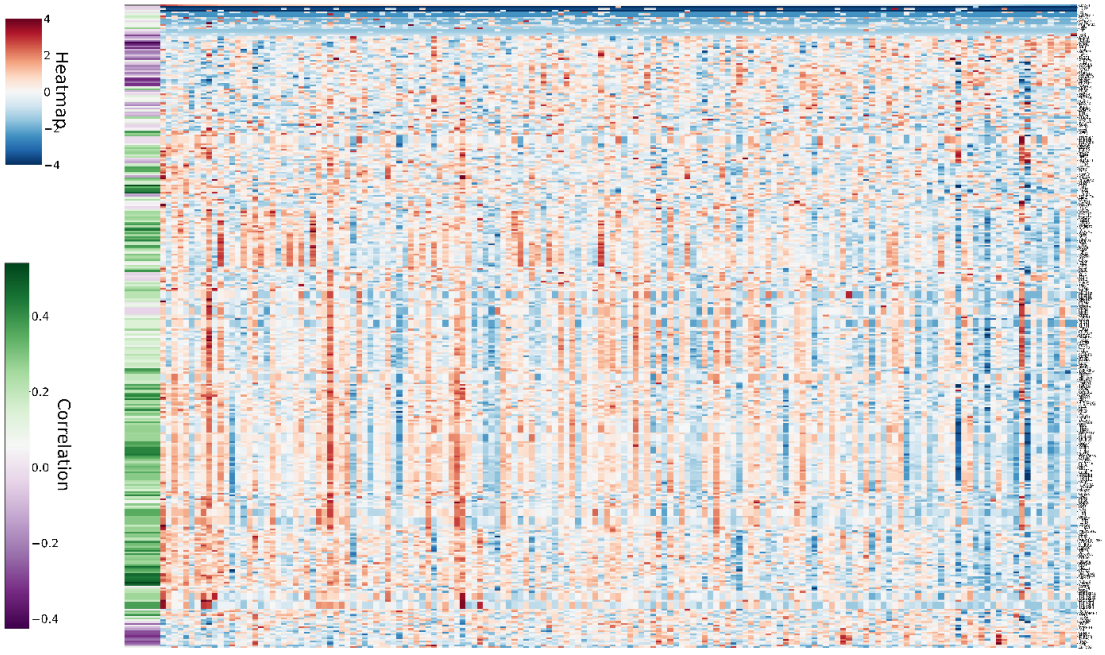

Glioblastoma

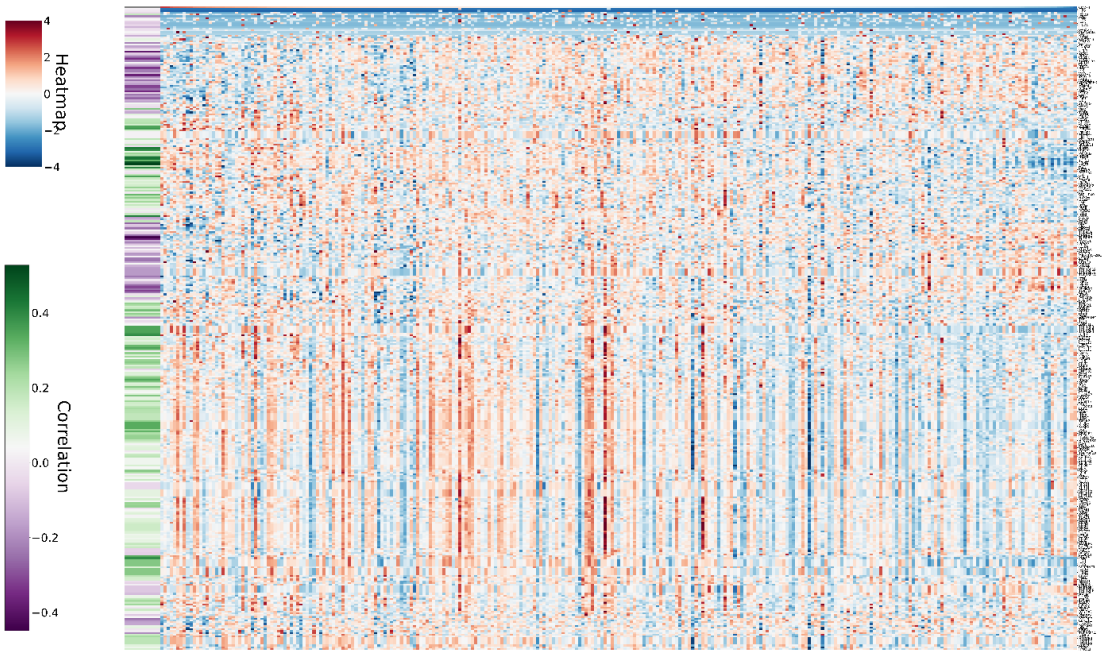

Kidney Renal Papillary Cell Carcinoma

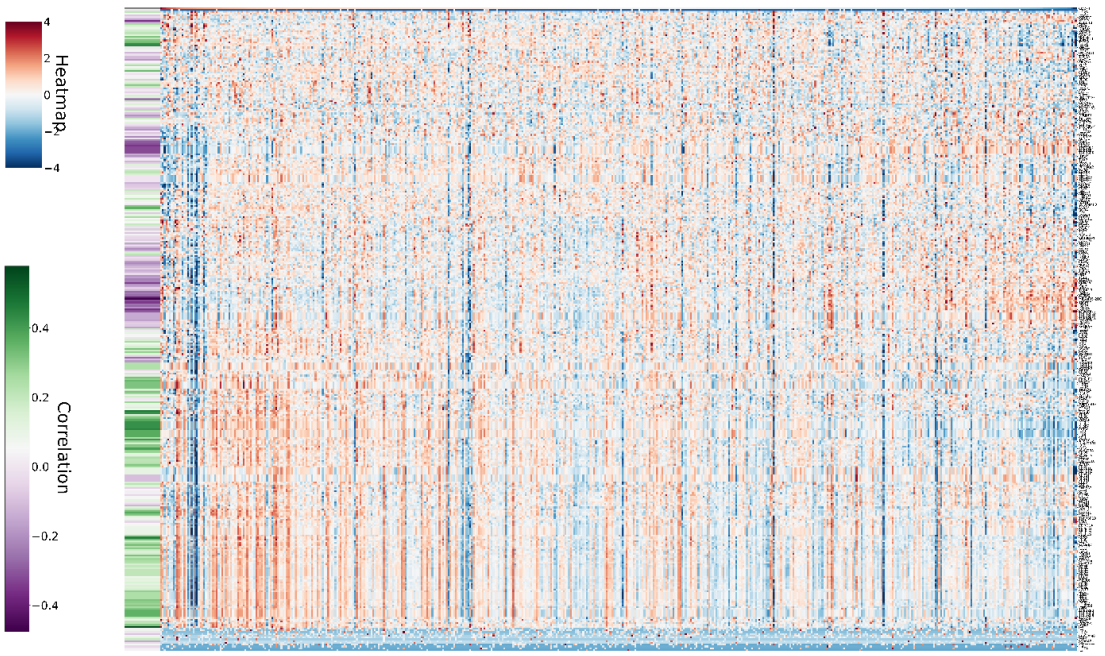

Kidney Renal Clear Cell

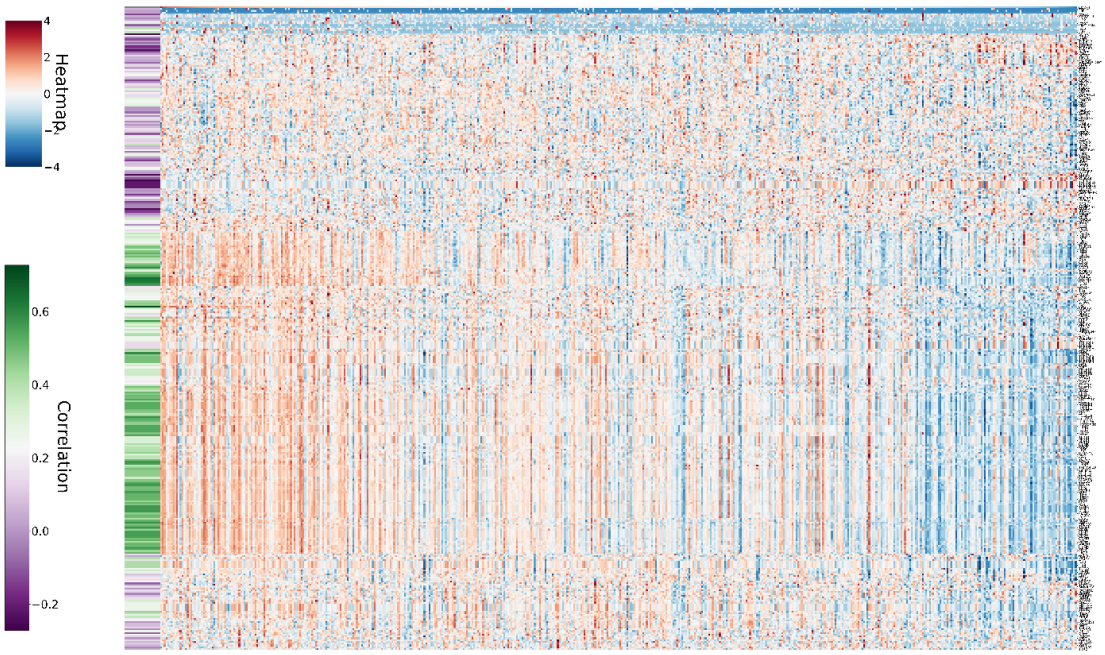

Head and Neck Squamous Cell

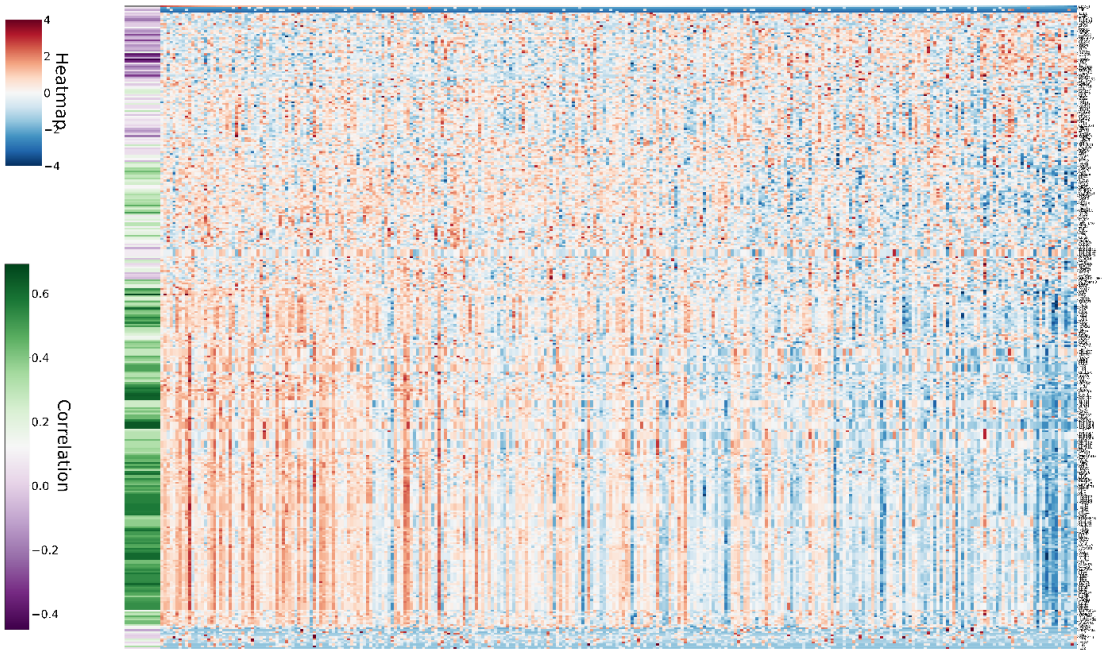

Cervical Squamous Cell

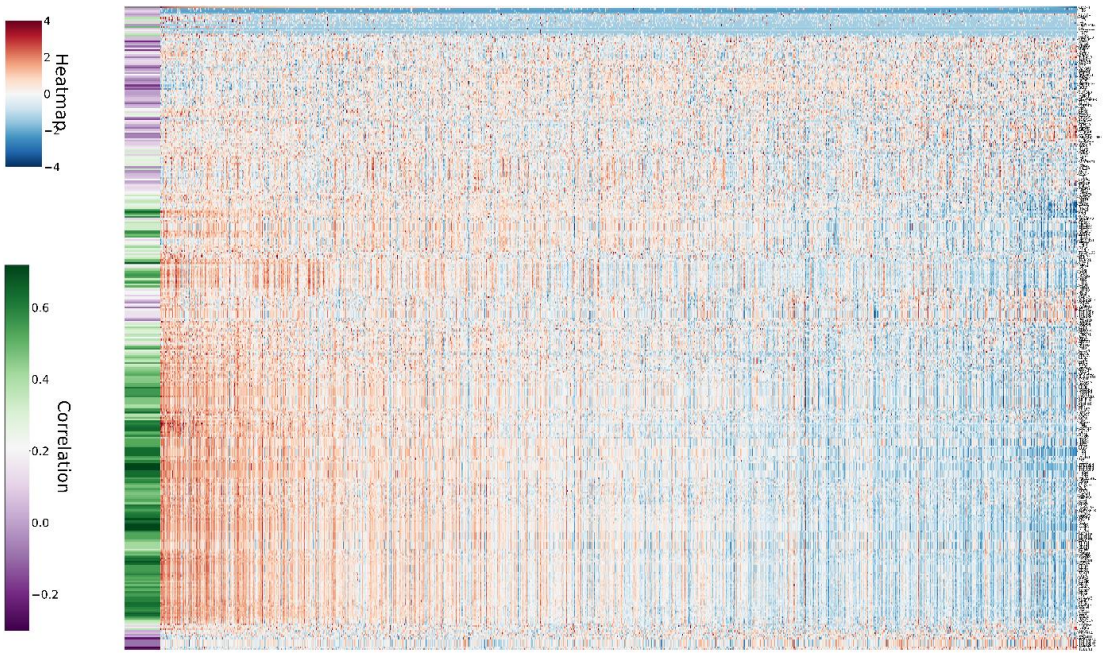

Breast Invasive Carcinoma

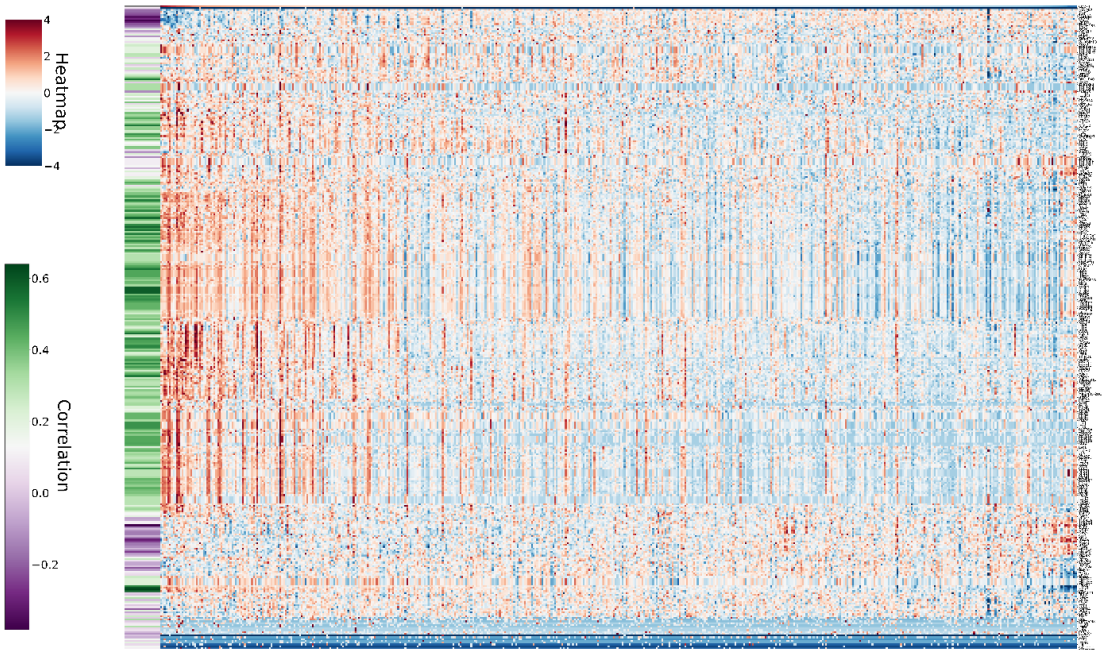

Brain Lower Gade Glioma

Supplementary Table 1. The full list of gene markers that significantly correlated with PDL1 expression in the supplementary figure 1 heatmaps. Pearson correlations (r) were computed between PDL1 and immune-related genes using z-score–normalised expression values. Correlations with r > 0.5 were considered strong positive associations, downloaded for each cancer type. Number of correlated genes were given as “n” for each cancer type.

Melanoma (n=128)	AIF1	BTN3A1	CCL3	CCL4	CCL5	CCR2	CCR3	CCR4	CCR5	CCR7	CD163	CD2	CD226	CD27	CD28
	CD38	CD3D	CD3E	CD4	CD40LG	CD48	CD52	CD69	CD7	CD86	CD8A	CD8B	CIITA	CLEC9A	CMKLR1
	CORO1A	CSF1R	CTSW	CXCL10	CXCL11	CXCL13	CXCL9	CXCR3	CXCR6	FASLG	FCGR1A	FOXP3	GATA3	GIMAP7	GNLY
	GZMA	GZMB	GZMH	GZMK	HAVCR2	HLA-DQA1	HLA-DRA	HLA-DRB1	HLA-E	ICOS	IDO1	IFI35	IFI44L	IFIT2	IFIT3
	IFNG	IKZF1	IL10	IL10RA	IL12B	IL12RB1	IL18	IL21R	IL2RA	IL2RB	IL2RG	IL32	IL7R	IRF1	IRF8
	ITGAL	ITGAM	ITGB7	JAK2	JAML	KLRB1	KLRD1	LAG3	LTA	LTB	LY9	LYZ	MIR155HG	NCR3	NKG7
	NLRP3	OAS1	OAS2	OAS3	OASL	PDCD1	PRDM1	PRF1	PTGER2	PTPRC	RSAD2	SELL	SELPLG	SH2D1A	SIGLEC10
	SLAMF6	SLAMF7	SOCS1	SPI1	SPN	STAT1	STAT4	TAGAP	TBX21	TIGIT	TNF	TNFRSF1B	TNFRSF9	TOX	TOX2
	TRIM21	WARS1	XAF1	XCL1	XCL2	ZBTB32	ZNF683								
Breast Cancer (n=101)	BTN3A1	CCL4	CCL5	CCR2	CCR4	CCR5	CD163	CD2	CD226	CD28	CD38	CD3D	CD3E	CD4	CD40LG
	CD48	CD68	CD69	CD86	CD8A	CIITA	CMKLR1	CTLA4	CXCL10	CXCL11	CXCL9	CXCR3	CXCR6	EOMES	FAS
	FASLG	FOXP3	GNLY	GZMA	GZMB	HAVCR2	HLA-DQA1	HLA-DRA	HLA-E	ICOS	IDO1	IFI16	IFI44L	IFIT2	IFIT3
	IFNG	IKZF1	IL10	IL10RA	IL12RB1	IL18R1	IL21R	IL2RA	IL2RB	IL2RG	IL6R	IL7R	IRF1	IRF4	IRF8
	ITGA4	ITGAL	ITGAX	ITGB7	JAK2	KLRD1	LIMS1	LTA	LY9	LYZ	MIR155HG	MX2	NKG7	OAS2	OAS3
	P2RX7	PDCD1	PRDM1	PRF1	PTPRC	RSAD2	SELL	SH2D1A	SIGLEC10	SLAMF6	SLAMF7	SPN	STAT1	STAT4	TAGAP
	TBX21	TIGIT	TNFRSF1B	TNFRSF9	TOX	WARS1	XAF1	XCL1	XCL2	ZEB2					
Colorectal Cancer (n=100)	AIF1	BATF3	BTN3A1	CCL18	CCL3	CCL4	CCL5	CCR2	CCR4	CCR5	CD163	CD2	CD226	CD28	CD38
	CD3D	CD3E	CD4	CD48	CD69	CD86	CD8A	CIITA	CMKLR1	CSF1	CSF1R	CTLA4	CTSW	CXCL10	CXCL11
	CXCL13	CXCL9	CXCR6	EOMES	FASLG	FCGR1A	GIMAP7	GNLY	GZMA	GZMH	GZMK	HAVCR2	HIF1A	HLA-DQA1	HLA-DRA
	HLA-DRB1	ICOS	IDO1	IFI16	IFI44L	IFIT2	IFIT3	IFNG	IKZF1	IL10	IL10RA	IL12RB1	IL18R1	IL1R1	IL21R
	IL2RA	IL2RB	IL7R	IRF1	IRF4	ITGA4	ITGAL	ITGAX	JAK2	KLRD1	LAG3	LIMS1	LTA	NKG7	NLRP3
	OAS2	OAS3	P2RX7	PDCD1	PRDM1	PRF1	PTPRC	SELL	SH2B3	SH2D1A	SIGLEC10	SLAMF7	SPI1	SPN	STAT1
	STAT4	TAGAP	TBX21	TIGIT	TNFRSF9	WARS1	XAF1	ZEB2	ZNF683						
Bladder (n=94)	AIF1	CCL18	CCL3	CCL4	CCL5	CCR5	CD109	CD163	CD2	CD226	CD38	CD3E	CD7	CD86	CD8A
	CIITA	CMKLR1	CSF1	CSF1R	CSF2	CTLA4	CXCL10	CXCL11	CXCL13	CXCL9	CXCR3	CXCR6	DPP4	EOMES	FAS
	FASLG	FCGR1A	FOXP3	GNLY	GZMA	GZMB	GZMH	HAVCR2	HLA-DQA1	HLA-DRA	HLA-DRB1	HLA-E	ICOS	IDO1	IFI44L
	IFIT2	IFIT3	IFITM1	IFITM3	IFNG	IKZF1	IL10RA	IL12RB1	IL21R	IL2RA	IL2RB	IL2RG	IL32	IL7R	IRF1
	IRF4	ITGA4	ITGAL	ITGAM	ITGAX	JAK2	KLRD1	LAG3	NKG7	NLRP3	P2RX7	PDCD1	PRF1	PTPRC	RSAD2
	SELPLG	SH2B3	SH2D1A	SIGLEC10	SLAMF6	SOCS1	SPI1	SPN	STAT1	STAT4	TAGAP	TBX21	TIGIT	TNF	TNFRSF9
	TRIM21	WARS1	ZNF683												
Ovarian (n=93)	BTN3A1	CCL5	CCR2	CCR4	CCR5	CCR7	CD163	CD2	CD226	CD27	CD38	CD3D	CD3E	CD4	CD40LG
	CD48	CD68	CD7	CD86	CD8A	CIITA	CTLA4	CTSW	CXCL10	CXCL11	CXCL13	CXCL9	CXCR3	CXCR6	EOMES
	FASLG	FCGR1A	FOXP3	GIMAP7	GNLY	GZMA	GZMB	GZMH	HAVCR2	HLA-E	ICOS	IDO1	IFI35	IFI44L	IFIT2
	IFIT3	IFNG	IKZF1	IL10RA	IL12RB1	IL21R	IL2RA	IL2RB	IL2RG	IRF1	IRF4	ITGA4	ITGAL	ITGAM	ITGAX
	JAK2	KLRD1	LAG3	LTA	LY9	LYZ	MX1	NKG7	OAS1	OAS2	OAS3	OASL	P2RX7	PDCD1	PRF1
	PTPRC	RSAD2	SELL	SELPLG	SH2D1A	SIGLEC10	SLAMF6	SLAMF7	STAT1	STAT4	TAGAP	TBX21	TIGIT	TRIM21	WARS1
	XAF1	ZNF683													

Prostate (n=68)	AHR	BTN3A1	CCR2	CCR4	CCR5	CCR6	CCR7	CD163	CD226	CD4	CD40LG	CD48	CD68	CD69	CD86
	CD8A	CIITA	CSF1	CSF1R	CXCR4	CXCR6	HAVCR2	HLA-DRA	HLA-E	ICOS	IFI16	IFI44L	IFIT2	IFIT3	IL10
	IL10RA	IL12RB1	IL21R	IL2RA	IL2RB	IL6R	IL6ST	IL7R	IRF4	ITGA4	ITGAL	ITGAM	JAK2	KLRD1	LY9
	NLRP3	P2RX7	PRDM1	PRF1	PTPRC	RORA	RSAD2	SELL	SELPLG	SH2B3	SIGLEC10	SLAMF6	SLAMF7	SPN	STAT1
	STAT4	TAGAP	TIGIT	TNFRSF1B	TNFRSF9	XAF1	ZEB2								
Lung ADC. (n=58)	AIF1	BTN3A1	CCL3	CCL4	CCR5	CD163	CD226	CD4	CD68	CD86	CD8A	CMKLR1	CSF1R	CTLA4	CXCL10
	CXCL11	CXCL9	CXCR6	FAS	FASLG	FCGR1A	GZMB	HAVCR2	ICOS	IFI16	IFIT3	IFNG	IKZF1	IL10	IL10RA
	IL12RB1	IL21R	IL2RA	IL2RB	IL7R	IRF1	ITGAL	ITGAM	ITGB7	JAK2	KLRD1	NLRP3	P2RX7	PDCD1	PTPRC
	SELPLG	SH2B3	SIGLEC10	SIRPA	SLAMF7	SPI1	STAT1	TAGAP	TBX21	TIGIT	TNFRSF9	WARS1			
Cervical (n=55)	CCL4	CCL5	CCR5	CD2	CD226	CD3E	CD4	CD48	CD86	CD8A	CTLA4	CXCL10	CXCL11	CXCL13	CXCL9
	CXCR6	FASLG	FOXP3	GZMB	GZMH	HAVCR2	HLA-E	ICOS	IDO1	IFIT3	IFNG	IKZF1	IL12RB1	IL21R	IL2RA
	IL2RB	IRF1	ITGAL	JAK2	KLRD1	NKG7	OAS2	OAS3	P2RX7	PRDM1	PRF1	PTPRC	RSAD2	SH2D1A	SIGLEC10
	SLAMF7	SPI1	SPN	STAT1	TAGAP	TBX21	TIGIT	TNFRSF9	WARS1						
Stomach (n=54)	BTN3A1	CCL3	CCL4	CCL5	CCR5	CD163	CD2	CD226	CD38	CD86	CD8A	CIITA	CTLA4	CXCL10	CXCL11
	CXCL9	CXCR6	FASLG	FCGR1A	GNLY	GZMA	GZMB	GZMH	HAVCR2	HLA-E	ICOS	IDO1	IFIT3	IFNG	IL12RB1
	IL21R	IL2RA	IL2RB	IRF1	ITGAE	ITGAL	ITGB7	JAK2	KLRD1	LAG3	NKG7	PDCD1	PRF1	PTPRC	SIGLEC10
	SLAMF7	STAT1	TAGAP	TBX21	TIGIT	TNFRSF9	WARS1	ZNF683							
Thyroid (n=53)	AHR	ATM	BHLHE40	BTN3A1	CCR2	CCR4	CCR5	CD163	CD226	CD28	CD68	CD69	CD86	CIITA	CSF1
	CTLA4	FAS	HAVCR2	HIF1A	HLA-DQA1	HLA-DRA	HLA-DRB1	HLA-E	ICOS	IFIT2	IFIT3	IKZF1	IL2RA	IL2RB	IL4R
	IL6R	IL6ST	IL7R	IRF8	ITGA4	ITGAM	JAK2	LIMS1	LYZ	NLRP3	OAS3	P2RX7	PTPRC	RSAD2	SPN
	STAT1	STAT3	TAGAP	TCF12	TIGIT	TNFRSF9	WARS1								
Head and Neck (n=42)	BTN3A1	CCL4	CCR5	CD226	CD69	CD8A	CIITA	CSF1	CXCL10	CXCL11	CXCL9	CXCR3	CXCR6	FASLG	GZMB
	HAVCR2	HLA-DRA	ICOS	IDO1	IFIT3	IFNG	IL10RA	IL12RB1	IL2RA	IL2RB	IRF1	ITGAL	JAK2	KLRD1	LAG3
	NKG7	OAS3	PDCD1	PRF1	PTPRC	SIGLEC10	SPN	STAT1	TBX21	TIGIT	WARS1				
Pancreatic (n=37)	BCL2L11	CCR4	CCR5	CD163	CD226	CD38	CD4	CD86	CSF1	CXCL10	CXCL9	HIF1A	ICOS	IDO1	IFIT2
	IL1R1	IL2RA	IL2RB	IL6ST	IL7R	ITGA1	ITGA4	JAK2	LIMS1	NLRP3	P2RX7	PRDM1	PTPRC	RORA	SH2B3
	STAT1	TAGAP	TCF12	TIGIT	TNFRSF9	ZEB2									
Sarcoma (n=24)	CCR4	CCR5	CD226	CIITA	CXCL10	CXCL9	CXCR6	EOMES	FASLG	HLA-DQA1	HLA-DRA	ICOS	IFNG	IL7R	IRF1
	ITGAL	JAK2	MIR155HG	P2RX7	PTPRC	SPN	STAT1	TIGIT							
Brain Lower (n=23)	BHLHE40	CCR5	CD109	CD226	CIITA	CXCL10	HLA-E	IKZF1	IL6R	IL6ST	JAK2	LIMS1	MX2	NFKBIZ	OAS2
	PTPRC	RUNX1	SH2B3	STAT1	STAT3	STAT6	VDR								
Hepatocellular carcinoma (n=14)	CD163	CIITA	CXCL9	EOMES	IFI16	IL2RA	IL2RB	ITGA4	JAK2	PRDM1	PTPRC	TAGAP	ZEB2		
Esophageal (n=11)	CCL4	CD86	CXCL10	CXCL9	GZMB	GZMH	ICOS	IFNG	LAG3	PRF1					
Pheochromocytoma (n=9)	ATM	IFIT2	IL6ST	JAK2	LIMS1	MX1	OAS3	RSAD2	STAT1						
Glioblastoma (n=3)	CSF1	IFNAR1													
Kidney Renal Clear (n=1)	JAK2														
Kidney Renal Papillary (n=1)	LIMS1														
Lung Suquamous Cell (n=1)	JAK2														